The Role of the Ste20-like Kinase in Embryonic Development and Neu-induced Mammary Tumorigenesis

Khalid Al-Zahrani

Department of Cellular and Molecular Medicine

Faculty of Medicine

University of Ottawa

Ottawa, Ontario, Canada

September 2018

This thesis is submitted as a partial fulfilment of the

Ph.D. program in Cellular and Molecular Medicine

Abstract

Over the past two decades, the mammalian Ste20-like kinase (SLK) has been characterized for its role in regulating cellular migration, proliferation and apoptosis in fibroblasts and myoblasts. In mammary epithelial cells, SLK has been shown to be required for efficient epithelial-to-mesenchymal transition and to be activated downstream of the HER2/Neu-oncogene to control chemotactic cellular migration. Here, we assessed the role of SLK in HER2/Neu-induced mammary tumorigenesis *in vivo*. As SLK is activated downstream of HER2/Neu, we hypothesized that the loss of SLK would significantly delay tumor progression in a mouse model of HER2-positive breast cancer. As we have shown that global attenuation of SLK kinase activity results in embryonic lethality, a conditional SLK knockout mouse model was generated. To study the role of SLK in HER2-positive breast cancer, we crossed these conditional SLK knockout mice with mice expressing HER2/Neu linked to Cre recombinase in the mammary luminal epithelium. Unexpectedly, we have demonstrated that conditional deletion of SLK significantly accelerates Neu-induced mammary tumor onset and decreases overall survival. SLK deletion results in the induction of Sox10 which drives mammary stem/progenitor activity and cooperates with HER2/Neu to drive tumor growth. Using the Cancer Genome Atlas, we have supported previous findings and validated Sox10 as a potential biomarker of the Triple-negative Breast Cancer subtype. Furthermore, we have uncovered that SLK deletion results in enhanced activation of both PDK1 and AKT. We provide evidence that Sox10 induction requires signaling through a novel AKT/Sox9-dependent pathway following SLK deletion. Taken together, our data suggests that SLK may be required to maintain cells in a fully differentiated state and that loss of SLK in HER2/Neu-induced breast cancer drives a more basal/stem-like phenotype through the induction of Sox10.

Table of Contents

List of Figures

List of Tables

Copyright Permissions

JOHN WILEY AND SONS LICENSE TERMS AND CONDITIONS

Mar 04, 2018

This Agreement between Khalid Al ("You") and John Wiley and Sons ("John Wiley and Sons") consists of your license details and the terms and conditions provided by John Wiley and Sons and Copyright Clearance Center.

License Number	4302010991236
License date	Mar 04, 2018
Licensed Content Publisher	John Wiley and Sons
Licensed Content Publication	Developmental Dynamics
Licensed Content Title	Essential role for the SLK protein kinase in embryogenesis and placental tissue development
Licensed Content Author	Khalid N. Al-Zahrani,Prabhjot Sekhon,Daniel R. Tessier,Julien Yockell-Lelievre,Benjamin R. Pryce,Kyla D. Baron,Grant A. Howe,Roshan K. Sriram,Kate Daniel,Marlene Mckay,Vivian Lo,Jennifer Quizi,Christina L. Addison,Andrée Gruslin,Luc A. Sabourin
Licensed Content Date	Jan 28, 2014
Licensed Content Pages	12
Type of use	Dissertation/Thesis
Requestor type	Author of this Wiley article
Format	Print and electronic
Portion	Figure/table
Number of figures/tables	8
Original Wiley figure/table number(s)	Figures 1-8
Will you be translating?	No
Title of your thesis / dissertation	The role of the Ste20-like kinase in embryonic development and Neu-induced mammary tumorigenesis.
Expected completion date	May 2018
Expected size (number of pages)	180
Requestor Location	Khalid Al-Zahrani 697B Sue Holloway Dr. Ottawa, ON K2J5R6 Canada Attn: Khalid Al-Zahrani
Publisher Tax ID	EU826007151
Total	0.00 CAD
Terms and Conditions	

TERMS AND CONDITIONS

This copyrighted material is owned by or exclusively licensed to John Wiley & Sons, Inc. or one of its group companies (each a"Wiley Company") or handled on behalf of a society with

which a Wiley Company has exclusive publishing rights in relation to a particular work (collectively "WILEY"). By clicking "accept" in connection with completing this licensing transaction, you agree that the following terms and conditions apply to this transaction (along with the billing and payment terms and conditions established by the Copyright Clearance Center Inc., ("CCC's Billing and Payment terms and conditions"), at the time that you opened your RightsLink account (these are available at any time at http://myaccount.copyright.com).

Terms and Conditions

- The materials you have requested permission to reproduce or reuse (the "Wiley Materials") are protected by copyright.

- You are hereby granted a personal, non-exclusive, non-sub licensable (on a stand-alone basis), non-transferable, worldwide, limited license to reproduce the Wiley Materials for the purpose specified in the licensing process. This license, **and any CONTENT (PDF or image file) purchased as part of your order,** is for a one-time use only and limited to any maximum distribution number specified in the license. The first instance of republication or reuse granted by this license must be completed within two years of the date of the grant of this license (although copies prepared before the end date may be distributed thereafter). The Wiley Materials shall not be used in any other manner or for any other purpose, beyond what is granted in the license. Permission is granted subject to an appropriate acknowledgement given to the author, title of the material/book/journal and the publisher. You shall also duplicate the copyright notice that appears in the Wiley publication in your use of the Wiley Material. Permission is also granted on the understanding that nowhere in the text is a previously published source acknowledged for all or part of this Wiley Material. Any third party content is expressly excluded from this permission.

- With respect to the Wiley Materials, all rights are reserved. Except as expressly granted by the terms of the license, no part of the Wiley Materials may be copied, modified, adapted (except for minor reformatting required by the new Publication), translated, reproduced, transferred or distributed, in any form or by any means, and no derivative works may be made based on the Wiley Materials without the prior permission of the respective copyright owner.**For STM Signatory Publishers clearing permission under the terms of the STM Permissions Guidelines only, the terms of the license are extended to include subsequent editions and for editions in other languages, provided such editions are for the work as a whole in situ and does not involve the separate exploitation of the permitted figures or extracts,** You may not alter, remove or suppress in any manner any copyright, trademark or other notices displayed by the Wiley Materials. You may not license, rent, sell, loan, lease, pledge, offer as security, transfer or assign the Wiley Materials on a stand-alone basis, or any of the rights granted to you hereunder to any other person.

- The Wiley Materials and all of the intellectual property rights therein shall at all times remain the exclusive property of John Wiley & Sons Inc, the Wiley Companies, or their respective licensors, and your interest therein is only that of having possession of and the right to reproduce the Wiley Materials pursuant to Section 2 herein during the continuance of this Agreement. You agree that you own no right, title or interest in or to the Wiley Materials or any of the intellectual property rights therein. You shall have no rights hereunder other than the license as provided for above in Section 2. No right, license or interest to any trademark, trade name, service mark or other branding ("Marks") of WILEY or its licensors is granted hereunder, and you agree that you shall not assert any such right, license or interest with respect thereto

- NEITHER WILEY NOR ITS LICENSORS MAKES ANY WARRANTY OR REPRESENTATION OF ANY KIND TO YOU OR ANY THIRD PARTY, EXPRESS, IMPLIED OR STATUTORY, WITH RESPECT TO THE MATERIALS OR THE ACCURACY OF ANY INFORMATION CONTAINED IN THE MATERIALS, INCLUDING, WITHOUT LIMITATION, ANY IMPLIED WARRANTY OF MERCHANTABILITY, ACCURACY, SATISFACTORY QUALITY, FITNESS FOR A PARTICULAR PURPOSE, USABILITY, INTEGRATION OR NON-INFRINGEMENT AND ALL SUCH WARRANTIES ARE HEREBY EXCLUDED BY WILEY AND ITS LICENSORS AND WAIVED BY YOU.

- WILEY shall have the right to terminate this Agreement immediately upon breach of this Agreement by you.

- You shall indemnify, defend and hold harmless WILEY, its Licensors and their respective directors, officers, agents and employees, from and against any actual or threatened claims, demands, causes of action or proceedings arising from any breach of this Agreement by you.

- IN NO EVENT SHALL WILEY OR ITS LICENSORS BE LIABLE TO YOU OR ANY OTHER PARTY OR ANY OTHER PERSON OR ENTITY FOR ANY SPECIAL, CONSEQUENTIAL, INCIDENTAL, INDIRECT, EXEMPLARY OR PUNITIVE DAMAGES, HOWEVER CAUSED, ARISING OUT OF OR IN CONNECTION WITH THE DOWNLOADING, PROVISIONING, VIEWING OR USE OF THE MATERIALS REGARDLESS OF THE FORM OF ACTION, WHETHER FOR BREACH OF CONTRACT, BREACH OF WARRANTY, TORT, NEGLIGENCE, INFRINGEMENT OR OTHERWISE (INCLUDING, WITHOUT LIMITATION, DAMAGES BASED ON LOSS OF PROFITS, DATA, FILES, USE, BUSINESS OPPORTUNITY OR CLAIMS OF THIRD PARTIES), AND WHETHER OR NOT THE PARTY HAS BEEN ADVISED OF THE POSSIBILITY OF SUCH DAMAGES. THIS LIMITATION SHALL APPLY NOTWITHSTANDING ANY FAILURE OF ESSENTIAL PURPOSE OF ANY LIMITED REMEDY PROVIDED HEREIN.

- Should any provision of this Agreement be held by a court of competent jurisdiction to be illegal, invalid, or unenforceable, that provision shall be deemed amended to achieve as nearly as possible the same economic effect as the original provision, and the legality, validity and enforceability of the remaining provisions of this Agreement shall not be affected or impaired thereby.

- The failure of either party to enforce any term or condition of this Agreement shall not constitute a waiver of either party's right to enforce each and every term and condition of this Agreement. No breach under this agreement shall be deemed waived or excused by either party unless such waiver or consent is in writing signed by the party granting such waiver or consent. The waiver by or consent of a party to a breach of any provision of this Agreement shall not operate or be construed as a waiver of or consent to any other or subsequent breach by such other party.

- This Agreement may not be assigned (including by operation of law or otherwise) by you without WILEY's prior written consent.

- Any fee required for this permission shall be non-refundable after thirty (30) days from receipt by the CCC.

- These terms and conditions together with CCC's Billing and Payment terms and conditions (which are incorporated herein) form the entire agreement between you and WILEY concerning this licensing transaction and (in the absence of fraud) supersedes all prior agreements and representations of the parties, oral or written. This Agreement may not be amended except in writing signed by both parties. This Agreement shall be binding upon and inure to the benefit of the parties' successors, legal representatives, and authorized assigns.

- In the event of any conflict between your obligations established by these terms and conditions and those established by CCC's Billing and Payment terms and conditions, these terms and conditions shall prevail.

- WILEY expressly reserves all rights not specifically granted in the combination of (i) the license details provided by you and accepted in the course of this licensing transaction, (ii) these terms and conditions and (iii) CCC's Billing and Payment terms and conditions.

- This Agreement will be void if the Type of Use, Format, Circulation, or Requestor Type was misrepresented during the licensing process.

- This Agreement shall be governed by and construed in accordance with the laws of the State of New York, USA, without regards to such state's conflict of law rules. Any legal action, suit or proceeding arising out of or relating to these Terms and Conditions or the breach thereof shall be instituted in a court of competent jurisdiction in New York County in the State of New York in the United States of America and each party hereby consents and submits to the personal jurisdiction of such court, waives any objection to venue in such court and consents to service of process by registered or certified mail, return receipt requested, at the last known address of such party.

WILEY OPEN ACCESS TERMS AND CONDITIONS

Wiley Publishes Open Access Articles in fully Open Access Journals and in Subscription journals offering Online Open. Although most of the fully Open Access journals publish open access articles under the terms of the Creative Commons Attribution (CC BY) License only, the subscription journals and a few of the Open Access Journals offer a choice of Creative Commons Licenses. The license type is clearly identified on the article.

The Creative Commons Attribution License

The Creative Commons Attribution License (CC-BY) allows users to copy, distribute and transmit an article, adapt the article and make commercial use of the article. The CC-BY license permits commercial and non-

Creative Commons Attribution Non-Commercial License

The Creative Commons Attribution Non-Commercial (CC-BY-NC)License permits use, distribution and reproduction in any medium, provided the original work is properly cited and is not used for commercial purposes.(see below)

Creative Commons Attribution-Non-Commercial-NoDerivs License

The Creative Commons Attribution Non-Commercial-NoDerivs License (CC-BY-NC-ND) permits use, distribution and reproduction in any medium, provided the original work is properly cited, is not used for commercial purposes and no modifications or adaptations are made. (see below)

Use by commercial "for-profit" organizations

Use of Wiley Open Access articles for commercial, promotional, or marketing purposes requires further explicit permission from Wiley and will be subject to a fee.

Throughout this thesis, images and text have been used with permissions from:

Ste20-like kinase SLK, at the crossroads. A matter of life and death. This is an Accepted Manuscript of an article published by Taylor & Francis in *Cell Adhesion & Migration* on *1 January 2013*, available online: https://www.tandfonline.com/doi/abs/10.4161/cam.22495

Abbreviations

ADP	Adenosine diphosphate
AKT	Protein kinase B
AR	Androgen receptor
ASK1	Apoptosis signal-regulating kinase 1
ATAC-seq	Assay for Transposase-Accessible Chromatin using sequencing
ATH	AT1-46 homology domain
ATP	Adenosine triphosphate
BAC	Bacterial artificial chromosome
BSA	Bovine serum albumin
cAMP	Cyclic adenosine monophosphate
CBP	CREB-binding protein
CD24	Cluster of differentiation 24
CD49f	Cluster of differentiation 49f
cDNA	Complementary DNA
ChIP	Chromatin immunoprecipitation
CREB	cAMP response element-binding protein
DAB	3,3'-diaminobenzidine
DAPI	4',6-diamino-2-phenylindole
DMEM	Dulbecco's modified eagle media
DNA	Deoxyribonucleic acid
Dom	Dominant megacolon phenotype
DTT	Dithiothreitol
E	Embryonic day
EDTA	Ethylenediaminetetraacetic acid
EGF	Epidermal growth factor
EGFR	Epidermal growth factor receptor
EGTA	Ethylene glycol-bis(β-aminoethyl ether)-N,N,N',N'-tetraacetic acid

EMT	Epithelial-to-mesenchymal transition
ER	Endoplasmic reticulum
ERM	Ezrin, Radixin and Moeisin
ESR1	Estrogen receptor 1
FAK	Focal adhesion kinase
fMaSCs	Fetal mammary stem cells
FBS	Fetal bovine serum
FDR	False discovery rate
FGF	Fibroblast growth factor
FGFR	Fibroblast growth factor receptor
FoxO	Forkhead box O
GFP	Green fluorescent protein
H&E	Haematoxylin and Eosin
HEPES	4-(2-hydroxyethyl)-1-piperazineethanesulfonic acid
HER2	Human epidermal growth factor receptor 2
HER3	Human epidermal growth factor receptor 3
HER4	Human epidermal growth factor receptor 4
HMG	High mobility group
HRG	Heregulin
HRP	Horseradish peroxidase
IPTG	Isopropyl β-D-1-thiogalactopyranoside
GCK	Germinal centre kinase
GSK3β	Glycogen synthase kinase 3β
GST	Glutathione S-Transferase
IRES	Internal ribosomal entry site
JNK1	c-Jun N-terminal kinase 1
LacZ	β-galactosidase
Lin	Lineage marker

LOK	Lymphocyte-oriented kinase
MAPK	Mitogen-activated protein kinase
MCS	Multiple-species conserved sequences
MDMECs	Mouse dermal microvascular endothelial cells
MED	Mediator polypeptide transcriptional coactivator complex
MEF	Mouse embryonic fibroblast
MEGS	Mammary epithelial growth supplement
MHC	Myosin heavy chain
MMTV	Mouse mammary tumor virus
MST1	Mammalian ste20-like kinase 1
mTOR	Mammalian target of rapamycin
mTORC1	Mammalian target of rapamycin complex 1
mTORC2	Mammalian target of rapamycin complex 2
NDL	neu-deletion mutant
NIC	NDL-IRES-Cre
PAK	p21-activated kinase
PARP	Poly (ADP-ribose) polymerase
PBP	Peroxisome-proliferator-activated receptor-binding protein
PBS	Phosphate buffered saline
PCNA	Proliferating cell nuclear antigen
PCR	Polymerase chain reaction
PDK1	Phosphoinositide-dependent-protein kinase 1
PECAM	Platelet endothelial cell adhesion molecule
PGR	Progesterone receptor
PH	Pleckstrin-homology
PH-PAK	PH domain-containing p21-activated kinase
PHLPP1	PH domain leucine-rich repeat protein phosphatase 1
PHLPP2	PH domain leucine-rich repeat protein phosphatase 2

PI3K	Phosphoinositide 3-kinase
PIP_3	Phosphoinositide(3,4,5)triphosphate
PLCγ	Phospholipase C γ
PLK1	Polo-like kinase 1
PMSF	Phenylnethylsulfonyl fluoride
PP2A	Protein phosphatase 2A
PtdIns	Phosphatidylinositol
PTEN	Phosphatase and tensin homolog
PVDF	Polyvinyldene difluoride
PyMT	Polyoma Middle-T-Antigen
qPCR	Quantitative polymerase chain reaction
RIPA	Radioimmunoprecipitation assay
RNA	Ribonucleic acid
rpm	Revolutions per minute
S6K	S6 kinase
SCID	Severe combined immune deficiency
SDS	Sodium dodecyl sulfate
SEM	Standard error of the mean
SH3	src homology 3
SIN1	Stress-activated map kinase-interacting protein 1
siRNA	Short interfering RNA
SLK	Ste20-like kinase
Sox	Sry HMG-box
Sry	Sex-determining region Y
TBST	Tris-buffered saline with Tween 20
TCA	Tricholoroacetic acid
TCGA	The cancer genome atlas
TGFβ	Transforming growth factor β

TMA	Tissue microarray
TNBC	Triple-negative breast cancer
TNF-α	Tumor necrosis factor α
TSC2	Tuberous sclerosis complex 2
TUNEL	Terminal deoxynucleotidyl transferase dUTP nick end labelling
UV	Ultraviolet
WS4	Waardenburg-Shah syndrome type 4
X-gal	5-bromo-4-chloro-3-indolyl-β-D-galactopyranoside
xPLKK1	Xenopus polo-like kinase kinase 1
ZO-1	Zona occludens 1

Significant Contributions

David P. Cook generated all the data analysis scripts, helped analyze and interpret TCGA dataset in Chapter 5. David also analyzed the microarray that was performed in Figure 4.9. A.

Christiano Tanese de Souza performed the subcutaneous injections shown in Figure 4.14.

John Abou-Hamad, under my supervision as an undergraduate student, performed the microarray validation qRT-PCR shown in Figure 4.9. B.

Jonathan Hodgins performed the CD133 and Sca1 staining, flow cytometry and analysis shown in Figure 4.10. C and D.

OHRI StemCore Laboratories performed the RNA hybridization and scanning of the Affymetrix Mouse Gene 2.0 ST Array shown in Figure 4.9. A.

The University of Ottawa Histology core performed the paraffin embedding and sectioning of all embryo, mammary gland and tumor samples.

Acknowledgements

First and foremost, I would like to thank the Canadian Breast Cancer Foundation for the two Fellowships which I was awarded over the first five years of my graduate studies. To the generous donors, I am eternally grateful for all your support. I would also like to thank the Government of Ontario for providing me with an Ontario Graduate Scholarship to fund the last year of my research.

Next, I would like to thank Dr. Luc Sabourin for his friendship, mentorship and guidance over the last six years. You have taught me that being wrong is okay and that the hard work will always make that black box a little clearer day by day. I would like to sincerely thank you for always being the devil's advocate and pushing me to be my best.

To my mom and dad, I will always love you and I dedicate this thesis to you. You have both taught me the value of hard work and I have seen how much you both have sacrificed to provide us with a better life. There is no way to repay that to you both and I am forever thankful and indebted to you both.

To Pascale, thank you for always listening to me talk about research no matter what time of day or night. Your patience has been a blessing and I love you for it. I am always grateful for you letting me do "just one more experiment". Thank you for always reminding me to spend time outside of the lab, introducing me to ultimate and always being there for me when I needed it most.

Lastly, to my lab mates and friends, thank you for making the lab such a fun place to work. Ben, Jill, Céd and John – you guys are truly special people and none of this work would be possible without you guys. Here is to all the late nights and weekends we have spent together in the lab!

Chapter 1

General Introduction.

1.1. The Ste20-like Kinase.

1.1.1. The Ste20 family of kinases.

There are over 500 different protein kinases in mammals that can be divided into four major categories: receptor tyrosine kinases, non-receptor tyrosine kinases, receptor serine/threonine kinases, and non-receptor serine/threonine kinases (1-6). Most protein kinases have a highly conserved catalytic domain which may reflect their evolution from a common precursor (7,8). The Ste20 family of non-receptor serine/threonine protein kinases represent one important subset of kinases involved in cellular proliferation, migration and terminal differentiation (9,10). The Ste20 kinase archetype is an important signaling molecule that has been well studied in yeast as a regulator of a mitogen-activated protein kinase- (MAPK-) dependent pathway involved in the control of the mating response (11).

In studying yeast Ste20, a group of similar Ste20-like kinases was identified in mammals due to their high degree of homology (12). These kinases can be subdivided into three major families based on their structure: p21-activated kinases (PAKs), pleckstrin-homology domain-containing PAKs (PH-PAKs) and germinal centre kinases (GCKs) (12).

1.1.2. Identification, structure and activation of the Ste20-like kinase.

The mammalian Ste20-like kinase (SLK) was first isolated from guinea pig liver, followed by the successful cloning of the mouse and human homologs (13-15). Mammalian SLK was first identified and characterized as a caspase 3-activated kinase which played a role in the induction of apoptosis (14,16-18). SLK was shown to be ubiquitously expressed in adult tissues and cell lines and predominantly expressed in the muscular and neuronal lineages of the developing embryo (14,19). SLK is classified as a GCK-related kinase and is comprised of an N-terminal Ste20 catalytic domain (amino acids 1-338), central coiled regions (amino

acids 339-788 and 825-1180) and a C-terminal AT1-46 homology (ATH) domain (amino acids 867-1178) (Figure 1.1.) (14,16,20-22).

The N-terminal catalytic domain is most similar to lymphocyte-oriented kinase (LOK) and mammalian ste20-like kinase 1 (MST1) in sequence homology with the characteristic Ste20 kinase domain motif (TPYWMAPE) located in subdomain VIII at amino acid position 193 (23). SLK contains an activation segment characterized by a DFG motif at the beginning of the region and an αEF/αF loop at the end (23). The activation segment of SLK has been shown to contain short helices located at the C-terminal end of the DFG motif (23). Activation loop phosphorylation of SLK has been mapped to T183 and S189 within subdomains VII and VIII, respectively (23,24). Phosphorylation of these two residues is required for maximal autoactivation (23,24). A putative caspase 3 cleavage site (DXXD) is also contained within the central coiled domain and is loosely conserved in several other species (16). Additionally, a putative consensus src homology 3 (SH3) binding site (PXXPX) is located at end of the coiled domain, although it is not entirely well conserved among species (16,25).

A number of protein kinases are regulated by autophosphorylation on at least one key residue in the activation segment, usually contained within the kinase domain of the protein (26). Autophosphorylation sites on SLK have been mapped to T183 and S189 through electron density map analysis obtained by mass spectrometry, however neither site appeared to be completely phosphorylated (23). Phosphorylation of residues T183 and S189 are the most important post-translational modifications required for the activation of SLK. Catalytic activity of an SLK^{T183A} mutant drops by 60% while an SLK^{S189A} or $SLK^{T183A/S189A}$ mutant showed an 80% reduction further supporting the requirement of these sites for maximal SLK activity (24). Although autophosphorylation of these residues enhances SLK activity, they may also be targets for other protein kinases. For kinases that require priming phosphorylation for

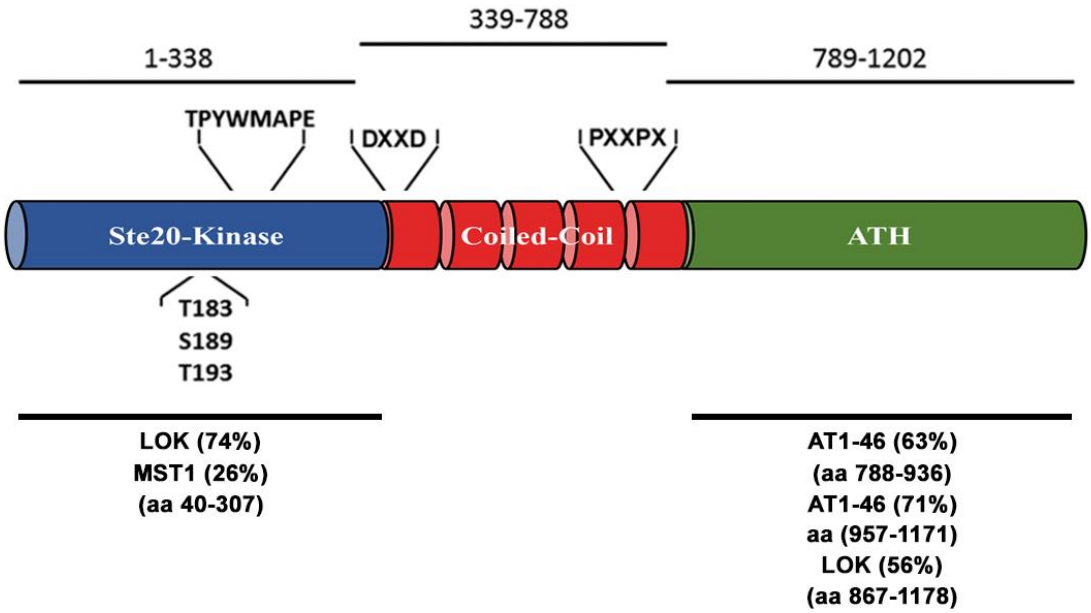

Figure 1.1. SLK structure and homologies. Schematic representation of murine SLK structure showing the Ste20 catalytic kinase domain at the N-terminus and the AT1-46 homology region at the C-terminus. Amino acid numbering is provided. The percentage homology for SLK to the related kinases within each domain are shown in parentheses. The Ste20 signature sequence (TPYWMAPE), the consensus caspase cleavage site (DXXD) and a putative SH3-binding domain are shown (PXXPX). Figure was adapted from (27).

maximal activation, the phosphate group often confers a conformational change within the activation segment that promotes or enhances substrate binding, compared to the non-phosphorylated activation segment which remains unstructured (28,29). As both T183 and S189 are never fully phosphorylated, it is possible that they are phosphorylated in a primary and secondary manner. The role of the secondary phosphorylation site has been suggested to be involved in substrate recruitment after the first phosphorylation event has stabilized the activation segment (30). Emphasizing the importance of T183 in SLK activation, this residue is a highly conserved phosphorylation site across diverse groups of protein kinases in addition to the Ste20 family (23).

The mechanism of SLK activation has not been fully elucidated and is under ongoing investigation. However, it has been demonstrated that SLK is able to homodimerize in a *trans* orientation and autophosphorylate (23). Supporting the critical role for homodimerization in SLK activation, an SLK^{Q185P} mutant which exists as a monomer in solution is unable to autophosphorylate (23). The C-terminus of SLK contains a coiled-coil region which may facilitate homodimerization by allowing the catalytic core to come into proximity of the activation segment on the *trans* molecule and phosphorylate it (21). The consensus target sequence of SLK appears to differ from its activation segment sequence, but SLK is still able to recognize and phosphorylate both (23).

The GCK-related kinases have been shown to contain a C-terminal autoregulatory region (31,32). It was then hypothesized that the ATH domain played a critical role in regulating SLK activity. Indeed, a truncation deleting the C-terminal two-thirds of the ATH domain ($SLK^{\Delta 950\text{-}1202}$) dramatically increases SLK kinase activity (16). Furthermore, an SLK truncation only expressing the kinase domain ($SLK^{1\text{-}373}$) has a 10-fold increase in kinase activity, suggesting that SLK activity may be regulated by multiple domains (16).

Interestingly, expression of part of the central coiled domain in addition to the kinase domain (SLK^{1-592}) has no effect on activity when compared to the full-length kinase (15). Likewise, our lab has shown that an SLK^{1-551} construct results in a reduction in kinase activity when compared to the SLK^{1-373} truncation supporting that an important region required for the regulation of SLK activity lies within amino acids 373 and 592 (16). These findings suggest that SLK is under complex regulation and that additional studies are required to fully understand the role of its various domains.

1.1.3. The role of SLK in apoptosis, cell cycle progression, migration and EMT.

SLK was initially identified as a mediator of apoptosis (14). Stable overexpression of SLK in myoblasts was sufficient to induce apoptosis through a JNK1-dependent pathway (14), consistent with the function of the Ste20 kinase homolog in the helminth parasite *Schistosoma mansoni* (14,33). Interestingly, expression of the full-length kinase inactive SLK mutant (SLK^{K63R}) was also sufficient to induce an apoptotic response, albeit significantly delayed compared to full-length SLK, implying that perhaps SLK can induce an apoptotic response in a kinase independent manner (14). Preceding apoptosis, SLK or SLK^{1-373} overexpression caused the dissolution of actin stress fibers, the distribution of actin to the cell periphery, membrane blebbing and loss of substrate adhesion (16). Additionally, incubation of recombinant SLK with either apoptotic lysate or purified caspase 3 resulted in cleavage of the active kinase and ATH domains (16). Cleavage and release of the active SLK fragment was also observed in response to apoptotic stimuli *in vitro* including c-myc overexpression, exposure to UV radiation or treatment with TNF-α (16). Together these results support a mechanism whereby an active fragment of SLK is released by caspase 3 during apoptosis and may mediate part of the apoptotic response. These *in vitro* findings were further corroborated in a renal ischemia-reperfusion injury model. SLK activity was shown to attenuate the ER

stress response, facilitate cytochrome C release and induce p38 activity through ASK1 (17). SLK overexpression in glomerular epithelial cells stimulated p53 transactivational activity through the JNK pathway (18). Consistently, overexpression of SLK in kidney glomerular podocytes resulted in injury and loss of this cell layer, accompanied by an increase in p38 activity (34). The multifaceted role of SLK in mediating the apoptotic response suggests that it may play a role in apoptosis-dependent physiological processes such as development and tumorigenesis (Figure 1.2.).

Initial characterization of SLK focused on the apoptotic response. However, the presence of active SLK in healthy exponentially dividing cells suggested that its function was much more complex. In search for an upstream activator of PLK1, SLK emerged as a candidate due to its high homology to the Xenopus polo-like kinase kinase 1 (xPLKK1) (35). PLK1 was identified as a novel substrate of SLK, which phosphorylates and activates PLK1 during the G2/M transition (35). Consistent with these observations, SLK kinase activity is highest during this phase of the cell cycle and overexpression of a dominant negative SLK^{K63R} arrests fibroblasts in G2/M (35,36). Supporting this, SLK was shown to be required for radial microtubule organization during interphase as depletion of SLK resulted in the inability of centrosomes to anchor or cap microtubules (20). Together, these data support a role for SLK in regulating the microtubule network during interphase allowing for efficient entry into mitosis and cell cycle progression (Figure 1.2.).

As SLK has been shown to associate with and regulate the microtubule and actin networks, its role in cellular migration was explored. Actin fibers are anchored at focal adhesions through protein complexes composed of integrins, focal adhesion kinase (FAK), src, vinculin and paxillin (37-39). In response to cell adhesion or migration stimuli, cells assemble focal adhesion complexes which recruit numerous other adaptor proteins that ultimately

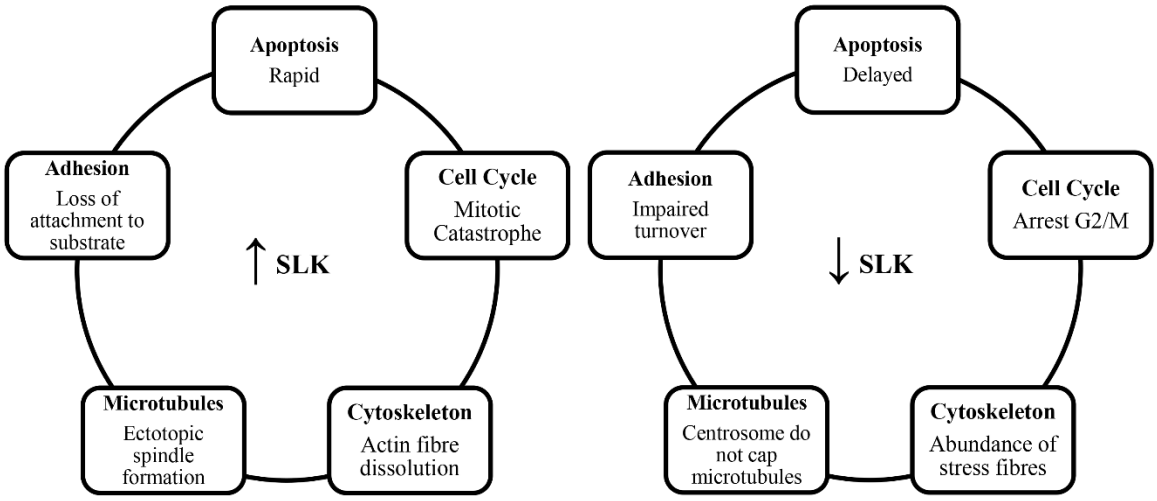

Figure 1.2. Summary of SLK functions in untransformed cell lines. Studies have shown that high levels of SLK activity induce apoptosis, loss of actin stress fibres, retraction from the substratum and ectopic spindle formation. Conversely, knockdown experiments or expression of a kinase inactive SLK construct results in delayed cell death, cell cycle arrest and inhibition of cellular migration. Together, these data suggest a role for SLK in multiple cellular processes. Whether the role of SLK is restricted to cytoskeletal remodelling in all cases remains to be verified. Figure was adapted from (27).

regulate focal adhesion turnover and cellular migration (Figure 1.3.) (38,39). Following fibronectin stimulation, SLK was found to colocalize with vinculin at large podosome-like adhesions (40). SLK knockdown resulted in an increase in the size and density of vinculin-positive adhesions, indicative of stable focal adhesions in non-migrating cells (41). Consistent with this role for SLK in focal adhesion turnover and cell migration, SLK kinase activity is highest in cells induced to migrate by scratch wounding when compared to non-motile cells (41,42). SLK activation was found to be dependent on c-src and the MAPK pathways as pre-treatment with either PP2 or U0126 inhibitors abrogated kinase activation following scratch wounding (41). Additionally, expression of the src family kinases was required for the recruitment of SLK to the leading edge and focal adhesions of actively migrating cells (41). Cellular migration across a substrate is dependent on the formation of a functional FAK/src complex initiated by autophosphorylation of FAK at Y397, focal adhesion assembly, turnover and movement along the substrate (41-47). Interestingly, nocodazole treatment of fibroblasts results in microtubule depolymerization and focal adhesion stabilization with high levels of pFAK Y397 (48). After stabilization of the focal adhesions, removal of nocodazole is followed by microtubule regrowth and cyclic changes in the levels of pFAK Y397 (48). SLK depletion in fibroblasts impairs the turnover of focal adhesions induced by nocodazole wash-out experiments, as measured by a sustained high level of pFAK Y397 and enlarged vinculin-positive adhesions (41). Lastly, our lab has shown that activated SLK regulates FAK-dependent focal adhesion turnover by phosphorylating paxillin at serine 250 (49). As such, expression of a paxillin^{S250T} mutant stabilized the levels of pFAK Y397, vinculin-positive adhesions and impaired cellular migration (49). Together, this body of work suggests that SLK is part of a microtubule-associated complex that targets focal adhesions for disassembly and therefore is a critical regulator of cellular migration (Figure 1.3.) (50,51).

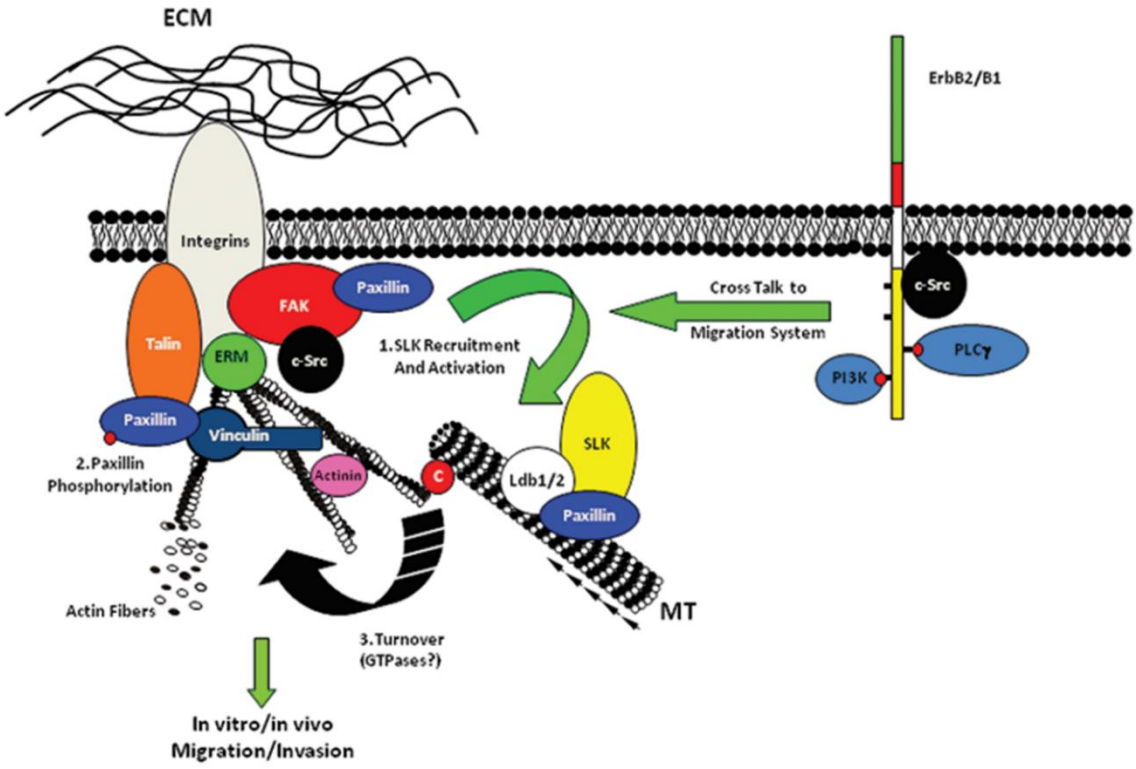

Figure 1.3. Integrating SLK signaling through HER2/ErbB2/Neu with the migratory network. Upon integrin engagement, the FAK/src complex is activated and focal contacts are assembled while SLK is held in an inactive conformation. Further signaling activates SLK through the microtubule network, along the actin stress fibers. SLK can phosphorylate paxillin near the focal adhesions to induce focal adhesion disassembly and turnover. Alternatively, microtubule-bound paxillin could be phosphorylated and recruited to newly formed adhesions and induce destabilization. Stimulation of growth factor receptors such as ErbB2 can also activate SLK through receptor-integrin cross talk. Figure was adapted from (27).

Consistent with the role for SLK in regulating cytoskeletal dynamics in the control of cell cycle and migration, our lab has shown that SLK is required for the cytoskeletal remodelling necessary to induce an efficient TGFβ-mediated epithelial-to-mesenchymal transition (EMT) (52). SLK knockdown delayed the breakdown of both ZO-1- and E-cadherin-positive epithelial junctions following TGFβ treatment suggesting that SLK loss results in a sustained epithelial phenotype (52). SLK knockdown was also shown to increase the expression of E-cadherin and decrease the expression of vimentin in human glioma cell lines, further supporting its role in maintaining an epithelial phenotype (53). Additionally, expression of the dominant negative SLK^{K63R} did not have the same effect as an SLK knockdown on blocking TGFβ-mediated EMT, demonstrating that this effect may be due to a scaffolding function of SLK independent of kinase activity (52). Overall SLK has been shown to be required for TGFβ-induced cytoskeletal changes and not the direct genetic program associated with EMT in both mammary and glioma cell lines (52,53).

1.2. An Overview of the Molecular Subtypes of Breast Cancer.

Breast cancer is the most common cancer in women, accounting for approximately 25% of all reported carcinomas worldwide (54). However, the molecular basis for the various breast cancer subtypes is not fully understood and the vast heterogeneity that exists within each tumor makes treatment an even more difficult task.

Breast cancer subtypes are most commonly classified based on the expression of the Estrogen Receptor (ESR1), Progesterone Receptor (PGR) and/or the Human Epidermal Growth Factor Receptor-2 (HER2) (55-58). ESR1 and PGR-positive breast cancers make up the Luminal A (Ki67-negative) and Luminal B (Ki67-positive) subtypes (55-58). The Luminal A and B subtypes are the most common, accounting for approximately 65% of all breast cancer cases (57). The Luminal subtypes tend to have the best prognostic outcome of all subtypes and

these tumors generally respond well to hormone therapy (59). The HER2-positive subtype is characterized by overexpression and amplification of HER2 with a prevalence of approximately 25-30% and a poor prognosis due to its association with highly metastatic breast cancers (57,60-62). The monoclonal antibody, trastuzumab (Herceptin), in combination with chemotherapy is currently the best form of treatment for HER2-positive breast cancers (63). Lastly, the triple-negative breast cancers (TNBCs) are defined by those that do not express HER2, ESR1 or PGR (58). TNBCs account for approximately 10% of all cases and have the worst prognosis and survival rates, as major therapeutic targets have not yet been identified for this subtype (57). This lack of biomarkers and/or drivers for this subtype makes them difficult to treat effectively and chemotherapy remains the standard of care treatment for TNBC (64-66).

1.3. HER2-positive Breast Cancer.

1.3.1. The HER2/Neu oncogene.

HER2/Neu/ErbB2 (HER2 in human; Neu in rat; ErbB2 in mouse) is an orphan transmembrane receptor belonging to the epidermal growth factor receptor (EGFR) family, along with EGFR (HER1), HER3 and HER4 (67). HER2 contains an extracellular domain composed of two ligand binding regions and two cysteine-rich regions, a short transmembrane domain, an intracellular catalytic tyrosine kinase domain and a carboxy terminal tail (68). HER2 can complex with HER1, HER3 and HER4, which are receptors for a variety of ligands including epidermal growth factor (EGF) and heregulin (HRG) (69). As an orphan receptor, HER2 does not have a known extracellular ligand and is therefore activated by forming complexes with the other HER proteins (70). Heterodimerization and subsequent activation of the intracellular kinase domain of HER2 is initiated by transphosphorylation of specific tyrosine residues within the cytoplasmic tail (71). Distinct docking proteins target these

phosphorylated residues and link activated HER2 to the Ras/MAPK-, PI3K- and src-signaling pathways (72,73). Under normal conditions these signaling cascades activate proliferative, apoptotic and survival pathways (72,73).

HER2 is an oncoprotein that is overexpressed in approximately 25-30% of human breast cancers (61,62). Patients whose tumors overexpress HER2 receptors present with a more metastatic and invasive disease with a poorer prognosis (61). Overexpression in breast cancer results in 40-100 fold increase in the HER2 receptor at the tumor cell surface (74). HER2 signaling follows a strict hierarchy, with HER2 being the preferred dimerization partner of EGFR, HER3 and HER4 (75). Therefore, the overexpression of HER2 observed in human breast cancers is sufficient to increase HER2-containing dimers despite the lack of a specific ligand (68). Evidence suggests that HER2-containing dimers have prolonged signaling and can escape normal feedback inhibition mechanisms. Following ligand binding and activation of the HER family, these molecules undergo either endocytic degradation (EGFR) or recycling (HER2, HER3 and HER4) to dampen their activity and prevent constitutive signaling (76). HER2 overexpression can dampen this feedback mechanism by preferentially dimerizing with EGFR and allowing the dimer to evade endocytic degradation, subsequently increasing the signal potency and duration (77,78).

Large scale sequencing efforts have uncovered rare somatic mutations within the HER2 kinase domain in human breast cancers. However, very little is known about the biological significance of these mutations (79). Despite the lack of somatic mutations in HER2, polymorphisms within the transmembrane domain have been discovered. The I655V allele, for example, results in the expression of a HER2 variant with a greater capacity for dimerization and downstream signaling (80). However, the association of this variant allele with breast cancer risk has been disputed in the literature with most studies reporting no

significant increase in the likelihood of developing breast cancer (81-83). Therefore, it is likely that the HER2-positive breast cancer subtype is driven by gene amplification and not mutational activation of HER2.

The oncogenic and transforming potential of both HER2 and Neu have been extensively characterized. Although both possess oncogenic potential, there are several significant differences between the human and rodent proteins. Overexpression of HER2 is sufficient to transform and induce tumorigenic growth in NIH3T3 fibroblasts (84,85). HER2 overexpression in the human luminal A breast cancer cell line, MCF-7, increased both estrogen-dependent and tamoxifen-resistant tumor growth in ovariectomized athymic nude mice (86). Lastly, HER2 was sufficient to reinitiate cellular proliferation in growth arrested mammary acini grown in three-dimensional basement membrane gels (87). Additionally, these mammary acini retained their basement membrane and lost their luminal cavity when transduced with HER2 homodimers, reminiscent of early stage mammary tumors (87). Unlike the human HER2, overexpression of the normal rat *c-neu* allele is not sufficient induce cellular transformation and the oncogenic potential of Neu requires a point mutation within the transmembrane domain (88). The point mutation results in a V664E mutated protein termed NeuNT (88). This mutation has been shown to enhance receptor homo- and heterodimerization and increases tyrosine kinase activity, significantly enhancing signaling downstream of Neu (89). Despite these differences, both human HER2 and the rat homolog Neu are potent oncogenes capable for transforming cells and driving tumorigenic growth.

1.3.2. Transgenic models of HER2/Neu-induced mammary tumorigenesis.

To date, numerous animal models have been established to confirm the oncogenic role of HER2/Neu. Among these, the most common involve the expression of *neu* (or an activating *neu* mutation) driven by the mouse mammary tumor virus (MMTV) promoter (90,91). The

MMTV promoter primarily drives gene expression in the luminal epithelial compartment starting at embryonic day 8.5 (90,92). Leaky expression from the MMTV promoter is observed in the salivary glands and in the testes of male mice, although to a significantly lower extent than in the mammary gland (90).

Initially, the constitutively active *neuNT* was driven from the MMTV promoter and transgenic females developed tumors involving the entire mammary gland by approximately 90 days of age (90). One caveat to this system is that HER2 is often overexpressed but not mutated in human breast cancers (79). Therefore, the role of *c-neu* in driving mammary tumor growth was assessed. Compared to the activated *neuNT*, MMTV-*c-neu* mice formed tumors with approximately twice the latency despite expressing similar levels of the oncogene (60). Interestingly, approximately 65% of these *c-neu* tumors arose from strains carrying somatic mutations within the transgene (93). Most of these mutations were in-frame, 5-12 amino acid deletions immediately upstream of the transmembrane domain (93). Additionally, these in-frame deletions showed an increased transformation potential *in vitro*, compared to wildtype Neu (93). Given that most of these tumors bear activating mutations, they likely represent a rate-limiting step in tumor initiation in the MMTV-*c-neu* model (93,94).

The observation that most MMTV-*c-neu* derived tumors arise from somatic in-frame deletion mutations has led to the generation of the most widely used MMTV-Neu transgenic model, the *neu* deletion (NDL) mutant (93,94). The MMTV-NDL2-5 transgenic line expresses a *neu* mutant harboring a deletion of five amino acids immediately upstream of the transmembrane domain adjacent to a C655W substitution, a critical cysteine residue for disulfide bonding (94). These mutations result in the constitutive activation of Neu, with an average mammary tumor onset of 161 days (94). A high proportion of tumors from the

MMTV-NDL2-5 transgenics resembled mammary adenocarcinomas and metastasized to the lungs (94).

The role of various proteins in HER2/Neu-driven breast cancer progression can be studied using global knockout models crossed into the MMTV-NDL2-5 transgenic background. However, this does not allow for the study of genes in which the global knockout model is lethal. To study the role of genes in regulating HER2/Neu-positive breast cancers in a mammary specific conditional knockout model, the MMTV-NDL2-5-IRES-Cre (NIC) model was established (95). The NIC model expresses the constitutively active Neu oncogene linked to Cre recombinase by an internal ribosomal entry sequence which effectively couples oncogene expression to Cre mediated recombination (95). This allows for the coupling of Neu expression to Cre and precludes the possibility of obtaining a Neu-positive tumor cell that escapes Cre-mediated recombination (95). Additionally, these tumors form mammary adenocarcinomas that histologically resemble human HER2-positive tumors (90,95).

Together, these transgenic models have significantly advanced the study of HER2-positive breast cancer initiation, progression, metastasis and chemotherapeutic resistance *in vivo* and serve as a powerful tool to further our understanding of this disease.

1.3.3. Current HER2-targeted therapies and clinical implications.

Initial studies into the identification of specific HER2-targeted therapies yielded murine antibodies against a cell surface domain of Neu that could inhibit the tumorigenic growth of Neu-transformed NIH3T3 fibroblasts *in vivo* (96). Following these studies a humanized monoclonal antibody, trastuzumab, which targets extracellular domain IV of HER2 was shown to inhibit proliferation of HER2-positive cell lines and enhance the antitumor function of other chemotherapeutic agents in xenograft models (97). Trastuzumab use for the treatment of HER2-positive breast cancers has led to significant reductions in relative risk of

death (20%), rate of recurrence (24%) and increased disease-free survival (48%) (98-101). Despite the clinical success, less than 35% of patients respond to an initial treatment and approximately 70% of patients who initially respond develop tumor progression and metastatic disease within a year of treatment (63,102). Additionally, trastuzumab cannot cross the blood-brain barrier and approximately 35% of treated patients eventually develop brain metastases (103).

Pertuzumab (Perjeta) is a second generation humanized monoclonal antibody targeted against HER2 (104). Pertuzumab binds directly to extracellular domain II of HER2, which is required for dimerization with HER3 (104,105). Therefore, pertuzumab treatment dampens the activation and downstream signaling of HER2 and inhibits breast cancer xenograft growth *in vivo* (106,107). When used in combination with trastuzumab, pertuzumab significantly improved patient outcome and overall survival in several clinical trials (108,109).

In addition to preventing HER2 dimerization, trastuzumab and pertuzumab can induce antibody-dependent cell-mediated cytotoxicity or phagocytosis both *in vitro* and *in vivo* (110,111). The Fc-portion of the HER2 antibodies have been shown to activate both natural killer cells and macrophages by binding to FC-receptors and ultimately leading to tumor cell destruction (110,111). Margetuximab (MGAH22), an Fc-optimised antibody targeting the same extracellular domain of HER2 as trastuzumab, was generated to improve the effector cell function of these antibodies (112).

Although numerous clinical trials have shown promise with HER2-targeted antibody therapies, many patients remain refractory to treatment (102). Developing a better understanding of the intracellular signaling downstream of HER2 may allow for the identification of novel therapeutic targets to overcome some of the shortcomings associated

with current treatments, potentially enhancing the efficacy of current anti-HER2 based therapies.

1.3.4. Implicating SLK in HER2/Neu-induced migration and chemotaxis.

HER2-induced transformation and invasion requires FAK (113) and our lab has shown that SLK is required for regulating focal adhesion dynamics downstream of FAK signaling (41). As such, a role for SLK in mediating chemotaxis and invasion of mammary cells expressing the HER2 oncogene was uncovered (114). Breast cancer cell lines expressing high levels of HER2 have been shown to express higher levels of SLK (114). Similarily, overexpression of the constitutively active NeuNT mutant is sufficient to increase SLK activity in cell lines with low basal levels of HER2 (114). Expression of SLK^{K63R} reduced heregulin-induced migration and chemotaxis in MCF-7, MDA-MD-231 and SkBr3 cell lines (114). Blockade of the MAPK and src family kinase pathways attenuates HER2-mediated SLK activation (114), consistent with their ability to attenuate SLK-mediated cellular migration (41). HER2 autophosphorylation on tyrosine 1201 and 1226/7 has been shown to couple HER2 to its downstream signaling cascades (115). The presence of either of these two autophosphorylation sites, in an otherwise phosphorylation-deficient Neu mutant (Neu^{NYPD}), is sufficient to activate SLK downstream of heregulin stimulation (114). Inhibition of PLCγ or PI3K inhibited SLK activation downstream of tyrosine 1201 and 1226/7, respectively (114). Overexpression of NeuNT in $FAK^{-/-}$ fibroblasts could not induce SLK activation following heregulin stimulation, suggesting that FAK is required in this process (114). Additionally, SLK was not activated following heregulin stimulation following treatment with the src inhibitor, PP2, or in fibroblasts missing the src-family of kinases (114). Although the role of SLK activation downstream of HER2 is not fully understood (Figure 1.3.), SLK presents itself as a potential therapeutic target in HER2-positive breast cancers. Specific inhibition of SLK may delay the

progression of HER2-positive tumors and may achieve favorable responses in a combinatorial therapeutic approach.

1.4. PI3K/AKT Signaling Downstream of HER2/Neu.

1.4.1. HER2/Neu signaling activates PI3K.

The importance of the HER2-PI3K pathway in breast cancer signaling cannot be overstated. The HER2-PI3K pathway is the most frequently altered oncogenic pathway across all cancer subtypes and its activation is responsible for tumor growth, drug resistance and metastasis (116). Heterodimerization with other HER proteins and subsequent activation of HER2 results in the transphosphorylation of specific tyrosine residues within the cytoplasmic tail of these receptors (71). Phosphorylated tyrosine residues on the HER proteins are recognized by SH2-containing proteins which bind and serve as adaptor molecules recruiting downstream signaling to the plasma membrane (71). Recruitment and activation of PI3K to active HER2-containing dimers is perhaps the most important downstream signal required for oncogenesis (68). PI3K is specifically recruited to HER2/HER3 heterodimers (Figure 1.4.) and HER3 is required for HER2-induced cellular transformation (117,118). HER3 contains seven putative phosphotyrosine binding motifs for PI3K whereas HER2 does not contain any, highlighting the importance of the HER2/HER3 heterodimer in recruiting and activating PI3K (119,120).

Once activated, PI3K phosphorylates the 3-hydroxyl group of the inositol ring of phosphatidylinositol (PtdIns) lipid substrates (121). Phosphorylation of these PtdIns modulate signaling downstream of PI3K by directly binding and localizing effector proteins at the plasma membrane (Figure 1.4.) (122). Effector proteins downstream of PI3K, including PDK1 and AKT, are recruited to the cell membrane and bind to the 3-phospho-inositides through their pleckstrin-homology (PH) domain (123).

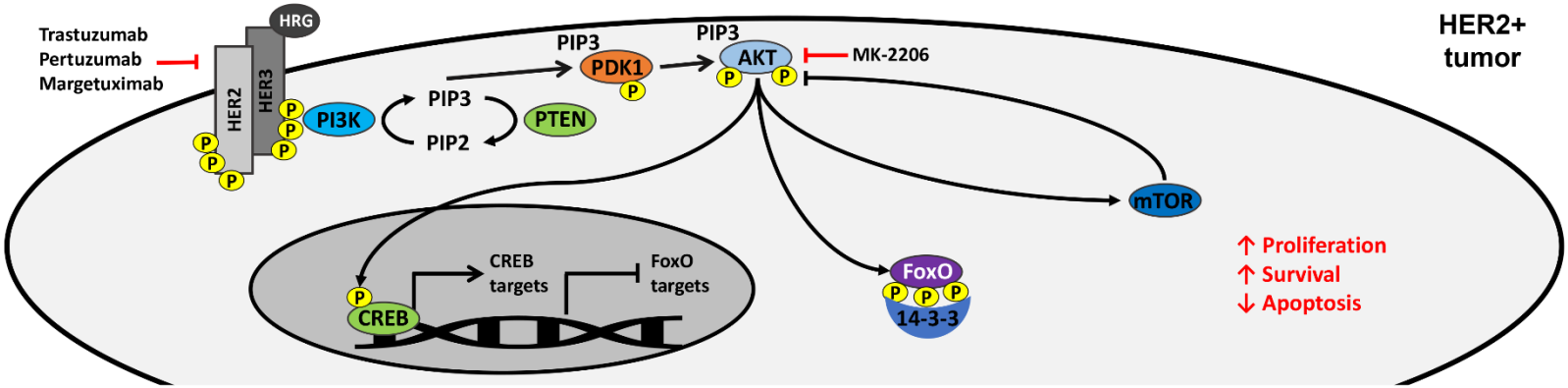

Figure 1.4. AKT signaling is activated downstream of HER2/Neu. Ligand binding to the HER family of receptors induces a conformational change and subsequent homo- or heterodimerization. Receptor dimerization results in activation and tyrosine phosphorylation of the intracellular tail providing a docking site for SH2-domain containing proteins. PI3K is recruited to the activated HER2/HER3 complex and phosphorylates phosphatidylinositol lipid substrates at the plasma membrane. These 2- or 3-phospho-inositides (PIP2 or PIP3, respectively) are bound by PH domaining containing proteins, including PDK1 and AKT. Binding of PDK1 and AKT to PIP3 relieves the autoinhibitory PH domain and allows for maximal activation of these kinases. PDK1 directly phosphorylates AKT at threonine 308 resulting in the activation of AKT. AKT activates the mammalian target or rapamycin (mTOR), which can feedback to inhibit AKT signaling. AKT directly controls transcription through phosphorylation of FoxO and CREB. Phosphorylation of FoxO results in its cytoplasmic sequestration through binding to 14-3-3 proteins while phosphorylation of CREB allows for maximal DNA binding and transcriptional cofactor recruitment. As such, AKT controls the transcription of pro-proliferative, pro-survival and anti-apoptotic genes downstream of the HER2/Neu oncogene.

Phosphorylation and generation of 3-phospho-inositides is a relatively fast process. These lipid species are rapidly dephosphorylated to prevent constitutive signaling through PI3K (124). One of the major phosphatases to catalyze this process and antagonize PI3K signaling is the tumor suppressor, PTEN (125). PTEN is frequently inactivated in cancers, especially Herceptin-resistant breast tumors, leading to sustained activation of PI3K and a more aggressive phenotype (126).

1.4.2. AKT is activated downstream of PI3K.

AKT is a serine and threonine protein kinase which is activated downstream of PI3K in virtually all tissues and cell lines (127). Ultimately, inactive AKT is recruited to the plasma membrane and binds to 2- or 3-phospho-inositides via its PH domain and is anchored in an open conformation (127). Activation of the PI3K signaling cascade results in the phosphorylation of two critical residues on AKT (128). The first residue, T308, is located within the activation segment of the kinase domain and the second residue, S473, is located within the C-terminal hydrophobic regulatory region (128). Fully phosphorylated AKT at the cell membrane is relatively short-lived. Activated AKT can generally be found intracellularly and can phosphorylate substrates for up to two hours post-stimulation (129,130). This suggests that once phosphorylated, AKT can dissociate from 3-phospho-insoitides and remain in an active conformation within the cytoplasm to phosphorylate its wide range of targets (129,131).

The major upstream kinase for AKT phosphorylation on T308 is the phosphoinositide-dependent-protein kinase 1 (PDK1) (132). Localization and binding of both PDK1 and AKT to 3-phospho-inositides at the plasma membrane induces conformational changes allowing PDK1 to phosphorylate AKT at T308 (Figure 1.4.) (130). In the inactive cytoplasmic conformation, the PH domain of AKT is inhibitory and overlaps the catalytic kinase domain

and prevents phosphorylation at T308 (130). Binding of the PH domain to 3-phospho-inositides removes this inhibition and releases the kinase domain for activation by PDK1 (130).

Phosphorylation of AKT at S473 is required for maximal activation and the primary kinase for the phosphorylation of this site is the mammalian target of rapamycin (mTOR) complex 2 (mTORC2) (133). As with PDK1 and AKT, mTORC2 is localized to the plasma membrane and binds to 3-phospho-inositides via a PH domain in the SIN1 component of the complex (134). This binding relieves the autoinhibition of mTOR kinase activity and allows for phosphorylation of AKT. While AKT phosphorylated solely at T308 has basal kinase activity, phosphorylation at S473 stabilizes the T308 phosphorylation and greatly enhances AKT activity (128).

Direct signaling through PDK1 and AKT is terminated by either lipid phosphatases, such as PTEN, which dephosphorylates membrane 3-phospho-inositides and prevents further membrane accumulation of AKT, or by protein phosphatases which directly inactivate AKT (125,127). Dephosphorylation of T308 is mainly catalyzed by protein phosphatase 2A (PP2A) whereas the PH domain leucine-rich repeat protein phosphatases (PHLPP1 and PHLPP2) are responsible for dephosphorylation of S473 (135,136).

In addition to inhibition by lipid and protein phosphatases, numerous feedback mechanisms exist to dampen the PI3K signaling axis (127). Amongst the most important of these feedback mechanisms is the effect of the downstream AKT effector, mTORC1 (Figure 1.4.). Treatment of cells with the mTORC1 inhibitor, rapamycin, enhances the responsiveness of AKT to insulin signaling, suggesting that mTORC1 is involved in dampening AKT signaling (137). Activation of mTORC1 results in the direct phosphorylation and degradation of the insulin receptor substrates which are responsible for scaffolding the insulin receptor to PI3K (138). Inhibition of mTORC1 also acutely activates EGFR, HER2, HER3 and HER4

which results in the membrane recruitment and activation of the PI3K-AKT signaling cascade (139).

1.4.3. AKT-mediated regulation of transcription – FoxO and CREB.

AKT directly phosphorylates numerous kinases, cell cycle regulators, E3 ubiquitin ligases, metabolic enzymes and transcription factors that control a multitude of diverse cellular processes (127,131). AKT phosphorylates serine or threonine residues within the consensus motif R-X-R-X-X-S/T-Φ (where X is any amino acid and Φ is a hydrophobic residue) (127). While AKT phosphorylates many targets, most notably glycogen synthase kinase 3 (GSK3α/β) and tuberous sclerosis complex 2 (TSC2), the phosphorylation of the Forkhead Box O (FoxO) family of transcription factors or cAMP response element-binding protein (CREB) are the predominant mechanisms by which AKT can directly regulate a transcriptional program (140-143).

Activation of AKT results in the translocation of FoxO proteins from the nucleus to the cytoplasm and a repression of their transcriptional program (142). AKT regulates the translocation and cytoplasmic retention of FoxO proteins through direct phosphorylation at three conserved residues (142). Phosphorylation of FoxO proteins at the N-terminus and within the nuclear localization signal creates a recognition sequence for the 14-3-3 phospho-binding proteins, which bind to and sequester FoxO in the cytoplasm (Figure 1.4.) (144). Therefore, AKT signaling suppresses the expression of FoxO target genes which have been shown to repress proliferation and growth or negatively feedback on the PI3K/AKT axis (145).

AKT activation has also been shown to directly phosphorylate CREB at serine 133 resulting in its activation (143). Upon activation, CREB recruits the CREB-binding protein (CBP) and together they activate a pro-survival and anti-apoptotic transcriptional program (Figure 1.4.) (146,147). Therefore, AKT has been shown to both repress (FoxO) and activate

(CREB) transcription factors through direct phosphorylation and promote the expression of proliferation, survival and anti-apoptotic genes.

1.4.4. AKT: mutational activation and therapies in breast cancer.

AKT is often hyperactivated in human cancers with most mutations affecting upstream effectors rather than AKT itself (148). These include amplification or somatic mutations in *EGFR*, *HER2*, *PDK1*, or *PIK3CA* or loss-of-heterozygosity and inactivating mutations in *PTEN* or *PHLPP* (127,148). The most common somatic activating mutation, occurring in approximately 2% of all breast cancers, is the AKT^{E17K} mutation (149). This mutation in the PH domain increases its affinity for 3-phospho-inositides, resulting in the accumulation and activation of membrane-bound AKT (149). The constitutive activation of AKT conferred by the E17K mutation results in hyperactivation of pro-growth and pro-survival pathways contributing to increased tumor proliferation and progression (131). Several phase I and II clinical trials utilizing allosteric or catalytic AKT inhibitors in breast cancer have been reported (150,151). The potent and orally bioavailable allosteric AKT inhibitor, MK-2206 (Figure 1.4.), which targets both the PH and catalytic kinase domains, induces cancer cell death and shows promising clinical outcomes when used in combination with either lapatinib or fulvestrant (150-152). Unlike catalytic inhibitors, these allosteric inhibitors target both the open and closed AKT conformations preventing membrane localization and maximal activation (152). Although MK-2206 has shown promise in clinical trials in combination with other chemotherapeutics, it has no effect as a single agent, suggesting that AKT blockade alone is not sufficient for the treatment of breast cancers (151).

1.5. An Emerging Role for Sox10 in Regulating Stem/Progenitor Activity in Development and Cancer.

1.5.1. The Sox family of proteins.

Sex-determining region Y (Sry) was the initial member of the Sry HMG-box (Sox) group of proteins and is critical for sex determination in males (153). The Sox proteins are a family of 20 transcription factors that share a similar high mobility group (HMG) domain (154). The HMG box, which is characteristic of the Sox proteins, contains two independent nuclear localization signals and one leucine-rich nuclear export signal which regulates the nucleocytoplasmic shuttling of these transcription factors (155). The Sox proteins can directly bind to DNA through their HMG box at a consensus motif of 5'-(A/T)(A/T)CAA(A/T)G-3' with the flanking sequences largely dictating specificity between different Sox proteins (156-158). Sox proteins have been shown to regulate transcription directly as bona fide transcription factors or indirectly through their ability to remodel chromatin (159,160).

There are nine groups of Sox genes in the mammalian genome: A, B1, B2 and C through H (154,161). Sox proteins within the same group share a greater than 80% sequence identity in their DNA-binding HMG domain (154,159,161). Additionally, Sox proteins within the same group tend to have overlapping functions and can at least partially compensate for one another (154,159). The Sox proteins have mainly been characterized based on their role in embryonic development. However, over the past decade, they have also been implicated in the prognosis and/or progression of a variety of diseases and cancers (154).

1.5.2. The SoxE family of transcription factors.

The SoxE family of proteins has three members: Sox8, Sox9 and Sox10 which share highly conserved dimerization, HMG, protein interaction (K2) and C-terminal transactivation domains (162,163). In addition to their role in sex determination, chondrogenesis and neural

development, the SoxE family has been shown to regulate tumor progression and stem/progenitor cell activity (164-169).

The first SoxE protein, Sox8, is probably the least characterized within this family. Sox8 tends to share a functional redundancy with Sox9 during development in the mammalian testis (170,171). Global deletion of Sox8 in mice results in a progressive spermatogenic failure and eventual infertility in males (172). Mutations within the *SOX8* locus in male patients have also been shown to contribute to male infertility and other reproductive anomalies (173). In addition to a role for Sox8 in male development, it has been postulated that Sox8 may have an oncogenic function in hepatocellular carcinoma and regulate cancer cell proliferation in concert with β-catenin (169).

Along with Sox8, Sox9 also plays a critical role during sexual development (171). Sox9 inhibits the generation of the female reproductive system by regulating the transcription of the anti-Müllerian hormone (AMH) in Sertoli cells (174). Additionally, Sox9 is the major target downstream of Sry during Sertoli cell differentiation and its expression is sufficient to rescue testis development in Sry-null XX gonads (175,176). Downregulation of Sox9 by deletion of a distal enhancer is also sufficient to induce sex reversal and female gonad development in male mice (177). Sox9 expression has been shown to be elevated in hepatocellular carcinoma and colorectal cancers where it correlates with a more aggressive phenotype (178,179). Sox2 signaling was shown to suppress Sox9 expression in lung cancer stem cells and loss of Sox2 results in a more differentiated and invasive phenotype through the induction of Sox9 (180). More recently, Sox9 has been validated as an ESR1-responsive gene that is sufficient to drive endocrine resistance, suggesting that it may be an interesting therapeutic target for luminal breast cancers (181).

Whereas Sox8 and Sox9 have primary functions in the development of the male reproductive system, Sox10 is involved in neural crest and peripheral nervous system development (163). In fact, Sox10 is the sole SoxE factor expressed in migrating neural crest cells and through their differentiation into glia, Schwann cells or neurons (163). The role of SoxE proteins in melanocyte development was first uncovered when the spontaneous mouse mutant Dominant megacolon phenotype (*Dom*) was linked to a single base pair insertion in the *Sox10* coding region (182,183). This truncation mutation ($Sox10^{Dom}$) serves as a model for Waardenburg-Shah syndrome type 4 (WS4) which is defined by sensorineural deafness, hypopigmentation and enteric aganglionosis (182,183). In cancer, Sox10 has predominantly been reported to enhance tumorigenesis, specifically in melanoma and basal-like breast tumors (165-167). However, in gastric cancers, it has been suggested that Sox10 has a tumor suppressive function (168).

1.5.3. Sox10 is a regulator of stem/progenitor cell activity.

As Sox10 is required for proper neural crest development and highly expressed in more aggressive human tumors (163,166), it is not surprising that a crucial role for Sox10 has been discovered in the regulation of stem/progenitor cell activity in neurons, melanocytes and mammary epithelium (164,184,185). In neurons, Sox10 is required in neural crest stem cells to maintain a multipotent state and restricts differentiation towards an oligodendrocyte lineage (185,186). While Sox10 also maintains the melanocyte stem cell population postnatally, it has also been shown to play a role in driving differentiation towards fully mature melanocytes (164). More recently, Sox10 has been shown to regulate the stem/progenitor population and mesenchymal state in mammary epithelial cells (184).

Transcriptomic analysis of fetal mammary stem cells (fMaSCs) revealed that Sox10 was among the most enriched transcription factors within this cell type (184). Within the fetal

mammary rudiment, Sox10 is often co-expressed with both cytokeratin 8 and 14 (a luminal and basal marker, respectively) in the same cell, suggesting the bipotent or stem-like nature of this lineage (184). Functionally, single Sox10-positive cells isolated from the mammary rudiment were able to form organoids in three-dimensional culture which architecturally resembled the mammary gland with both luminal and basal lineages present (184). In contrast, Sox10-negative cells were unable to efficiently form organoids (184). Sox10-positive basal cells were also able to repopulate a cleared mammary fat pad in limiting dilution experiments, whereas no successful transplantation was observed for the Sox10-negative population (184).

More recently, using ATAC-seq, binding motifs for the Sox family of proteins have been shown to be enriched in the open chromatin of fMaSCs (187). Intra-tumoral heterogeneity also directly relates to Sox10 levels in several murine mammary tumor models (187). Interestingly, *Sox10* expression within these tumors was found to correlate with the acquisition of a more de-differentiated, mesenchymal phenotype (187). Sox10 has been shown to directly bind to the promoter of genes involved in EMT, stem/progenitor maintenance and neural crest cell identity (187). Moreover, hemizygous expression of *Sox10* in a murine model of basal-like breast cancer was sufficient to significantly delay tumor progression and increase overall survival (187). In addition to the functional role of Sox10 in the mammary stem/progenitor population, Sox10 has been suggested to mark a triple-negative or basal-like subtype of breast cancer (166,167,184). Therefore, fully elucidating the mechanisms behind the induction and function of Sox10 may provide an interesting therapeutic window in the treatment of these breast cancers.

1.5.4. Regulation of Sox10 gene expression.

Sox10 has been shown to be required for numerous developmental processes and to enhance tumor growth and progression in various cancers. Although it regulates

stem/progenitor activity in melanocytes and mammary epithelial cells, the signaling that modulates the expression of Sox10 is largely unknown (188).

To dissect these signaling pathways, comparative sequence analyses identified 14 multiple-species conserved sequences (MCS) that control *Sox10* expression (189). Use of transgenic mice expressing *LacZ* under the control of these MCS sequences revealed two regions (MCS4 and MCS7) driving *LacZ* expression overlapping with endogenous *Sox10* expression (189). Both MCS4 and 7 contain dimeric SoxE binding sites that are required for functional enhancer activity of these sequences, suggesting that Sox10 can be regulated by either itself, Sox8 or Sox9 (189). Although some reports corroborate the findings that Sox9 can induce *Sox10* expression, some studies report that these two proteins repress each other's expression, suggesting that perhaps this regulation is context dependent (165,190,191).

Both MCS4 and MCS7 have been used to identify another direct transcriptional activator of Sox10. Peroxisome-proliferator-activated receptor-binding protein (PBP) was shown to bind directly at these enhancer regions in Notch4-immortalizaed luminal mammary epithelial cells and PBP knockout significantly decreased *Sox10* expression (192). PBP binds to the enhancer region of the *Sox10* promoter and recruits the mediator polypeptide transcriptional coactivator complex which is required for successful transcription initiation by RNA polymerase II (Figure 1.5.) (192,193).

Additional conservation between species can be observed within the first intron of *sox10* in zebrafish (194). Binding sites for Lef1, Sox9, Notch and β-catenin have all been identified in zebrafish and found to be conserved in mammalian species (194). Additionally, these four transcription factors have been shown to regulate reporter construct expression under the control of the intron 1 regulatory region in zebrafish models (194).

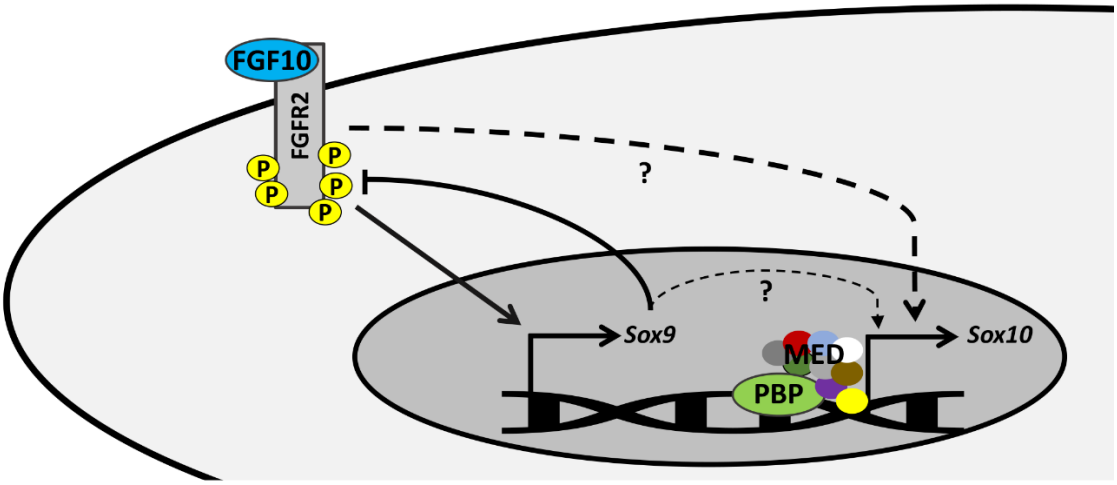

Figure 1.5. The mechanisms controlling Sox10 expression are largely unknown. Fibroblast growth factor (FGF) signaling, specifically through FGFR2, is sufficient to induce the expression of both *Sox9* and *Sox10*. However, whether the induction of *Sox9* precedes and subsequently activates *Sox10* expression remains to be determined. Sox9 is a direct transcriptional activator of genes that negatively feedback on the FGF signaling system. In addition to FGF signaling, peroxisome-proliferator-activated receptor-binding protein (PBP) was shown to bind directly to the *Sox10* enhancer Notch4-immortalizaed luminal mammary epithelial cells and induce *Sox10* expression. PBP binds to the enhancer region of the *Sox10* promoter and recruits the mediator polypeptide transcriptional coactivator complex (MED) which is required for successful transcription initiation by RNA polymerase II. Despite the critical role for Sox10 in neural crest development, cancer progression and stem/progenitor cell maintenance and function, the mechanisms regulating its expression have not been well characterized.

Lastly, fibroblast growth factor (FGF) signaling has been shown to regulate both the expression and function of Sox10 in ocular gland and mammary epithelial cells (184,191). Interestingly, both studies report a specificity for FGF10 in regulating *Sox10* expression through its specific receptor, FGFR2 (184,191). Conditional knockout of *Fgfr2* in the conjunctival epithelium was sufficient to abolish the expression of both *Sox9* and *Sox10* in these cells (191). Additionally, deletion of Sox9 in these cells reduced signaling through FGFR2 by downregulating the expression of several FGF-pathway target genes, suggesting that a feedback mechanism may exist between these two pathways (191). Inhibition of FGFR is also sufficient to reduce *Sox10* expression in both fMaSCs and luminal progenitor derived organoids and reduce their sphere-forming capacity (184). Despite this critical role for FGF signaling in regulating *Sox9* and *Sox10* expression (Figure 1.5.), the direct transcription factor(s) and/or mechanisms responsible have not yet been identified.

1.6. Thesis Objectives and Hypotheses.

Studies from our laboratory have demonstrated that SLK is ubiquitously expressed in adult tissues and highly expressed in embryonic stem cells and the muscular and neuronal lineages of the developing embryo (14,19,195,196). To investigate the role of SLK *in vivo*, we assessed the effect of an SLK-targeted gene trap on embryonic development. We hypothesized that global deletion of SLK would result in embryonic lethality with significant developmental defects in the myotome and neuronal compartments. Using this SLK-targeted gene trap, we observed that embryos develop normally to embryonic day 12.5 at which point they begin resorbing. We have attributed this defect to improper vascularization within the placentae of these embryos. Overall, we have concluded that decreased kinase activity during embryonic development is lethal and that a conditional knockout approach should be used to study the potential roles of SLK in adult tissues and disease.

Our lab has previously shown that SLK is activated downstream of Neu and is required for Neu-mediated cellular migration (114). Additionally, we and others have demonstrated that SLK is required for efficient epithelial-to-mesenchymal transition (52,53). To test these observations *in vivo*, our second objective was to cross a recently generated conditional SLK allele into a Neu-induced mammary tumor model. We hypothesized that conditional *Slk* deletion would significantly delay Neu-induced mammary tumor progression and increase overall survival in mice. Contrary to our hypothesis, we have observed that SLK deletion accelerates mammary tumor onset and increases mammary stem/progenitor activity through the induction of Sox10.

Sox10 contributes to mammary stem/progenitor function and has begun to gain attention as a potential biomarker of the triple-negative breast cancer subtype (166,167,184,197). As we observed the induction of Sox10 following SLK deletion in the context of Neu-expressing cell lines, our third objective was to confirm that Sox10 expression was highest in triple-negative breast cancer as compared to the Luminal A/B or HER2-positive subtypes. Therefore, we interrogated The Cancer Genome Atlas containing RNA-seq from 1246 invasive human breast cancer samples. We have confirmed that Sox10 expression is highest in the triple-negative subtype using gene-level quantification, correlated Sox10 expression with a more stem-like phenotype and validated the transcriptomic data by histochemistry.

Functional FGF signaling is required for both Sox10 expression and stem/progenitor activity in fetal mammary stem cells and epithelial organoids (184). However, the regulation of Sox10 expression in mammary epithelial tumors remains largely unknown. As Sox10 is highly expressed in triple-negative breast cancer and at least in part contributes to Neu-induced tumor growth following SLK deletion, our last objective was to further elucidate the

mechanisms that regulate the induction of Sox10 in mammary tumors. We have uncovered that Sox10 expression requires signaling through the PI3K/PDK1/AKT signaling axis downstream of Neu. Additionally, we have demonstrated that Sox9 acts as a direct transcriptional activator of Sox10 in SLK-deficient mammary tumor cells in an AKT dependent manner.

Chapter 2

Materials and Methods.

2.1. Animal Care.

2.1.1. Mouse Lines and Husbandry.

All mouse lines were bred and maintained on an FVB/N background. Initial C57 mice were backcrossed onto FVB/N mice (Jackson Laboratory) for at least two generations in house. DNA from these offspring were sent for advanced speed congenics genotyping to assess the FVB/N content using microsatellite analysis. Mice with the highest FVB/N contribution (>85%) were used in the first generation of experimental crosses. The BCO415 line (NIH Gene-trap Consortium) was established at the transgenics facility at McGill University. $SLK^{fl/fl}$ transgenic mice were generated as previously described (198). MMTV-Cre, MMTV-NeuNDL and MMTV-NIC transgenic mice were a kind gift from Dr. William Muller (McGill University). Rosa26R-LacZ reporter mice (JAX003309) were purchased from Jackson Laboratory. MMTV-Cre, MMTV-NeuNDL and MMTV-NIC females were not used as breeders and all other female breeders were euthanized after having four litters. Animal care and husbandry was performed according to Animal Care and Veterinary Service guidelines at the University of Ottawa.

2.1.2. Genotyping.

Ear or tail clips were taken from mice at the time of weaning or embryos, respectively. Tissue samples were processed using proteinase K and genomic DNA was isolated using the DNeasy Blood and Tissue Kit following the manufacturer's protocol (QIAGEN). Genomic DNA was used for genotyping by polymerase chain reaction using the KAPA 2x Genotyping Mastermix (Kapa Biosystems). Genotyping PCR was performed as follows: an initial 95°C denaturation for 3 minutes followed by 35 cycles of denaturation at 95°C for 15 seconds, annealing at 5°C lower than the primer melting temperature for 15 seconds and elongation at 72°C for 30 seconds. A final elongation at 72°C for 4 minutes was performed prior to cooling

the samples to 4°C. Genotyping reactions were all run on 2% agarose gels. A list of genotyping primers and corresponding annealing temperatures used throughout these studies can be found in Table 2.2.

2.1.3. Subcutaneous Injections.

For subcutaneous injections, 8-12-week-old SCID Hairless Congenic mice were purchased from Charles River. $1.5x10^6$ of the indicated tumor cell line was resuspended in 100 μL of a 1:1 PBS:Matrigel mixture and this was injected into the right flank of recipient mice. The PBS:Matrigel mixture was injected into the left flank as a contralateral control. Following injections, mice were palpated every three days and tumor diameter was measured. Mice were sacrificed when the first mouse within each experiment reached a final tumor diameter of 10 mm.

2.1.4. Tumor Measurements.

All mammary and subcutaneous tumors were palpated and measured every three days. The largest diameter of the tumor was measured at each timepoint and tumor volume was calculated using the following formula: volume = $(4/3)*(\pi)*(r^3)$, where r is the tumor radius. Tumor onset was defined as the time where the first palpable tumor reached a tumor volume of 0.5 cm^3 and endpoint was defined by a total cumulative tumor burden of 1.7 cm^3 as defined by University of Ottawa Animal Care and Veterinary Service Guidelines.

2.2. Histology.

2.2.1. Formalin Fixation, Paraffin Embedding and Sectioning.

Embryos, mammary glands and tumors were harvested and fixed in 10% buffered formalin phosphate for 24 hours and then transferred to 70% ethanol for storage. Tissues were formalin fixed and paraffin embedded at the University of Ottawa Histology Core. Paraffin blocks were stored at room temperature protected from light until sectioned at 5 μm.

2.2.2. X-gal Staining.

Embryos or mammary glands from either BCO415 or MMTV-Cre Rosa26R-LacZ transgenic mice were stained using standard X-gal histochemistry. Samples were fixed for 30 minutes in 1% formaldehyde, 0.5% glutaraldehyde in PBS. Tissues were then washed three times in detergent buffer (PBS containing 0.02% NP40, 0.01% Na-Deoxycholate and 2 mM $MgCl_2$). After the last wash, tissues were incubated in staining solution (1 mg/mL X-gal, 5 mM $K_3Fe(CN)_6$, 5 mM $K_4Fe(CN)_6$ and 1 mM EGTA in detergent buffer) overnight with gentle agitation and protected from light. Excess stain was removed with successive PBS washes and storage at 4°C. Whole mounts and embryos were photographed using an upright dissecting microscope equipped with a camera.

2.2.3. Immunohistochemistry.

Tissue sections were deparaffinized and subjected to antigen retrieval in 10 mM citrate buffer (pH 6.0) for 10 minutes in a pressure cooker. Endogenous peroxidase was quenched with 3% hydrogen peroxide for 15 minutes at room temperature. Sections were blocked in 5% donkey serum in PBS for an hour and incubated with the indicated primary antibody overnight at 4°C followed by incubation with the appropriate HRP-conjugated secondary antibody at room temperature for 30 minutes. All incubations were performed in blocking solution. For mouse monoclonal antibodies on mouse tissues, mouse-on-mouse blocking solution (Vector Laboratories) was added to the blocking step. Sections were then incubated in DAB substrate (Sigma Aldrich) and counterstained with Haematoxylin. Sections were dehydrated in ethanol prior to clearing in three changes of xylene before mounting the slides. Sections were imaged using the Aperio Scanscope (Leica Biosystems) and images were processed and/or analyzed using Imagescope or ImageJ. Antibodies used for immunohistochemistry can be found in Table 2.1.

2.2.4. Immunofluorescence.

For immunofluorescence, 1.5 x 10^5 cells were seeded on sterile coverslips in 6-well plates. Following the indicated treatment, the coverslips were fixed with 4% paraformaldehyde for 10 minutes at room temperature. The coverslips were then washed twice in PBS and cells were permeabilized with 0.1% Triton X-100 in PBS for 5 minutes at room temperature. The cells were then washed three times with PBS and blocked for an hour at room temperature in 1.5% donkey serum. Blocking was then removed and the indicated primary antibody was added at the appropriate dilution in 1.5% donkey serum for one hour at room temperature. The cells were then washed three times with PBS and the appropriate fluorescent secondary was added in 1.5% donkey serum for one hour at room temperature protected from light. The coverslips were then washed three times in PBS and mounted on slides with mounting media containing DAPI (Vector Laboratories) and sealed with nail polish. Antibodies used for immunofluorescence can be found in Table 2.1.

2.3. Plasmids and Cloning.

The following plasmids were purchased from Addgene: pBABE (#1764), pBABE-Sox10 (#64890), pE1B-C-F/Sox10-MCS4 (#20243) and pE1B-C-F/Sox10-MCS7 (#20246). The following plasmids were purchased from Origene: pCMV6-myc-DDK-PDPK1 (NM_031268) and pCMV6-myc-DDK-Sox9 (NM_011448). The following plasmids were a kind gift from Dr. Pieter Siegel, McGill University: pMSCV-puro and pMSCV-NeuNT.

The pE1B-C-F vector was generated by digesting pE1B-C-F/Sox10-MCS4 with XhoI and NheI for one hour at 37°C and purifying the 4909 bp band from a 0.8% agarose gel using the QIAGEN Gel Extraction Kit (28704) following the manufacturer's protocol. The purified backbone was blunted using T4 DNA ligase (Invitrogen, M0202) and the blunt product was re-ligated using T7 DNA ligase (Invitrogen, M0318).

Fragments of the Sox10 promoter were amplified by PCR from Bacterial Artificial Chromosome (BAC) RP23-424P8 which contains up to 12 kb of the Sox10 promoter and was purchased from The Centre of Applied Genomics (SickKids, Toronto, Canada). Each fragment of the Sox10 promoter was amplified using the indicated primers in Table 2.2. PCR products were digested with KpnI and XhoI (which were included in the forward or reverse primer, respectively) for two hours at 37°C. Digested products were purified from a 0.8% agarose gel using the QIAGEN Gel Extraction Kit (28704) and ligated into pGL3P which was linearized with KpnI and XhoI.

pGEX-Sox9 was generated by PCR amplifying Sox9 cDNA from pCMV6-myc-DDK-Sox9.1 HA-Sox9 with the indicated primers in Table 2.2. The PCR product was digested with BamHI and XhoI (which were included in the forward or reverse primer, respectively) for one hour at 37°C. Digested products were purified from a 0.8% agarose gel using the QIAGEN Gel Extraction Kit (28704) and ligated into pGEX-4T2 which was linearized with BamHI and XhoI.

pGEX-Sox9$^{1-223}$ was generated by linearizing and purifying pGEX-Sox9 with SmaI and NotI. The linear fragment was then blunted with Klenow (New England Biolabs) and purified from a 0.8% agarose gel using the QIAGEN Gel Extraction Kit (28704). The linearized vector was then incubated with T4 DNA ligase (New England Biolabs) to generate the circular plasmid.

Sox9 S181A mutants were generated using either pGEX-Sox9$^{1-223}$ or pCMV6-myc-DDK-Sox9 as template. The point mutation was generated using the QuickChange XL Site-directed Mutagenesis Kit according to the manufacturer's protocol. The primers used to generate the point mutations are listed in Table 2.2. Positive clones were confirmed by Sanger sequencing.

2.4. Cell Culture.

2.4.1. Isolation of Mouse Embryonic Fibroblasts.

Mouse embryonic fibroblasts (MEFs) were harvested from E14.5 embryos. Embryos were collected by caesarian section of timed matings. A portion of the tail was taken for genotyping and the internal organs were removed before trypsin digestion of the remainder of the embryo. Isolated MEFs were plated in DMEM supplemented with 10% FBS, 1% Penicillin/Streptomycin and 1% L-glutamine. Primary MEFs were used for all experiments using the BCO415 SLK-targeted gene trap model. $SLK^{fl/fl}$ MEFs were immortalized by continuously passaging the cells through every three days until they reached crisis and then changing the media every three days while they remained senescent. Cells were considered immortalized and ready for experimental use once they had begun to rapidly proliferate and had achieved a doubling time of approximately 24 hours. Immortalized pools were used in all experiments unless otherwise indicated.

2.4.2. Isolation of $SLK^{fl/fl}$ NDL Cell Lines.

To establish mammary epithelial $SLK^{fl/fl}$ tumor cells, tumor bearing $SLK^{fl/fl}$ NDL females were sacrificed at a tumor volume of 1 cm^3. Tumors were minced in 2 mL of digestion media (49% DMEM/F12, 50% accutase, 1% Pencillin/Streptomycin and 1 mg/mL collagenase) and incubated in a 50 mL Falcon tube for 5 hours at 37°C in a shaking incubator at 225 rpm. The digested tumor was diluted 1:1 with BSA wash buffer (0.2% BSA in DMEM/F12) and filtered through a 40 μm mesh cell strainer. Cells were pelleted and washed twice in BSA wash buffer. Red blood cells were then lysed with a 4:1 mixture of NH_4Cl:1% BSA in PBS for 3 minutes at room temperature. Pellets were then washed once with BSA wash buffer and digested with accutase for 10 minutes at 37°C to disaggregate cell clumps. Accutase was neutralized with the addition of two volumes of BSA wash buffer. To isolate the lineage

marker negative (Lin^-) mammary epithelial tumor cells from this mixture, the Mouse Mammary Stem Cell Enrichment Kit (Stemcell Technologies) was used according to the manufacturer's protocol without the addition of either CD24 or CD49f antibodies. Following isolation, the cells were seeded in DMEM/F12 media containing 10% FBS, 1% mammary epithelial growth supplement (Life Technologies), 1% Penicillin/Streptomycin and 1% L-glutamine. Media was changed every second day and cultures were passaged when 80% confluency was achieved. Cells were considered ready for experimental use once they achieved a doubling time of approximately 24 hours.

2.4.3. Routine Cell Culture.

All mammary tumor cell lines were maintained in DMEM/F12 containing 10% FBS, 1% mammary epithelial growth supplement (Life Technologies), 1% Penicillin/Streptomycin and 1% L-glutamine. All mammary tumor cell lines were used within 25 passages of initial isolation. NMuMG cells were maintained in DMEM containing 10% FBS, 4 mM HEPES, 8 mg/mL Insulin, 1% Penicillin/Streptomycin and 1% L-glutamine. All other cell lines used were maintained in DMEM containing 10% FBS, 1% Penicillin/Streptomycin and 1% L-glutamine. Cells were cultured at 37°C in a humidified incubator set at 5% CO_2. Cells were routinely passaged at a one in ten dilution every 2-3 days. All cell lines were tested for mycoplasma contamination monthly by routine PCR analysis.

2.4.4. Plasmid Transfection.

For plasmid and siRNA transfections, cells were seeded such that they would reach approximately 75% confluency the day of transfection. Lipofectamine 3000 was used for all transfections according to the manufacturer's protocol using 8 μg of plasmid or 100 nM of siRNA. Plasmid transfections were performed for 24-72 hours depending on the experiment

while siRNA transfections were performed for 72 hours. Successful plasmid or siRNA transfection was assessed by Western blot and/or qPCR analysis.

2.4.5. Retroviral Production and Transduction.

To produce retroviral particles, 293T cells were seeded in 10 cm plates such that they were at approximately 90% confluency at the time of viral packaging. To package retrovirus, the 293T cells were transfected using Lipofectamine 3000 with 1 μg of retroviral construct, 889 ng of pUMVC and 111 ng of pCMV-VSV-G. The day following transfection, the media was replaced with 5 mL of serum-free DMEM for a further 24 hours. The media, now containing crude retrovirus, was filtered through a 0.44 μm filter and supplemented with 8 μg/mL of polybrene and 5 mL of serum-free media was added back onto the 293T cells. Cells to be infected were trypsinized and infected with 3 mL of virus containing media in suspension for 4 hours. The following day, the infection was repeated, and appropriate selection was applied to the cells for 7 days. Successful selection and retroviral integration was assessed by Western blot and/or qPCR analysis.

2.4.6. Boyden Chamber Migration Assay.

Boyden chambers were pre-coated using 40 μg/mL rat tail collagen type I overnight at 4°C. Boyden chambers were then washed and stored in PBS at 4°C for up to a month. Cells were starved in serum free DMEM/F12 overnight prior to performing the migration assay. Cells were then counted and $5x10^4$ cells were plated in 400 μL of DMEM/F12 containing 1% FBS into the upper chamber. The lower chamber was filled with 400 μL of the same media. Cells were left to migrate through the filter for 8 hours. The chambers were then washed three times with PBS and cells remaining on the top side of the membrane were removed with a cotton swab. The membranes were fixed for 10 minutes in 10% buffered formalin phosphate at room temperature. The Boyden chambers were then washed twice with PBS and stained for

30 minutes with 0.5% crystal violet in 25% methanol. Excess crystal violet was removed in serial washes of ddH_2O and membranes were left to dry overnight at room temperature. Membranes were mounted onto slides and slides were scanned using the Aperio Scanscope (Leica Biosystems). Cells were counted from ten random fields of view and averaged per filter.

2.4.7. Proliferation Assay.

For proliferation assays, $5x10^4$ cells were seeded in triplicate 60 mm plates per timepoint. At the indicated time, cells were collected by trypsinization and pelleted at 1200 rpm for 3 minutes at room temperature. Pellets were washed once with PBS and resuspended in 2 mL of media. Cells were then stained with trypan blue and counted in triplicate using a Vi-Cell Counter and the number of viable cells per day was quantified. All proliferation assays were performed for at least three independent biological replicates.

2.4.8. Colony Forming Assay.

For colony formation, 100 μL of Matrigel (Cultrex) was plated out on 4-well glass chamber slides (Life Technologies) and allowed to solidify at 37°C. $1x10^4$ cells were seeded per chamber in 400 μL of DMEM/F12 media containing 2% FBS and 1x MEGS (Life Technologies). Media was changed on the cells every other day for the duration of the assay. Colonies were counted 4 and 8 days after seeding and ten random fields of view per chamber were chosen for quantification. Colonies with an area over 5000 μm^2 were considered positive and enumerated per field of view.

2.4.9. Focus Forming Assay.

For focus forming assays, Rat-1 fibroblasts were seeded at 75% confluency in triplicate 10 cm plates. The following day, the indicated retroviral constructs were transfected. The Rat-1 fibroblasts were then cultured for up to 18 days depending on the assay with a full media change every three days. At the end of the experiment, each plate was washed twice with PBS

and fixed for 10 minutes in ice cold methanol. Foci were then stained with 3 mL of 0.5% crystal violet in 25% methanol for 5 minutes. The residual crystal violet solution was aspirated, and the plates were washed thoroughly with ddH_2O and allowed to dry overnight at room temperature. Foci with a diameter greater than 1.5 mm were quantified.

2.4.10. Mammosphere Forming Assay.

Primary mammospheres were established by plating $1x10^3$ cells that were disaggregated by passing the cells through a 25-gauge needle three times. Cells were washed once in PBS and resuspended in 500 μL of DMEM/F12 media containing 1x MEGS and 1x B27 supplements (Life Technologies). For assays using inhibitors, the indicated concentration was added to the resuspended cells. Cells were plated in 24 well Ultra-Low Attachment Flat Bottom Plates (Corning) and spheres were left to grow for one week before quantification. The mammosphere forming efficiency was defined as the percentage of spheres with a diameter of greater than 15 μm over the total number of cells seeded per well. Secondary mammospheres were plated by disaggregating the primary mammospheres with 0.5% trypsin 0.2% EDTA for 3 minutes and achieving a single cell suspension using a 25-gauge needle. Secondary spheres were seeded between 0.3 and $1x10^3$ cells per well and allowed to grow for one week.

2.4.11. Capillary Morphogenesis.

The organization of mouse dermal microvascular endothelial cells (MDMECs) into capillary networks was assessed by plating cells onto Cultrex Basement Membrane Extract (Trevigen). Cells were transfected with the indicated SLK targeted siRNA for 48 hours prior to plating. Cultrex was polymerized at 37°C for 30 minutes in 24-well plates and $5x10^4$ cells were plated in single wells containing Endothelial Cell Medium with Supplement (Cell Biologics). At least three independent experiments were performed with independent siRNA

transfections. Images were collected 24 hours after plating and analysis of capillary formation was performed as previously described (199).

2.5. RNA Expression Analysis.

2.5.1. Tissue and Cell Lysis.

Tissues and cell lines were collected in 1 mL of Trizol buffer, thoroughly homogenized and left to sit at room temperature for 10 minutes. For tissue samples, insoluble material was pelleted at 12000 x g for 10 minutes at 4°C. To the supernatant, 200 µL of chloroform was added and the samples were vortexed for 15 seconds and then left to sit at room temperature for 5 minutes. Phase separation was performed by centrifugation at 12000 x g for 15 minutes at 4°C and the upper aqueous phase was transferred to a new tube. Nucleic acids were then precipitated for 10 minutes at room temperature by adding one volume of isopropanol and vortexing thoroughly. The nucleic acids were pelleted by centrifugation at 12000 x g for 10 minutes at 4°C. Pellets were washed with 70% ethanol and centrifuged at 7500 x g for 5 minutes. The nucleic acid pellet was then dried at room temperature for 10 minutes and resuspended in 100 µL of RNase-free water. Samples were then treated with DNase using the RNeasy Mini Kit (QIAGEN). Purified RNA was quantified using a nanodrop and purity was assessed using the A260/230 and A260/280 ratios.

2.5.2. Reverse Transcription and First Strand cDNA Synthesis.

For first strand cDNA synthesis, a 13 µL mixture containing 500 ng of RNA, 50 ng of random primers, 250 ng of oligo$(dT)_{12\text{-}18}$ and 10 nmol of dNTP mix was incubated at 65°C for 5 minutes. Reverse transcription was performed using Superscript III Reverse Transcriptase (Life Technologies) according to the manufacturer's protocol. Briefly, to the 13 µL sample, 4 µL of 5X First Strand Buffer, 1 µL of RNase OUT, 1 µL of 0.1 M DTT and 1 µL of SuperScript III reverse transcriptase were added. Samples were then incubated at 25°C for 5 minutes, 55°C

for 60 minutes and 70°C for 15 minutes. Samples were then diluted to 200 µL in nuclease-free water prior to storage at -20°C.

2.5.3. Quantitative Realtime-PCR.

For qRT-PCR analysis, a mastermix was set up containing 17.5 µL of 2X iTaq Universal SYBR Green Supermix (BioRad), 2.1 µL of the indicated primers (10µM), 3.5 µL of diluted cDNA and 11.9 µL of nuclease-free water. For each mastermix, 10 µL was added to triplicate wells in a 96-well qPCR plate. Plates were run on an Applied Biosystems 7500 Real-Time Fast PCR thermocycler. The PCR reaction started with an initial hold and denaturation at 50°C for 5 minutes and 95°C for 10 minutes, respectively, followed by 40 cycles of denaturation at 95°C for 15 seconds and Annealing and Extension at 60°C for 60 seconds. Relative mRNA expression was calculated using the $\Delta\Delta C_T$ method and normalizing to total levels of ribosomal 18S. The primers used for qRT-PCR can be found in Table 2.2.

2.5.4. Microarray Analysis.

Microarray analysis was performed using total RNA from three independent $SLK^{fl/fl}$ and $SLK^{-/-}$ NDL cell lines hybridized to the Mouse Gene 2.0 ST Array (Affymetrix). RNA hybridization was performed by the StemCore Laboratories at the Ottawa Hospital Research Institute. Microarray data analysis was carried out in the r statistical programming environment with Bioconductor.

2.6. Protein Expression Analysis.

2.6.1. Tissue and Cell Lysis.

Tissues and cell lines were collected and homogenized in RIPA lysis buffer containing protease inhibitors (0.05% SDS, 1% Triton X-100, 1% NP-40, 50 mM Tris-HCl, pH 7.5, 150 mM NaCl, 2 mM EDTA, pH 8.0, 12 mM Na-Deoxycholate, 10 mM NaF, 1 mM DTT, 10 mM β-glycerophosphate, 0.6 mM $NaVO_3$, 1 mM PMSF, 10 µg/mL leupeptin, 10 µg/mL aprotinin,

10 μg/mL pepstatin and 100 μM benzamide). Lysates were incubated on ice for 10 minutes with occasional vortexing. Lysates were cleared by centrifugation at 14000 rpm for 10 minutes at 4°C. Protein concentrations were determined using Bradford reagent (Biorad) and stored at -80°C.

2.6.2. Western Blotting.

Equal amounts of protein lysate (10-40 μg) were prepared in PBS containing 1x SDS sample buffer (50 mM Tris-HCl, 100 mM DTT, 2% SDS, 0.1% bromophenol blue and 10% glycerol) and denatured at 100°C for 5 minutes prior to electrophoresis. Lysates were electrophoresed on polyacrylamide gels (8-12%) for 45 minutes at 45 mA in 1x SDS running buffer (25 mM Tris-HCl, 192 mM glycine and 0.1% SDS). The samples were then transferred to a PVDF membrane at 100 V for 90 minutes in 1x transfer buffer (48 mM Tris-HCl, 39 mM glycine and 20% methanol). Membranes were probed with the indicated primary antibody overnight at 4°C in TBST (50 mM Tris, pH 7.4, 150 mM NaCl, 0.05% Tween 20) containing 5% BSA. Primary antibody was removed and the membranes were washed three times in TBST. Appropriate HRP-conjugated secondary antibodies were added in TBST containing 5% BSA for one hour at room temperature. Secondary antibody was removed and the membranes were washed three times in TBST. Reactive proteins were detected by chemiluminescence (Perkin Elmer) and exposure to X-ray film. The antibodies used for Western blot can be found in Table 2.1.

2.6.3. Immunoprecipitation.

For immunoprecipitation, equal amounts of total protein lysate (200-400 μg) were immunoprecipitated with 1 μg of the indicated primary antibody and 20 μL of Protein A sepharose beads (GE Healthcare) with rotation at 4°C for 2 hours. The beads were then washed three times with NETN (20 mM Tris-HCl, pH 8.0, 1 mM EDTA, pH 8.0, 200 mM NaCl and

0.5% NP-40) and once in PBS. The beads were resuspended in 20 μL of PBS containing 1x SDS sample buffer (50 mM Tris-HCl, 100 mM DTT, 2% SDS, 0.1% bromophenol blue and 10% glycerol) and denatured at 100°C for 5 minutes prior to electrophoresis. Antibodies used for immunoprecipitation can be found in Table 2.1.

2.6.4. GST-fusion Protein Production.

RP bacteria were transformed with the indicated GST or GST-fusion plasmids and glycerol stocks were stored at -80°C. Glycerol stocks were used to inoculate 3 mL of LB broth containing the appropriate antibiotic and cultures were left to grow overnight at 37°C with shaking at 225 rpm. The 3 mL cultures were then expanded to 30 mL and left to shake at 225 rpm for 1 hour at 37°C. GST-fusion protein production was then induced with 1 mM IPTG for 2 hours at 37°C with shaking at 225 rpm. The bacterial cultures were then pelleted at 3000 rpm for 15 minutes at 4°C. Bacterial pellets were lysed in 500 μL of RIPA lysis buffer containing protease inhibitors (0.05% SDS, 1% Triton X-100, 1% NP-40, 50 mM Tris-HCl, pH 7.5, 150 mM NaCl, 2 mM EDTA, pH 8.0, 12 mM Na-Deoxycholate, 10 mM NaF, 1 mM DTT, 10 mM β-glycerophosphate, 0.6 mM $NaVO_3$, 1 mM PMSF, 10 μg/mL leupeptin, 10 μg/mL aprotinin, 10 μg/mL pepstatin and 100 μM benzamide) and incubated on ice for 15 minutes with occasional vortexing. Lysates were then sonicated with three 15 seconds pulses and cleared by centrifugation at 14000 rpm for 30 minutes at 4°C. GST-fusion proteins were then purified with 20 μL of GST-sepharose beads (GE Healthcare) using the immunoprecipitation protocol.

2.6.5. *In vitro* Kinase Assay.

For *in vitro* kinase assays, samples were immunoprecipitated as indicated above. Following the three washes with NETN, beads were washed once with 1x kinase buffer (20 mM Tris-HCl, pH 7.4, 0.25 mM $NaVO_3$, 1 mM NaF, 10 mM β-glycerophosphate, 1 mM DTT and 15 mM $MgCl_2$). The beads were then resuspended in 20 μL of 1x kinase buffer and the

reactions were initiated by the addition of 1 μL of [^{32}P]γATP (5 μCi/μL, Perkin Elmer) and incubated for 30 minutes at 30°C with mixing every 10 minutes. For recombinant kinase assays with GST-fusion proteins, 200 ng of recombinant human GST-AKT fusion protein (Sigma Aldrich, SRP-5001) was added to the kinase assay mastermix. The reactions were terminated with the addition of 4x SDS sample buffer (200 mM Tris-HCl, 400 mM DTT, 8% SDS, 0.4% bromophenol blue and 40% glycerol) and denatured at 100°C for 5 minutes prior to electrophoresis. Samples were electrophoresed and transferred to a PVDF membrane as indicated above. Incorporation of the radiolabelled phosphate was detected by autoradiography and the efficiency of the immunoprecipitation was determined by Western blot for the immunoprecipitated protein.

2.6.6. Cytoplasmic/Nuclear Fractionation.

To separate the cytoplasmic and nuclear fractions, cells were collected and pelleted at 1300 x g for 5 minutes at 4°C and resuspended in 200 μL of cytoplasmic lysis buffer (20 mM HEPES, 0.5% NP-40, 50 mM NaCl, 3 mM $MgCl_2$ and 292 mM sucrose). Samples were incubated with rotation for 10 minutes at 4°C followed by centrifugation at 1300 x g for 5 minutes at 4°C. The supernatant was collected as the cytoplasmic fraction and insoluble material was further cleared at 17200 x g for 10 minutes at 4°C. The remaining pellet, containing the nuclear fraction, was washed with 200 μL of cytoplasmic lysis buffer for 10 minutes with rotation at 4°C then centrifuged at 16000 x g for 1 minute at 4°C to collect the nuclei. The pellet was then resuspended in 100 μL of RIPA lysis buffer containing protease inhibitors (0.05% SDS, 1% Triton X-100, 1% NP-40, 50 mM Tris-HCl, pH 7.5, 150 mM NaCl, 2 mM EDTA, pH 8.0, 12 mM Na-Deoxycholate, 10 mM NaF, 1 mM DTT, 10 mM β-glycerophosphate, 0.6 mM $NaVO_3$, 1 mM PMSF, 10 μg/mL leupeptin, 10 μg/mL aprotinin, 10 μg/mL pepstatin and 100 μM benzamide) and incubated on ice for 10 minutes. Nuclei were

then lysed by sonication and cleared at 17200 x g for 10 minutes at 4°C. Protein samples were then quantified by Bradford assay, denatured and electrophoresed as indicated above.

2.6.7. Flow Cytometry.

For flow staining and analysis, cells were trypsinized for 3 minutes and pelleted at 1200 rpm for 5 minutes at 4°C. Cells were washed once in flow buffer (PBS containing 1% BSA) and plated in a 96-well V-bottom plate. Cells were washed once in PBS and stained with Zombie NIR Live/Dead dye (BioLegend) at a 1/500 dilution in PBS for 20 minutes on ice protected from light. Cells were then washed once with flow buffer and pelleted at 2000 rpm for 3 minutes at 4°C. Samples were then blocked with mouse Fc Block (BD Biosciences) at a 1/200 dilution in flow buffer for 20 minutes on ice protected from light. Cells were then washed with flow buffer and pelleted at 2000 rpm for 3 minutes at 4°C. The indicated antibodies were then prepared at the appropriate dilution listed in Table 2.1 and added to the cells for 20 minutes on ice protected from light. Extra wells were included for both unstained and single-color viability dye. For single color-control wells, 30 μL of UltraComp beads (eBioscience) was added with the appropriate antibody. Samples were then washed three times in flow buffer and run on a BD LSRFortessa flow cytometer. FlowJo was used to analyze the data.

2.7. Lipid Extraction and PI(3,4,5)P_3 Quantification.

To extract intracellular lipids, media was removed from cell culture plates and cells were incubated for 5 minutes in ice cold 0.5 M TCA. Cells were then collected and pelleted at 3000 rpm for 5 minutes at 4°C. Cells pellets were washed twice with 3 mL of 5% TCA in 1 mM EDTA. Neutral lipids were then extracted with two incubations of MeOH:$CHCl_3$ (2:1) for 10 minutes each. Acidic lipids were then extracted from the pellet in MeOH:$CHCl_3$:12 M HCl (80:40:1) for 25 minutes at room temperature. To the supernatant, 0.25 volumes of $CHCl_3$ and 0.5 volumes of 0.1 M HCl were added to extract the lower organic fraction containing

$PI(3,4,5)P_3$. The organic fraction was dried in a vacuum dryer at room temperature and dried lipids were stored at -20°C until use. Levels of intracellular $PI(3,4,5)P_3$ were detected using the PIP_3 Mass ELISA Kit (K-2500s, Echelon Biosciences) following the manufacturer's protocol.

2.8. Analysis of DNA and Chromatin.

2.8.1. Bisulfite Sequencing.

Genomic DNA for bisulfite conversion was isolated using the DNeasy Blood and Tissue Kit following the manufacturer's protocol (QIAGEN). Bisulfite conversion of genomic DNA was performed using the EpiTect Plus DNA Bisulfite Kit (QIAGEN) following the manufacturer's protocol. Promoter regions of control and bisulfite converted DNA was amplified using the primers indicated in Table 2.2 using Taq polymerase (Invitrogen). Amplicons were subcloned into pGEM-T (Promega) according to the manufacturer's protocol. Five clones for each conversion reaction were picked, miniprepped and sequenced to identify methylated cytosine residues.

2.8.2. Luciferase Assay.

For luciferase assays, 1.5×10^5 cells were seeded in triplicate wells of a 6-well plate. The following day, the cells were transfected using Lipofectamine 3000 with 1.25 μg of the appropriate pGL3P reporter construct and 1.25 μg of pRL-CMV (encoding Renilla luciferase) for 48 hours. Luciferase assays were performed using the Dual Luciferase Assay Reporter System (Promega). Cells were collected in 1.5 mL Eppendorf tubes and lysed in 100 μL of 1X passive lysis buffer with rotation at room temperature for 30 minutes. Lysates were cleared by centrifugation at 13000 rpm for 10 minutes at room temperature. 20 μL of each sample was transferred in triplicate into a black-sided 96-well plate with a clear bottom. 100 μL of resuspended Luciferase Assay Substrate was added to each well and read using a luminometer

with a read time of 10 seconds and a 2 second delay per well. 100 µL of Stop and Glo solution was then added to each well and read using a luminometer with a read time of 10 seconds and a 2 second delay per well. Luciferase counts were normalized to the pRL-CMV counts to account for differences in transfection efficiency between wells.

2.8.3. Chromatin Immunoprecipitation.

For chromatin immunoprecipitation, $5x10^6$ cells from each condition were seeded in two 15 cm plates and cultured for 48 hours. Cells were then crosslinked in 1% formaldehyde for 10 minutes at room temperature. The formaldehyde was then quenched with the addition of glycine to a final concentration of 125 mM. Nuclear extraction, chromatin digestion, and immunoprecipitation and DNA elution were all performed using the SimpleChip Kit (Cell Signaling Technologies) according to the manufacturer's protocol with the addition of a pre-clearing step with beads alone prior to the immunoprecipitation. 10 µg of chromatin was used per immunoprecipitation with 1 µg of the indicated antibody. Following chromatin IP and DNA cleanup, 6.5 µL of chromatin was mixed with 35 µL of iTaq Universal SYBR Green Supermix (BioRad), 6.5 µL of the indicated primers (5µM) and 21 µL of nuclease-free water. The PCR reaction was started with an initial hold and denaturation at 50°C for 5 minutes and 95°C for 10 minutes, respectively, followed by 40 cycles of denaturation at 95°C for 15 seconds and Annealing and Extension at 60°C for 60 seconds. The percent input was then calculated as follows: Percent Input = 2% x $2^{(C[T]\ 2\%Input\ Sample\ -\ C[T]\ IP\ Sample)}$. The antibodies used for chromatin immunoprecipitation can be found in Table 2.1. The primers used for ChIP-qPCR can be found in Table 2.2.

2.9. Bioinformatics and Analysis of The Cancer Genome Atlas Database.

2.9.1. Access of The Cancer Genome Atlas Database.

Gene-level RNA-seq (v2) counts from the cohort of invasive breast carcinoma samples from The Cancer Genome Atlas (n=1246, (200)) were collected using the R package recount2 (201). Counts were scaled to account for differences in library size across all samples.

2.9.2. Stratification of Molecular Breast Cancer Subtypes.

HER2, ESR1 and PGR expression (z-score of log2 counts) was calculated from each of the 1246 invasive breast carcinoma samples. Hierarchical clustering was used to group patients by the expression pattern of each receptor, revealing a group of putative TNBC, HER2-positive and Luminal A/B patients.

2.9.3. Identification of Marker Genes.

Marker genes were identified using an ANOVA to identify genes that are differentially expressed across all molecular subtypes. Differentially expressed genes were filtered with a Benjamini-Hochberg-adjusted p-value < 0.01 (ANOVA) across all subtypes with a minimum log2 fold change of 4 (16-fold) between the subtype with the lowest expression and the one with the highest expression.

2.9.4. Data Analysis Scripts.

All analysis scripts required to reproduce these findings are available at: https://github.com/dpcook/tcga_breast_cancer.

2.10. Reproducibility and Statistical Analyses.

For all *in vitro* experiments, at least three independent biological replicates were performed and all data is represented as the mean with error bars representing the standard error of the mean (SEM). For quantification of histological or immunofluorescent images, at least three or ten biological replicates were performed for *in vitro* or *in vivo* samples,

respectively. For each independent image, ten random fields of view were quantified per and all graphs are presented as the mean of all biological replicates +/- SEM. For tumor cell injections, at least six mice were injected per cell type and the mean tumor volume at each timepoint is presented +/- SEM.

Power calculations were performed in order to estimate that 25 mice were needed per genotype in order to detect a significant ($p<0.05$) 30 day change in survival between $SLK^{+/+}$, $SLK^{+/fl}$ or $SLK^{fl/fl}$ NIC mice with a power of 0.80. These calculations were performed using a mean survival of 184 days for NIC mice with a population standard deviation of 39 days.

For statistical analysis with only two comparisons, a students t-test was used with a significance cut-off of $p<0.05$. For greater than two comparisons a one-way ANOVA was performed using a Tukey post-hoc test. Kaplan-Meier survival was analyzed using a Mantel-Cox log-rank test.

Table 2.1. List of Antibodies. A list of antibodies, catalog numbers, applications and dilutions that were used throughout this thesis is provided here.

Antibody	Company	Catalog Number	Western	IF	IHC-P	Flow	IP/ChIP
SLK	Custom	-	1:10000	-	1:500	-	0.75 µg
α-tubulin	Sigma	T1568	1:5000	-	-	-	-
β-Gal	Cell Signaling Technology	2372	-	-	1:500	-	-
FAK	BD Biosciences	610088	1:1000	-	-	-	-
ERM	Cell Signaling Technology	3142	1:1000	-	-	-	-
Paxillin	BD Biosciences	612405	1:1000	-	-	-	-
MHC	R&D Systems	MAB44470	-	-		-	-
Tuj-1	Neuromics	MO15013	-	-	1:200	-	-
Cleaved Caspase 3	Cell Signaling Technology	9661	1:1000	-	1:200	-	-
Smooth Muscle Actin	Abcam	ab7817	-	-	1:400	-	-
PECAM-1	Santa Cruz	sc-1506	-	-	1:200	-	-
Neu	Calbiochem	OP15	1:2000	-	-	-	-
Cre	Millipore	69050	1:10000	-	-	-	-
β-actin	Sigma	A5316	1:20000	-	-	-	-
Ki67	Millipore	ab9260	-	-	1:50	-	-
Cyclin D1	Santa Cruz	sc-20044	1:200	-	-	-	-
PCNA	Santa Cruz	sc-56	1:500	-	-	-	-
phospho ERK 1/2 Y204	Santa Cruz	sc-7383	1:2000	-	-	-	-
ERK1/2	Santa Cruz	sc-154	1:2000	-	-	-	-
PARP	Cell Signaling Technology	9542	1:2000	-	-	-	-
Cytokeratin 8	Abcam	ab53280	1:2000	-	-	-	-

Sox10	Cell Signaling Technology	89356	1:1000	-	-	-	-
Sox10	Novus	NBP2-44474	-	-	1:400	-	-
CD133 (BV421)	Biolegend	141213	-	-	-	2 µg/mL	-
Sca1 (BV510)	BD Biosciences	565507	-	-	-	2 µg/mL	-
phospho S6 S235/236	Cell Signaling Technology	2211	1:5000	-	-	-	-
S6	Santa Cruz	sc-74459	1:2000	-	-	-	-
phospho AKT S473	Cell Signaling Technology	4060	1:1000	-	-	-	-
AKT	Cell Signaling Technology	9272	1:2000	-	-	-	-
PI3K	BD Biosciences	610045	1:1000	-	-	-	-
PTEN	Cell Signaling Technology	9552	1:2000	-	-	-	-
phospho PDK1 S241	Cell Signaling Technology	3061	1:1000	-	-	-	-
PDK1	Cell Signaling Technology	5662	1:2000	1:200	-	-	-
phospho SLK S189	Custom	-	1:1000	-	-	-	-
HA	Sigma	H6908	1:5000	-	-	-	2 µg
c-myc	Sigma	M4439	1:5000	-	-	-	-
phospho ErbB3 Y1289	Cell Signaling Technology	4791	1:1000	-	-	-	-
ErbB3	Cell Signaling Technology	12708	1:1000	-	-	-	-
CREB	Cell Signaling Technology	9197	1:1000	-	-	-	-
FoxO3a	Cell Signaling Technology	12829	1:1000	-	-	-	-
FoxO1	Cell Signaling Technology	2880	1:1000	-	-	-	-
GAPDH	Cell Signaling Technology	2118	1:2000	-	-	-	-
Lamin A/C	Cell Signaling Technology	4744	1:2000	-	-	-	-
phospho Sox9 S181	Abcam	ab59252	1:500	-	1:100	-	-
Sox9	Novus	NBP1-8555	1:2000	-	-	-	1 µg

Rabbit IgG - HRP Conjugate	BioRad	170-6515	1:5000	-	-	-	-
Mouse IgG- HRP Conjugate	BioRad	170-6516	1:5000	-	-	-	-
Rabbit IgG- AF555 Conjugate	Abcam	ab150074	-	1:1000	-	-	-

Table 2.2. List of Primers. A list of primers and their applications that were used throughout this thesis is provided here.

Primer	Assay	Primer Sequence
BCO415 forward	Genotyping	GAGCAGGTCAGCCAGTCCAATAG
BCO415 reverse	Genotyping	CTCTCAGGCGGTTAGTGTGCTCTT
LacZ forward	Genotyping	CACCGATCGCCCTTCCCAACAGT
LacZ reverse	Genotyping	TGCCGCTCATCCGCCACAT
Floxed SLK forward	Genotyping	TGAGGACCTGGGGAGATTGCT
Floxed SLK reverse	Genotyping	ATGCAGCTGTATCTTCACAAG
Rosa26R forward	Genotyping	AAAGTCGCTCTGAGTTGTTAT
Rosa26R reverse	Genotyping	GGAGCGGGAGAAATGGATATG
Rosa26R common	Genotyping	GCGAAGAGTTTGTCCTCAACC
Cre forward	Genotyping	GGATTGCTTATAACACCCTGTTACG
Cre reverse	Genotyping	TATTCGGATCATCAGCTACACCAGAG
Floxed SLK forward	Recombination PCR	TTGGGGGATGGCTTCGTGCTT
Floxed SLK reverse	Recombination PCR	ATGCAGCTGTATCTTCACAAG
Floxed SLK common	Recombination PCR	TGAGGACCTGGGGAGATTGCT
Sox10 promoter -6904/-5995 forward	Cloning	GCGGTACCCTCTTTCCTGTCCAA
Sox10 promoter -6904/-5995 reverse	Cloning	CGCTCGAGAGCAGATCACATTGG
Sox10 promoter -4565/-3503 forward	Cloning	GCGGTACCTCCCTGATACCACAT
Sox10 promoter -4565/-3503 reverse	Cloning	CGCTCGAGATACCCTGGGGTGCT
Sox10 promoter -3484/-2495 forward	Cloning	GCGGTACCTATTGACCTGAGGTG
Sox10 promoter -3484/-2495 reverse	Cloning	CGCTCGAGTCCCTCCTCTTGGAG
Sox10 promoter -1859/+359 forward	Cloning	CCGGTACCTAGGCTGTAGAGGTGAG

Sox10 promoter -1859/+359 reverse	Cloning	CCCTCGAGCATGTCGCTCCCGGCCG
pGEXSox9 forward	Cloning	CAGGATCCAATCTCCTGGACCCCTTCATG
pGEXSox9 reverse	Cloning	CACTCGAGTCAGGGTCTGGTGAGCTG
m18S forward	qRT-PCR	AGTCCCTGCCCTTTGTACACA
m18S reverse	qRT-PCR	GATCCGAGGCCTCACTAAAC
mSLK forward	qRT-PCR	ACCGAGATCTAAAAGCTGGCA
mSLK reverse	qRT-PCR	ACCCAGGGACCAAACATCAG
mLgr6 forward	qRT-PCR	GAGGACGGCATCATGCTGTC
mLgr6 reverse	qRT-PCR	GCTCCGTGAGGTTGTTCATACT
mFam107a forward	qRT-PCR	CGCTGGTCAGTGTGGTGATT
mFam107a reverse	qRT-PCR	AGAGCACCGTCGCAGGAAT
mCcl9 forward	qRT-PCR	CCCTCTCCTTCCTCATTCTTACA
mCcl9 reverse	qRT-PCR	AGTCTTGAAAGCCCATGTGAAA
mLama4 forward	qRT-PCR	GGGGAGTACCTGAATGTTCACATG
mLama4 reverse	qRT-PCR	CTACATCCAACTGAACCACATTTGAATCTC
mApod forward	qRT-PCR	CTTCACCACAGCCAAAGGAC
mApod reverse	qRT-PCR	CGGGCAGTTCGCTTGATCTG
mMcpt8 forward	qRT-PCR	CTGAAGAGGATGTTCCTG
mMcpt8 reverse	qRT-PCR	GTGGGGTTTGGACTCTGT
mGria3 forward	qRT-PCR	GGTCATTCTCACGGAGGATTC
mGria3 reverse	qRT-PCR	GGTGTTCTGGTTGGTGTTGTA
mSerpine2 forward	qRT-PCR	CACATGGGATCGCGTCCATC
mSerpine2 reverse	qRT-PCR	CAGCACTTTACCAACTCCGTTTA

mSlc35f1 forward	qRT-PCR	CTGGGTAAGTCCACGACAGG
mSlc35f1 reverse	qRT-PCR	GGGCTGGTGCTGTATTCCTC
mEgln3 forward	qRT-PCR	AGGCAATGGTGGCTTGCTATC
mEgln3 reverse	qRT-PCR	GCGTCCCAATTCTTATTCAGGT
mB4galt6 forward	qRT-PCR	GGGTCTCCAATCGCTCTCTG
mB4galt6 reverse	qRT-PCR	ATAAAGAGGTACGTGTTGGCG
mTimp3 forward	qRT-PCR	CTTCTGCAACTCCGACATCGT
mTimp3 reverse	qRT-PCR	GGGGCATCTTACTGAAGCCTC
mParvb forward	qRT-PCR	AAGGACGAGTCTTTCTTGGGC
mParvb reverse	qRT-PCR	GGGGCCATTGGAGAGTTGAT
mPtprn forward	qRT-PCR	ACCAAGGTTGCCAGAGAATGG
mPtprn reverse	qRT-PCR	CCTGCCAGTACAGCAGTCAAT
mHhip forward	qRT-PCR	CCAGCCAGTTGGAAAGATGC
mHhip reverse	qRT-PCR	TGTGGTGTACATGAGTGATTACCT
mPtpn22 forward	qRT-PCR	GGTTGAGGAAGCCGGAGAG
mPtpn22 reverse	qRT-PCR	TCAGATGTCCCACTGCATTC
mMamdc2 forward	qRT-PCR	GTGTGGCTTTGACTCCGTGT
mMamdc2 reverse	qRT-PCR	GCCTGCAAATCAGAACTCAGC
mSox10 forward	qRT-PCR	AGGTTGCTGAACGAAAGTGAC
mSox10 reverse	qRT-PCR	CCGAGGTTGGTACTTGTAGTCC
mL1cam forward	qRT-PCR	AAAGGTGCAAGGGTGACATTC
mL1cam reverse	qRT-PCR	TCCCCACGTTCCTGTAGGT
mLcn2 forward	qRT-PCR	ACTTCCGGAGCGATCAGTT

mLcn2 reverse	qRT-PCR	CAGCTCCTTGGTTCTTCCAT
mMuc15 forward	qRT-PCR	CAATCTCATGGTGACAACTCCTT
mMuc15 reverse	qRT-PCR	GGGAGGAACAGAATATGTCGAGG
mMme forward	qRT-PCR	CTCTCTGTGCTTGTCTTGCTC
mMme reverse	qRT-PCR	GACGTTGCGTTTCAACCAGC
mCeacam1 forward	qRT-PCR	ATTTCACGGGGCAAGCATACA
mCeacam1 reverse	qRT-PCR	GTCACCCTCCACGGGATTG
mPdgfrb forward	qRT-PCR	TTCCAGGAGTGATACCAGCTT
mPdgfrb reverse	qRT-PCR	AGGGGGCGTGATGACTAGG
mPrex2 forward	qRT-PCR	TCACAGCAGTGGGCATATTGT
mPrex2 reverse	qRT-PCR	CCCTTTCCGACGTTCTCTTTCT
mEya4 forward	qRT-PCR	TCCTTGGCCCTGCTAAGAG
mEya4 reverse	qRT-PCR	TGCCTATTTTTGTTGCGCTGT
mSox8 forward	qRT-PCR	TGGAGTCTGGTGCCTATGCCTGT
mSox8 reverse	qRT-PCR	GCCGAGCACTGCATCAGCTTTGT
mSox9 forward	qRT-PCR	CATCAAGACGGAGCAGCTGAG
mSox9 reverse	qRT-PCR	ATGGTCAGCGTAGTCGTATTG
Sox10 distal forward	Bisulfite Sequencing	ATTTATTTAGGGTTTGGTATGTGTA
Sox10 distal reverse	Bisulfite Sequencing	CCACCTCTAATAAATCTTATTCCTC
Sox10 proximal forward	Bisulfite Sequencing	ATTAGAGGTGGAGTTGAGTTTTGTG
Sox10 proximal reverse	Bisulfite Sequencing	ATTCCTTCTTAACCTTACCCAATTC
Sox10 promoter +103 forward	ChIP-qPCR	TGGGACCCGACGGCGGCGGCGGTG
Sox10 promoter +103 reverse	ChIP-qPCR	CTTGCTCTTGCTGGCACCGTTGAC

Sox10 promoter -349 forward	ChIP-qPCR	GGTGGGAAATTCCAGGGGCCCGGA
Sox10 promoter -349 reverse	ChIP-qPCR	CTGATCCCAACCGTCTCTAGGTGT
Sox10 promoter -1643 forward	ChIP-qPCR	CACTGAGAAGAGAAAAGGACACTA
Sox10 promoter -1643 reverse	ChIP-qPCR	ACACTGAGAAAAGACAGGAACTGC
Sox10 promoter -2260 forward	ChIP-qPCR	GCGCTTCTGAGGCCGGGCGGGCGC
Sox10 promoter -2260 reverse	ChIP-qPCR	CTCCCTTCTCTTCCCTGTGCCCAG
Sox10 promoter -6175 forward	ChIP-qPCR	CCCTCGCTCTGTCCAGATTAATG
Sox10 promoter -6175 reverse	ChIP-qPCR	AGCAGATCACATTGGTAGACATGTAG
Sox10 promoter -6642 forward	ChIP-qPCR	ACAGAGATGAGCCATGTGAAAATAAG
Sox10 promoter -6642 reverse	ChIP-qPCR	AGCTGTCAGCAGCCTGGGCAAGGG
Sox9 S181A mutagenesis forward	Site directed mutagenesis	GCCCCGGCGGAGGCGGACAAGCGGAG
Sox9 S181A mutagenesis reverse	Site directed mutagenesis	CTCCGCTTGTCCGCCTCCGCCGGGGC

Chapter 3

Regulation of SLK catalytic activity is required for normal embryonic development.

3.1. Introduction and Rationale.

Successful embryonic and placental development requires the proper temporal and spatial coordination of many important cellular processes including adhesion, cytoskeletal reorganization, apoptosis, cell cycle control and migration [reviewed in (202-204)]. Over the past two decades, SLK has been shown to play a critical role in most of these processes *in vitro* (14,16,18,20,35,36,40,45,49,205,206), however a limited number of *in vivo* models have been established to study SLK. The *in vivo* functions of SLK have been studied using tissue-specific overexpression of either wildtype or kinase-dead SLK, which has established SLK as a mediator of muscle specific differentiation and fusion and for recovery from podocyte injury in the kidney (34,195,196). Our lab has also shown that SLK is highly expressed in embryonic stem cells and the muscular and neuronal lineages of the developing mouse embryo (19). Therefore, we aimed to assess the role of SLK during embryonic development using a globally expressed gene-trapped allele. As SLK is ubiquitously expressed in adult tissues with preferential expression in muscular and neuronal compartments of the developing embryo (14,19,195,196), we hypothesized that global expression of a gene-trapped *Slk* allele would result in developmental defects and embryonic lethality.

3.2. Generation and characterization of an *Slk* gene-trapped allele.

Embryonic stem cells harboring an *Slk*-targeted gene-trapped allele (BCO415 or RRJ117) was obtained from the Wellcome Trust Sanger Institute, NIH (Gene Trap Consortium). Insertion of the *Engrailed* (En-2)-β-Geo (pGT0-lxr) cDNA within the *Slk* locus, downstream of exon 10, was validated by 5'RACE. Insertion of the β-Geo cassette downstream of exon 10 within the BCO415 or RRJ117 embryonic stem cell lines results in an in-frame splicing event and the expression of an SLK-LacZ fusion protein that is approximately 50 kDa larger than endogenous SLK (Figure 3.1. A, B). The resulting SLK-

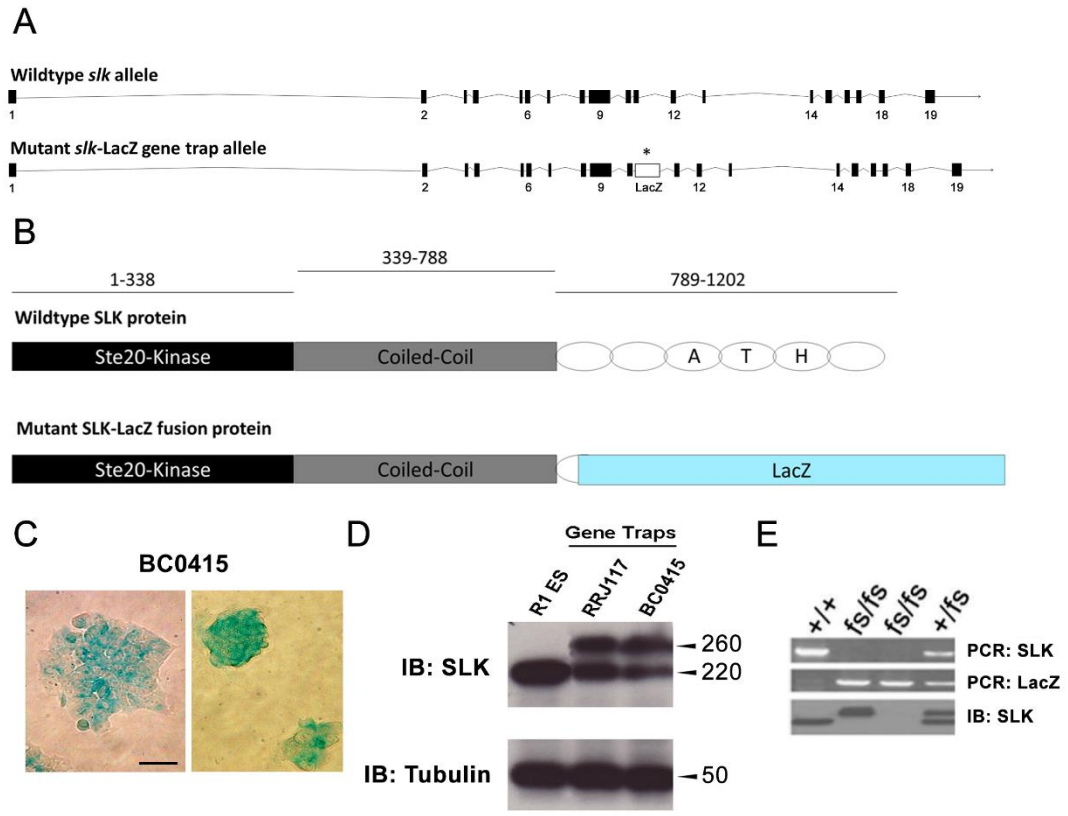

Figure 3.1. Generation of an SLK-targeted gene trap. (A) Schematic representation of endogenous *Slk* and BCO415 SLK-targeted gene trap construct. The BCO415 construct was purchased from the Wellcome Trust Sanger Institute, NIH. A β-Geo cDNA was inserted downstream of SLK exon 10 and validated by 5'RACE analysis. **(B)** Schematic representation of endogenous SLK and SLK-LacZ fusion protein. Insertion of LacZ downstream of exon 10 results in the production of an in frame, functional SLK-LacZ fusion protein. This fusion kinase lacks most of the C-terminal ATH region but contains the catalytic kinase domain. **(C)** Validation of SLK-LacZ fusion protein expression in embryonic stem cells. Cells were stained with X-gal and representative images were taken with (left) and without (right) feeder cells. **(D)** Total cell lysates from control (R1 ES), BCO415 and RRJ117 (an additional SLK-targeted gene trap construct) were analyzed for SLK-LacZ fusion protein expression. Both gene traps show expression of the higher molecular weight SLK-LacZ fusion protein (260 kDa) and endogenous SLK protein (220 kDa), whereas R1 ES cells only express endogenous SLK protein. **(E)** Polymerase chain reaction and Western blot analysis on genomic DNA and whole embryo lysate of E10.5 embryos showing the various combinations of SLK-LacZ genotype and protein expression patterns. Scale bar = 25 μm. Figure was adapted from (207).

LacZ fusion protein retains the N-terminus and contains both the catalytic and coiled-coil domains but lacks the C-terminal ATH domain due to the insertion of the LacZ cassette.

To confirm expression of the SLK-LacZ fusion protein within the BCO415 embryonic stem cell line, X-gal staining was performed with and without a feeder layer of irradiated fibroblasts (Figure 3.1. C). X-gal staining was selective to the BCO415 embryonic stem cells and no staining was observed on the feeder layer, suggesting that the SLK-LacZ fusion protein is highly and selectively expressed in the embryonic stem cells. Western blot analysis for endogenous and LacZ-fusion SLK was performed on R1, RRJ117 and BCO415 embryonic stem cells (Figure 3.1. D). Both gene-trapped lines express equal amounts of the wildtype and LacZ-fusion SLK validating that the in frame splicing between exon 10 and the LacZ cassette generate a stable protein product. The BCO415 clone was used for blastocyst injections and the subsequent production of chimeric mice.

Following germline transmission, the BCO415 line was crossed into an FVB/N background and embryos were collected at embryonic day (E) 10.5 for genotyping and proteotyping. At E10.5 the mice were genotyped for the presence of the wildtype *Slk* allele (primers span the LacZ cassette insertion site) or LacZ cDNA. Presence of the gene-trapped LacZ-fusion allele was given the designation "fs". Wildtype ($SLK^{+/+}$) mice genotype positive for wildtype SLK and negative for LacZ, heterozygote ($SLK^{+/fs}$) mice genotype positive for both wildtype SLK and LacZ and homozygous ($SLK^{fs/fs}$) mice genotype negative for endogenous SLK and positive for LacZ (Figure 3.1. E). Surprisingly, proteotyping of $SLK^{fs/fs}$ E10.5 embryos by Western blot analysis revealed that only about half of those embryos expressed any detectable levels of the SLK-LacZ fusion (Figure 3.1. E).

Our lab has previously shown that SLK is preferentially expressed in the neuronal and skeletal muscle lineages of the developing embryo (19,195,196). To validate these findings

and further characterize SLK expression in the developing embryo, we performed X-gal staining and β-galactosidase histochemistry on $SLK^{+/fs}$ embryos. Embryos were harvested by caesarian section at either E12.5 or E14.5 and fixed in 10% formalin for either whole mount staining or paraffin embedded sectioning. As previously described for endogenous SLK (19,195,196), whole mount X-gal staining of $SLK^{+/fs}$ E12.5 embryos showed high levels of SLK-LacZ fusion protein in the developing limb buds, forebrain, eyes and dorsal root ganglia (Figure 3.2. A, B). Similarly, anti-β-galactosidase immunohistochemistry of E14.5 paraffin sections shows high expression of SLK-LacZ fusion protein in the eye, epidermis, muscle, cartilage, bone and fetal liver (Figure 3.2. C-G).

3.3. Homozygous expression of the *Slk* gene-trapped allele is embryonic lethal.

To assess any development defects in the BCO415 line, the mice were bred to homozygosity. Heterozygote mating pairs were set up and pups were weaned at postnatal day (P) 21. Interestingly, no $SLK^{fs/fs}$ homozygote pups were seen at weaning (n=106 pups) suggesting that homozygous expression of the *Slk* gene-trapped allele is lethal (Figure 3.3. A). As no death of pups was observed between litter birth and weaning, we concluded that homozygous expression of the *Slk* gene-trap was embryonic lethal.

To further investigate the apparent embryonic lethality in our model, timed mating pairs of heterozygotes were set up. Embryos were collected from these timed matings at E10.5, E12.5 and E14.5 (n=38, 69 and 112, respectively). A hind limb from each embryo was removed for genotyping and a normal Mendelian distribution of $SLK^{+/+}$, $SLK^{+/fs}$ and $SLK^{fs/fs}$ embryos was observed across all three gestational time points (Figure 3.3. A). Despite observing $SLK^{fs/fs}$ embryos across all the gestational timepoints, severe morphological defects were detected approximately 40% of the time at E12.5 and in all the E14.5 embryos (Figure 3.3. B). Additionally, no $SLK^{fs/fs}$ embryos could be detected at E16.5 within the uterus, and

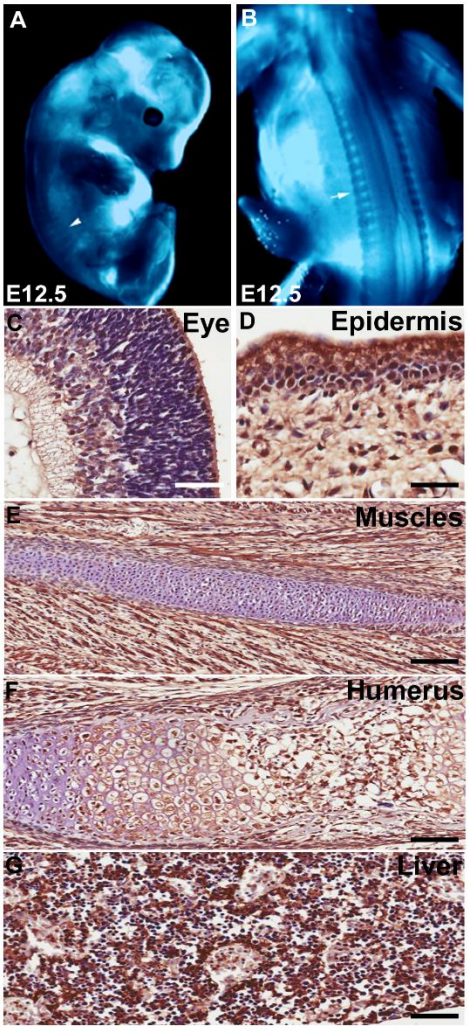

Figure 3.2. SLK is expressed in the developing embryo. (A) E12.5 $SLK^{+/fs}$ embryos were harvested by caesarean section and stained with X-gal. A lateral view of the stained embryo reveals a high level of SLK expression in the limb buds (arrow), forebrain and myotome (arrowhead). **(B)** A dorsal view of the embryo shows high level of SLK expression in the dorsal root ganglia (white arrow). **(C-G)** E14.5 $SLK^{+/fs}$ embryos were harvested by caesarean section, fixed and paraffin embedded. LacZ immunohistochemistry was performed and the eye (C), epidermis (D), muscle (E), bone (F) and liver (G) all reveal a high level of SLK-LacZ fusion protein expression. Scale bar = 50 μm in (C, D); 100 μm in (E-G). Figure was adapted from (207).

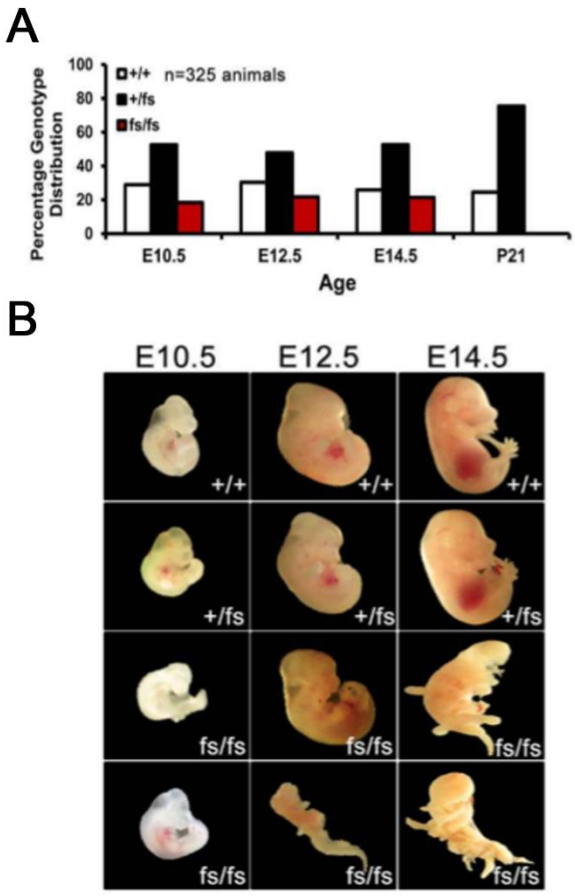

Figure 3.3. Homozygous SLK-LacZ fusion protein expression is embryonic lethal. (A) Timed matings of $SLK^{+/fs}$ male and female animals were collected at E10.5, 12.5, 14.5 or post-natal day 21 (P21). Tail (embryos) or ear (weanlings) clips were digested and used for genotyping. Normal Mendelian ratios of all three genotypes were observations at all three gestational timepoints. However, no $SLK^{fs/fs}$ pups were seen at weaning. A total of 325 animals were genotyped across all four time points. **(B)** Embryos were photographed after being harvested. Approximately 40% of $SLK^{fs/fs}$ embryos displayed severe morphological defects at E12.5, while all $SLK^{fs/fs}$ embryos at 14.5 were showing severe morphological defects and signs of resorption. Figure was adapted from (207).

complete resorption of these embryos could be detected at each implantation site (assessed by an empty amniotic sac with no discernable embryo) by this timepoint. These data suggest that an embryonic lethality is occurring asynchronously in the $SLK^{fs/fs}$ embryos between E10.5 and E14.5.

3.4. SLK-LacZ fusion protein has reduced kinase activity.

One possibility for the embryonic lethality observed in the $SLK^{fs/fs}$ embryos is that the SLK-LacZ fusion protein product has aberrant kinase activity or is unable to recognize substrate, given that the C-terminal ATH domain has been shown to be essential for binding of necessary co-factors to SLK (208,209). Therefore, we measured the kinase activity of the SLK-LacZ fusion protein *in vitro*. E12.5 embryos were collected and SLK kinase activity was assayed by immunoprecipitation and incubation with purified Histone H1 as a substrate in the presence of [^{32}P]γATP (Figure 3.4.). SLK kinase activity towards Histone H1 was reduced by approximately 60% in $SLK^{+/fs}$ embryos and 80% in $SLK^{fs/fs}$ embryos, suggesting that the SLK-LacZ fusion protein cannot efficiently phosphorylate exogenous substrate resulting in a hypomorphic phenotype. This reduction in substrate phosphorylation is likely due to either steric hinderance of the LacZ domain or tetramerization of the SLK-LacZ fusion protein (as opposed to the normal dimerization of endogenous SLK), both of which would prevent efficient substrate access.

3.5. Homozygous expression of the *Slk* gene-trapped allele results in severe muscular and neuronal defects within the developing embryo.

The first signs of developmental defects within the developing $SLK^{fs/fs}$ embryos arose when approximately half of these embryos at E12.5 had no discernable expression of the SLK-LacZ fusion protein (Figure 3.1. E). Interestingly, embryos which lacked any expression of the SLK-LacZ fusion protein were those that presented with the most pronounced gross

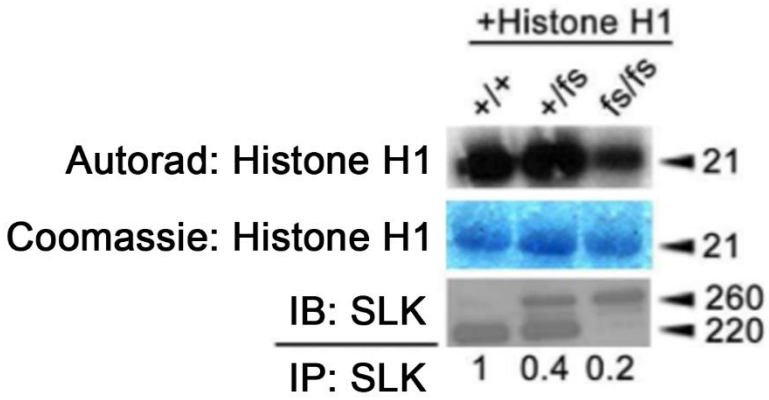

Figure 3.4. The SLK-LacZ fusion protein is unable to efficiently phosphorylate substrate. Total embryo lysates were collected from E12.5 embryos and SLK kinase activity was assayed by immunoprecipitation and *in vitro* phosphorylation of recombinant Histone H1. Relative Histone H1 phosphorylation levels (shown below each lane) were determined after normalization to total Histone H1 (Coomassie) and total SLK (blot). Figure was adapted from (207).

morphological defects (Figure 3.3. B). One possible explanation for the loss of SLK-LacZ fusion protein within $SLK^{fs/fs}$ embryos is that these embryos are actively being resorbed, which is ultimately coupled with a significant amount of protein degradation. To further assess this possibility, protein lysates from E10.5, E12.5 and E14.5 embryos were probed for several cytoskeletal proteins, including paxillin, FAK, ERM and α-tubulin. $SLK^{fs/fs}$ embryos showed reduced or undetectable levels of these cytoskeletal proteins when compared to either $SLK^{+/+}$ or $SLK^{+/fs}$ controls (Figure 3.5.). Importantly, the loss of cytoskeletal proteins within the $SLK^{fs/fs}$ embryos becomes more severe as the gestational age increases and directly correlates with embryos that present with major morphological defects (Figure 3.5.).

As SLK has been shown to be highly expressed in the muscular and neuronal lineages of the developing embryo (19,195,196), we aimed to assess potential developmental defects within these compartments. As most embryos did not present with any gross morphological defects at E10.5, we began our analysis at this gestational timepoint. Early muscle masses were analyzed by anti-myosin heavy chain (MHC; MF20) immunohistochemistry, however, no obvious defects were observed in the E10.5 $SLK^{fs/fs}$ embryos (Figure 3.6. A, B). Next, we assessed the neuronal compartment and observed a marked decrease in the size of the neural tube by Tuj1 histochemistry within the $SLK^{fs/fs}$ embryos at E10.5 (Figure 3.6. C, D). As SLK is required for cell cycle progression (36), it is possible that the neuronal precursor population may fail to expand resulting in a reduced number of differentiated neurons and ultimately a smaller neuronal compartment. The failure to observe similar defects in the early myotome may be due to different thresholds of SLK activity being required in neuronal tissue. Alternatively, early myogenic precursors may not require SLK activity for growth and differentiation.

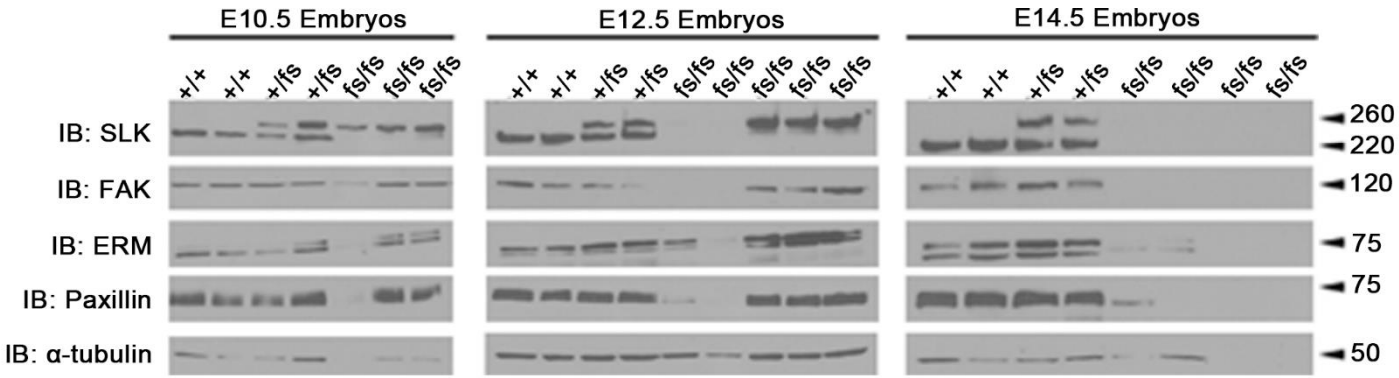

Figure 3.5. Degradation of major cytoskeletal components is observed in SLK$^{fs/fs}$ embryos by E14.5. Total embryo extracts were probed for the expression of major cytoskeletal components including FAK, ERM, paxillin and tubulin. These embryos have lost expression of these markers between E12.5 and E14.5 corresponding to the period of observed embryonic lethality. Figure was adapted from (206).

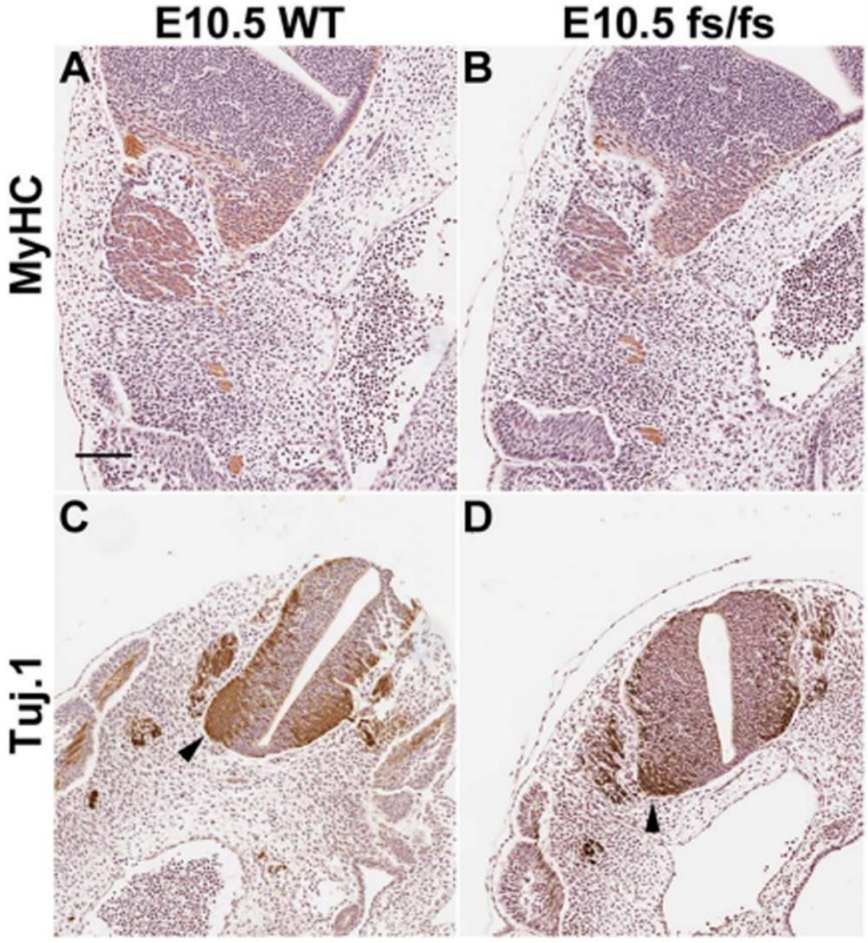

Figure 3.6. Defects in the neuronal compartments in SLK$^{fs/fs}$ embryos at E10.5. (A, B) Myosin Heavy Chain (MyHC) immunohistochemistry was performed on E10.5 embryo sections. No appreciable differences in the size or structure of the myogenic compartment between wildtype and SLK gene-trapped mice could be observed at this timepoint. **(C, D)** Tuj1 immunohistochemistry was performed on E10.5 embryo sections and the posterior neural tube was analyzed. A smaller neural compartment is observed in the SLK$^{fs/fs}$ embryos (black arrow). Scale bar = 100 μm. Figure was adapted from (207).

Although approximately 40% of $SLK^{fs/fs}$ embryos at E12.5 presented with severe morphological defects, haematoxylin and eosin (H&E) staining of all E14.5 revealed marked defects in the brains, eyes, muscles, viscera and limbs with differentiated cells being detected but showing a marked developmental delay and aberrant structural organization (Figure 3.7. A-D). Using MHC and Tuj1 as markers, we further characterized the defects within the muscular and neuronal compartments, respectively, at these later gestational timepoints. Analysis of the myogenic compartment showed organized clusters of myofibers within the intercostal area of $SLK^{+/+}$ embryos at E12.5 that expanded in E14.5 embryos (Figure 3.7. E, G). Conversely, $SLK^{fs/fs}$ embryos at E12.5 displayed a smaller and less structured myogenic compartment with MHC-positive cells scattered throughout the ribcage (Figure 3.7. F). By E14.5, the MHC-positive myofibers were very sparse and completely unstructured (Figure 3.7. H). Although the Tuj1-positive neuronal compartment was smaller in $SLK^{fs/fs}$ embryos at E12.5 (Figure 3.7. H), significant degeneration of these compartments could be observed by E14.5 (Figure 3.7. L, P). Whereas $SLK^{+/+}$ embryos started to display Tuj1-positive dorsal root ganglia which were well-organized and patterned between vertebrae, $SLK^{fs/fs}$ embryos displayed spatially disorganized Tuj1-positive cell clusters which aligned in a dorsoventral pattern with the vertebrae (Figure 3.7. Q-T).

In addition to observing defects in the myogenic and neuronal compartments of the developing embryos, we also observed a marked reduction in the overall size and cellularity of $SLK^{fs/fs}$ embryos compared to their littermates starting at E12.5. Quantification of the total cell number by H&E staining of paraffin sections revealed a 33% reduction in the number of cells within $SLK^{fs/fs}$ embryos when compared to $SLK^{+/+}$ littermates at E12.5 (Figure 3.8. A). Supporting the observations that $SLK^{fs/fs}$ embryos are being resorbed and display extensive protein degradation, propidium iodide staining of single cell suspensions from $SLK^{fs/fs}$

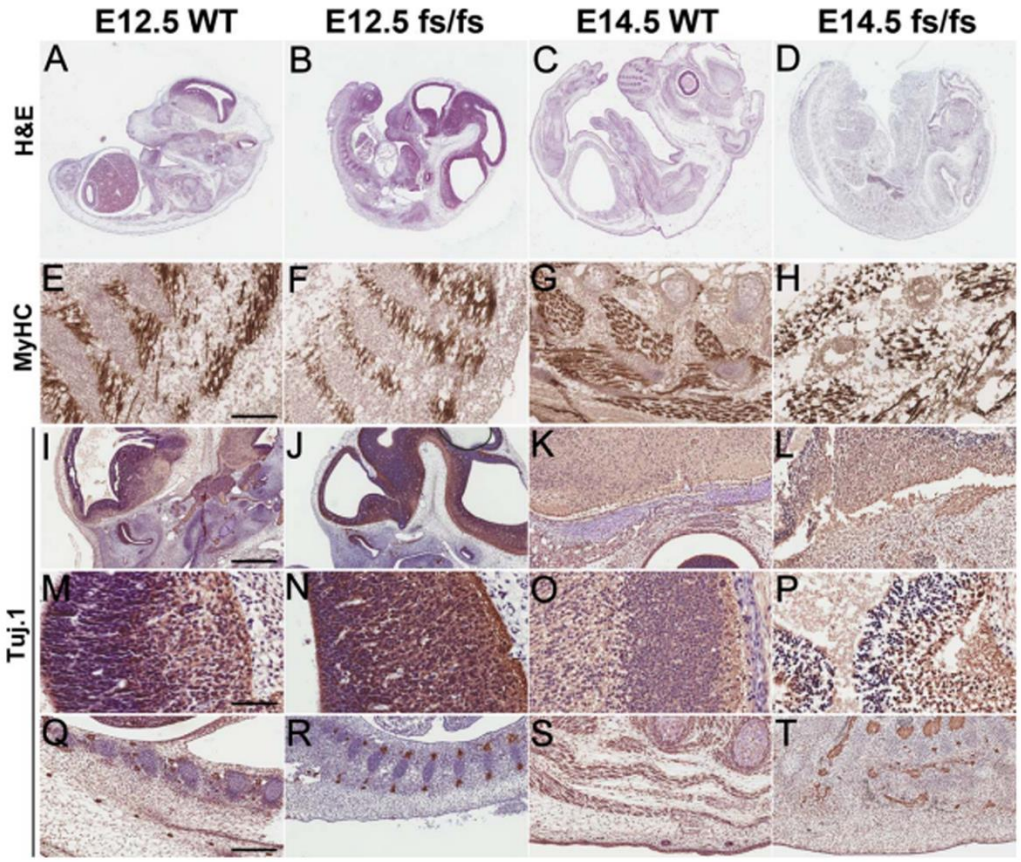

Figure 3.7. Defects in the myogenic and neuronal compartments in SLK$^{fs/fs}$ embryos at E12.5 and E14.5. (A-D) Hematoxylin and Eosin staining was performed on E12.5 and E14.5 embryo sections. As approximately 40% of SLK$^{fs/fs}$ embryos at E12.5 present with a severe phenotype (see Fig. 3.3.), a representative embryo of a moderate phenotype is shown. Marked defects in the SLK$^{fs/fs}$ embryos can be observed in the brain, eyes, muscles, viscerae and limbs. **(E-H)** Myosin Heavy Chain (MyHC) immunohistochemistry was performed on embryo sections. A less structured myogenic compartment was observed throughout the ribcage of SLK$^{fs/fs}$ embryos at E12.5, becoming very sparse and completely unstructured by E14.5. (**I-L)** Tuj1 immunohistochemistry was performed on embryo sections. Significant degeneration and a significant decrease in Tuj1-positive cells was observed in SLK$^{fs/fs}$ embryos at E14.5. **(M-P)** High magnification from panels I-L. **(Q-T)** Tuj1 immunohistochemistry is shown along the vertebral axis and dorsal root ganglia. SLK$^{fs/fs}$ embryos display spatially disorganized Tuj1-positive cell clusters and very little expansion of the dorsal root ganglia at both E12.5 and E14.5. Scale bar = 50 μm in E-H, M-P; 100 μm in I-L, Q-T. Figure was adapted from (207).

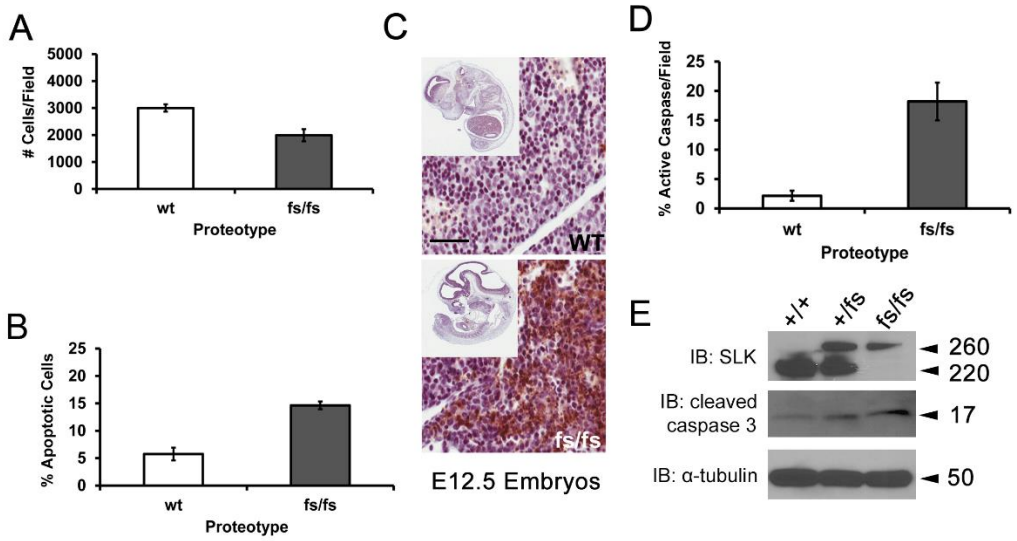

Figure 3.8. Reduced cellularity and increased apoptosis within SLK$^{fs/fs}$ embryos. (A) Hematoxylin and Eosin staining was performed on E12.5 embryo sections and the total number of nuclei was counted from five independent embryos per genotype. Three random fields of view were averaged per embryo. A 33% reduction in total cellularity was observed in the SLK$^{fs/fs}$ embryos. **(B)** E12.5 embryos were disaggregated into single cell suspensions and stained with propidium iodide. Three embryos per genotype were analyzed by flow cytometry and the percentage of apoptotic cell is represented. A three-fold increase in the percentage of apoptotic cells was observed in SLK$^{fs/fs}$ embryos. **(C)** Cleaved caspase 3 immunohistochemistry was performed on E12.5 embryo sections and a representative field of view from both genotypes is shown (n=5 embryos/genotype). **(D)** The total percentage of cleaved caspase 3-positive cells from each random field of view were scored from the staining performed in (C). A significant increase in the percentage of cleaved caspase 3 was observed in SLK$^{fs/fs}$ embryos. **(E)** Total embryo lysates from E12.5 embryos were probed for cleaved caspase 3 with SLK$^{fs/fs}$ embryos showing an increase. Scale bar = 50 μm. P-value < 0.05 for A, B and D. Figure was adapted from (207).

embryos revealed a three-fold increase in the number of apoptotic cells compared to $SLK^{+/+}$ embryos at E12.5 (Figure 3.8. B). This increase in apoptosis was confirmed by Western blot analysis and immunohistochemistry for cleaved caspase 3 (Figure 3.8. C-E). Taken together, these data suggest that SLK plays an important role in embryonic development, patterning and the maintenance/expansion of multiple embryonic compartments, which cannot be compensated for by the SLK-LacZ fusion protein.

3.6. Homozygous expression of the *Slk* gene-trapped allele results in abnormal placental differentiation and vascularization.

Proper placental development and perfusion is critical required for normal embryonic development (202,210). Furthermore, the observed increased in neuronal size in several of the smaller $SLK^{fs/fs}$ embryos would support potential placental defects as previously reported (211). To gain further insight into the mechanisms underlying the embryonic lethality, we analyzed the placentae at E12.5 and E14.5. The placenta is comprised of three distinct layers: the maternal tissue, junctional zone and labyrinth (202), and all of the placentae across genotypes and gestational timepoints displayed all three layers (Figure 3.9. A-D).

Although all three placental layers were identifiable, $SLK^{fs/fs}$ placentae at E12.5 had labyrinth tissue that was hypovascular and devoid of fetal blood as evidenced by a significant reduction in eosin-positive staining (Figure 3.9. E, F). Similarly, smooth muscle actin histochemistry of $SLK^{fs/fs}$ placentae at E12.5 revealed the presence of thin-walled and enlarged vasculature compared to $SLK^{+/+}$ placentae which have completely collapsed by E14.5 (Figure 3.9. M-P). Additionally, hemorrhaging and pooling of maternal blood is readily observed around the periphery of the labyrinth in $SLK^{fs/fs}$ placentae at both E12.5 and E14.5 further supporting the hypothesis that these tissues are hypovascular (Figure 3.9. A-D). As expression of the SLK-LacZ fusion protein results in placental vascular defects, we also analyzed the

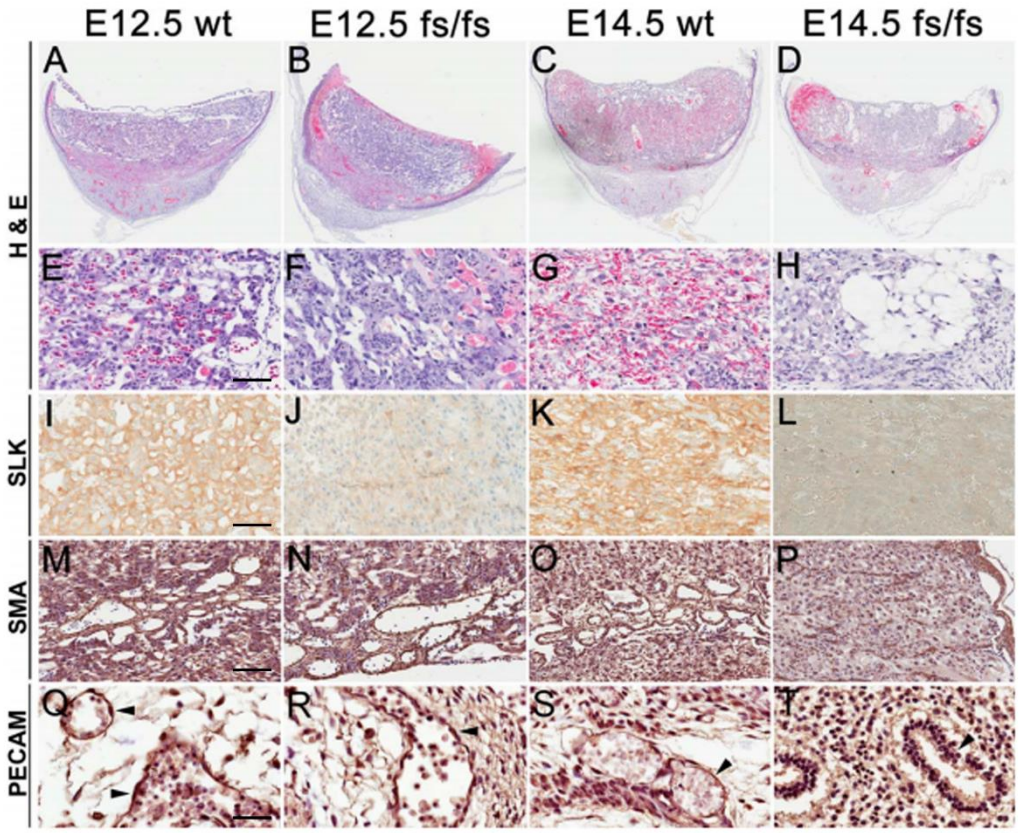

Figure 3.9. Abnormal differentiation and vascularization in the SLK$^{fs/fs}$ placentae. (A-D) Hematoxylin and Eosin staining was performed on E12.5 and E14.5 placental sections. The maternal tissue, junctional zone and labyrinth were readily detectable in both genotypes at both gestational timepoints. Hemorrhaging of fetal blood around the outside of SLK$^{fs/fs}$ placentae was observed. **(E-H)** Representative images of labyrinth tissue, showing proper perfusion of fetal blood throughout SLK$^{+/+}$ but not SLK$^{fs/fs}$ placentae at both E12.5 and E14.5. **(I-L)** SLK histology was performed on placental sections. Reduced SLK staining was observed throughout the labyrinth of SLK$^{fs/fs}$ placentae. **(M-P)** Smooth muscle actin (SMA) histology was performed on placental sections. Abnormal vascularization was observed in SLK$^{fs/fs}$ placentae at E12.5 which results in complete vessel collapse by E14.5. **(Q-T)** For comparison, whole embryo sections were stained with PECAM to detect the presence of blood vessels (arrowheads). Apparently normal vasculature was observed in SLK$^{fs/fs}$ embryos at E12.5, however, SLK$^{fs/fs}$ embryos at E14.5 were devoid of any PECAM-positive vasculature. Scale bar = 50 μm in E-L, Q-T; 100 μm in M-P. Figure was adapted from (207).

vasculature in $SLK^{+/+}$ and $SLK^{fs/fs}$ embryos. Immunohistochemistry for PECAM shows normal vasculature in $SLK^{+/+}$ embryos at E12.5 and E14.5 characterized by well defined PECAM-positive blood vessels containing circulating blood cells (Figure 3.9. Q, S). Similarly, $SLK^{fs/fs}$ embryos at E12.5 displayed apparently normal vasculature (Figure 3.9. R). However, structures reminiscent of collapsed blood vessels could be observed in $SLK^{fs/fs}$ embryos at E14.5, although PECAM-positive structures could not be detected. These data suggest that the placental defects ultimately result in vascular collapse and death in developing embryos.

Coupled with the abnormal vasculature, the labyrinth tissue also appeared to be less differentiated in the $SLK^{fs/fs}$ placentae. At E12.5, $SLK^{fs/fs}$ placentae did not contain the typical syncytiotrophoblast morphology which should be apparent at this timepoint (Figure 3.9. E, F). A similar phenotype was also observed in the E14.5 placentae, although a larger proportion of acellular lesions were observed (Figure 3.9. G, H). Of interest, the observed defects within the placentae were localized to the junctional zone and labyrinth but not the maternal tissue suggesting that these phenotypes are of an embryonic origin. Remarkably, immunostaining for SLK was absent in junctional zone and labyrinth of all $SLK^{fs/fs}$ placentae starting at E12.5 (Figure 3.9. I-L), which contrasts with the 50% of embryos that have lost expression at the same gestational timepoint. This suggests that the developmental defects observed in the placenta precede those in the embryo and that proper expression and/or regulation of SLK activity is required for both placental and embryonic development.

3.7. Homozygous expression of the *Slk* gene-trapped allele reduces cellular proliferation *in vitro*.

Our lab has previously shown that SLK is required for proper cell cycle progression and proliferation (36). Therefore, one possibility for the decreased cellularity observed in the $SLK^{fs/fs}$ embryos (Figure 3.8. A) could be due to a reduction in cellular proliferation in addition

to the increase in apoptosis (Figure 3.8. B-E). To test this hypothesis, primary mouse embryonic fibroblasts (MEFs) were isolated from E12.5 embryos of all three genotypes and subject to *in vitro* proliferation assays. As previously reported for cells overexpressing a dominant negative SLK construct (36), direct counts over time revealed that $SLK^{fs/fs}$ MEFs grew significantly slower than $SLK^{+/+}$ MEFs (Figure 3.10. A). Interestingly, we observed an intermediate phenotype with $SLK^{+/fs}$ MEFs suggesting a dose dependence for SLK expression in regulating cellular proliferation (Figure 3.10. A). However, no differences in cell viability could be observed across the three genotypes, as measured by trypan blue uptake (Figure 3.10. B). This suggests that the decreased growth rate observed in the $SLK^{fs/fs}$ MEFs is not a direct result of a reduction in cell viability. Furthermore, it is likely that the increased cell death observed within the $SLK^{fs/fs}$ placentae and embryos is likely due to impaired placental vascularization rather than apoptosis induced by an absence of functional SLK.

3.8. *Slk* knockdown impairs capillary morphogenesis *in vitro*.

Our lab has previously reported that SLK activity is required for cellular migration and efficient focal adhesion turnover (40,41,49). As the process of placental vascularization requires efficient cellular migration (212), we hypothesized that homozygous expression of the SLK-LacZ fusion protein within the endothelial cells of the placenta impairs their angiogenic properties. To test whether these defects were cell autonomous, we assessed whether knockdown of *Slk* in mouse dermal microvascular endothelial cells (MDMECs) would impair capillary morphogenesis *in vitro*. Knockdown of *Slk* within MDMECs resulted in approximately 60% less protein expression than the non-targeting control (Figure 3.11. A). Following knockdown, MDMECs were plated on Matrigel and assayed for capillary formation (199). When compared to non-targeting controls, *Slk* knockdown significantly impaired the number of capillaries and branching (Figure 3.11. B, C). Combined with our *in vivo*

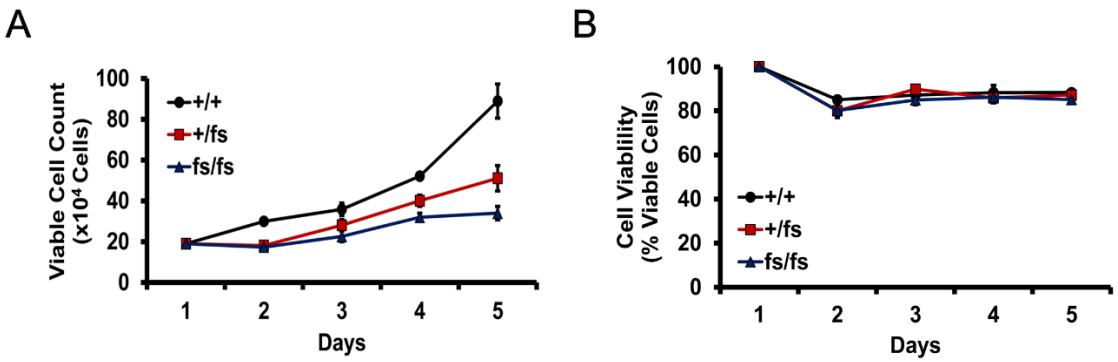

Figure 3.10. Catalytic activity of SLK is required for cellular proliferation *in vitro*. (A) Mouse embryonic fibroblasts (MEFs) were established from E12.5 embryos (three independent embryos were used per genotype). $2x10^5$ cells were plated in triplicate and the number of viable cells were counted daily by trypan blue exclusion. $SLK^{+/fs}$ and $SLK^{fs/fs}$ MEFs show reduced proliferation as compared to $SLK^{+/+}$ MEFs. P-value < 0.05 between all three genotypes. **(B)** Cell viability was determined by trypan blue exclusion over the proliferation timecourse. No differences between any of the three genotypes was observed. Figure was adapted from (207).

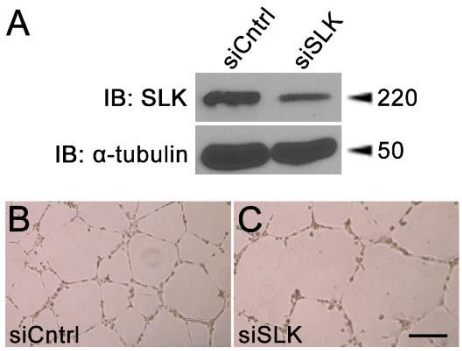

Figure 3.11. SLK is required for endothelial cell branching *in vitro*. (A) Mouse dermal microvascular endothelial (MDME) cells were treated with siCntrl or siSLK for 48 hours. Cells were harvested and assessed for efficient SLK knockdown by Western blot. **(B, C)** MDME cells that were treated with siCntrl or siSLK were subject to capillary morphogenesis assay for 24 hours. Cells treated with siSLK showed a reduced ability to form capillaries on Matrigel. Scale bar = 25 μm. Figure was adapted from (207).

observations showing reduced vascularization within the labyrinth of $SLK^{fs/fs}$ placentae, these *in vitro* capillary morphogenesis assays support a role for SLK in regulating efficient angiogenesis.

3.9. Homozygous deletion of SLK is preimplantation lethal.

Although the *Slk* targeted gene trap provides an interesting insight into the possible roles for SLK during embryonic development, some of the observed effects may be attributed to the in-frame splicing event and the expression of LacZ at the C-terminus of SLK. LacZ has been shown to tetramerize (213), whereas SLK dimerization is required for efficient substrate phosphorylation (214). Therefore, it is possible that the observed embryonic lethality occurs due to the aberrant function of a tetrameric SLK-LacZ fusion protein and this may not be the case for a global knockout. Our lab has recently generated a conditional SLK knockout mouse (198), which can be used to assess whether global deletion of SLK is embryonic lethal.

To assess the effects of global SLK deletion on embryonic development, we crossed our conditional SLK knockout mice with β-actin-Cre transgenic mice (Figure 3.12. A). The β-actin-Cre transgenic mice allow for expression of Cre recombinase under the control of the β-actin promoter and is therefore expressed at E0.5 in all embryonic cells before the blastocyst stage. Timed matings of $SLK^{+/fl}$ β-actin-Cre were established and weanlings were genotyped at weaning. Interestingly, the total number of weanlings were not significantly reduced in these crosses compared to that of control FVB/N matings (Figure 3.12. B). Despite the apparently normal litter sizes from these matings, no homozygote SLK-null animals were genotyped in a total of 116 weanlings (Figure 3.12. C). One possibility for these observations is that $SLK^{-/-}$ embryos did not implant in the uterine lining at the blastocyst stage. In support of the possibility that $SLK^{-/-}$ blastocysts failed to implant, uterine horns of pregnant $SLK^{+/fl}$ β-actin-

A

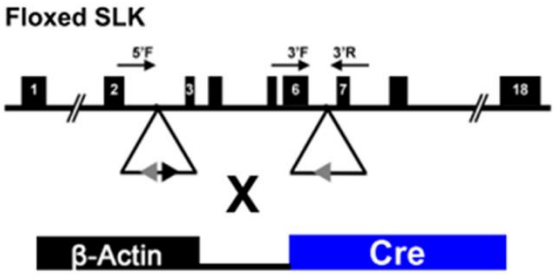

B

	Actual	Expected
Wildtype ($SLK^{+/+}$)	36	29
Heterozygote ($SLK^{+/-}$)	80	58
Knockout ($SLK^{-/-}$)	0	29

Figure 3.12. Conditional SLK deletion at E0.5 results in embryonic lethality. (A) Schematic representation of the conditional *Slk* allele which was crossed into β-actin-Cre transgenic mice. **(B)** Timed matings of $SLK^{+/fl}$ β-actin-Cre male and female animals were collected at post-natal day 21. Ear clips were digested and used for genotyping. No viable SLK knockout pups were found at weaning despite apparently normal litter sizes suggesting that $SLK^{-/-}$ blastocysts had failed to implant in the uterine lining.

Cre females were assessed for signs of resorption at 12.5 days of pregnancy and no signs of resorption could be identified.

3.10. Summary.

Proper embryonic development is regulated by multiple signaling networks which when altered can result in severe developmental defects and lethality. Although SLK is highly expressed in the neuronal and muscular lineages of the developing embryo (19,195,196), little is known about its specific function in the development of these organs. Using a gene-trapped *Slk* allele, we have shown that the activity of the SLK-LacZ fusion protein generated by the SLK gene trap is markedly reduced. This results in proliferative and angiogenic defects in the fetal placenta, leading to an embryonic lethal phenotype. However, marked developmental defects were also observed in the myogenic and neuronal compartments, suggesting an important role for SLK in the development of those structures. Lastly, homozygous deletion of SLK at E0.5 also results in an embryonic lethality further supporting an important role for SLK in early development.

Chapter 4

Conditional deletion of *Slk* in Neu-induced mammary tumors results in an accelerated tumor onset.

4.1. Introduction and Rationale.

Previously, our lab and others have shown that SLK plays an important role in regulating cellular proliferation, focal adhesion turnover and apoptosis (14,18,20,36,40,49). Furthermore, we have shown that SLK is catalytically activated downstream of Neu and requires proper docking of either PI3K or PLCγ to the cytoplasmic domain of Neu for maximal activation (114). Overexpression of dominant negative SLK in NMuMG cells expressing constitutively active Neu significantly impaired heregulin-stimulated cellular migration and invasion (114). Recently, SLK has been discovered to play an important role in regulating TGFβ-mediated EMT (52,53). Knockdown of SLK in NMuMG cells significantly delayed the breakdown of both E-cadherin and ZO-1 positive junctions following TGFβ treatment, suggesting that loss of SLK promotes a more epithelial morphology (52,53).

As SLK is activated downstream of Neu in a PI3K/PLCγ dependent manner (114), is required for Neu-driven cell motility (114) and functions to promote TGFβ-mediated EMT (52,53) we sought to assess the role of SLK in regulating Neu-induced mammary tumorigenesis *in vivo*. Given these previously defined roles for SLK in mammary epithelial cells, we hypothesized that conditional SLK deletion in Neu-positive mammary tumors would significantly delay tumor onset and increase overall survival in a murine model of the HER2 subtype.

4.2. Conditional deletion of *Slk* does not impair virgin mammary gland development.

Prior to assessing the role of SLK in Neu-induced mammary tumorigenesis, we first assessed whether SLK deletion in the luminal mammary epithelium results in any developmental defects. To test this, we crossed conditional SLK knockout mice (198) with MMTV-Cre transgenic mice expressing a Rosa26R-LacZ reporter. In this model, Cre recombinase is under the control of the mouse mammary tumor virus (MMTV) promoter,

which is primarily expressed in the luminal epithelial compartment starting at embryonic day 8.5 (90,92). Mammary glands from $SLK^{+/+}$ and $SLK^{fl/fl}$ MMTV-Cre Rosa26R-LacZ mice at 10 weeks of age were harvested, subjected to X-gal staining and either wholemounts or paraffin-embedded blocks were prepared. X-gal stained mammary wholemounts revealed no significant difference in gross morphology or ductal architecture, number of terminal end buds or ductal branch points, suggesting that SLK deletion does not have a significant impact on virgin mammary gland development (Figure 4.1.).

4.3. Conditional deletion of *Slk* accelerates Neu-induced mammary tumor initiation.

As we have previously reported that SLK is activated downstream of Neu and is required for TGFβ-mediated EMT (52,114) we hypothesized that SLK deletion in a Neu-induced mammary tumor model would significantly delay tumorigenesis. To assess the effect of SLK deletion on Neu-induced mammary tumorigenesis, we crossed conditional SLK knockout mice with MMTV-NIC transgenic mice (Figure 4.2.). The NIC model expresses the constitutively active Neu oncogene linked to Cre recombinase by an internal ribosomal entry sequence which effectively couples oncogene expression to Cre mediated recombination. Additionally, these tumors form mammary adenocarcinomas that histologically resemble human HER2-positive tumors (90).

To assess the role of SLK in Neu-induced mammary tumorigenesis, mice were palpated biweekly to assess mammary tumor onset and endpoint. Contrary to our initial hypothesis, $SLK^{fl/fl}$ NIC mice developed tumors on average 51 days sooner than control $SLK^{+/+}$ mice (Figure 4.3. A). Consistent with the accelerated tumor onset, $SLK^{fl/fl}$ NIC mice reached endpoint with a median survival of 137 days compared to the 173 days for $SLK^{+/+}$ NIC control mice (Figure 4.3. B). Of note, the average time from tumor onset to endpoint within each group is not affected with an average time of 13 days (Figure 4.3. C). Interestingly, $SLK^{+/fl}$ NIC mice

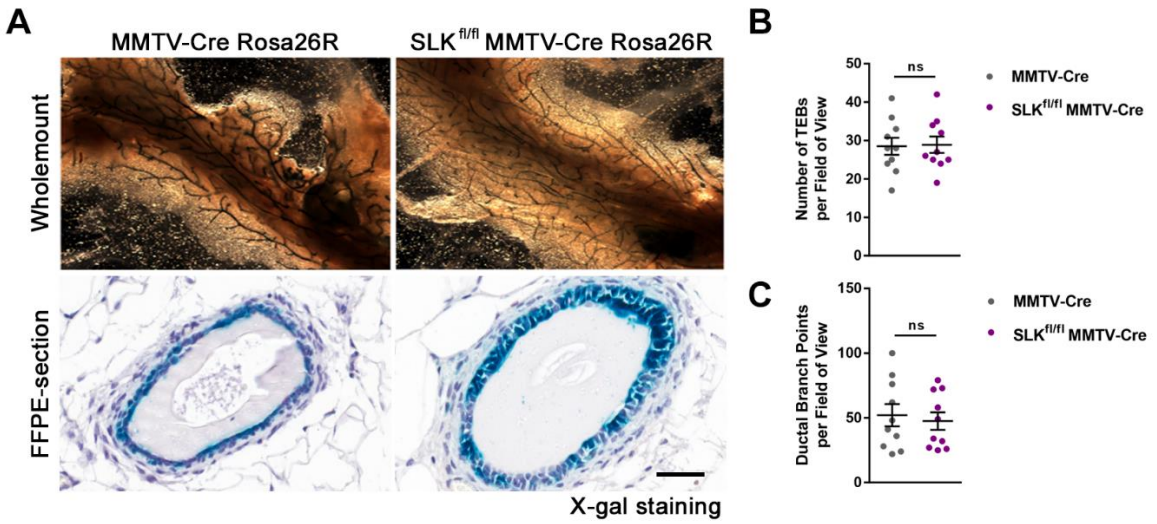

Figure 4.1. Conditional *Slk* deletion does not impair normal virgin mammary gland development. (A) Mammary glands were harvested from virgin MMTV-Cre or SLK$^{fl/fl}$ MMTV-Cre mice that were crossed into the Rosa26R reporter strain at 8-12 weeks of age (n=10 mice/genotype). Mammary glands were stained with X-gal and either wholemounts or formalin fixed paraffin embedded sections were made. Representative images of wholemounts or 4 μm cross sections are shown. **(B)** The number of terminal end buds (TEBs) per field of view were enumerated from the wholemounts in (A). **(C)** The number of ductal branch points were enumerated per field of view from the wholemounts in (A). No significant differences in the number of TEBs or ductal branch points were observed in the wholemount sections. Wholemount pictures were captured at 4x magnification. Scale bar = 25 μm.

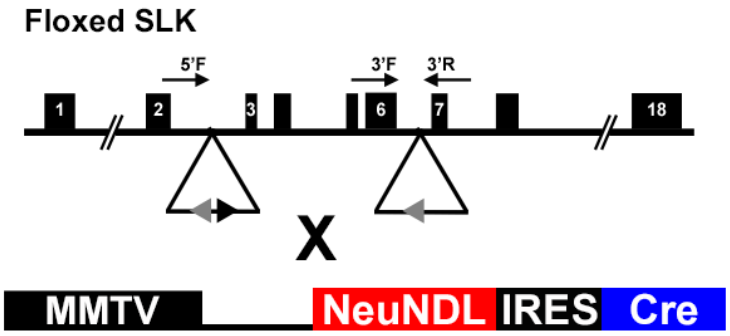

Figure 4.2. Schematic representation of the SLK$^{fl/fl}$ NIC animal model. The SLK floxed allele was generated as previously described (198) and crossed with the MMTV-NIC transgenic mice (90). The mouse mammary tumor virus (MMTV) promoter is expressed in the mammary luminal epithelium as early as embryonic day 8.5. Expression of bicistronic NeuNDL and Cre recombinase allow for coupled oncogenic expression and SLK deletion in this model.

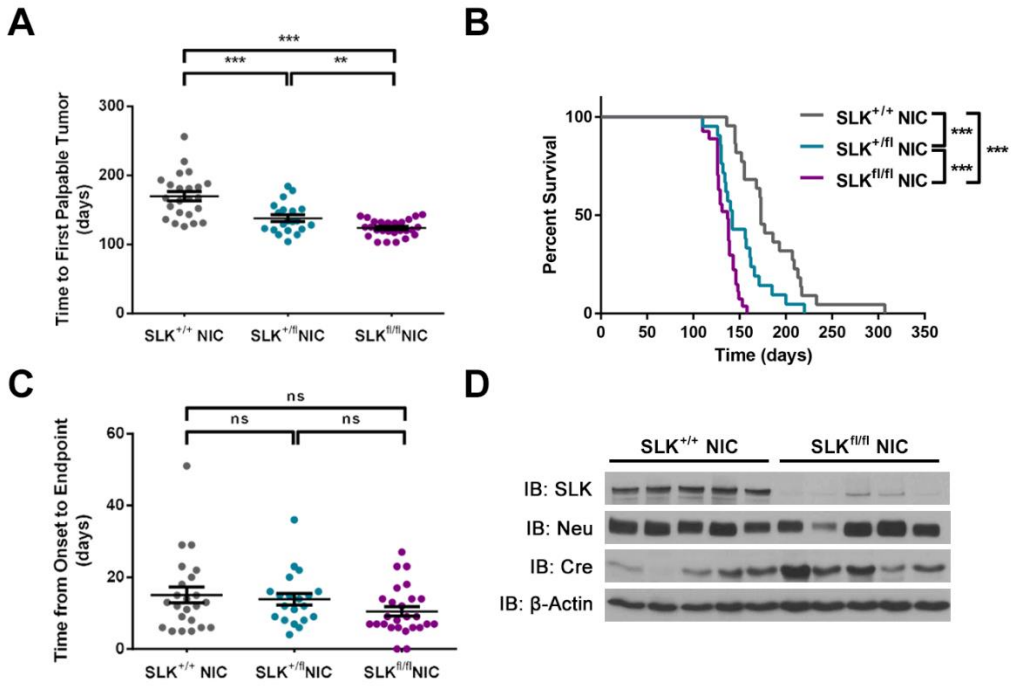

Figure 4.3. Conditional *Slk* deletion in a Neu-induced mammary tumor model significantly accelerates tumor onset and reduces overall survival. (A) Tumor bearing animals ($n \geq 20$ mice/genotype) were palpated biweekly for initial tumor formation which was defined by the initial palpation of a 0.5 cm^3 tumor. $SLK^{fl/fl}$ showed an accelerated tumor onset and developed tumors approximately 40 days faster than control mice. **(B)** Tumor bearing animals ($n \geq 20$ mice/genotype) were palpated biweekly for tumor growth and endpoint was assessed at a total cumulative tumor burden of 1.7 cm^3. A significant difference in overall survival was observed between all three genotypes. **(C)** The average time from tumor onset to endpoint for each animal was calculated. Interestingly, no differences were observed between all three genotypes suggesting that SLK deletion accelerates tumor onset but does not impact tumor progression. **(D)** Total tumor lysates (n=5 tumors/genotype) were probed for SLK, Neu and Cre to validate expression of the NIC transgene and Cre-mediated recombination of the *Slk* allele in our animal model. ** represents $p<0.005$ and *** represents $p<0.0005$.

showed an intermediate phenotype and developed tumors as well as reached endpoint in between the other two genotypes (Figure 4.3. A-C), suggesting that there is a dose dependency for SLK in the process of tumor initiation. Consistently, Western blot analysis on endpoint tumors confirmed the expression of Neu and Cre, as well as efficient deletion of SLK, implying that faster tumor onset is not likely the result of a population of cells that escaped recombination of the *Slk* allele (Figure 4.3. D). Together, these data demonstrate that loss of SLK in the context of Neu-induced mammary tumorigenesis accelerates tumor initiation but does not significantly alter tumor progression.

As SLK-deficient mammary tumors were palpable sooner than controls, we assessed mammary glands from $SLK^{+/+}$ and $SLK^{fl/fl}$ NIC mice at 4-16 weeks of age for evidence of hyperplastic lesions. Haematoxylin and Eosin staining of these mammary glands revealed a significant increase in the average size of each lesion and the average area of each mammary gland covered in hyperplastic lesions at 16 weeks of age in the $SLK^{fl/fl}$ NIC mammary glands. However, no differences were observed from 4-12 weeks of age (Figure 4.4.).

SLK has been shown to regulate both cellular proliferation and apoptosis (16,18,20,36), therefore we investigated whether these processes contributed to the accelerated tumor onset observed in the $SLK^{fl/fl}$ NIC mice. The proliferative index was measured by Ki67 histochemistry on endpoint tumors. No differences between control and SLK-deficient mammary tumors could be observed in the percentage of Ki67-positive nuclei (Figure 4.5. A, B). Consistent with the Ki67 histology, no differences in PCNA or cyclin D1 were observed by Western blot analysis (Figure 4.5. C). Although proliferation within these tumors remained unchanged, a significantly smaller fraction of TUNEL-positive cells was observed in $SLK^{fl/fl}$ NIC tumors accompanied by a reduction in both cleaved PARP and caspase 3 (Figure 4.6.),

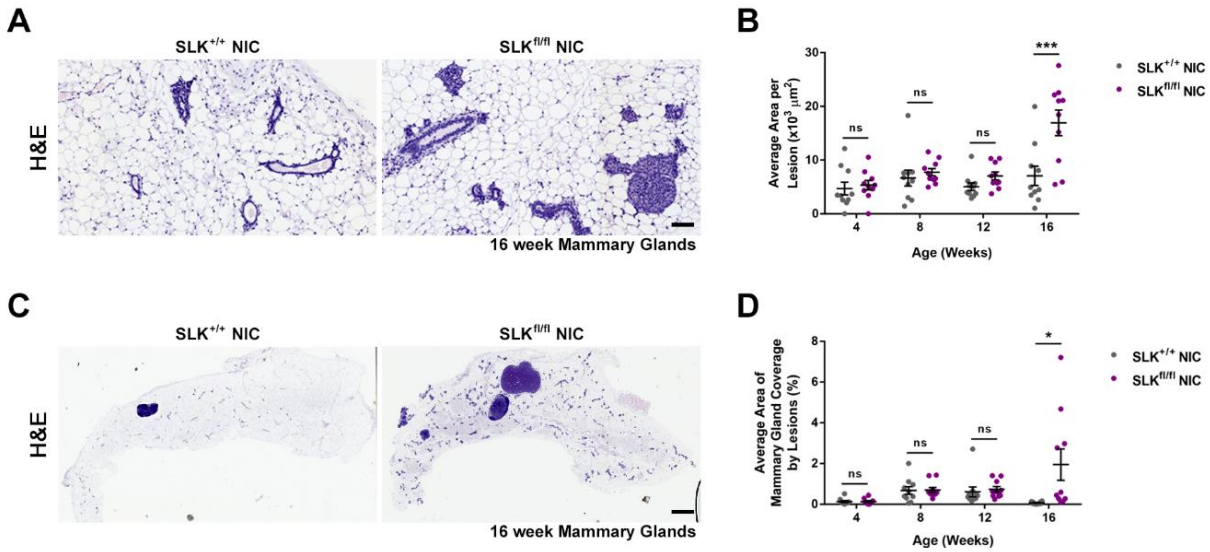

Figure 4.4. Conditional *Slk* deletion results in larger hyperplastic lesions by 16 weeks of age in Neu-induced mammary tumors. (A) Mammary glands were harvested from NIC or $SLK^{fl/fl}$ NIC mice at 4, 8, 12 and 16 weeks of age (n=5 mice/genotype). Mammary glands were stained fixed in formalin fixed and paraffin embedded sections were made. Representative images of haematoxylin and eosin stained mammary glands are shown from mice at 16 weeks of age. **(B)** The average area of each hyperplastic lesion per mammary gland was quantified at each timepoint. A significant increase in the average area per lesion was observed at 16 weeks. **(C)** Representative images of haematoxylin and eosin stained whole hyperplastic mammary gland sections at 16 weeks of age. **(D)** The average area of each mammary gland that was covered by hyperplastic epithelium was quantified for each mammary gland at each timepoint. An increase in total mammary gland coverage in hyperplastic lesions was observed by 16 weeks. * represents $p<0.05$, *** represents $p<0.0005$ and ns represents no statistical difference. Scale bar = 50 µm in A; 0.5 mm in C.

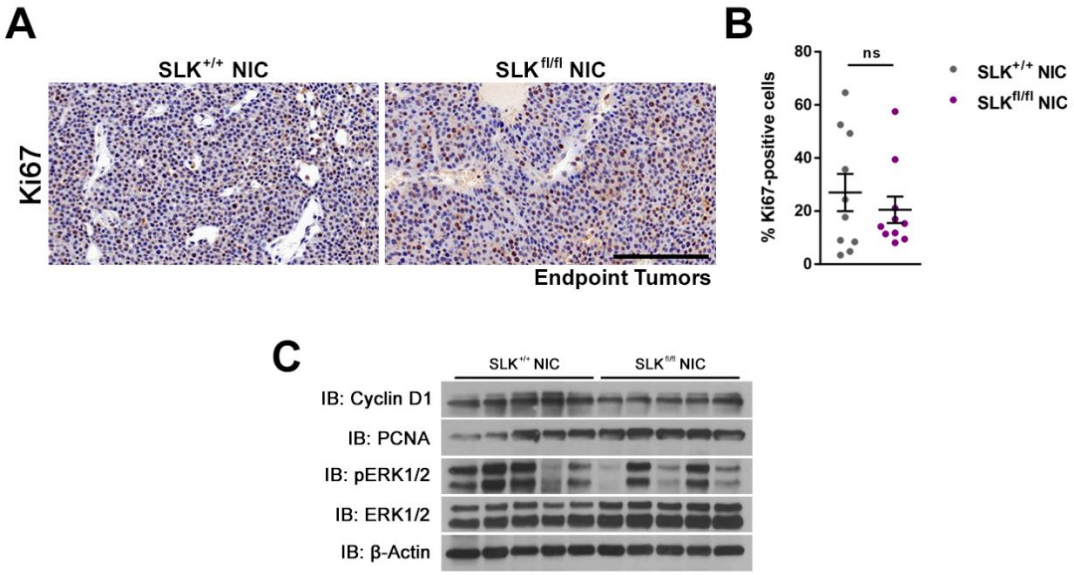

Figure 4.5. Conditional *Slk* deletion in Neu-induced mammary tumors has no effect on cellular proliferation. (A) Ki67 histochemistry was performed on $SLK^{+/+}$ NIC and $SLK^{fl/fl}$ NIC tumor sections (n=10 tumors/genotype) and representative images are shown for each genotype. **(B)** The percentage of Ki67-positive nuclei was counted on at least ten fields of view per tumor and is represented. No differences in Ki67 staining was observed. **(C)** Western blot analysis was performed for proliferative markers including Cyclin D1, PCNA and pERK on endpoint tumor lysate (n=5 tumors/genotype). No differences were observed between genotypes in proliferative markers. ns represents no statistical difference. Scale bar = 150 μm.

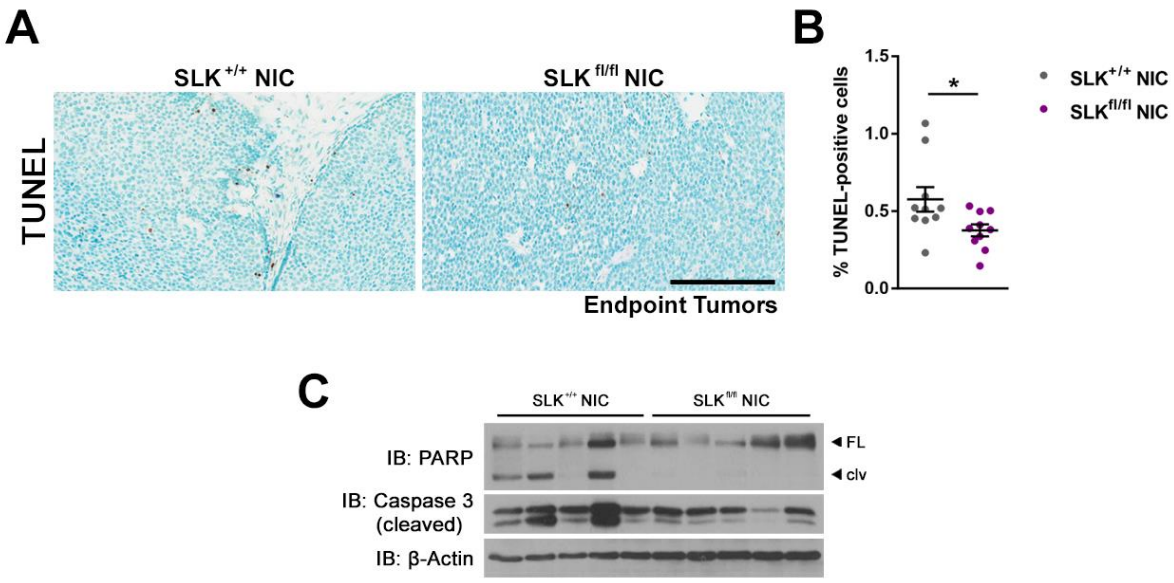

Figure 4.6. Conditional *Slk* deletion in Neu-induced mammary tumors results in tumors which are less apoptotic. (A) TUNEL staining was performed on $SLK^{+/+}$ NIC and $SLK^{fl/fl}$ NIC tumor sections (n=10 tumors/genotype) and representative images are shown for each genotype. **(B)** The percentage of TUNEL-positive cells was counted on at least ten fields of view per tumor and is represented. Significantly fewer TUNEL-positive cells were observed in the $SLK^{fl/fl}$ NIC tumors. **(C)** Western blot analysis was performed for apoptotic markers including PARP and cleaved caspase3 on endpoint tumor lysate (n=5 tumors/genotype). Less cleaved PARP and cleaved caspase 3 were observed in the SLK knockout tumor lysate. * represents $p<0.05$. Scale bar = 150 μm.

suggesting that SLK-deficient mammary tumors are more resistant to apoptosis which may contribute to the overall acceleration in tumor onset.

4.4. SLK deletion increases anchorage-independent growth *in vitro*.

To gain further insights into the mechanisms responsible for the accelerated growth of SLK-deficient mammary tumors, we investigated the effects of SLK deletion in a Neu-transformed mammary tumor cell line *in vitro*. Establishment and immortalization of NIC cell lines results in a significant reduction in the expression of Neu during cell culture (data not shown). Therefore, we opted to use the MMTV-NeuNDL model to generate our cell lines. The NeuNDL model differs from the NIC model in that it lacks the IRES-Cre cDNA. Conditional SLK knockout mice were crossed with MMTV-NeuNDL transgenics and primary mammary tumor ($SLK^{fl/fl}$ NDL) cells were established from endpoint tumors (Figure 4.7. A). The *slk* locus was inactivated using a GFP-Cre adenovirus and recombined cells were isolated by flow sorting for GFP expression to establish a pure $SLK^{-/-}$ NDL cell line. Efficient recombination was confirmed by PCR, qRT-PCR and Western blot analysis (Figure 4.7. B-D).

We first characterized the migratory and proliferative properties of the $SLK^{fl/fl}$ and $SLK^{-/-}$ NDL cell lines *in vitro*. No differences in haptotactic cell migration were observed when comparing $SLK^{fl/fl}$ and $SLK^{-/-}$ NDL cells in Boyden chamber transwell assays (Figure 4.8. A, B). Although no differences in cellular proliferation could be observed up to four days, $SLK^{-/-}$ NDL cells continued to proliferate after this point while the growth rate of the $SLK^{fl/fl}$ NDL cells plateaued (Figure 4.8. C). During the proliferation assay, we observed that the cells reached confluency at day five, at which point the SLK knockout cells continued to proliferate (Figure 4.8. C). One possibility for the increased growth rate of the $SLK^{-/-}$ NDL cells is that they no longer respond to contact inhibition and continue to proliferate once confluency has been achieved. To test this, anchorage independent growth was assessed by the ability of both

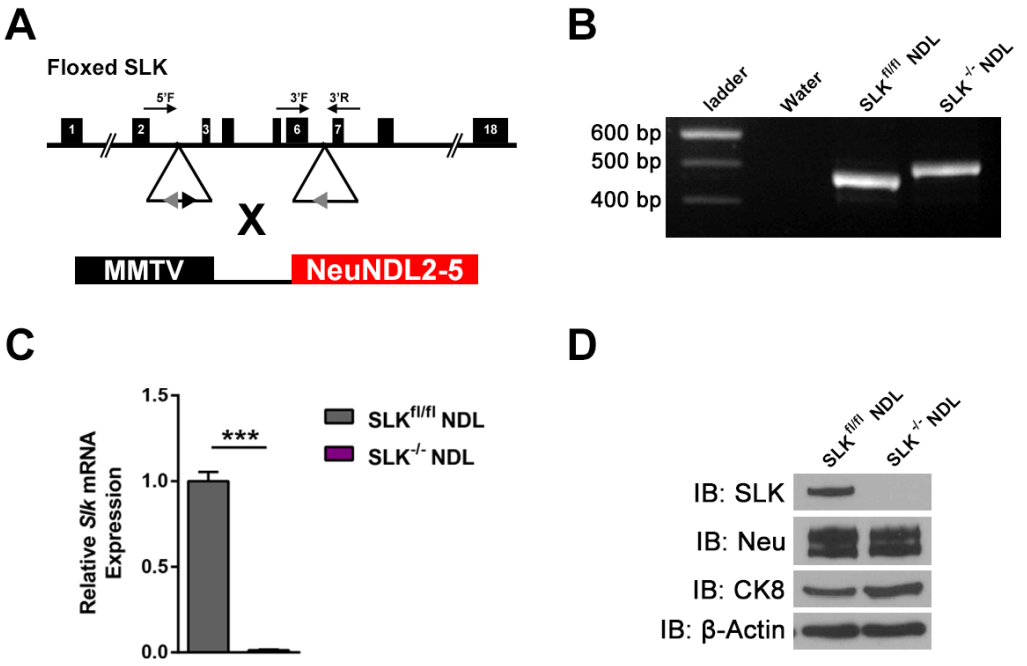

Figure 4.7. Generation and characterization of an SLK$^{-/-}$ NDL cell line. (A) Schematic representation of the SLK floxed allele and the MMTV-NeuNDL transgenic allele. This cross was used to generate tumor bearing females and subsequent generation an SLK$^{fl/fl}$ NDL cell line (n = 2 independent isolates of cells). **(B)** Cells were flow sorted for GFP expression following adenoviral-GFP (SLK$^{fl/fl}$ NDL) or GFP-Cre (SLK$^{-/-}$ NDL) infection. Recombination of the *Slk* allele was assessed using the primers outlined in (A). **(C)** No detectable *Slk* transcript was observed by qPCR analysis up to 50 passages following flow sorting for GFP. **(D)** Western blot analysis for SLK, Neu and CK8 was performed to confirm the luminal epithelial Neu-positive origin of our SLK$^{fl/fl}$ and SLK$^{-/-}$ NDL cell lines. *** represents $p<0.0005$.

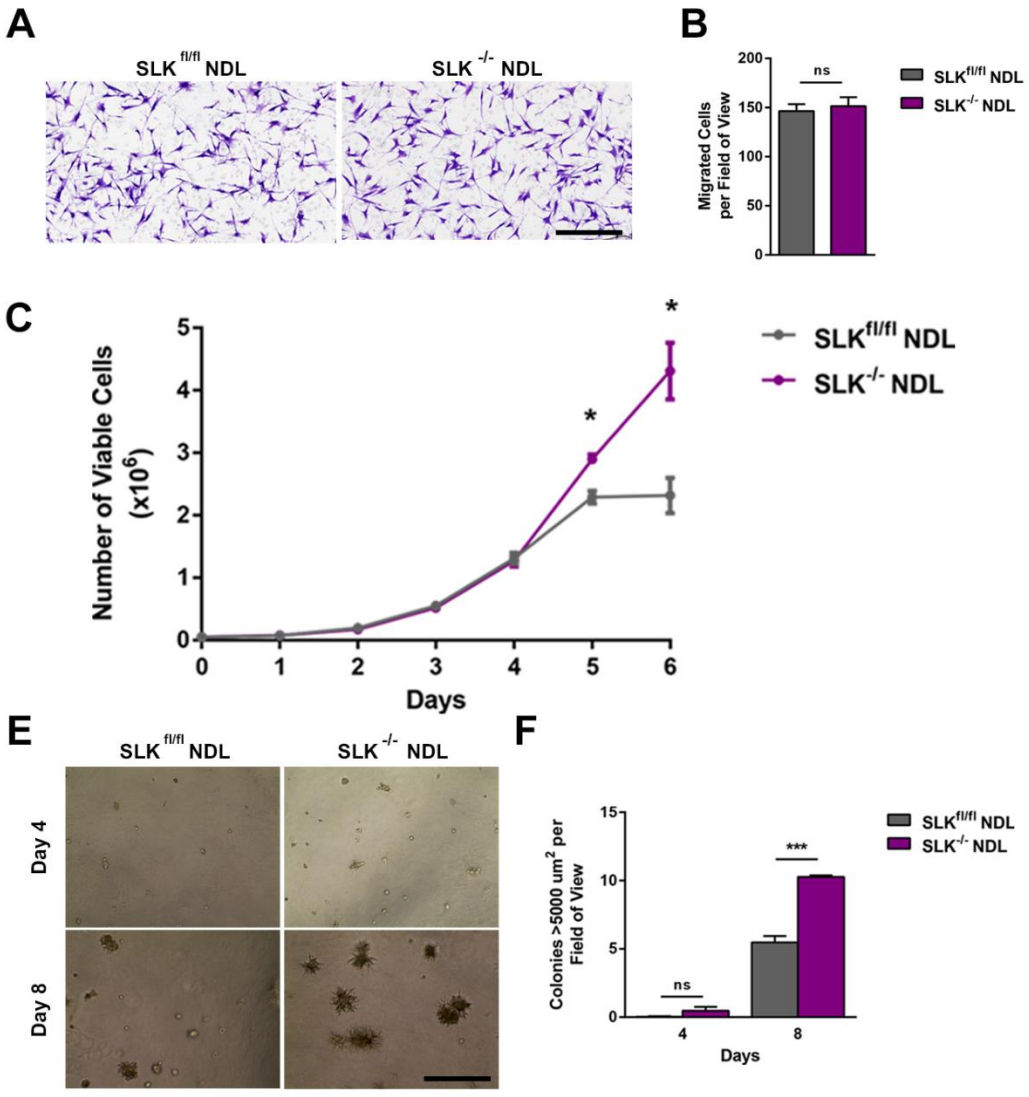
A
SLK fl/fl NDL
SLK -/- NDL
B
ns
SLKfl/fl NDL
SLK-/- NDL
Migrated Cells per Field of View
200
150
100
50
0
C
Number of Viable Cells (x10^6)
Days
SLKfl/fl NDL
SLK-/- NDL
*
*
E
SLK fl/fl NDL
SLK -/- NDL
Day 4
Day 8
F
Colonies >5000 um^2 per Field of View
ns
***
4
8
Days
SLKfl/fl NDL
SLK-/- NDL

Figure 4.8. SLK deletion in NeuNDL expressing cells does not impair cellular migration but increases cellular proliferation at high densities. (A) $SLK^{fl/fl}$ or $SLK^{-/-}$ NDL cells were subject to a haptotactic migration assay using a Boyden chamber transwell. $5x10^4$ cells were seeded per chamber in triplicate and allowed to migrate through the chamber for eight hours. Cells on the bottom of the chamber were stained with crystal violet and mounted on a slide prior to quantification. A representative field of view for each slide is shown. **(B)** For each chamber, ten random fields of view were chosen for quantification and the data is represented as the mean of three independent biological replicates +/- SEM. No differences in haptotaxis was observed following SLK deletion. **(C)** $SLK^{fl/fl}$ or $SLK^{-/-}$ NDL cells were seeded at $5x10^4$ cells per plate and proliferation was measured over six days by counting the number of viable cells per day by trypan blue exclusion. Triplicate plates were counted for each cell line on each day and the assay was performed four times. No differences in proliferation can be observed up to four days at which point the plates both appear to be confluent. Following this timepoint the $SLK^{-/-}$ NDL cells appear to have a growth advantage and continue to proliferate. **(D)** $SLK^{fl/fl}$ or $SLK^{-/-}$ NDL cells were subject to an anchorage independent growth assay. A total of 5000 cells were seeded in 4-well chamber slides pre-plated with a layer of Matrigel. Cells were seeded in full media containing 2.5% v/v Matrigel and allowed to grow with fresh media supplemented every two days. Representative images from both cell lines and time points are shown. **(E)** Colonies were photographed at four and eight days and colonies >5000 μm^2 were enumerated on ten random fields of view per chamber. Data is represented as the mean number of colonies from three independent biological replicates +/- SEM. A significant increase in the number of colonies is observed for the $SLK^{-/-}$ NDL cell line. * represents $p<0.05$, *** represents $p<0.0005$ and ns represents no statistical difference. Scale bar = 300 μm in A; 100 μm in D.

cell lines to form colonies in Matrigel. Consistent with the hypothesis that $SLK^{-/-}$ NDL cells can grow in low anchorage conditions, these cells formed approximately twice the number of colonies (Figure 4.8. D, E).

4.5. *Sox10* is induced in response to SLK-loss in Neu-induced mammary tumors and cells.

The observed enhanced tumor growth in the absence of SLK suggests the activation of alternate pathways. To investigate this, we performed microarray analysis using total RNA from three independent passages of $SLK^{fl/fl}$ and $SLK^{-/-}$ NDL cells. Our analysis revealed the presence of 27 genes, including *Slk*, whose mean fold change was greater than 1.5 with an adjusted p-value<0.05 between control and SLK knockout cells (Figure 4.9. A). The microarray results were validated by qRT-PCR and two reported stem cell markers were significantly upregulated in the $SLK^{-/-}$ NDL cell line, *Lgr6* (215) and *Sox10* (184) (Figure 4.9. A, B). Although Lgr6 has recently been reported as a stem cell marker in mouse skin squamous cell carcinoma (215), our attention was drawn to Sox10, which has been shown to regulate mammary stem/progenitor activity and is a marker of the TNBC subtype (166,184).

Although we have observed a 10-fold increase in the levels of *Sox10* transcript and at the protein level in SLK knockout tumor cells (Figure 4.9. B, C), we assessed the levels of Sox10 *in vivo*. We performed Sox10 histochemistry on both hyperplastic mammary glands and on endpoint tumors. Consistent with the larger number of hyperplasia at 16 weeks of age in the $SLK^{fl/fl}$ NIC mice, these lesions also had a two-fold increase in the percentage of Sox10-positive nuclei when compared to $SLK^{+/+}$ NIC mice (Figure 4.9. D, E). Although this difference was apparent at the hyperplastic stage, we did not detect any changes in endpoint tumors, supporting the observations that progression to endpoint is unaffected between the two groups (Figure 4.9. D, E).

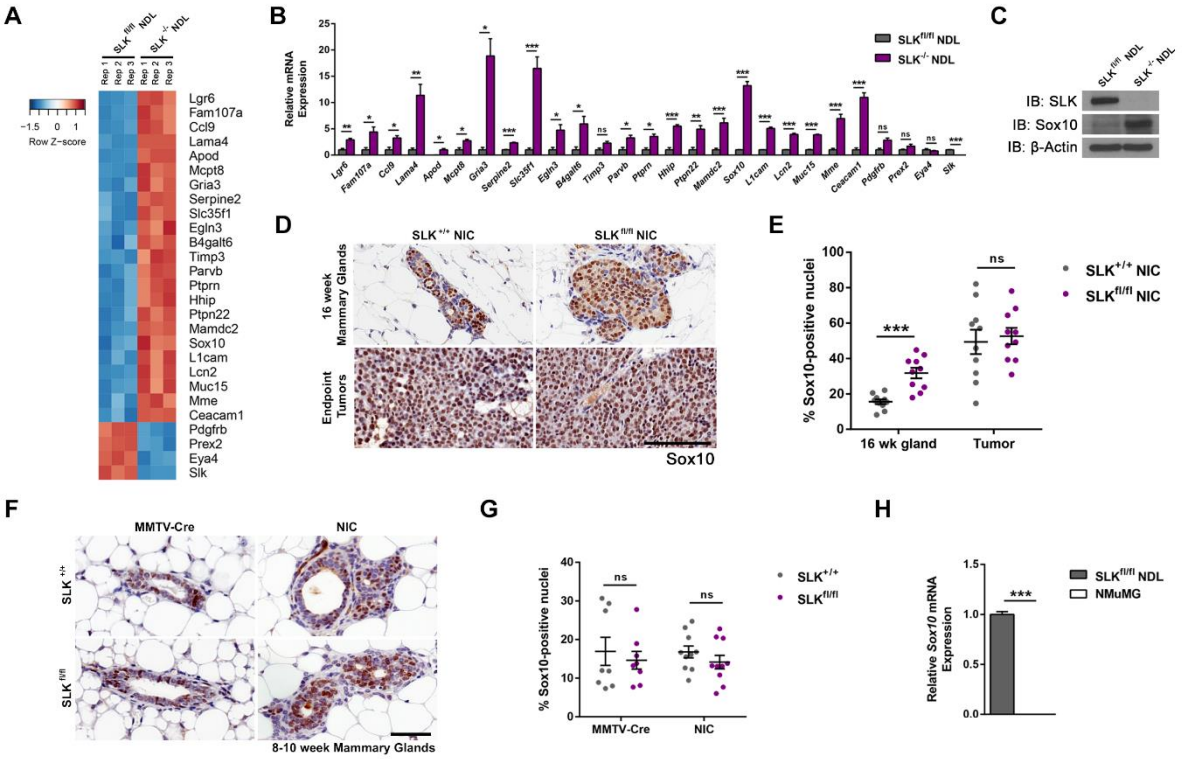

Figure 4.9. SLK deletion induces the upregulation of *Sox10* in NeuNDL expressing cell lines and hyperplasias. (A) Microarray analysis was performed using total RNA extracted from three independent $SLK^{fl/fl}$ NDL and $SLK^{-/-}$ NDL biological replicates. Total RNA was hybridized to the Mouse Gene 2.0 ST Array (Affymetrix). Data analysis was carried out in the r statistical programming environment with Bioconductor. Data for genes whose mean fold change was greater than 1.5 with an adjusted $p<0.05$ is represented as a heatmap. **(B)** Validation of microarray expression changes by qPCR analysis for all the genes identified in (A). **(C)** Western blot analysis was performed to validate that SLK deletion results in the upregulation of Sox10 protein. **(D)** Sox10 histochemistry was performed on $SLK^{+/+}$ NIC and $SLK^{fl/fl}$ NIC hyperplastic mammary glands and endpoint tumor sections (n=10 glands or tumors/genotype) and representative images are shown for each genotype. **(E)** The percentage of Sox10-positive nuclei was counted on at least ten fields of view per hyperplastic mammary gland or tumor and is represented. A significant increase in Sox10-positive nuclei was observed in the hyperplastic lesions of $SLK^{fl/fl}$ NIC mice. **(F)** Sox10 histochemistry was performed on MMTV-Cre and NIC mammary glands collected between eight and ten weeks of age ($n \geq 8$ mammary glands/transgenic line). Representative images are shown for each transgenic line and genotype. **(G)** The percentage of Sox10-positive nuclei was counted on at least ten fields of view per transgenic line and is represented. No differences in Sox10 nuclear staining could be observed in these mammary glands. **(H) S**ignificantly less *Sox10* transcript was observed by qPCR analysis in normal murine mammary epithelial (NMuMG) cells as compared to the $SLK^{fl/fl}$ NDL cells. * represents $p<0.05$, ** represents $p<0.005$, *** represents $p<0.0005$ and ns represents no statistical difference. Scale bar = 100 μm.

Sox10 has been shown to regulate mammary stem/progenitor activity (184). Therefore, we rationalized that SLK deletion may increase the mammary stem/progenitor pool through the induction of Sox10. SLK deletion in the context of the NIC model resulted in the upregulation of Sox10 by 16 weeks of age, however, we assessed whether the induction of Sox10 occurred earlier in this model or in the absence of the NeuNDL oncogene. To test this, mammary glands from virgin $SLK^{+/+}$ and $SLK^{fl/fl}$ MMTV-Cre and NIC mice at 10-12 weeks of age were stained for Sox10. No differences in nuclear Sox10 were observed in either transgenic line suggesting that SLK deletion does not increase the progenitor population and that the induction of Sox10 likely requires oncogenic Neu at early stages of tumor onset (Figure 4.9. F, G). Supporting this, *Sox10* expression was found to be significantly lower in normal murine mammary epithelial cells compared to the $SLK^{fl/fl}$ NDL cell line (Figure 4.9. H). As we observe both an increase in nuclear Sox10 staining and a significant increase in the number and size of hyperplastic lesions following SLK deletion we assessed whether Sox10 was driving the accelerated tumor initiation in this model.

4.6. SLK deletion increases stem/progenitor activity *in vitro*.

Sox10 has been shown to define basal/triple negative-like breast cancers and regulate mammary stem/progenitor activity (166,167,184). As *Sox10* is induced following SLK deletion, we hypothesized that the loss of SLK in Neu-induced mammary tumors results in a less differentiated basal-like phenotype, reminiscent of the TNBC subtype (216). Although the increased proliferation and anchorage independent growth suggests that the SLK knockout tumor cells have more stem/progenitor activity, we performed a mammosphere forming assay to validate our hypothesis. Interestingly, the mammosphere forming efficiency of the $SLK^{-/-}$ NDL cells in a primary passage was approximately twice that of the $SLK^{fl/fl}$ NDL controls (Figure 4.10. A, B). To confirm that these mammospheres are formed from stem-like cells, the

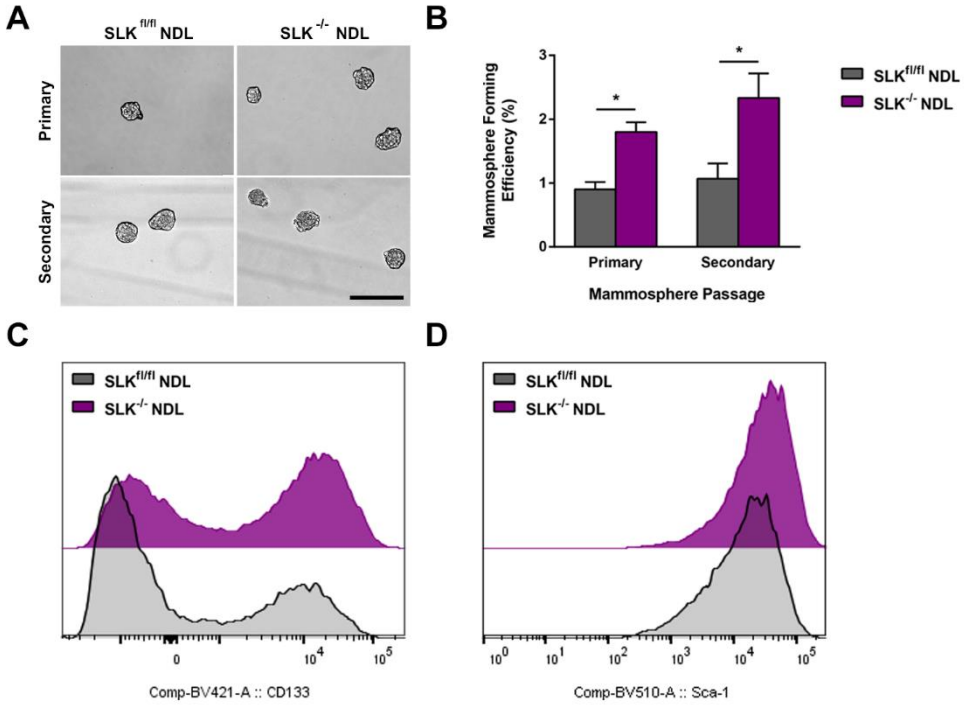

Figure 4.10. SLK deletion in NeuNDL expressing cells increases mammosphere forming efficiency. (A) The mammosphere forming efficiency of the $SLK^{fl/fl}$ and $SLK^{-/-}$ NDL cell lines was assessed by plating 1000 cells per well in 24-well low attachment plates and allowing primary mammospheres to form for seven days. Secondary mammospheres were plated by disaggregating the primary passage and seeding these cells for a further seven days. Representative images from both cell lines and mammosphere passage are shown. **(B)** The mammosphere forming efficiency was calculated as the percentage of spheres per well with a diameter greater than 15 μm over the total number of cells that were seeded. Data is represented as the mean mammosphere forming efficiency from three independent biological replicates +/- SEM. **(C, D)** $SLK^{fl/fl}$ and $SLK^{-/-}$ NDL cells were stained for CD133 (C) and Sca1 (D) and analyzed by flow cytometry. An increase in both the number of CD133-positive cells and Sca1 staining intensity was observed following SLK deletion. * represents $p<0.05$. Scale bar = 100 μm.

primary mammospheres were disaggregated and assessed for their secondary sphere forming potential. Consistent with the primary mammospheres, $SLK^{-/-}$ NDL cells had twice the mammosphere forming potential of the control cells (Figure 4.10. A, B). Given the increase in mammosphere forming efficiency, we assessed the surface expression of the stem cell markers, CD133 and Sca1. An increase in staining for both CD133 and Sca1 was observed by flow cytometry in the $SLK^{-/-}$ NDL cells (Figure 4.10. C, D). Together, these results indicate that loss of SLK in Neu-induced mammary tumors may result in the acquisition of a less differentiated, stem-like phenotype with a greater tumor initiating capacity.

4.7. Sox10 drives stem/progenitor activity *in vitro* following SLK deletion.

Sox10 has been shown to regulate the stem/progenitor activity of mammary epithelial cells (184). Together with the observations that SLK deletion induces *Sox10* expression and increases mammosphere formation we tested whether Sox10 was sufficient to drive this phenotype. To begin, we stably overexpressed retroviral pBABE-Sox10 into the $SLK^{fl/fl}$ NDL cell line which express very low basal levels of Sox10 and assessed whether any of the induced genes from the microarray were Sox10 responsive. Interestingly, several genes including *Ceacam1* and *L1cam* which are upregulated following SLK deletion, are also increased following stable overexpression of Sox10 (Figure 4.11. A). Additionally, Sox10 expression was sufficient to recapitulate the increase in proliferation following growth to confluency that was observed in the $SLK^{-/-}$ NDL cells (Figure 4.11. B), suggesting that Sox10 may be driving the anchorage independent growth that was observed following SLK deletion.

To corroborate our findings with the stable overexpression of Sox10 in the $SLK^{fl/fl}$ NDL cell line, we performed transient Sox10 knockdown using two independent siRNA sequences in the $SLK^{-/-}$ NDL cells expressing high levels of Sox10. The best two independent Sox10 siRNAs consistently knocked down *Sox10* expression by 50-60% which was sufficient

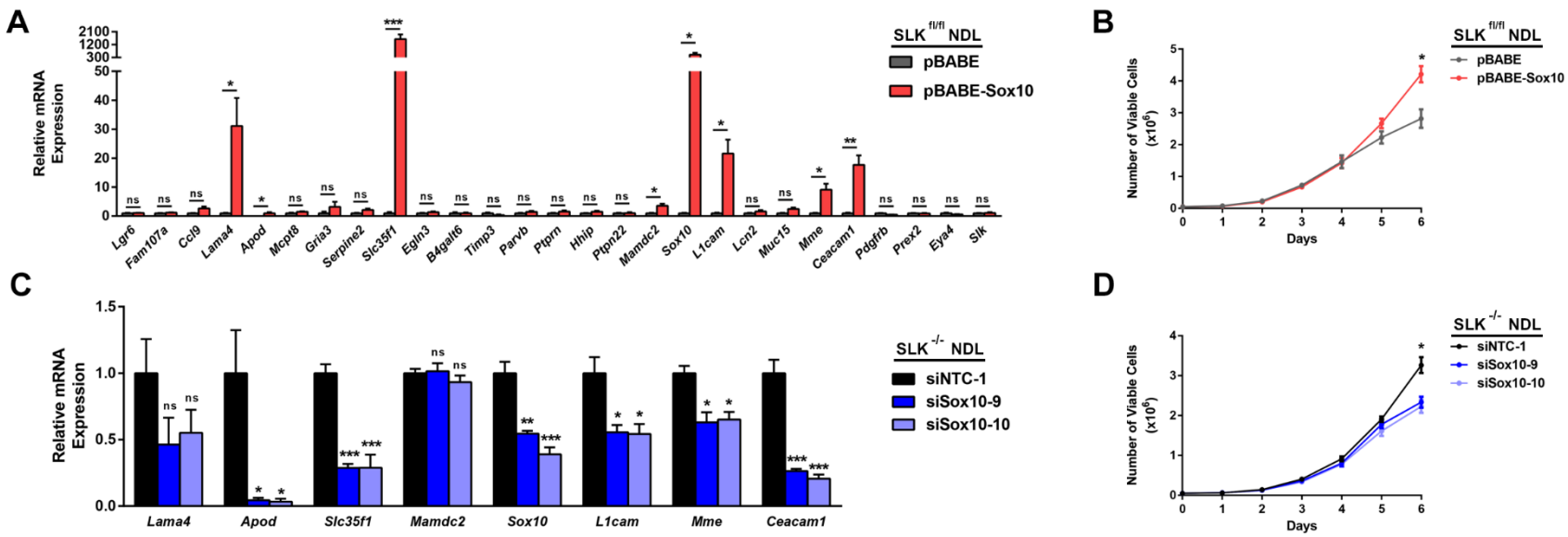

Figure 4.11. Sox10 is in part responsible for the transcriptional and proliferative phenotype following SLK deletion in NeuNDL expressing cells. (A) SLK$^{fl/fl}$ NDL cells were stably transduced with either pBABE or pBABE-Sox10 expressing retrovirus and selected for with puromycin. Validation of microarray expression changes by qPCR analysis for all the genes identified in Figure 4.9. A was performed. **(B)** SLK$^{fl/fl}$ NDL cells expressing either pBABE or pBABE-Sox10 were seeded at 5x10^4 cells per plate and proliferation was measured over six days by counting the number of viable cells per day by trypan blue exclusion. Triplicate plates were counted for each cell line on each day and the assay was performed three times. The pBABE-Sox10 expressing cells continued to proliferate at higher densities. **(C)** SLK$^{-/-}$ NDL cells were treated with siNTC-1 (non-targeting), siSox10-9 or siSox10-10 at 100 nM for 72 hours and total RNA was extracted. qPCR analysis was performed for the genes which were modulated by Sox10 overexpression in (A). **(D)** SLK$^{-/-}$ NDL cells treated with siNTC-1, siSox10-9 or siSox10-10 at 100 nM for 48 hours were seeded at 5x10^4 cells per plate and proliferation was measured over six days by counting the number of viable cells per day by trypan blue exclusion. Every two days the siRNA transfection was replenished. Triplicate plates were counted for each cell line on each day and the assay was performed three times. Sox10 knockdown resulted in a reduction in cellular proliferation compared to the SLK$^{-/-}$ NDL cell line at higher densities. * represents p<0.05, ** represents p<0.005, *** represents p<0.0005 and ns represents no statistical difference.

to significantly reduce the expression of the other Sox10-responsive genes (Figure 4.11. C). Similarly, treatment of the $SLK^{-/-}$ NDL cells with Sox10 siRNAs reduced proliferation following growth to confluency as evidenced by significantly lower viable cell counts between days five and six (Figure 4.11. D). Together, these data indicate that Sox10 expression is sufficient to recapitulate part of the transcriptional program induced by SLK deletion. Furthermore, it is sufficient to promote proliferation beyond confluency.

To confirm that Sox10 is conferring an increase in mammary stem/progenitor activity *in vitro*, $SLK^{fl/fl}$ NDL pBABE-Sox10 cells were assessed for their mammosphere forming potential. Consistent with our previous observations, stable overexpression of Sox10 resulted in a significant increase in mammosphere forming efficiency in both primary and secondary mammosphere assays (Figure 4.12.). Additionally, mammospheres formed from the pBABE-Sox10 overexpressing cell lines formed significantly larger mammospheres on average when compared to the pBABE controls (Figure 4.12. A). Therefore, expression of Sox10 is sufficient to increase the stem/progenitor activity of $SLK^{fl/fl}$ NDL cells and may contribute to the accelerated tumor onset that we observe *in vivo*.

4.8. Sox10 is not sufficient to drive transformation but cooperates with Neu.

We have shown that Sox10 is able to drive a stem/progenitor phenotype in our *in vitro* culture system and that Sox10 may drive the transcription of several of the genes induced following SLK deletion *in vitro*. We also have reported that SLK is required for Neu-induced chemotaxis and invasion (114). Therefore, we hypothesized that loss of SLK may hinder Neu-induced tumorigenesis and that Sox10 may act as an oncogenic driver accelerating tumor onset in the $SLK^{fl/fl}$ NIC mice.

To test whether Sox10 was sufficient to drive cellular transformation and oncogenesis, we performed focus forming assays in Rat-1 fibroblasts. Rat-1 fibroblasts have previously

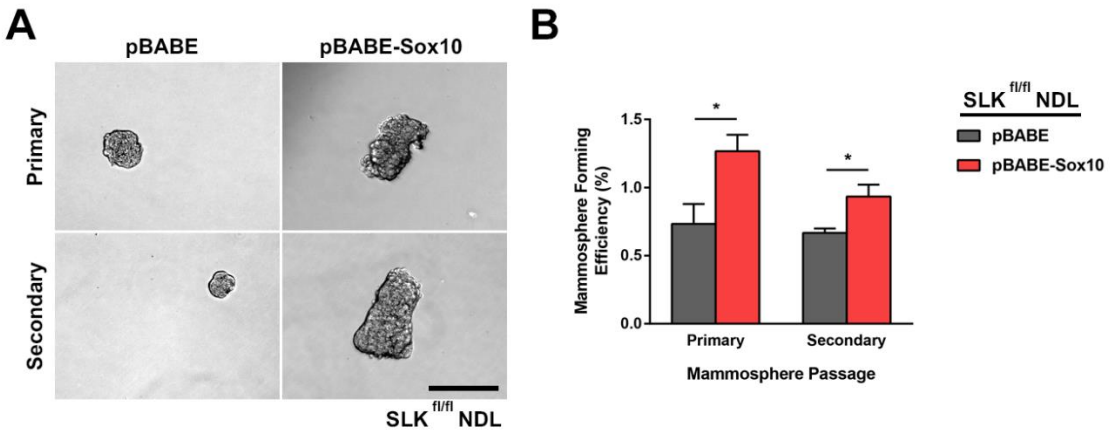

Figure 4.12. Sox10 expression is sufficient to increase the mammosphere forming potential of NeuNDL expressing cells. (A) The mammosphere forming efficiency of the SLK$^{fl/fl}$ NDL cell lines expressing either pBABE or pBABE-Sox10 was assessed by plating 1000 cells per well in 24-well low attachment plates and allowing primary mammospheres to form for seven days. Secondary mammospheres were plated by disaggregating the primary passage and seeding these cells for a further seven days. Representative images from both cell lines and mammosphere passage are shown. **(B)** The mammosphere forming efficiency was calculated as the percentage of spheres per well with a diameter greater than 15 μm over the total number of cells that were seeded. Data is represented as the mean mammosphere forming efficiency from three independent biological replicates +/- SEM. * represents $p<0.05$. Scale bar = 100 μm.

been used in the characterization and validation of the transformation potential of the Neu oncogene (71). Therefore, we selected this cell line as an appropriate model system. Rat-1 fibroblasts were seeded and allowed to grow to confluency prior to transduction with pBABE or pBABE-Sox10 vectors. As a positive control, pMSCV-NeuNT was transduced into these cells and resulted in the formation of over 200 foci following 21 days in culture (Figure 4.13. A, B). However, the expression of Sox10 alone was not sufficient to induce foci formation above the levels of the vector alone control, suggesting that Sox10 alone cannot drive transformation of the Rat-1 fibroblasts (Figure 4.13. A, B).

Despite the inability for Sox10 to transform Rat-1 fibroblasts in focus forming assays, we postulated that perhaps Sox10 can cooperate with an oncogenic stimulus such as Neu. As $SLK^{fl/fl}$ NIC tumors initiate faster than controls and since these hyperplastic lesions have increased levels of nuclear Sox10, we tested whether Sox10 could cooperate with oncogenic Neu and increase foci formation in Rat-1 fibroblasts. Rat-1 fibroblasts were seeded and grown to confluency prior to transduction with Sox10, NeuNT or both vectors together. Whereas our previous focus forming assay was performed for 21 days, these foci were cultured for 12 days to assess any differences early on. As with our previous assay, NeuNT was sufficient to induce foci formation above vector controls while Sox10 was not sufficient to transform these cells (Figure 4.13. C, D). Consistent with our hypothesis, the combination of NeuNT and Sox10 significantly enhanced foci formation five-fold above NeuNT alone. Therefore, although Sox10 alone is not sufficient to transform Rat-1 fibroblasts, it is able to cooperate with oncogenic NeuNT to increase its transforming capacity. To further explore the pro-tumorigenic potential of Sox10, we performed subcutaneous injections of $SLK^{fl/fl}$ NDL cells stably expressing either pBABE or pBABE-Sox10 into the right flank of immunocompromised female mice. Consistent with the increase in anchorage independent growth and mammosphere

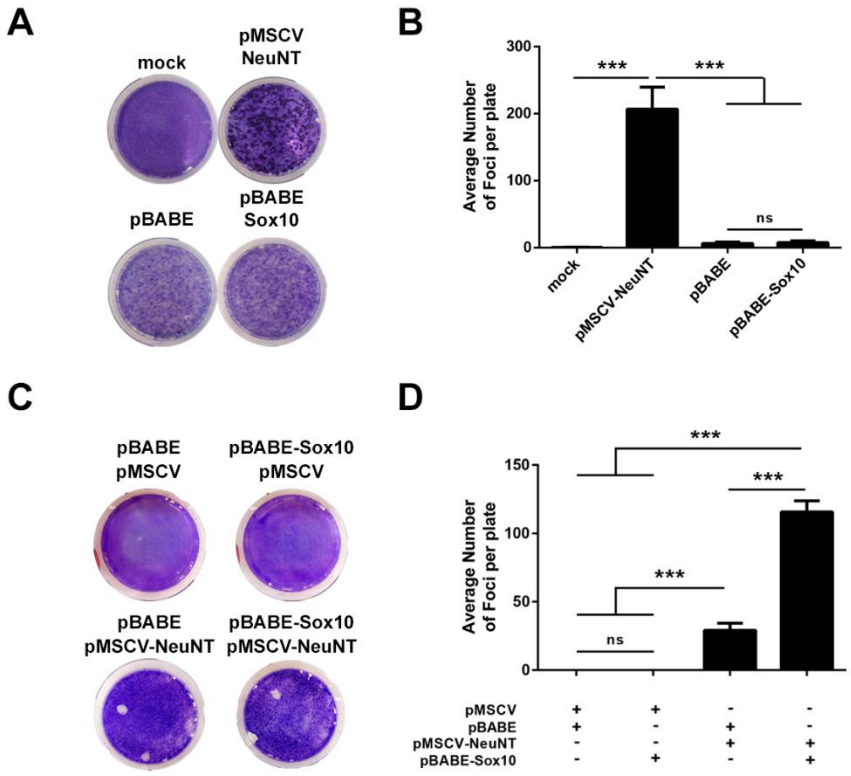

Figure 4.13. Sox10 alone is not sufficient to transform fibroblasts but can enhance the oncogenic potential of Neu. (A) Focus forming assay was performed on Rat-1 fibroblasts transiently transfected with NeuNT, pBABE or pBABE-Sox10. Cells were plated at 75% confluency and grown for 18 days with fresh media supplemented every 72 hours. Cells were fixed in methamol and stained with crystal violet. Three independent plates were seeded and transfected per condition and a representative plate from each condition is shown. **(B)** The total number of foci with a diameter of greater than 1.5 mm per plate was quantified from all three independent biological replicates and is represented as the mean +/- SEM. Sox10 expression is not sufficient to induce foci formation above control levels. **(C)** Focus forming assay was performed on Rat-1 fibroblasts transiently transfected with NeuNT, pBABE-Sox10 or both in combination. Cells were plated at 75% confluency and grown for 10 days with fresh media supplemented every 72 hours. Cells were fixed in methamol and stained with crystal violet. Three independent plates were seeded and transfected per condition and a representative plate from each condition is shown. **(D)** The total number of foci with a diameter of greater than 1.5 mm per plate was quantified from all three independent biological replicates and is represented as the mean +/- SEM. Sox10 expression is not sufficient to induce foci formation above control levels, however in combination with NeuNT is able to enhance the transformation potential of Neu. *** represents $p<0.0005$.

forming potential, Sox10 overexpressing cells formed tumors that grew significantly faster than the vector control *in vivo* (Figure 4.14. A). Additionally, Sox10 expressing tumors were significantly larger at endpoint when compared to tumors from control animals (Figure 4.14. B, C). Together, these data support the notion that Sox10 enhances transformation and tumor growth of Neu-expressing cell lines both *in vitro* and *in vivo*.

4.9. Summary.

HER2-positive breast cancers account for approximately 25% of all reported breast cancer cases and these tumors tend to have a poorer prognosis and clinical outcome due to their association with an increased metastatic potential (57,60-62). Our lab has shown that SLK plays an important role in regulating an epithelial to mesenchymal transition and that SLK is required for heregulin-induced chemotaxis and migration in Neu-expressing mammary cell lines (52,114). Therefore, we hypothesized that SLK may be required for Neu-induced mammary tumorigenesis *in vivo* and a potential therapeutic target in the treatment of HER2-positive breast cancers. Contrary to our initial hypothesis, conditional deletion of SLK in a Neu-induced mammary tumor model significantly accelerated tumor onset and reduced overall survival in our murine model. Consistent with the accelerated tumor onset, SLK-deficient mammary glands expressing the Neu oncogene developed larger and more numerous hyperplastic lesions by 16 weeks of age. To investigate the mechanisms involved in accelerating tumor onset in this model, we generated an SLK knockout NDL cell line *in vitro*. $SLK^{-/-}$ NDL cells show increased mammosphere forming potential, suggesting higher numbers of stem/progenitor cells following SLK deletion. Interestingly, microarray analysis revealed that expression of the mammary stem/progenitor marker, *Sox10,* was significantly higher in the SLK knockout cell line. These observations were validated *in vivo* with a significant increase in the percentage of Sox10-positive nuclei in SLK-null hyperplastic mammary glands.

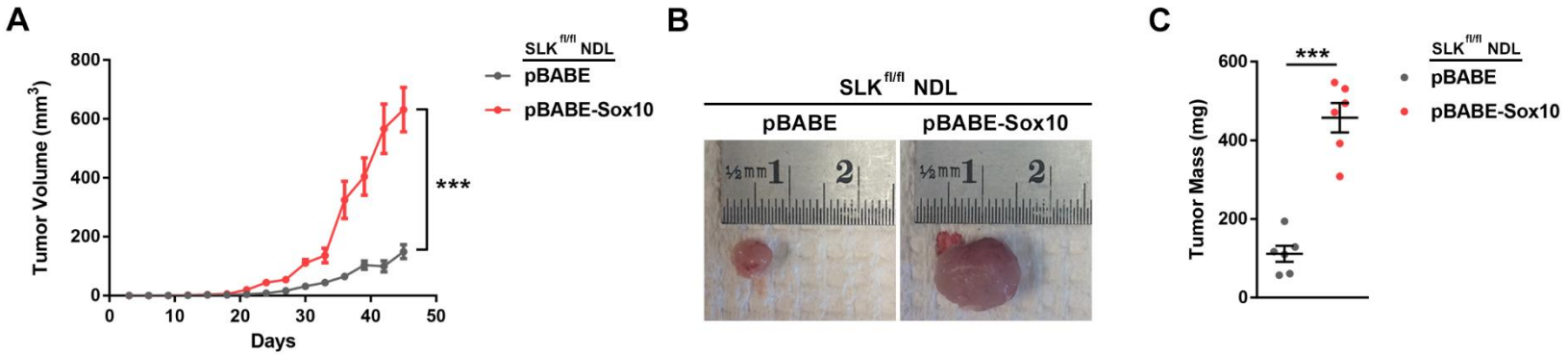

Figure 4.14. Sox10 expression enhances subcutaneous tumor growth of NeuNDL cell in immunocompromised mice. **(A)** SLK$^{fl/fl}$ NDL cells were stably transduced with either pBABE or pBABE-Sox10 and 1.5 x 10^6 cells (in 50% Matrigel) were injected subcutaneously into Scid Hairless Congenic female mice (n=6 mice/cell line). Tumors were measured every three days and mice were sacrificed when the largest tumor reached 15 cm in diameter. Sox10 expression significantly enhanced tumor growth compared to the vector control. **(B)** Representative tumors from both groups are shown with a ruler for scale. Tumors from the pBABE-Sox10 group are significantly larger at endpoint. **(C)** The average mass of each tumor was measured and represented as the mean +/- SEM. *** represents $p<0.0005$.

Lastly, stable expression of Sox10 was sufficient to recapitulate both the increase in mammosphere forming efficiency and tumor growth in a subcutaneous injection model, suggesting that Sox10 may be a key regulator of the accelerated tumor onset observed in $SLK^{fl/fl}$ NIC mice.

Chapter 5

Sox10 is an independent marker of the Triple-negative Breast Cancer subtype.

5.1. Introduction and Rationale.

Breast cancer subtypes are most commonly classified based on the expression of the Estrogen Receptor (*ESR1*), Progesterone Receptor (*PGR*) and/or the Human Epidermal Growth Factor Receptor-2 (*HER2*) (55-58). The Luminal A and B subtypes are the most common and account for approximately 65% of all breast cancer cases (57). The Luminal subtypes tend to be *ESR1* and *PGR*-positive, have the best prognostic outcome and generally respond well to hormone therapy (55-59). The HER2-positive subtype accounts for approximately 25% of all breast cancers and is characterized by amplification and overexpression of *HER2*. HER2-positive tumors tend to have a poorer prognostic outcome due to their association with an increased metastatic potential (57,60-62). Lastly, the Triple-negative breast cancers (TNBCs) are defined by those that do not express *HER2*, *ESR1* or *PGR* (58). TNBCs account for approximately 10% of all cases and have the worst prognosis and survival rates, as major therapeutic targets have not yet been identified for this subtype (57). As biomarkers and/or drivers of TNBCs have not been fully identified, chemotherapy remains the standard of care treatment option (64-66).

Identifying biomarkers and/or therapeutic targets for TNBCs has been an ongoing area of research over the last two decades. However, a lack of standardization in detection methods (compared to those used for diagnosing Luminal A/B- or HER2-positive tumors (217)) has led to a large degree of variation within the literature on whether certain genes are true markers of the TNBC subtype (218,219). Despite these inconsistencies, Sox10 has gained increasing attention as a novel biomarker for basal/TNBCs over the past decade (166,167). As *Sox10* expression is acquired in SLK-null mammary hyperplasias and tumor cell lines, we aimed to assess the validity of *SOX10* expression as an independent marker of the TNBC subtype using

1246 invasive breast cancer samples and whether SLK deletion in Neu-induced tumors drives a more basal/TNBC program through *Sox10* induction.

5.2. Luminal A/B, HER2-positive and Triple-negative subtypes can be defined by four distinct expression signatures.

We first aimed to stratify the RNA-Seq data available from The Cancer Genome Atlas according to the three major breast cancer subtypes: *HER2*-positive, *ESR1*/*PGR*-positive and Triple-negative. Gene-level quantifications from RNA-Seq data of 1246 invasive breast cancer samples from The Cancer Genome Atlas (200) were clustered based on their expression of *HER2*, *ESR1* and *PGR*. This resulted in three distinct putative subtypes: A HER2-positive, a Luminal A/B subtype which is *ESR1*/*PGR*-positive and a TNBC subtype lacking expression of all three receptors (Figure 5.1.).

Next, we sought to define an expanded gene expression signature associated with these subtypes to identify novel biomarkers. Additionally, we were interested in whether *SOX10* expression could be used to define its own unique subtype. To perform this, we identified differentially expressed genes (ANOVA, FDR < 0.01) with a minimum log2 fold change of 4 (16-fold) across subtypes. This resulted in four clusters of genes with distinct expression patterns between subtypes, which we have termed “Marker Clusters”, comprising 112 genes (Figure 5.2; Table 5.1.).

5.3. Luminal A/B and HER2-positive breast cancers have a defined gene signature.

The Marker Cluster 3 corresponded to genes whose expression is highest in the Luminal A/B subtype and contained the canonical markers *ESR1* and *PGR* (Figure 5.3; Table 5.1.). Other genes within this cluster include *CCDC170, WNK4* and *AGR3* (Table 5.1.) which have been reported to be implicated in these cancers (220-222).

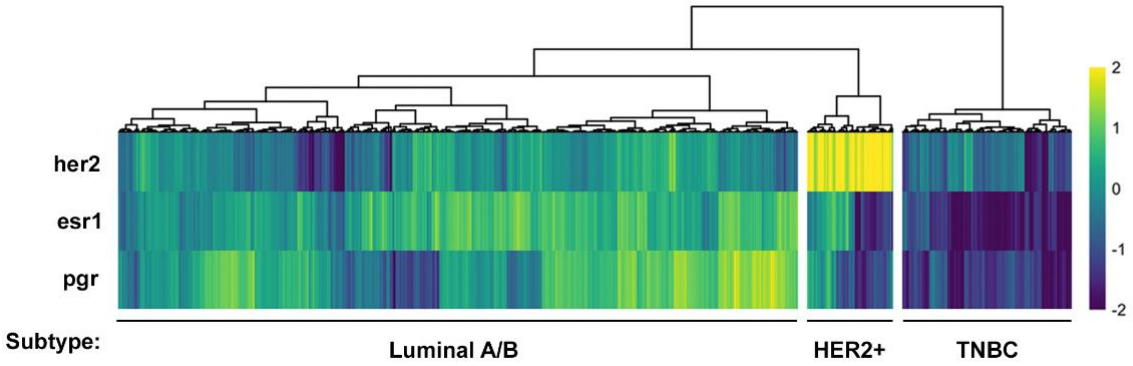

Figure 5.1. Stratification of human breast cancer samples from *The Cancer Genome Atlas* database into three putative breast cancer subtypes. Receptor heatmap of *HER2*, *ESR1* and *PGR* expression (z-score of log2 counts) across 1246 patient samples. Each column represents the expression values for an individual patient sample. Hierarchical clustering was used to group patients by the expression patterns of each receptor. This clustering revealed a group of putative TNBC, HER2-positive and Luminal A/B patients. Figure was adapted from (223).

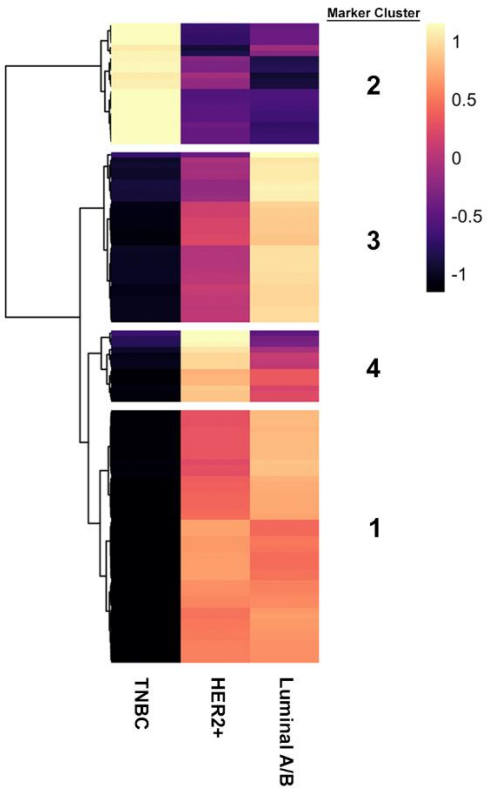

Figure 5.2. Four distinct marker clusters can be stratified from three putative breast cancer subtypes. Marker heatmap showing the average expression (z-score) of 112 marker genes across the three molecular subgroups identified in Figure 5.1. Each row represents an individual gene. Marker genes were identified by using an ANOVA to identify genes that are differentially expressed across molecular subtypes. Differentially expressed genes were defined as those with an FDR-adjusted p-value < 0.01 and a log2 fold-change > 4 between the lowest and highest expressing subtype. Hierarchical clustering was used to define four groups of marker genes with similar expression patterns across subtype. Figure was adapted from (223).

Table 5.1. Top 20 identified genes for each Marker Cluster identified across HER2+, Luminal A/B and TNBC subtypes. The four Marker Clusters (and the putative group that they define) are provided with the top genes identified for each cluster with an FDR-adjusted p-value <0.01 and a log2 fold-change > 4 between the lowest and highest expressing subtypes. For clusters with more than 20 genes, only the top 20 are shown here. These genes correspond to those identified by hierarchical clustering in Figure 5.2. Table was adapted from (223).

Marker Cluster 1 (Mosaic)	Marker Cluster 2 (High in TNBC)	Marker Cluster 3 (Luminal A/B)	Marker Cluster 4 (HER2+)
AR	*SOX10*	*PGR*	*ERBB2*
PIP	*ROPN1*	*ESR1*	*CEACAM5*
CLC7A2	*GABRP*	*CCDC170*	*CEACAM6*
ABCC8	*VGLL1*	*GRPR*	*ABCC11*
F7	*MSLN*	*WNK4*	*NXPH1*
BCAS1	*CA9*	*CHAD*	*ABCC12*
CA12	*GABBR2*	*AFF3*	*GRB7*
BPIFB2	*HORMAD1*	*GFRA1*	*PNMT*
DHRS2	*ZIC1*	*CPB1*	*MUCL1*
TMC5	*ART3*	*CLSTN2*	*LRRC26*
ARG2	*FABP7*	*PGLYRP2*	*UGT2B11*
GATA3	*A2ML1*	*KCNJ3*	*PP14571*
SCGB2A2	*FDCSP*	*NEK10*	*DSCAM-AS1*
LRRC31	*PRAME*	*GRIK3*	-
MLPH	*KRT16*	*DNALI1*	-
FOXA1	*SBSN*	*SERPINA6*	-
HMGCS2	*PPP1R14C*	*SYT9*	-
TTC6	*CT83*	*NAT1*	-
CYP4B1	*NKX1-2*	*CST9*	-
SYTL5	-	*AGR3*	-

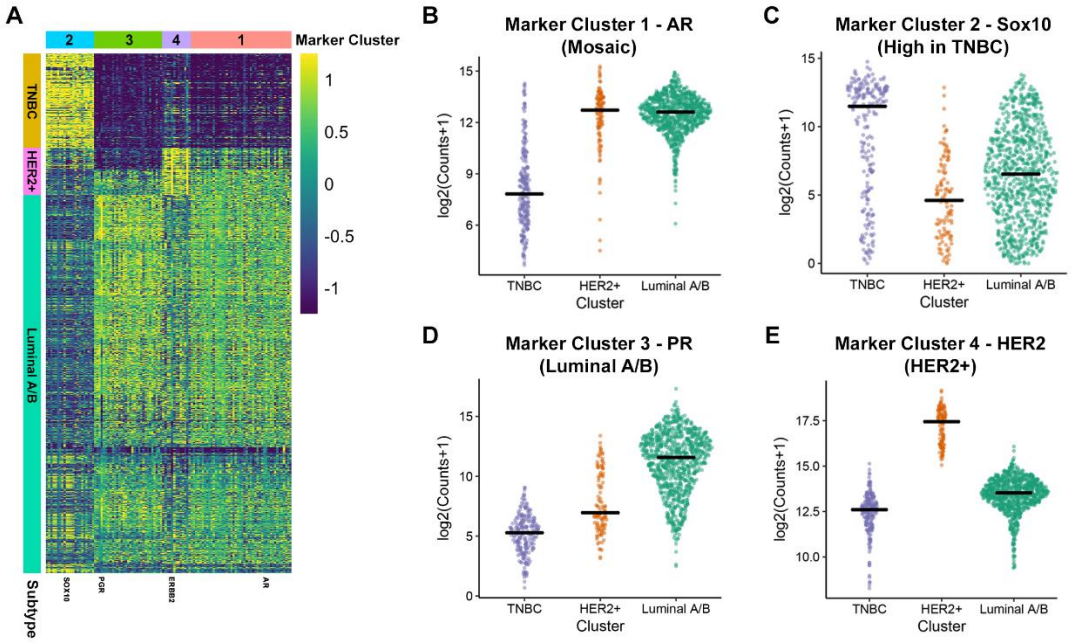

Figure 5.3. Identification of gene markers for the HER2-positive, Luminal A/B and TNBC subtypes. (A) Marker heatmap showing the expression (z-score of log2 counts) of 112 marker genes. Each row represents the expression of a single gene across each patient sample (columns). The rows of the heatmap are ordered identically to the receptor heatmap in Figure 5.1. **(B-E)** Expression of a representative identified marker across molecular subtypes is shown for each of the four identified marker groups. Each plot provides the distribution of log2 expression values of *AR* (B), *SOX10* (C), *PGR* (D) and *HER2* (E) across subtypes. The black line represents the median expression value for each subtype. Figure was adapted from (223).

Marker Cluster 4 genes are enriched in HER2-positive breast cancers and includes *ERBB2* (*HER2*), *GRB7* and *CEACAM6* (Figure 5.3; Table 5.1.). This subtype was well-defined, with all samples expressing higher levels of *HER2* than the mean of all samples. As with the Luminal cluster of genes, most genes making up this cluster have been implicated in HER2-positive breast cancer signaling and progression (224,225).

5.4. Two Marker Clusters define a Triple-negative gene signature.

Two remaining Marker Clusters corresponded to gene expression patterns which defined the TNBC subtype. Firstly, we identified Marker Cluster 1, termed the "mosaic" cluster, as the grouping of genes that were significantly increased in both the HER2-positive and Luminal A/B subtypes when compared to the TNBC subtype (Figure 5.3; Table 5.1.). Therefore, this cluster is composed of genes whose expression values are lowest in the TNBC subtype. Interestingly, this cluster contains *AR* and one its target genes, *PIP* (226) which are bot expressed at much lower levels in TNBC tumors when compared to the other two subtypes (Figure 5.3.).

Given that Marker Cluster 1 contains genes that are generally downregulated in TNBC tumors compared to HER2-positive and Luminal A/B tumors, we investigated Marker Cluster 2, which contained genes that are significantly enriched in the TNBC subtype. Intriguingly, the most striking differences in our differential expression analysis were the genes that showed increased expression in the absence of *HER2*, *ESR1* and *PGR*. This can be observed in the first column of the marker heatmap in Figure 5.2. and in the top rows of the marker heatmap averaged across clusters in Figure 5.3. A. *SOX10* is among the most differentially expressed genes within the TNBC subtype (Figure 5.3. C) and has gained increasing attention as a novel biomarker for these tumors over the past decade (166,167). Within the TNBC cluster, tumors

tend to express higher levels of Sox10 than any other subtype (Figure 5.3. C), providing further evidence that Sox10 is in fact a biomarker for the TNBC subtype.

5.5. *SOX10* can be used as an independent biomarker of the TNBC subtype.

The current strategy for identifying TNBC tumors is to assess patients for the absence of *HER2*, *ESR1* and *PGR*, which is the approach we initially used when analyzing the TCGA dataset (Figure 5.1.). However, identifying a gene or set of genes whose expression defines a subtype could improve clinical diagnosis, may provide a better insight into the disease and allow for the possible discovery of novel therapeutics. One of the strongest candidates for a bona fide biomarker of the TNBC subtype that others have identified (166,167,197) and we have confirmed here, is Sox10 (Figure 5.3. A, C; Table 5.1.). To further validate whether SOX10 is a biomarker of the TNBC subtype, we performed unsupervised clustering of the TCGA dataset based on the expression of *HER2*, *ESR1*, *PGR* and *SOX10*. We predicted that if SOX10 was a biomarker of the TNBC subtype, adding its expression analysis to the clustering performed with *HER2*/*ESR1*/*PGR* alone (Figure 5.1.) would not change the proportion of patient samples within each putative subtype. Confirming this hypothesis, the three putative subtypes remained effectively identical when *SOX10* expression was added to the clustering analysis (Figure 5.4.). Although Sox10 expression is highest in the TNBC subtype, it is interesting to note that most HER2-positive samples have very low expression of *SOX10* while the Luminal A/B subtype has more variable *SOX10* expression (Figure 5.4.).

To corroborate the findings drawn from our analysis, we performed immunohistochemical staining of 104 human breast cancer samples for Sox10. In accordance with our transcriptomic analyses, Sox10 histochemistry revealed an increased staining intensity and more prominent nuclear localization in the TNBC tumors than within the HER2

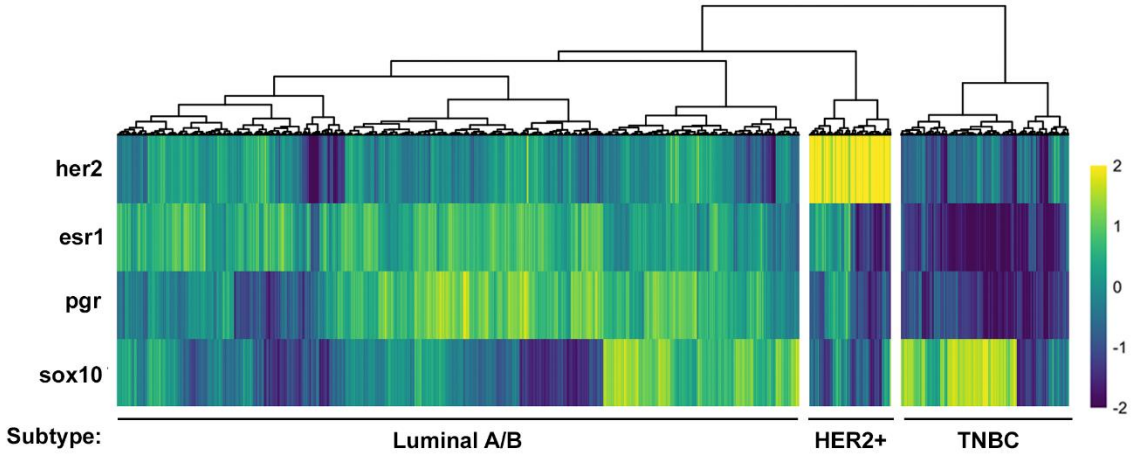

Figure 5.4. Sox10 expression can be used to independently identify the TNBC subtype. Heatmap of HER2, ESR1, PGR and Sox10 expression (z-score of log2 counts) across all samples. Each column represents the expression values for an individual patient sample. Hierarchical clustering was used to group patients by the expression patterns of each gene. This clustering revealed a group of putative TNBC, HER2-positive and Luminal A/B patients which was almost identical to that in Figure 5.1. suggesting that Sox10 expression defines the TNBC subtype. Figure was adapted (223).

and Luminal A/B cores (Figure 5.5.). Together, our data suggests that at levels of both the transcriptome and proteome, Sox10 is a strong candidate biomarker for the TNBC subtype.

5.6. Sox10 correlates with a more basal/stem-like phenotype in the TNBC but not Luminal A/B subtype.

The TNBC subtype is often associated with increased stem cell activity which may result in these tumors being more resistant to conventional therapeutics (64,216). We have also identified that *SOX10* is amongst the most differentially upregulated genes in the TNBC subtype (Table 5.1.). Interestingly, Sox10 transcriptional activity has been shown to be sufficient to reprogram pluripotent cells into a multipotent state and more specifically has been shown to regulate the stem/progenitor activity of mammary epithelial cells (184,227). Therefore, we aimed to assess whether S*OX10* expression was correlated with an increase in stemness. To perform this analysis, we utilized a recent study in which the stemness indices for all TCGA samples were calculated (228) and plotted stemness index against *SOX10* expression (Figure 5.6.). Interestingly, high *SOX10* expression correlated with high stemness only in the TNBC subtype, whereas Luminal A/B tumors which had higher levels of *SOX10* tended towards a lower stemness index (Figure 5.6.). These data suggest that either Sox10 is not the only driver of the stem-like phenotype in TNBC tumors or that Luminal A/B and HER2 tumors possess a pro-differentiation program that is able to overcome the basal/stem-like state driven by Sox10.

5.7. Loss of SLK induces several genes that correlate with the TNBC subtype, including Sox10.

SLK deletion in Neu-induced mammary tumors results in an increased mammosphere forming efficiency driven at least in part by the induction of *Sox10* (Figure 4.10. and 4.12.).

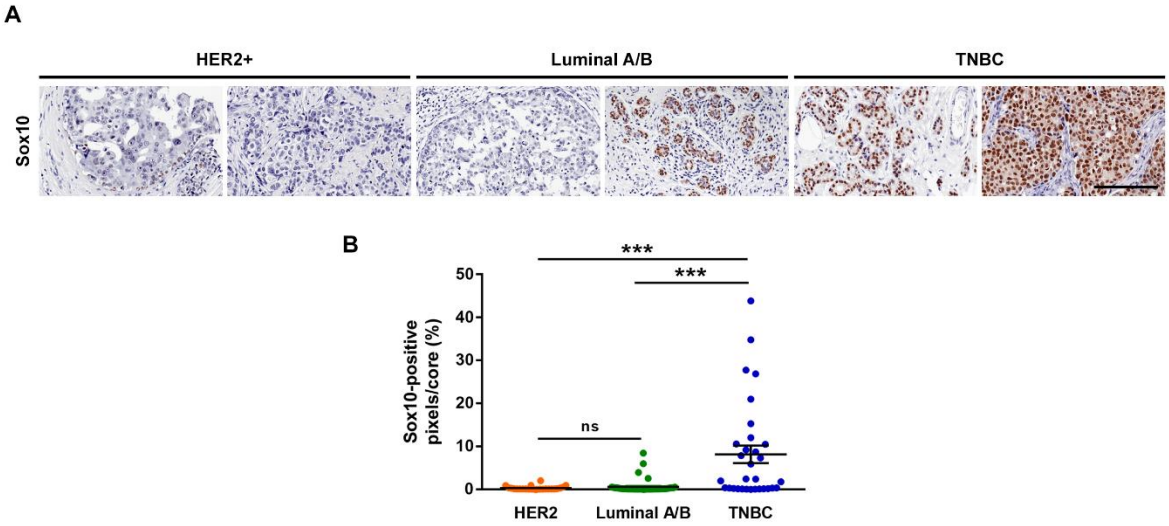

Figure 5.5. Sox10 histochemistry can be used as a predictor of the TNBC subtype. (A) Human breast cancer TMA BR20810 was purchased from US Biomax and contains 104 breast cancer cases across all three major subtypes as defined by HER2, ESR1 and PGR staining intensities. Sox10 histochemistry was performed and two representative cores from each subtype are shown. **(B)** Each core was quantified for the positive-pixel intensity of the Sox10 staining. A significant increase in the Sox10 staining intensity was observed in the TNBC tumor cores. Scale bar = 200 μm. Figure was adapted from (223).

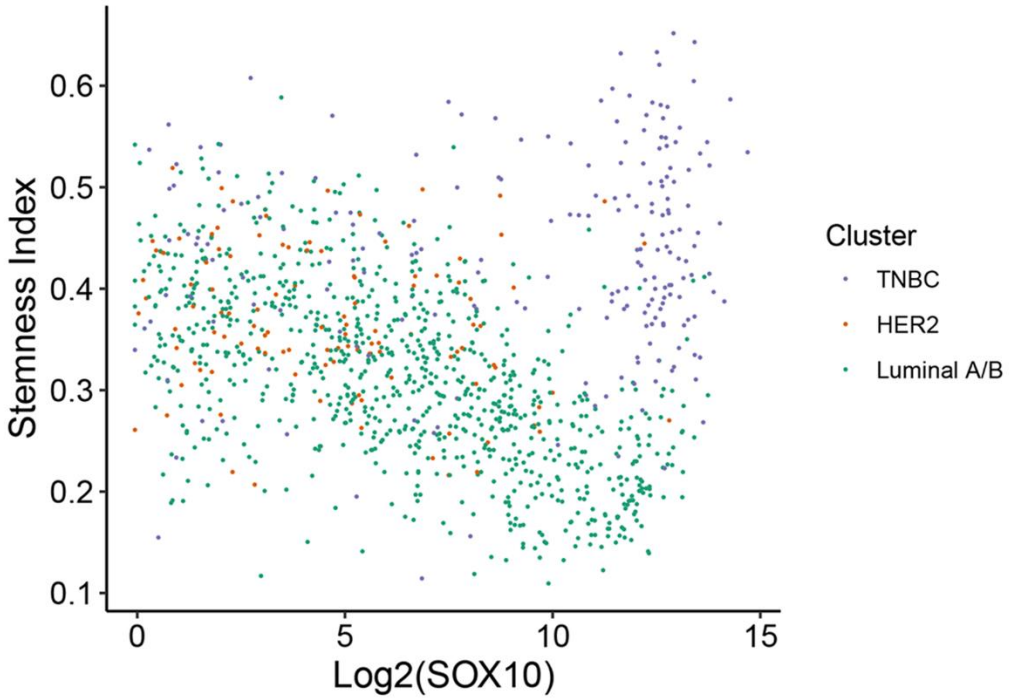

Figure 5.6. Sox10 expression correlates with a more basal/stem-like phenotype in TNBC. Stemness index for all 1246 patients from the TCGA dataset were previously calculated (228) and plotted against *SOX10* expression (log2). Individual samples were color coded according to their identified molecular subtype (Figure 5.1.). Figure was adapted from (223).

Here, we have also shown that *SOX10* is a marker of the TNBC subtype (Figure 5.3. C) and that high *SOX10* expression correlates with an increased stemness index within these tumors (Figure 5.6.). Therefore, we aimed to assess which other genes that were induced following SLK deletion also correlated with a TNBC/basal-like phenotype.

To test whether any genes other than Sox10 could be correlated with a more TNBC-like subtype, we correlated the expression strength of all the differentially expressed genes from the $SLK^{-/-}$ NDL microarray (Figure 4.9.) with their matched expression strength in the TNBC subtype from the TCGA dataset. As predicted, *Sox10* had the strongest positive correlation of all induced genes in the microarray with the TNBC subtype, however, several other genes including *Lcn2*, *Muc15*, *L1cam*, *Serpine2* and *Ceacam1* also showed string expression in both the microarray and TNBC patient samples (Figure 5.7. A). Although the expression of *Slk* is artificially low in the microarray samples (due to Cre-mediated recombination), we did observe that *Slk* expression seemed to negatively correlate with TNBC marker strength (Figure 5.7. A). Additionally, analysis of the TCGA dataset shows that the mean expression for *Slk* is significantly reduced in human TNBC breast cancers as compared to HER2-positive tumors (Figure 5.7. B).

To independently corroborate the transcriptional data from the TCGA dataset, we performed immunohistochemical staining for both SLK and Sox10 on human breast cancer cores. Consistent with the lower level of *SLK* expression in TNBC tumors and higher levels of *SOX10* expression within the same subtype, we observed an inverse correlation in SLK and Sox10 histochemistry (Figure 5.7. C). Tumor cores with low levels of HER2-positive staining tended to have very low levels of SLK in the cytoplasm, but very prominent nuclear Sox10 (Figure 5.7. C). Conversely, as HER2-positivity increased, a more prominent signal for SLK

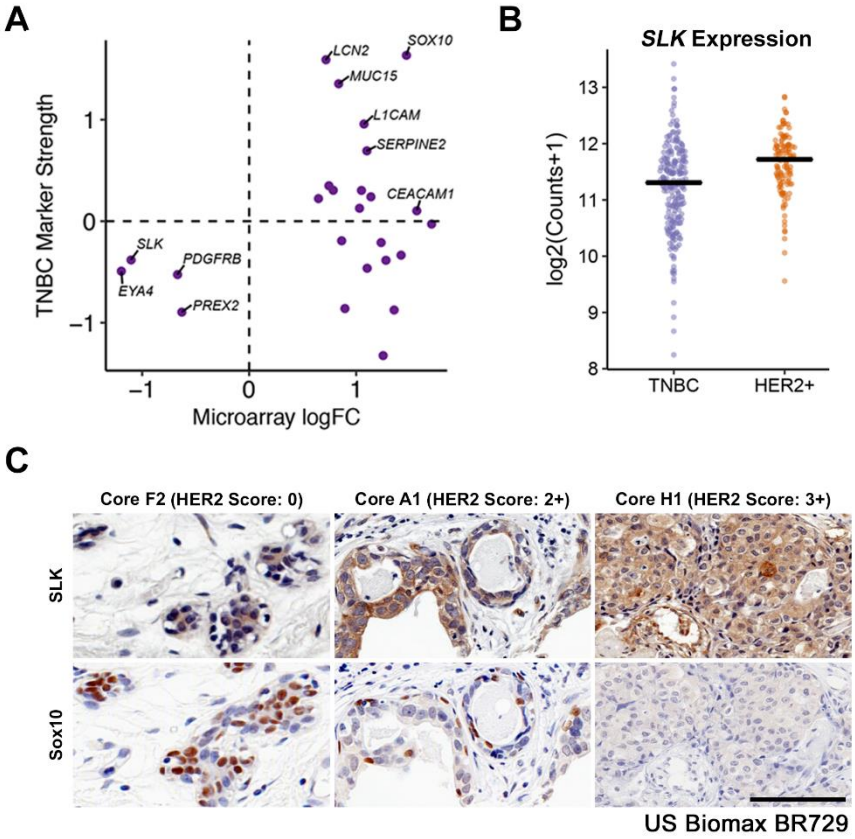

Figure 5.7. SLK deletion results in a more TNBC-like signature. (A) Microarray analysis was performed using total RNA from three independent $SLK^{fl/fl}$ and $SLK^{-/-}$ NDL cell lines hybridized to the Mouse Gene 2.0 ST Array (Affymetrix). Data analysis was carried out in the r statistical programming environment with Bioconductor. The log fold change was plotted for each gene from the microarray and correlated to its expression strength within the TNBC subtype from the TCGA dataset. Several genes that are induced following SLK deletion have strong expression in the TNBC subtype. **(B)** SLK expression (log2) was plotted for each individual patient sample from the TCGA dataset that was identified as HER2-positive or Triple-negative. The black line represents the median expression value for each subtype. **(C)** Human breast cancer TMA BR729 was purchased from US Biomax. Serial slides containing 72 HER2-positive breast cancer cases were stained for SLK and Sox10. Each core was scored by US Biomax for its HER2-positivity and three representative cores are shown. SLK expression was significantly higher in tumor cores with a greater HER2-positivity and was also inversely correlated with Sox10 expression. Scale bar = 200 μm.

was observed in the cytoplasm coupled with a reduction in the nuclear Sox10 staining intensity (Figure 5.7. C).

5.8. Summary.

Here, we have analyzed 1246 invasive breast cancer samples from the TCGA database and demonstrated that *SOX10* is highly expressed in *HER2*/*ESR1*/*PGR*-low tumors and is a candidate biomarker for the TNBC subtype. Additionally, high expression of *SOX10* was correlated with a greater stemness index in the TNBC tumors. We have also observed that *SOX10* and *SLK* expression have an inverse correlation within human patient samples and that *SLK* expression is lowest within the TNBC subtype. Lastly, we have shown that SLK deletion in Neu-induced mammary tumor cell lines results in the acquisition of genes which are highly expressed in TNBC tumors. Additionally, we have observed an inverse expression pattern between SLK and Sox10 in human cancers, with low SLK/high Sox10 expression in TNBC tumors. These data suggest that SLK may be required to maintain a differentiated state in the context of Neu-induced mammary tumors and upon downregulation or deletion of SLK, tumors induce the expression of *Sox10* and subsequently acquire a more basal/TNBC-like phenotype.

Chapter 6

Sox10 induction following SLK deletion in Neu-induced mammary tumors requires signaling through an AKT/Sox9-dependent pathway.

6.1. Introduction and Rationale.

Our lab has shown that SLK is activated downstream of Neu and is required for heregulin-stimulated chemotaxis (114). To assess the role of SLK in Neu-induced mammary tumorigenesis *in vivo*, we have crossed conditional SLK knockout mice (198) with MMTV-NIC transgenic mice (90). Conditional deletion of SLK in Neu-induced mammary tumors results in an accelerated tumor onset and reduced overall survival (Figure 4.3. A, B). Loss of SLK in Neu-expressing cell lines and tumors results in the induction of the triple-negative breast cancer marker, Sox10 (Figure 4.9.).

As Sox10 has been shown to mark and regulate the stem/progenitor population in neural crest, melanocyte and mammary epithelial cells (164,184,185), we assessed the stem/progenitor activity in our SLK knockout cell line. Following SLK deletion, an increase in mammosphere forming potential accompanied by higher surface expression of the stem cell markers, CD133 and Sca1 was observed (Figure 4.10.). We have confirmed the previous findings that Sox10 is sufficient to drive increased stem/progenitor activity in mammary epithelial cells by overexpression Sox10 in $SLK^{fl/fl}$ NDL tumor cells (Figure 4.12.). Additionally, we have shown that Sox10 overexpression cooperates with Neu in the transformation process (Figure 4.13.) and drives a significant increase in subcutaneous tumor growth in immunocompromised mice (Figure 4.14.). Together, these results suggest that Sox10 is critical for the earlier mammary tumor onset that is observed following SLK deletion.

Despite the importance of Sox10 in neuronal development, stem cell maintenance and tumor development, little is known about the mechanisms regulating its expression (164,166,167,184,185,229). FGF signaling has been shown to play a major role in regulating both the expression and function of Sox10. However, the transcriptional machinery responsible for its induction is unknown (Figure 1.5.) (184,191). Here, we have reported that

Sox10 is a bona fide marker of the triple-negative subtype (Figure 5.5.). Additionally, we have observed that Sox10 is a critical regulator of the phenotype observed following SLK deletion in Neu-induced mammary tumors and cell lines (Figure 4.9., 11.), we sought to investigate the signaling mechanisms that mediate the induction of Sox10.

6.2. Induction of *Sox10* requires PI3K-dependent signaling following SLK deletion.

SLK has previously been shown to signal downstream of Neu in a PLCγ- and PI3K-dependent manner (114). Therefore, we first assessed whether Sox10 expression was dependent on either PLCγ or PI3K signaling. $SLK^{fl/fl}$ and $SLK^{-/-}$ NDL cells were treated with either U-73122 or LY-294002 to inhibit PLCγ or PI3K, respectively. Inhibition of PLCγ had no significant effect on the expression of *Sox10* in either cell line, suggesting that *Sox10* induction is not dependent on PLCγ signaling (Figure 6.1. A). Conversely, inhibition of PI3K in $SLK^{-/-}$ NDL cells led to a 40% reduction in *Sox10* mRNA levels (Figure 6.1. B). Therefore, the induction of *Sox10* following SLK deletion in this tumor model is at least partially dependent on PI3K signaling. However, it is likely that other mechanisms contribute to the induction of *Sox10* as PI3K-inhibtion does not completely restore expression to control levels (Figure 6.1. B).

Activation of PI3K by receptor tyrosine kinases, including Neu, results in the phosphorylation of phosphatidylinositol lipid substrates and generation of the 3-phosphoinositide, PIP_3 (121). PI3K-dependent signaling then proceeds through two downstream effectors, PDK1 and AKT, which bind to the newly generated PIP_3 lipid moiety and are primed for maximal activation (121,128,130). As PDK1 and AKT are two downstream mediators of the PI3K-depedent signaling cascade, we hypothesized that pharmacological inhibition of those kinases would repress *Sox10* expression in SLK knockout mammary tumor cells. $SLK^{fl/fl}$ and $SLK^{-/-}$ NDL cells were treated with LY-294002, PDK1 inhibitor II or MK-

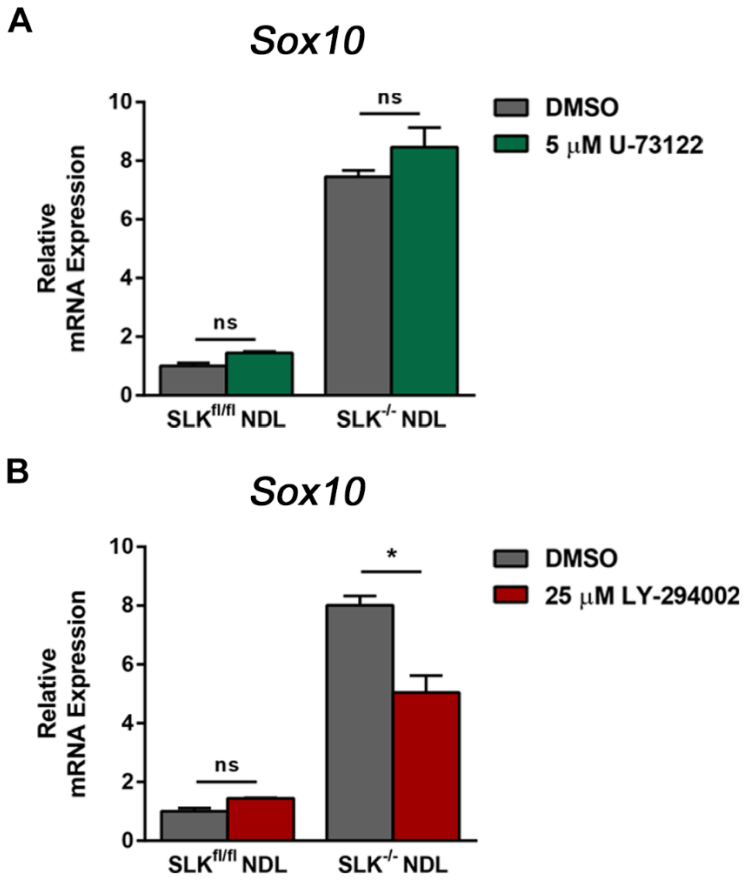

Figure 6.1. *Sox10* expression is dependent on PI3K signaling in SLK$^{-/-}$ NDL cells. (A) SLK$^{fl/fl}$ and SLK$^{-/-}$ NDL cells were treated with the PLCγ inhibitor, U-73122, for 72 hours. The levels of *Sox10* transcript was assessed by qPCR analysis. No significant differences in *Sox10* were observed following treatment. **(B)** SLK$^{fl/fl}$ and SLK$^{-/-}$ NDL cells were treated with the PI3K inhibitor, LY-294002, for 72 hours. The levels of *Sox10* transcript was assessed by qPCR analysis. *Sox10* expression was significantly reduced in the SLK-knockout cells following PI3K-inhibition. * represents $p<0.05$ and ns represents no statistical difference.

2206 to inhibit PI3K, PDK1 or AKT, respectively. Consistently, inhibition of all three kinases resulted in a significant reduction in *Sox10* expression following 72 hours of treatment (Figure 6.2. A-C). Inhibition of PI3K or PDK1 results in a 30-40% reduction in *Sox10* mRNA transcript at this timepoint (Figure 6.2. A, B). Interestingly, the 30-40% reduction in *Sox10* expression observed following PI3K or PDK1 inhibition was sufficient to reduce the amount of Sox10 protein to nearly undetectable levels (Figure 6.2. D). To eliminate the possibility that these compounds have different potencies in inhibiting the PI3K signaling cascade, we assessed the levels of active ribosomal S6 protein which is a common signaling node for all three kinases. S6 was found to be completely inactivated at the highest dose for all three inhibitors (Figure 6.2. D). This strongly suggests that the induction of *Sox10* following SLK deletion is primarily AKT-dependent.

As inhibition of PI3K, PDK1 or AKT is sufficient to downregulate the expression of *Sox10* at the transcriptional level, we tested whether this signaling cascade was upregulated in SLK-deficient tumors and cell lines. Additionally, an increase in the PI3K/PDK1/AKT axis would increase pro-survival and anti-apoptotic signaling and enhance tumorigenesis in line with our initial observations in the $SLK^{fl/fl}$ NIC model (Figure 4.3. A, B) (116,127). We first assessed the levels of both PI3K and PTEN in the $SLK^{fl/fl}$ and $SLK^{-/-}$ NDL cells and observed no differences in overall protein expression between the two cell lines (Figure 6.3. A). This suggests that loss of SLK does not affect transcription or protein stability of either PI3K or PTEN. Intracellular PIP_3, which is required for the maximal activation of both PDK1 and AKT, is produced when PI3K directly phosphorylates PIP_2 (121). Therefore, measuring the intracellular levels of PIP_3 by mass ELISA is a surrogate readout for the overall activity of PI3K (230). No differences in the total amount of PIP_3 was detected between $SLK^{fl/fl}$ and

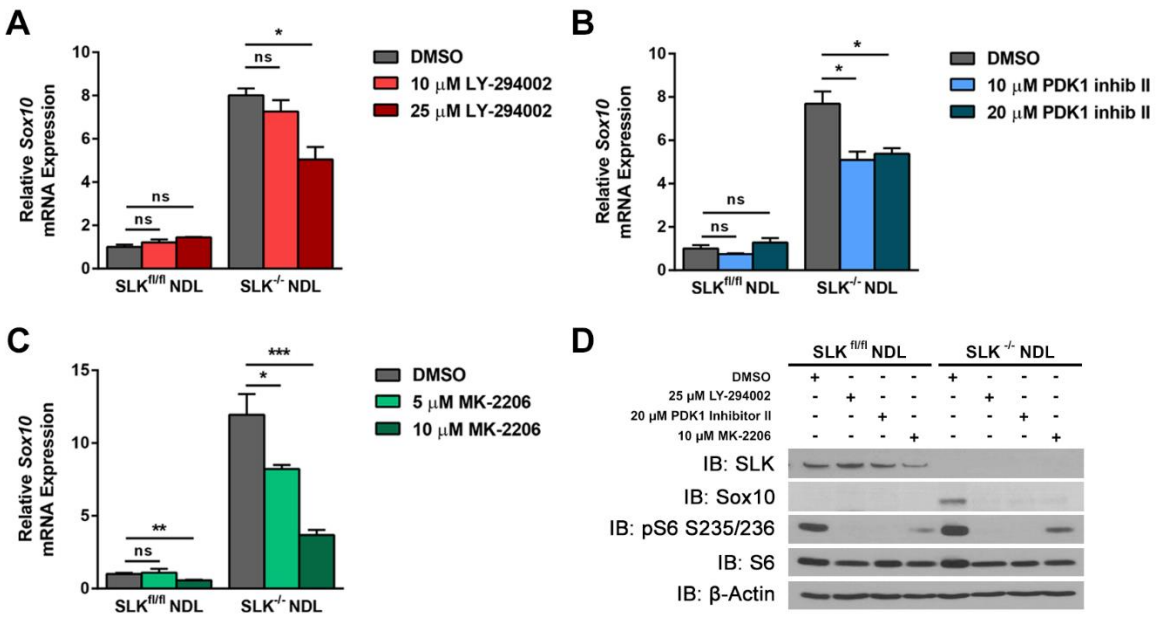

Figure 6.2. Inhibition of PI3K, PDK1 or AKT significantly reduces *Sox10* expression in SLK$^{-/-}$ NDL cells. (A) SLK$^{fl/fl}$ and SLK$^{-/-}$ NDL cells were treated with two different concentrations of the PI3K inhibitor, LY-294002, for 72 hours. The levels of *Sox10* transcript was assessed by qPCR analysis. **(B)** SLK$^{fl/fl}$ and SLK$^{-/-}$ NDL cells were treated with two different concentrations of the PDK1 inhibitor, PDK1 inhibitor II, for 72 hours. The levels of *Sox10* transcript was assessed by qPCR analysis. **(C)** SLK$^{fl/fl}$ and SLK$^{-/-}$ NDL cells were treated with two different concentrations of the AKT inhibitor, MK-2206, for 72 hours. The levels of *Sox10* transcript was assessed by qPCR analysis. *Sox10* expression was significantly reduced in the SLK-knockout cells following PI3K-, PDK1- or AKT-inhibition. **(D)** SLK$^{fl/fl}$ and SLK$^{-/-}$ NDL cells were treated with PI3K, PDK1 or AKT inhibitors at the highest indicated concentration from (A-C) for 72 hours. Following treatment, whole cell lysates were analyzed for levels of Sox10 and phosphorylation of ribosomal protein S6 by Western blot. Inhibition of PI3K, PDK1 or AKT at these concentrations significantly reduces ribosomal protein S6 activity to a similar degree. * represents $p<0.05$, ** represents $p<0.005$, *** represents $p<0.0005$ and ns represents no statistical difference.

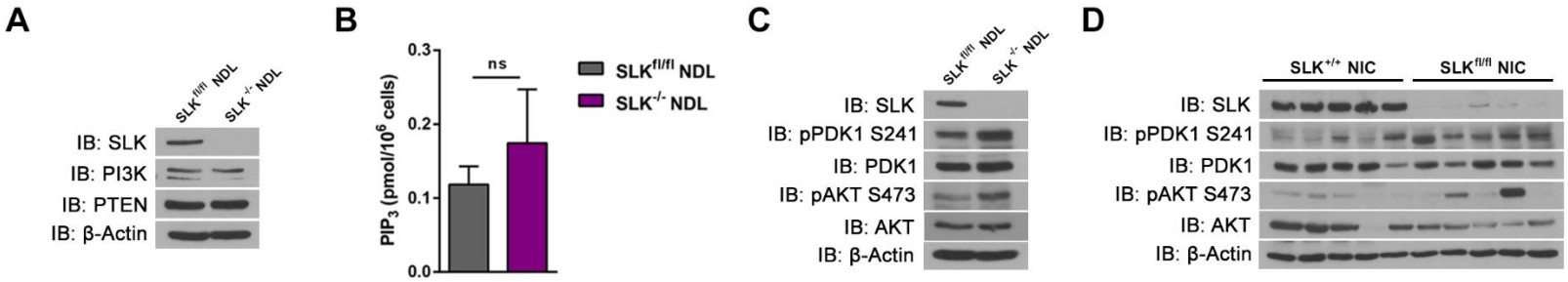

Figure 6.3. SLK deletion in NeuNDL tumor cells results in constitutive PDK1 and AKT activation. (A) Levels of PI3K and PTEN were assessed in $SLK^{fl/fl}$ and $SLK^{-/-}$ NDL cells by Western blot. No appreciable differences were observed between the two cell lines. **(B)** PI3K and PTEN activity was assessed by measuring the intracellular levels of PIP_3 by mass ELISA. Data is represented as the mean mass of PIP_3 detected per million cells from three independent biological triplicates +/- SEM. **(C)** $SLK^{fl/fl}$ and $SLK^{-/-}$ NDL cells were assessed for PDK1 and AKT activity by Western blot analysis. The levels of pPDK1 S241 and pAKT S473 are significantly higher in the $SLK^{-/-}$ NDL cells. **(D)** PDK1 and AKT activity was assessed in $SLK^{+/+}$ and $SLK^{fl/fl}$ NIC tumor lysates. Consistently elevated levels of pPDK1 S241 was observed in the $SLK^{fl/fl}$ NIC tumors. Levels of pAKT S473 also appear to be higher in the SLK knockout samples when normalized to the total amount of AKT in each sample. ns represents no statistical difference.

$SLK^{-/-}$ NDL cells (Figure 6.3. B). Overall, these results suggest that loss of SLK does not alter the overall activity of PI3K or PTEN *in vitro*.

Although PI3K activity was not affected by the deletion of SLK, we investigated the possibility that SLK directly alters PDK1 and/or AKT activity. Interestingly, consistently elevated levels of active PDK1 and AKT were observed in SLK-deficient tumor cells as compared to controls (Figure 6.3. C). The findings were corroborated qualitatively *in vivo* where $SLK^{fl/fl}$ NIC tumors tended to have higher levels of active PDK1 and AKT (Figure 6.3. D). Therefore, SLK deletion increases the activity of PDK1 and AKT in a PI3K-indepdent or downstream manner.

6.3. SLK and PDK1 activity are reciprocally regulated through a negative feedback mechanism.

As the deletion of SLK results in an increase in PDK1 and AKT activity independent of PI3K and PIP_3 levels, we hypothesized that SLK regulates a negative feedback mechanism on one or both proteins downstream of Neu. To determine whether SLK was upstream of PDK1 and AKT, we stimulated $SLK^{fl/fl}$ NDL cells with heregulin and assessed the kinetics of activation of these kinases (Figure 6.4. A). Maximal SLK activation was observed at 90 minutes following stimulation with heregulin (Figure 6.4. A), consistent with previous reports (114). Unexpectedly, heregulin-stimulated activation of both PDK1 and AKT occurred prior to the maximal SLK kinase activity (Figure 6.4. A). Additionally, the downregulation of PDK1 and AKT activity occurred after maximal SLK activation (Figure 6.4. A). Interestingly, we observed that the activation of PDK1 following heregulin-stimulation was cyclic, with two independent waves of activation observed over two hours (Figure 6.4. A). As SLK deletion results in increased PDK1 activity, this data suggests that PDK1 is activated prior to SLK and that SLK may feedback on this signal and inhibit PDK1.

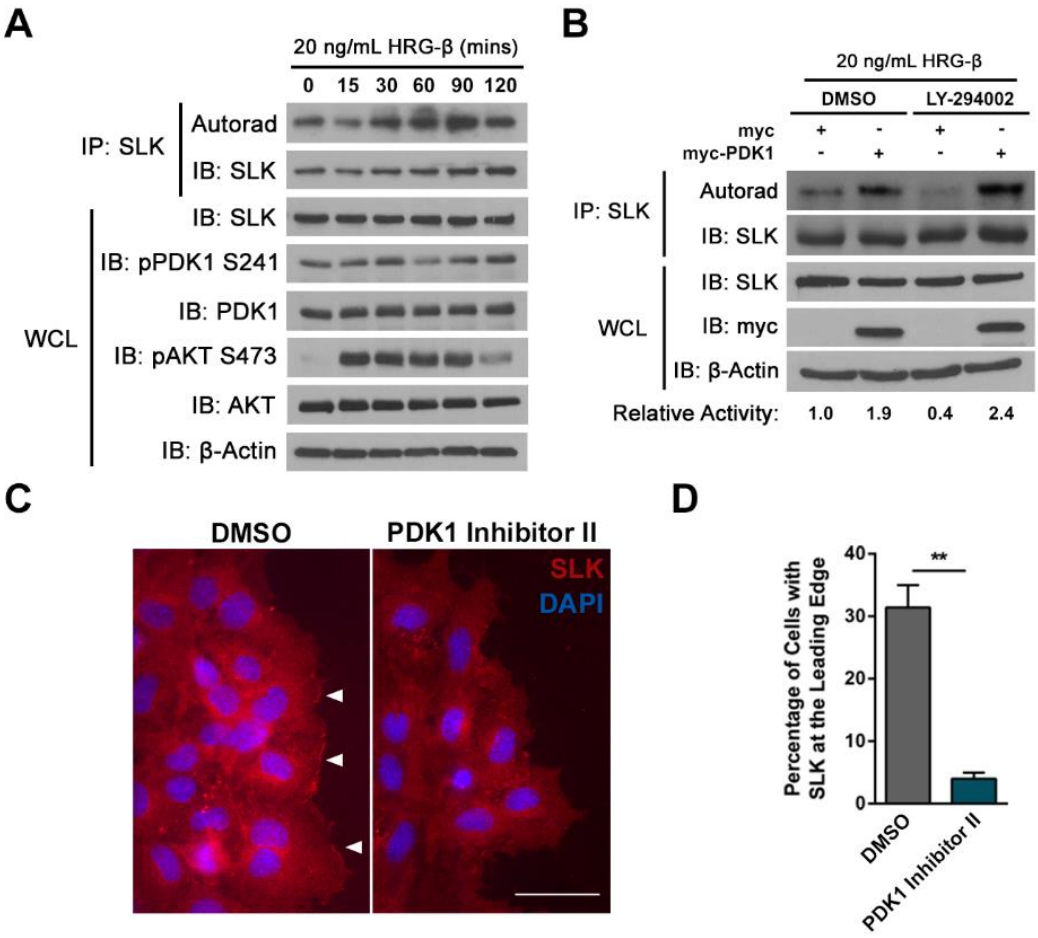
A
20 ng/mL HRG-β (mins)
0 15 30 60 90 120
IP: SLK
Autorad
IB: SLK
WCL
IB: SLK
IB: pPDK1 S241
IB: PDK1
IB: pAKT S473
IB: AKT
IB: β-Actin
B
20 ng/mL HRG-β
DMSO
LY-294002
myc
myc-PDK1
IP: SLK
Autorad
IB: SLK
WCL
IB: SLK
IB: myc
IB: β-Actin
Relative Activity: 1.0 1.9 0.4 2.4
C
DMSO
PDK1 Inhibitor II
SLK
DAPI
D
Percentage of Cells with SLK at the Leading Edge
**
DMSO
PDK1 Inhibitor II
E
SLK fl/fl NDL
SLK -/- NDL
0 15 30 45 60 0 15 30 45 60
IB: SLK
IB: pErbB3 Y1289
IB: ErbB3
IB: pPDK1 S241
IB: PDK1
IB: β-Actin

Figure 6.4. SLK and PDK1 are reciprocally regulated through a negative feedback mechanism. (A) $SLK^{fl/fl}$ NDL cells were serum-starved overnight and stimulated with heregulin-β (HRG-β) for up to two hours. SLK activity was assessed by kinase assay and activity of PDK and AKT by Western blot analysis. A spike in both pPDK1 S241 and pAKT S473 precedes maximal SLK activation. **(B)** $SLK^{fl/fl}$ NDL cells were transfected with myc or myc-PDK1 and serum starved overnight in the presence of DMSO or the PI3K inhibitor, LY-294002. Cells were then stimulated with heregulin-β for two hours and subject to an SLK kinase assay. Expression of PDK1 rescues SLK activity in the presence of LY-294002 following heregulin-stimulation. **(C)** NIH-3T3 fibroblasts were grown to confluency on coverslips and serum-starved overnight. Cells were then treated with PDK1 Inhibitor II for six hours and stimulated to migrate by scratch-wounding the confluent monolayer for 45 minutes. Cells were then fixed and stained for SLK. SLK can be observed at the leading edge of DMSO treated control cells (white arrowhead). **(D)** For each coverslip, ten random fields of view were chosen for quantification and the data is represented as the mean of three independent biological replicates +/- SEM. A significant decrease in the proportion of cells with SLK staining at the leading edge is observed following PDK1 inhibition. **(E)** $SLK^{fl/fl}$ and $SLK^{-/-}$ NDL cells were treated serum-starved overnight and stimulated with heregulin-β for one hour. Cell lysates were collected at the indicated timepoints and probed for pPDK1 S241 to assess PDK1 activity. PDK1 cycles between an active and inactive state following heregulin-stimulation in SLK-expressing but nor SLK-knockout NDL cells. ** represents $p<0.005$. Scale bar = 50 μm.

We first tested whether PDK1 overexpression was sufficient to activate SLK in the presence of heregulin. $SLK^{fl/fl}$ NDL cells were transiently transfected with myc-PDK1 and stimulated with heregulin for 90 minutes. Overexpression of PDK1 was sufficient to induce a two-fold increase in heregulin-stimulated SLK kinase activity compared to the vector control (Figure 6.4. B). Furthermore, overexpression of PDK1 was sufficient to rescue heregulin-stimulate SLK activity in the presence of a PI3K inhibitor (Figure 6.4. B). Our lab has previously observed that PDK1 is required for SLK-dependent cellular migration in fibroblasts (unpublished data). We have reported that SLK is readily localized to the leading edge of migrating fibroblasts on a scratch-wounded confluent monolayer, where it is fully activated (41). NIH-3T3 fibroblasts were grown to confluency and pre-treated with a PDK1 inhibitor for 6 hours prior to scratch-wounding. Consistent with the observation that PDK1 is sufficient to induce SLK activation, inhibition of PDK1 significantly reduced that number of fibroblasts with SLK-positive staining at the leading edge (Figure 6.4. C, D). This suggests that PDK1 is at least partially responsible for regulating SLK localization to the leading edge and maximal activation downstream of PI3K.

As we have observed that PDK1 activation precedes that of SLK and is sufficient to induce SLK activation, we tested the hypothesis that SLK may signal to inhibit PDK1 signaling. To do this, $SLK^{fl/fl}$ and $SLK^{-/-}$ NDL cells were both treated with heregulin for 60 minutes and PDK1 activity was assessed by western blot. Consistent with our previous data, PDK1 activation in control cells cycled between an active and inactive state following heregulin-stimulation with peak activation observed every 30 minutes (Figure 6.4. E). However, PDK1 activity did not oscillate in the $SLK^{-/-}$ NDL cells and remained consistently elevated and higher throughout the timecourse (Figure 6.4. E). As SLK-deficient cells failed

to decrease PDK1 activity following heregulin-stimulation, we concluded that SLK is required to inhibit PDK1 in a negative feedback mechanism.

6.4. Sox10 is sufficient to rescue stem/progenitor function following PI3K-pathway inhibition.

We have previously observed that $SLK^{-/-}$ NDL cells have an increased mammosphere forming capacity (Figure 4.10.) and that overexpression of Sox10 in control cells is sufficient to mimic this phenotype (Figure 4.12.). Therefore, we aimed to assess whether inhibition of PI3K, PDK1 or AKT was sufficient to reduce the mammosphere forming potential of $SLK^{-/-}$ NDL cells. Consistent with our previous results, SLK knockout cells had a three-fold increase in mammosphere forming efficiency when compared to control cells in the presence of DMSO (Figure 6.5. A, B). Inhibition of PI3K, PDK1 or AKT resulted in a significant reduction in the mammosphere forming efficiency of both cell lines (Figure 6.5. A, B). These observations were confirmed in both primary and secondary mammosphere assays (Figure 6.5. A, B). Although these results correlate with *Sox10* expression they do not explicitly confirm that the reduction in stem/progenitor activity is a direct result of *Sox10* downregulation. We next assessed whether ectopic expression of Sox10 would prevent the decrease in mammosphere forming efficiency that was observed by inhibiting PI3K, PDK1 or AKT. Consistent with previous reports showing that Sox10 is required for mammary stem/progenitor activity (184,187), stable overexpression of Sox10 in $SLK^{fl/fl}$ NDL cells was sufficient to rescue the reduction in mammosphere forming potential caused by inhibition of PI3K, PDK1 or AKT (Figure 6.5. C, D). Interestingly, Sox10 expression only partially rescued the formation of primary and secondary mammospheres when treated with LY-294002 or PDK1 inhibitor II but virtually a complete rescue was observed when treated with the AKT inhibitor, MK-2206

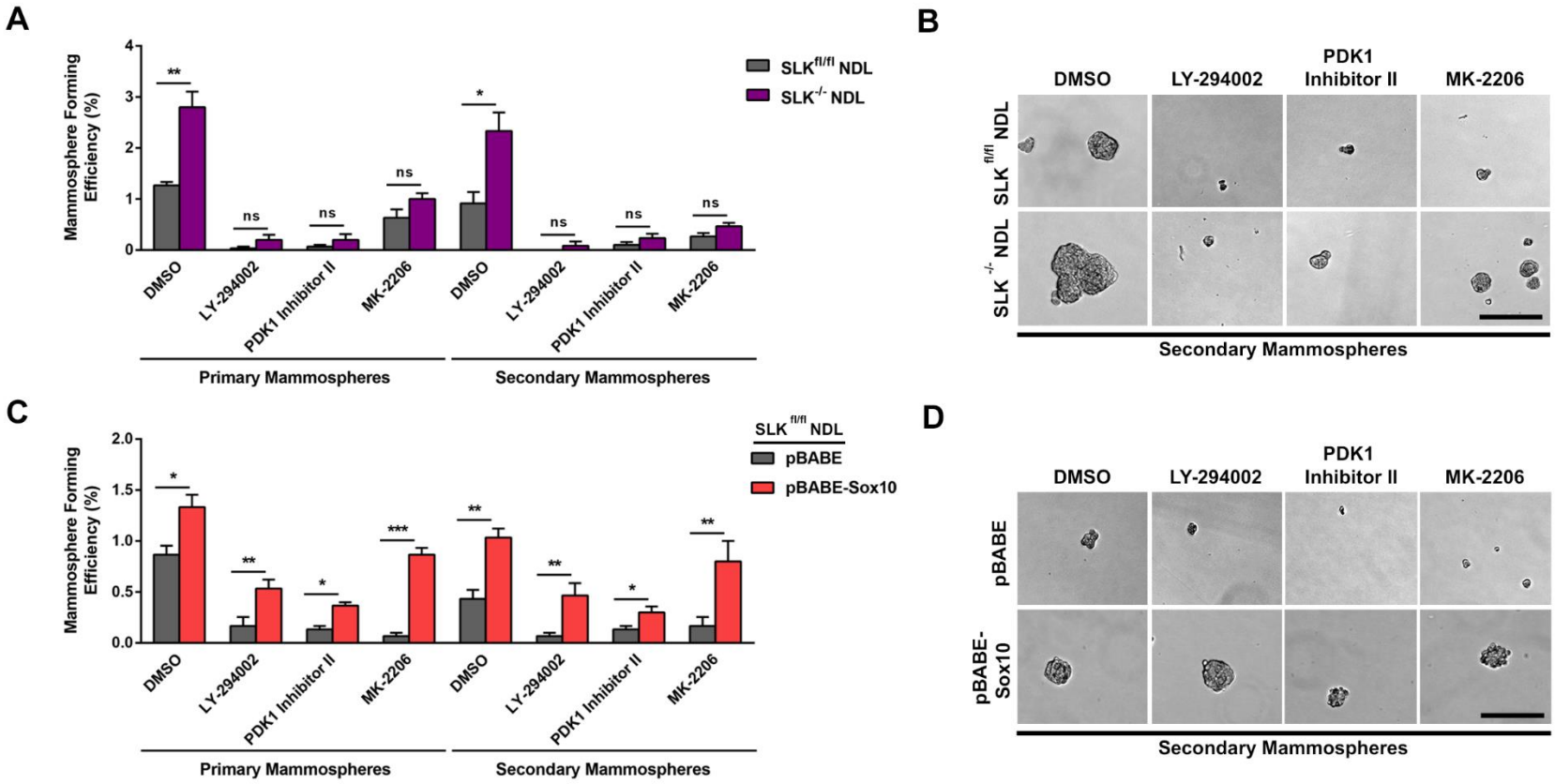
A
Mammosphere Forming Efficiency (%)
SLK fl/fl NDL
SLK -/- NDL
DMSO
LY-294002
PDK1 Inhibitor II
MK-2206
Primary Mammospheres
Secondary Mammospheres
B
PDK1 Inhibitor II
SLK fl/fl NDL
SLK -/- NDL
Secondary Mammospheres
C
SLK fl/fl NDL
pBABE
pBABE-Sox10
D
pBABE
pBABE-Sox10

Figure 6.5. The mammosphere forming potential of $SLK^{-/-}$ NDL cells is dependent on PI3K-signaling and can be rescued by Sox10 expression. (A) The mammopshere forming potential of $SLK^{fl/fl}$ and $SLK^{-/-}$ NDL cells was assessed by plating 1000 cells per well in 24-well low attachment plates and allowing primary mammospheres to form for seven days in the presence of LY-294002, PDK1 Inhibitor II or MK-2206. Secondary mammospheres were plated by disaggregating the primary passage and seeding the cells for a further seven days. The mammosphere forming efficiency from both cell lines and mammosphere passages was calculated as the percentage of spheres per well with a diameter greater than 15 μm over the total number of cells that were seeded. Data is represented as the mean mammosphere forming efficiency from three independent biological replicates +/- SEM. **(B)** Representative images from both mammosphere passages and cell lines is shown. Inhibition of PI3K, PDK1 or MK-2206 significantly inhibits the mammosphere forming potential of $SLK^{fl/fl}$ and $SLK^{-/-}$ NDL cell lines. **(C)** The same experiment was carried out as in (A) but using $SLK^{fl/fl}$ NDL cells expressing either pBABE or pBABE-Sox10. **(D)** Representative images from both mammosphere passages and cell lines is shown. Expression of Sox10 is sufficient to rescue mammosphere forming efficiency in the presence of PI3K pathway inhibitors. * represents $p<0.05$, ** represents $p<0.005$, *** represents $p<0.0005$ and ns represents no statistical difference. Scale bar = 100 μm.

(Figure 6.5. C, D). This observation supports the notion that AKT is the major regulator of Sox10 and that inhibition of PI3K or PDK1 is not sufficient to entirely block AKT activity. Alternatively, PI3K and PDK1 may be critical for other cellular functions whereas AKT is a major downstream regulator of stemness and *Sox10* expression. Furthermore, we have provided evidence that Sox10 is a major regulator of stem/progenitor activity in luminal-derived Neu-induced mammary tumor cells *in vitro*.

6.5. *Sox10* expression is regulated by several upstream promoter elements in SLK-deficient Neu-induced mammary tumor cells.

As we have shown that *Sox10* expression is regulated by AKT (Figure 6.1. C) and that Sox10 enhances both stem/progenitor activity (Figure 4.12., 6.5. C, D) and tumor growth *in vivo* (Figure 4.14.), we aimed to identify the direct mechanisms downstream of AKT regulating its expression.

The *SOX10* promoter has previously been shown to be epigenetically silenced in human gastric cancers and metastatic melanoma (168,231). We hypothesized that the *Sox10* gene was hypermethylated in $SLK^{fl/fl}$ NDL cells as the basal level of expression is low *in vitro*. We identified two putative CpG islands immediately upstream of the *Sox10* transcription start site using MethPrimer CpG island prediction software (Figure 6.6. A) (232). To assess whether the *Sox10* gene was methylated, we treated $SLK^{fl/fl}$ and $SLK^{-/-}$ NDL cells with 5-aza-2'-deoxycytidine for five days to effectively eliminate any methylation marks within the genome. Following treatment only a modest increase in *Sox10* mRNA was observed in the $SLK^{-/-}$ NDL cells with no significant differences observed in the controls (Figure 6.6. B). The lack of *Sox10* induction following 5-aza-2'-deoxycytidine treatment suggests that these putative CpG islands are not heavily methylated in either cell line. To verify that promoter hypermethylation was

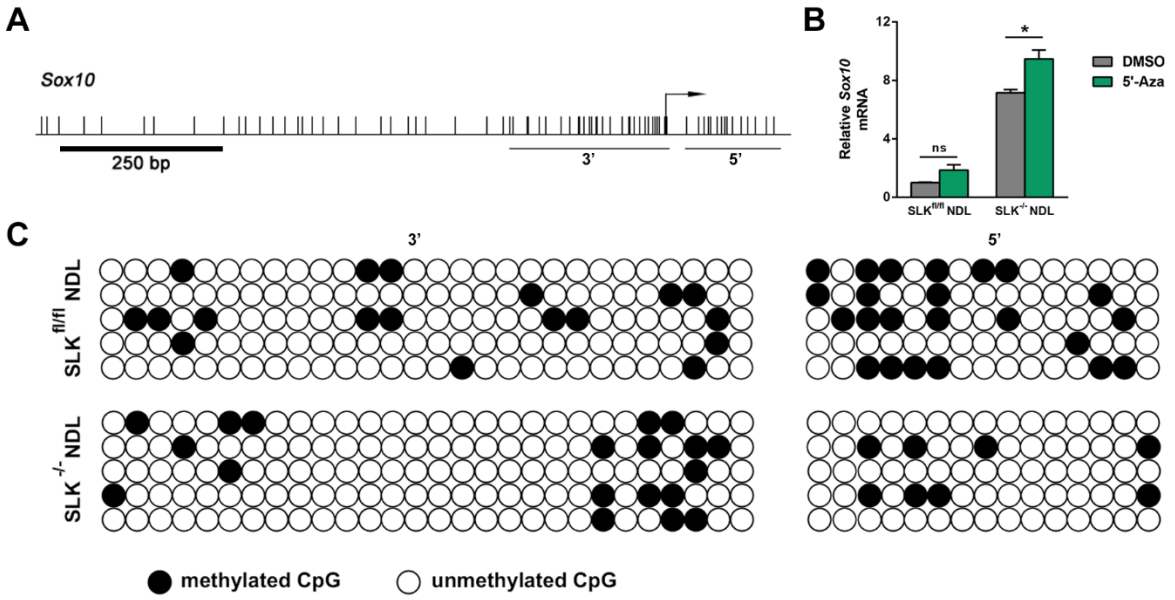

Figure 6.6. Induction of *Sox10* following SLK deletion is not due to promoter demethylation. (A) Schematic representation of the murine *Sox10* gene. The transcriptional start site is indicated by the forward arrow. The location of all CG dinucleotides are represented as individual vertical lines. MethPrimer CpG island prediction software (232) was used to identify potential CpG islands and are shown as the underlined regions. **(B)** $SLK^{fl/fl}$ and $SLK^{-/-}$ NDL cells were treated with 5-aza-2'-deoxycytidine (5'-Aza) for five days. The media and 5'-Aza was replenished daily. The levels of *Sox10* transcript was assessed by qPCR analysis and only a modest increase in expression was observed in the $SLK^{-/-}$ NDL cells. **(C)** Bisulfite sequencing of genomic DNA from $SLK^{fl/fl}$ and $SLK^{-/-}$ NDL cells was performed. Five independent clones from each cell lines were sequenced. A representative plot of methylated (filled) and unmethylated (open) CpG repeats from the two putative CpG islands identified in (A) is presented. No appreciable differences were observed in the methylation status in either cell line for both CpG islands. * represents $p<0.05$ and ns represents no statistical difference.

not responsible for the repression of *Sox10* in SLK-expressing tumor cells *in vitro*, we isolated genomic DNA and performed bisulfite sequencing on both putative CpG islands and compared the methylation pattern in both $SLK^{fl/fl}$ and $SLK^{-/-}$ NDL cells. Using this approach, we have validated that only approximately 20% of cytosines within these CpG islands are methylated in either cell line with no significant differences observed following SLK deletion (Figure 6.6. C). Together, these results indicate that demethylation of the *Sox10* promoter is not responsible for *Sox10* induction following SLK deletion.

As epigenetic silencing is not responsible for the differential expression of *Sox10* in $SLK^{fl/fl}$ and $SLK^{-/-}$ NDL cells, we sought to identify regulatory regions around the *Sox10* gene that directly control its expression. Comparative sequence analyses have previously identified multiple-species conserved sequences (MCS) that control *Sox10* expression (189). In luminal mammary epithelial cells, peroxisome-proliferator activated receptor-binding protein (PBP) was shown to directly bind to MCS4 and MCS7 resulting in the recruitment of the mediator complex and transcriptional initiation by RNA polymerase II (192,193). As MCS 4 and MCS7 have been shown to regulate *Sox10* expression in mammary epithelial cells, we tested whether these enhancer elements were differentially regulated in $SLK^{fl/fl}$ and $SLK^{-/-}$ NDL cells. Interestingly, both enhancer elements drove luciferase activity above the levels of the control vector, however, no significant differences between cell lines was observed (Figure 6.7. A). This suggests that perhaps basal expression of *Sox10* is driven by these enhancer sequences, although they are not responsible for the ten-fold increase in *Sox10* observed in the $SLK^{-/-}$ NDL cells.

As little is known about the mechanisms regulating *Sox10* transcription outside of the MCS sequences, we generated luciferase assay constructs driven by five independent Sox10 promoter elements within 7 kb of the transcription start site. Initially, we observed that the

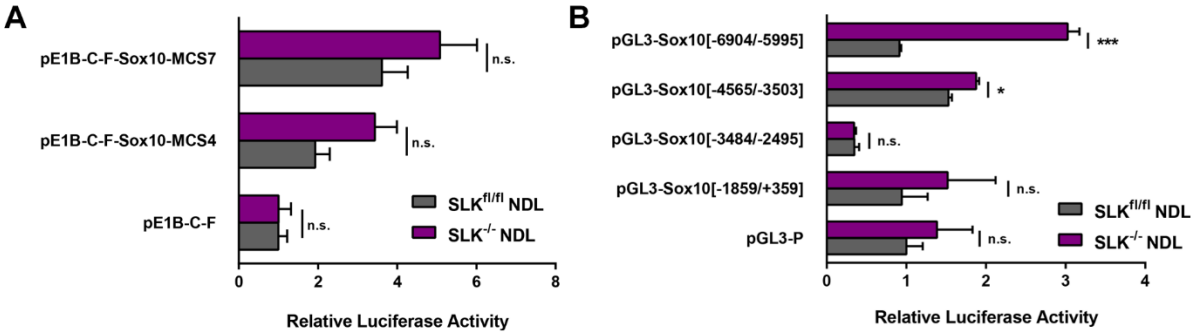

Figure 6.7. A 1 kb fragment of the Sox10 promoter differentially regulates luciferase activity in SLK$^{fl/fl}$ and SLK$^{-/-}$ NDL cells. (A) Two multiple-species conserved sequences (MCS4 and 7) that have been shown to control *Sox10* expression were assessed for their ability to drive luciferase activity in SLK$^{fl/fl}$ and SLK$^{-/-}$ NDL cells. Both MCS4 and MCS7 increased luciferase activity above the control vector (pE1B-C-F), however, no differences were observed between the two cell lines. **(B)** Approximately 1 kb fragments of the Sox10 promoter were cloned into pGL3 and assessed for their ability to drive luciferase activity in SLK$^{fl/fl}$ and SLK$^{-/-}$ NDL cells. The -6904/-5995 promoter element was differentially regulated between the two cell lines. Raw light units from the luciferase constructs were normalized to Renilla for each technical sample. Data from (A) and (B) is represented as the mean luciferase activity from three independent biological replicates +/- SEM. * represents $p<0.05$, ** represents $p<0.005$, *** represents $p<0.0005$ and ns represents no statistical difference.

-3484/-2495 fragment of the promoter contained a repressive element which decreased luciferase activity by approximately 75% in both $SLK^{fl/fl}$ and $SLK^{-/-}$ NDL cell lines and may account for the lower basal expression of *Sox10* in cultured mammary epithelial tumor cell lines (187) (Figure 6.7. B). Differential regulation of luciferase activity was observed in the two most distal promoter fragments between $SLK^{fl/fl}$ and $SLK^{-/-}$ NDL cells (Figure 6.7. B). Intriguingly, the -6904/-5995 promoter element showed a three-fold increase in luciferase activity in the SLK knockout cells, whereas that same element was inactive in the control cell line (Figure 6.7. B). As such, we have identified at least one region within the *Sox10* promoter which is differentially regulated between $SLK^{fl/fl}$ and $SLK^{-/-}$ NDL cells.

6.6. Sox9 is activated in an AKT-dependent manner and controls *Sox10* gene expression.

To identify the transcriptional machinery regulating *Sox10* expression on the -6904/-5995 region of the promoter, we first assessed the nuclear localization of known transcription factors that are AKT-responsive. We focused on AKT-regulated transcription factors as we have shown that AKT activity is required for maintenance of *Sox10* expression in SLK knockout mammary tumor cells (Figure 6.2. C). AKT has been shown to directly regulate CREB, FoxO and FoxA1 nuclear localization and transcriptional activity (142,143,167). Therefore, their cytoplasmic/nuclear distribution were assessed. Although no differences were observed between cell lines, it was interesting to note that CREB and FoxA1 are exclusively nuclear and that FoxO1 and FoxO3a are retained within the cytoplasm in this model (Figure 6.8.).

Further analysis of the -6904/-5995 promoter fragment revealed the presence of three consensus SoxE (Sox8, 9 and 10) binding sites within this region. To identify which SoxE genes are expressed in the Neu-induced mammary tumor cell lines, we performed qRT-PCR analysis. No detectable *Sox8* expression was observed in control or SLK knockout mammary

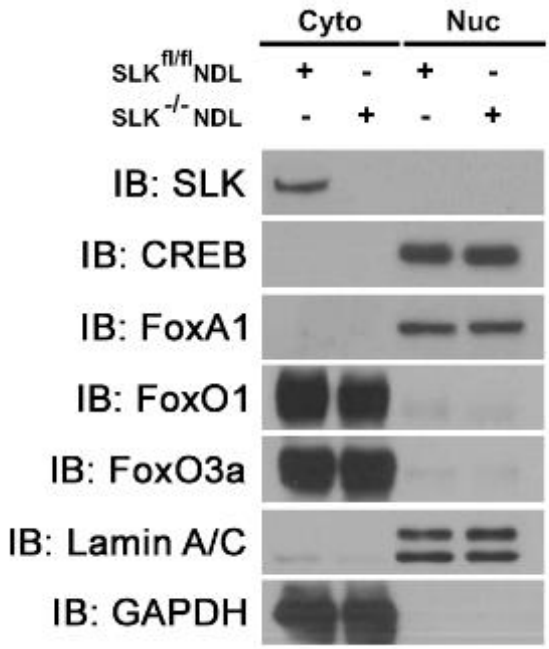

Figure 6.8. SLK deletion does not alter the nuclear localization of AKT-regulated transcription factors. Cytoplasmic (Cyto) and Nuclear (Nuc) fractions were separated from $SLK^{fl/fl}$ and $SLK^{-/-}$ NDL cells and harvested for protein lysate. The subcellular localization of AKT-regulated transcription factors was assessed by Western blot analysis. In these cells, CREB and FoxA1 remained exclusively nuclear while FoxO1 and FoxO3a were retained within the cytoplasm. No appreciable differences could be observed between cell lines. Lamin A/C and GAPDH were used as nuclear and cytoplasmic loading controls, respectively.

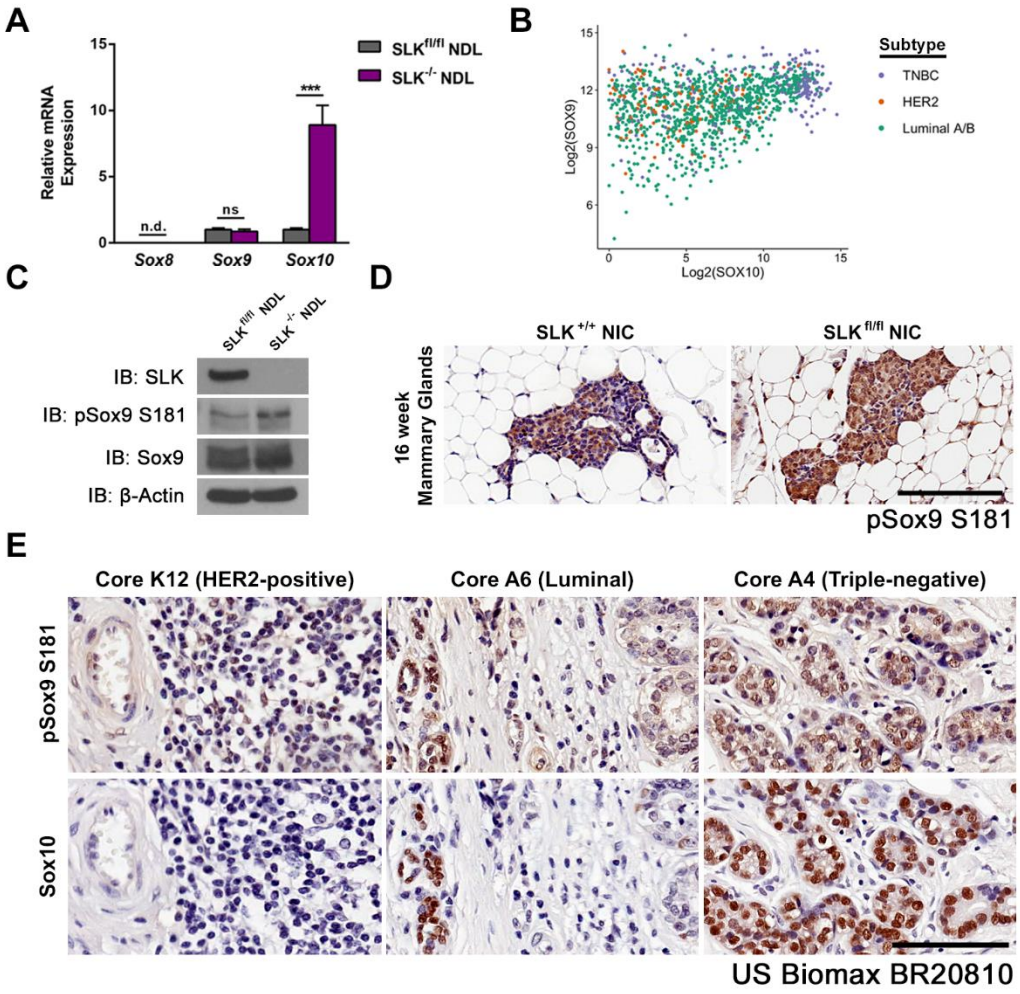

Figure 6.9. SLK deletion results in an increase in phosphorylated Sox9. (A) The expression level of the SoxE family was assessed in $SLK^{fl/fl}$ and $SLK^{-/-}$ NDL cells by qRT-PCR. No detectable (n.d.) expression of *Sox8*, no change in the levels of *Sox9* and a consistent ten-fold increase in *Sox10* was observed between the two cell lines. **(B)** The TCGA dataset was interrogated for expression of *SOX9* and *SOX10* across all breast cancer subtypes. Co-expression of both genes was observed in these patient samples with a Pearson correlation coefficient of 0.351. **(C)** $SLK^{fl/fl}$ and $SLK^{-/-}$ NDL cells were assessed for Sox9 expression and activity using a total or pS181 antibody, respectively. A consistent increase in phosphorylated Sox9 was observed in the SLK knockout tumor cell line when compared to the controls. **(D)** Sox9 histochemistry was performed on $SLK^{+/+}$ and $SLK^{fl/fl}$ NIC hyperplastic glands and endpoint tumor sections (n=10 glands/genotype) and representative images are shown for each genotype. Hyperplastic lesions within the SLK knockout mammary glands have considerably greater levels of phosphorylated Sox9. **(E)** Human breast cancer TMA BR20810 was purchased from US Biomax and contains 104 breast cancer cases across all three major subtypes as defined by HER2, ESR1 and PGR staining intensities. pSox9 S181 and Sox10 histochemistry was performed on serial sections and two representative cores from each subtype are shown. pSox9 S181 and Sox10 staining are positively correlated with higher staining in the TNBC subtype. *** represents $p<0.0005$ and ns represents no statistical difference. Scale bar = 100 μm in D; 200 μm in D.

tumor cells and no difference in the overall levels of *Sox9* was observed (Figure 6.9. A). Although reciprocal expression between Sox9 and Sox10 is observed in melanoma (165), analysis of TCGA data revealed a positive correlation between these two genes (Figure 6.9.B). We assessed the levels of Sox9 activity in our tumor cell lines by Western blot analysis for phosphorylated Sox9. Consistent with the positive correlation observed in breast cancer data sets, the levels of pSox9 S181 was much greater in the $SLK^{-/-}$ NDL cells, suggesting increased activity in this cell line compared to the control (Figure 6.9. C). We corroborated these results *in vivo* where we observed a significant increase in pSox9 S181-positive staining within the hyperplastic lesions of $SLK^{fl/fl}$ NIC mice at 16 weeks of age compared to NIC control mammary glands (Figure 6.9. D). Lastly, we have validated the positive correlation between active Sox9 and Sox10 levels by histochemical analysis of serial human tissue microarrays across HER2-positive, Luminal A/B and triple-negative breast cancer (Figure 6.9. E).

As we have observed increased activity for both AKT and Sox9 following SLK deletion in the Neu-induced mammary tumor cells (Figure 6.3. C, 6.9 C), we assessed the possibility that Sox9 is activated downstream of AKT and regulates *Sox10* expression. Treatment of $SLK^{fl/fl}$ and $SLK^{-/-}$ NDL cells with the AKT inhibitor, MK-2206, resulted in a significant decrease in the levels of Sox10 and phosphorylated Sox9, suggesting that Sox9 is activated in an AKT-dependant manner (Figure 6.10. A). To further validate that this AKT/Sox9 axis was responsible for the regulation of the -6904/-5995 promoter element, we performed a luciferase assay in the presence of MK-2206. Consistent with this element being the AKT-regulated region of the Sox10 promoter, treatment of the $SLK^{-/-}$ NDL cells with MK-2206 was sufficient to reduce luciferase activity back down to control levels (Figure 6.10. B).

Given this close connection between AKT and Sox9 in the regulation of *Sox10* expression, we assessed whether Sox9 is a direct target of AKT. Interestingly, the

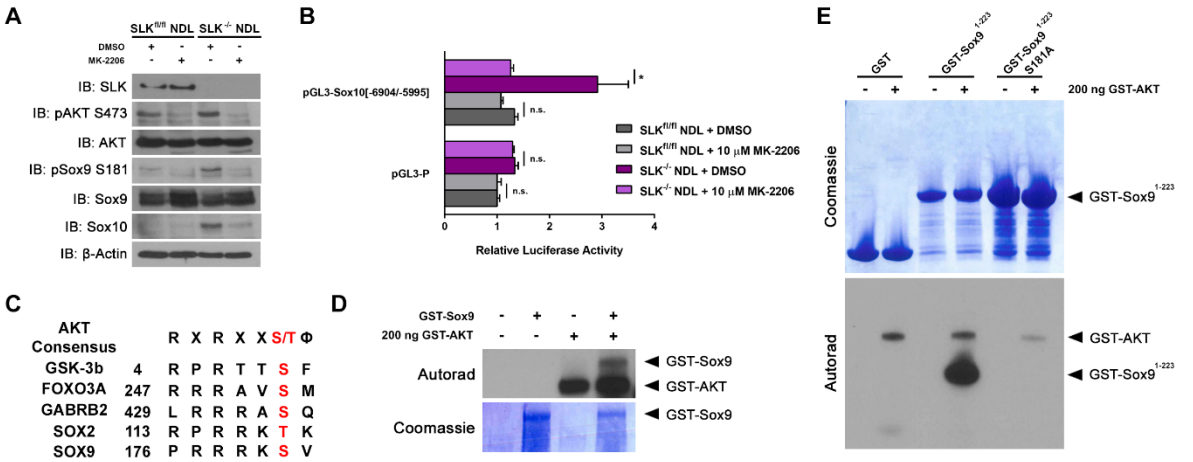

Figure 6.10. Sox9 phosphorylation and *Sox10* expression AKT-dependent. (A) Sox9 S181 phosphorylation in $SLK^{fl/fl}$ and $SLK^{-/-}$ NDL cells was assessed following treatment with the AKT inhibitor, MK-2206, for 72 hours by Western blot analysis. Treatment with MK-2206 significantly reduced AKT and Sox9 phosphorylation. **(B)** Luciferase assays were performed in the presence or absence of MK-2206 using the responsive -6904/-5995 element of the Sox10 promoter. A three-fold increase in luciferase activity was observed from the -6904/-5995 element in $SLK^{-/-}$ NDL cells when compared to controls. However, AKT inhibition was sufficient to reduce luciferase activity down to basal levels. Raw light units from the luciferase constructs were normalized to Renilla for each technical sample. Data is represented as the mean luciferase activity from three independent biological replicates +/- SEM. **(C)** The consensus AKT recognition sequence where X is any amino acid, the phosphorylated serine (S) or threonine (T) is in red and Φ is any hydrophobic amino acid. Bona fide AKT substrates are aligned to the consensus AKT substrate motif. Sox9 contains a putative AKT substrate recognition sequence at S181. **(D)** A recombinant kinase assay was performed using GST-Sox9 and 200 ng of recombinant GST-AKT. AKT phosphorylates Sox9 *in vitro*. **(E)** A recombinant kinase assay using GST-$Sox9^{1-223}$ or $Sox9^{1-223}$ S181A as substrates. * represents $p<0.05$ and ns represents no statistical difference.

phosphorylation site on Sox9 at S181 is very similar to the conserved AKT consensus sequence and shares a high degree of conservation with several bona fide AKT targets (Figure 6.10. C) (233-236). *In vitro* kinase assays using recombinant GST-AKT show direct phosphorylation of Sox9, suggesting that Sox9 may be a direct AKT target (Figure 6.10. D).

6.7. Sox9 transcriptional activity but not DNA binding is required for *Sox10* induction.

We have identified that the -6904/-5995 region of the Sox10 promoter is significantly more active in $SLK^{-/-}$ NDL cells, is AKT-responsive and contains three consensus SoxE binding motifs (Figure 6.7. B, 6.10. B). Additionally, we have shown that AKT inhibition is sufficient to decrease Sox9 phosphorylation on S181 (Figure 6.10 A). Therefore, we aimed to test whether Sox9 was directly bound to this promoter element and differentially controlling *Sox10* expression in the $SLK^{fl/fl}$ or $SLK^{-/-}$ NDL cells. For ChIP-qPCR, we immunoprecipitated Sox9 from both cell line and assessed binding to the -6904/-5995 promoter element using two different primer sets spanning the three putative SoxE binding sites. Although we observed a significant enrichment for Sox9 on this Sox10 promoter element above IgG in both the $SLK^{fl/fl}$ and $SLK^{-/-}$ NDL cells, no significant differences were observed between the two cell lines (Figure 6.11.). As a negative control, we also performed ChIP-qPCR on a putative SoxE binding site that was not responsive in our initial luciferase assays (Figure 6.7. B). This element, within exon 1, was not bound by Sox9 in either cell line suggesting that the enrichment we observe with the other fragments is not due to non-specific chromatin pulldown by the Sox9 antibody (Figure 6.11.).

Since Sox9 is present on the Sox10 promoter of both cell lines we hypothesized that the increase in Sox9 phosphorylation observed in the SLK knockout mammary tumor cells results in increased transcriptional activity. To test this, we transiently overexpressed myc, myc-Sox9 or myc-Sox9 S181A in $SLK^{-/-}$ NDL cells and performed a luciferase assay using the

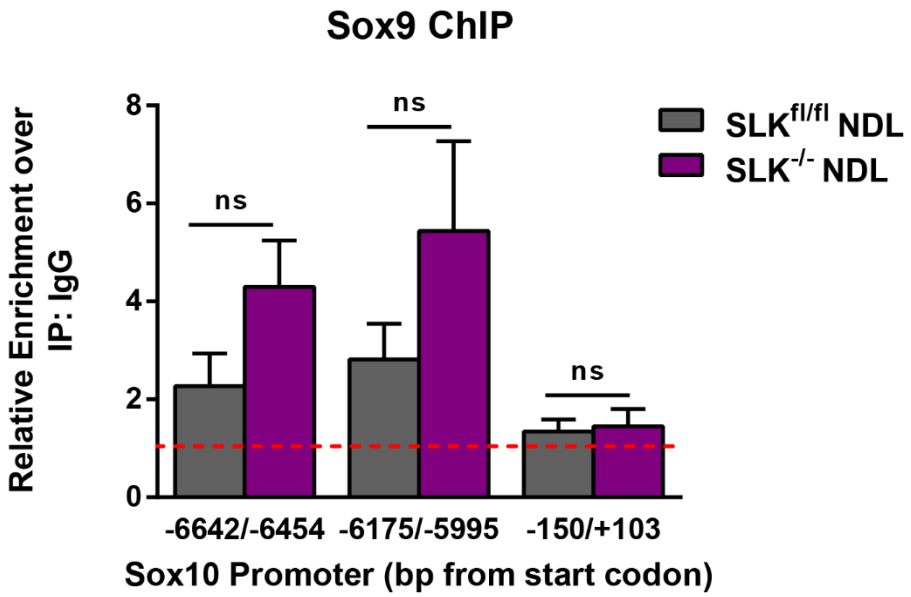

Figure 6.11. Sox9 S181 phosphorylation does not enhance DNA binding on the Sox10 promoter. Chromatin immunoprecipitation was performed on $SLK^{fl/fl}$ and $SLK^{-/-}$ NDL cells to assess Sox9 binding to the -6904/-5995 region of the Sox10 promoter. Following Sox9 immunoprecipitation, qPCR analysis was performed across three putative SoxE binding sites within the -6904/-5995 fragment of the Sox10 promoter. Sox9 binding to the Sox10 promoter was found to be significantly enriched at these SoxE binding sites when compared to IgG immunoprecipitation (dashed red line) or a negative control element within exon one (-150/+103). No significant differences in Sox9 enrichment on the chromatin was observed between the $SLK^{fl/fl}$ and $SLK^{-/-}$ NDL cell lines. ns represents no statistical difference.

-6904/-5995 fragment of the Sox10 promoter. Consistent with our previous data, we observed a two- to three-fold increase in luciferase activity from the Sox10 promoter fragment with the myc vector control (Figure 6.12. lanes 1 and 2). Additionally, we observed an AKT-dependent increase in luciferase activity following heregulin-stimulation in these cells (Figure 6.12. lanes 3 and 4). These controls further support the notion that *Sox10* induction from the -6904/-5995 promoter element is dependent on Neu signaling through AKT. To validate that these signals are dependent on Sox9 transcriptional activity, we assessed luciferase activity in the presence of myc-Sox9 or a myc-Sox9 S181A mutant which has reduced transcriptional activity (237). Surprisingly, in unstimulated cells, both wildtype and mutant Sox9 were sufficient to increase luciferase activity four-fold above background (Figure 6.12. lanes 5 and 6 compared to lanes 9 and 10). However, following stimulation with heregulin, a two-fold increase in luciferase activity was observed in myc-Sox9 expressing cells, whereas no significant change in luciferase activity was observed in cells expressing the myc-Sox9 S181A mutant (Figure 6.12. lanes 6 and 7 compared to lanes 10 and 11). As was observed in the myc transfected cells, the increased luciferase activity following heregulin-stimulation in myc-Sox9 transfected cells was completely dependent on AKT activity (Figure 6.12. lanes 7 and 8). Together these data suggest that the -6904/-5995 region of the Sox10 promoter is an AKT-responsive element which requires the transcriptional activity of Sox9.

6.8. Summary.

Here, we have shown that inhibition of the PI3K-signaling module downstream of Neu in SLK knockout tumor cells is sufficient to reduce *Sox10* levels (Figure 6.2.). The role for PI3K-dependent signaling modulating *Sox10* expression is further supported by the elevated levels of PDK1 and AKT activity in SLK knockout tumors and cell lines (Figure 6.3. C, D). Our results suggest that SLK is activated downstream of Neu in a PI3K-dependent manner and

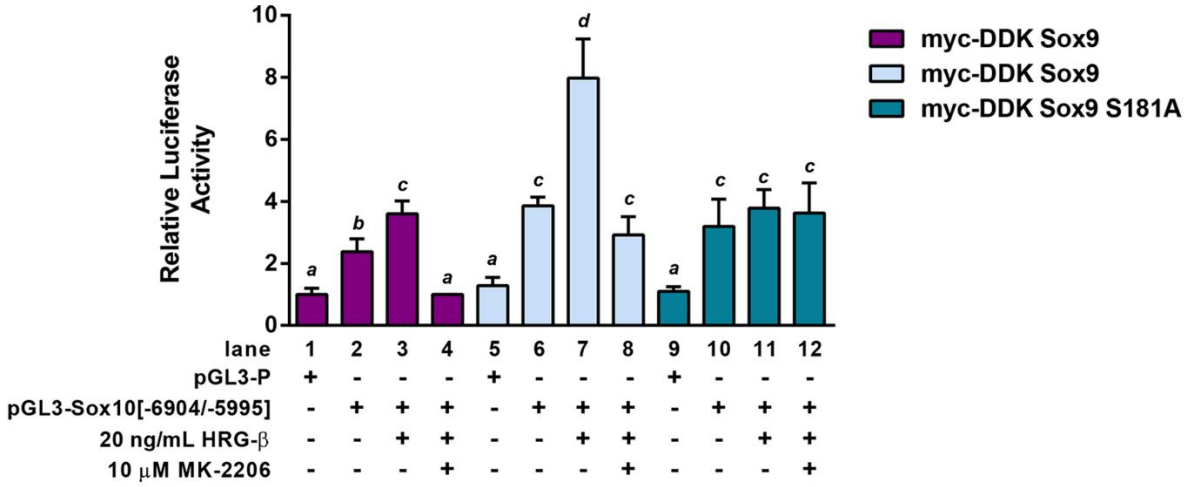

Figure 6.12. Sox9 phosphorylation at serine 181 is required for transactivation of the Sox10 promoter. Luciferase assays using the -6904/-5995 element of the Sox10 promoter was used to evaluate the role of Sox9 in controlling Sox10 expression. $SLK^{-/-}$ NDL cell were transfected with myc (purple bars), myc-Sox9 (light blue bars) or myc-Sox9 S181A (teal bars) and the indicated luciferase vectors for 48 hours. Cells were treated with heregulin-β (HRG-β), AKT inhibitor (MK-2206) or vehicle control for two hours prior collecting the cell lysate. Heregulin treatment significantly enhances luciferase activity driven by the Sox10 promoter in an AKT-dependent manner (lanes 3 and 4 and lanes 7 and 8) Heregulin-stimulation significantly increases luciferase activity in the myc-Sox9 but not myc-Sox9 S181A expressing cells (lanes 7 and 10). Raw light units from the luciferase constructs were normalized to Renilla for each technical sample. Data is represented as the mean luciferase activity from three independent biological replicates +/- SEM. All bars with the same letter are not statistically significant from each other. *a* compared to *b*: $p<0.05$, *a* compared to *c* or *d*: $p<0.005$, *b* compared to *c*: $p<0.05$, *b* compared to *d*: $p<0.005$ and *c* compared to *d*: $p<0.05$.

is required for feedback inhibition of PDK1 to dampen this signaling axis. Therefore, SLK deletion in Neu-induced mammary tumors and cell lines removes this feedback mechanism resulting in constitutive activation of PDK1 and AKT. Loss of SLK in this model also increases mammary stem/progenitor function likely due to the induction of *Sox10*. We have shown that AKT can activate Sox9 and that this novel pathway is responsible for the acquisition of *Sox10* in SLK-deficient mammary tumor cell lines. Using human breast cancer samples, we have also shown a correlation between the expression of Sox10 and Sox9 activity at both the RNA and protein levels. Lastly, we have shown that Sox9 is directly bound to and activates the Sox10 promoter. Importantly, this work has uncovered a novel mechanism in which HER2-positive breast cancers may acquire a more basal/stem-like Sox10-positive and together with triple-negative breast cancers, may benefit greatly from AKT-targeted therapies.

Chapter 7

General Discussion.

7.1. Deciphering the Roles of SLK During Embryogenesis.

7.1.1. The role of SLK in embryonic and placental development.

Proper embryonic development is regulated by multiple signaling networks which when altered can result in severe developmental defects and lethality. Although SLK is highly expressed in the neuronal and myogenic lineages of the developing embryo (19,195,196), little is known about its specific function in the development of these organs. Using a gene-trapped *Slk-LacZ* fusion allele, which is a functional hypomorph, we have shown that SLK is ubiquitously expressed across most organs during embryonic development and that proper regulation of the catalytic function of SLK is required for normal embryonic development.

As the gene-trapped *Slk* allele still contains the core catalytic kinase domain and lacks only the N-terminal ATH domain, we were surprised to observe such a dramatic phenotype. Despite the presence of the entire kinase domain, the SLK-LacZ fusion protein had reduced kinase activity when compared to endogenous SLK. One possibility for this reduction in catalytic activity is steric hinderance and substrate access caused by the presence of the LacZ moiety. Activation of SLK relies on efficient homodimerization in a head-to-tail orientation and autophosphorylation (214) whereas LacZ has been shown to tetramerize (213). This altered tetrameric SLK-LacZ fusion protein may not be able to readily autoactivate resulting in the reduced catalytic activity that we observed. Another possibility is that the C-terminal ATH domain of SLK is required to mediate the catalytic activity of SLK. In fact, both Ldb1/2 and LMO4 have been shown to regulate the activity of SLK and bind to the C-terminus of the kinase (208,209). This would suggest that the ATH domain is critical for SLK regulation by allowing for efficient homodimerization and/or the recruitment and binding of necessary co-factors.

To investigate the role of SLK in development, gene-trapped animals were bred to homozygosity which resulted in severe developmental defects and embryonic lethality. Further investigation revealed an increase in apoptosis accompanied with a marked disorganization of the neuronal and myogenic compartments in E12.5 and E14.5 *Slk-LacZ* homozygous ($SLK^{fs/fs}$) embryos. Previous reports have suggested that SLK is required for apoptosis and is cleaved by caspase 3 during this process (16,18). However, no differences in apoptosis have been observed in cultured MEFs (unpublished data), suggesting that the differences in apoptosis that we observed in $SLK^{fs/fs}$ embryos is a cell autonomous phenotype. Interestingly, the reports implicating SLK in the apoptotic signaling cascade have been performed by overexpression of either full length or a constitutively active truncated SLK which may account for the differences observed between the two systems.

Somites give rise to the dermomyotome, sclerotome and endothelial cells as well as guide the migration of neural crest cells and spinal nerve axons. Somitogenesis depends on several growth factor gradients whereby somites are deposited along the length of the embryo which requires proper coordination of cell migration and focal adhesion dynamics (238,239). We have observed that $SLK^{fs/fs}$ embryos display disorganized myogenic and neuronal compartments and underdeveloped viscerae. Our lab has previously shown that SLK regulates focal adhesion dynamics and cell migration (40,41). As SLK is expressed in myogenic precursors and neuronal stem cells (19,195), one possibility is that it is required for the migration of progenitor cells and proper tissue organization.

As with our SLK gene-trap model, p38, Mek1, B-Raf, Erk2 and Pak4 knockouts are embryonic lethal at around E12.5 and display defects in extraembryonic tissues (240-244). As with the SLK-targeted gene trap, a Pak4 knockout is embryonic lethal at E11.5 because of decreased cellular proliferation, particularly within the nervous system (244,245). A reduction

in cellular proliferation within the developing embryo is unlikely to be the sole reason for the embryonic lethality observed in our model. However, knockout mouse models that display embryonic lethality between E10.5 and E12.5 often present with placental abnormalities and/or embryonic vascular defects (202). As with the $SLK^{fs/fs}$ placentae, $Pak4^{-/-}$ placentae were reported to have a reduction in the number of blood vessels and a decreased cellularity throughout the labyrinth (245).

Placental development is critical for normal embryonic development. Therefore, one explanation for the increase in apoptosis within the embryo is abnormal vascular function. Analysis of placental tissues revealed abnormal blood vessel formation and severe hemorrhaging of $SLK^{fs/fs}$ placentae. Supporting a previously identified role for SLK in smooth muscle vasodilation (45), knockdown of *Slk* in MDMECs resulted in a significant reduction in capillary formation *in vitro*. SLK has been shown to phosphorylate and inactivate RhoA leading to vessel relaxation and vasodilation of endothelial cells (45). Therefore, we speculate that the SLK-LacZ fusion is unable to phosphorylate RhoA resulting in an accumulation of its activated GTP-bound form. Activated GTP-RhoA would result in increased vasoconstriction which may account for the collapsed SMA-positive vasculature within $SLK^{fs/fs}$ placentae. The restricted vasculature with these placentae would lead to a lack of appropriate nutrient and gas exchange between the maternal circulation and the embryo, ultimately inducing apoptosis throughout the embryo, resulting in the observed protein degradation and embryonic lethality.

We have shown that deletion of SLK at E0.5 using a β-actin-Cre transgenic mouse model results in an early embryonic lethality as no viable pups were ever born. Additionally, we have not observed any signs of resorption within the uterus of pregnant females from $SLK^{+/fl}$ β-actin-Cre timed matings. These data suggest that SLK deletion at the blastocyst stage may impair the ability for these blastocysts to migrate to and implant into the uterine lining.

This could be validated by flushing blastocysts from the uterine horns at E3.5 and genotyping. If no SLK-null blastocysts are detected, it would strongly support the hypothesis that SLK-null blastocysts fail to migrate to the uterus and implant. However, if SLK-null blastocysts are detected from the flushed uterine horns, it would suggest that they may implant and become resorbed early on.

7.1.2. The role of SLK in muscle development.

SLK has been shown to be most highly expressed in the developing muscular and neuronal lineages (19,195). Homozygous expression of the *Slk*-targeted gene trapped allele resulted in a significant reduction in the MyHC- and MyoD- positive populations in the developing muscle. Interestingly, the muscular defects observed within the gene-trap model may be a direct result of the reduced angiogenesis within the placenta and not as a direct effect of reduced kinase activity within the myogenic compartment. However, muscle-specific expression of a dominant negative SLK^{K63R} resulted in viable mice with enhanced regeneration *in vivo* (196). Additionally, SLK^{K63R} expression in this model was driven from the human skeletal actin (HSA) promoter. The HSA promoter is differentiation-specific and therefore SLK^{K63R} would not be expressed in undifferentiated myoblasts during early embryonic development.

To corroborate some of these findings, our lab has generated a conditional SLK allele and we have generated a muscle-specific SLK knockout using the Myf5-Cre knock-in mouse (198). Myf5 is expressed at E10.5-12.5 in the developing limb buds, which allows for Cre expression in the developing myogenic compartment prior to the formation of mature myofibers (246). In contrast to our *Slk*-targeted gene trap, SLK-deletion in the myogenic compartment resulted in an apparently normal myogenic compartment within the developing embryo (198). Although mice were viable, a progressive myopathy, impaired muscle function

and delayed regeneration was observed in the $SLK^{fl/fl}$ Myf5-Cre mice (198). Interestingly, muscle-specific deletion of SLK resulted in the mislocalization of focal adhesion proteins at the periphery of the myofibers (198). Together, these data support the notion that SLK is necessary for myofiber integrity but is dispensable for embryonic myogenesis, suggesting that the myogenic defects observed in the $SLK^{fs/fs}$ embryos are likely due to aberrant vascularization of the placenta.

7.1.3. The role of SLK in mammary gland development.

One potential explanation for the accelerated tumor onset observed following SLK deletion is that SLK knockout mammary glands could have impaired development and subsequent increase in the progenitor cell population. The MMTV promoter which drives the NIC transgene is primarily expressed in the luminal epithelial cell compartment (90) and therefore SLK deletion in the basal epithelium, myoepithelium or adipose tissue is highly unlikely to occur. Expression of Cre recombinase was confirmed in the luminal epithelial cells through positive X-gal staining of virgin mammary glands in the Rosa26R-LacZ reporter line (Figure 4.1.). Normal virgin mammary gland development was not affected by SLK deletion as evidenced by the apparently normal ductal structure and branching observed in virgin mice (Figure 4.1.). Similarly, the number of Sox10-positive cells was not changed, suggesting that the increase in tumor initiation rate following SLK deletion is not due to the expansion of progenitor populations. Although SLK deletion does not affect virgin mammary ductal outgrowth, the exact role of SLK in mammary gland development remains to be elucidated.

Pregnancy, lactation and involution are three key phases of adult mammary gland development that involve extensive rounds of coordinated differentiation, proliferation and apoptosis (247-249). Proliferation of the luminal epithelium is critical during early and late pregnancy where formation of lobuloalveolar structures prepares these cells for efficient milk

production and secretion (247). Conditional deletion of β1 integrin, an essential mediator of extracellular matrix signaling, in the luminal epithelial cells, reduced cellular proliferation and lobuloalveolar development during pregnancy. This is accompanied by a marked reduction in FAK levels (250,251). As SLK has been shown to be an important mediator of FAK-dependent migration and required for efficient cell cycle progression (20,35,36,41,49,252), SLK may play a critical role in β1 integrin/FAK-dependent lobuloalveolar expansion during pregnancy. Following pregnancy and lactation most of the secretory epithelium is removed with a week of weaning and the gland is remodelled to a pre-pregnant state (249). This involution of the mammary gland is biphasic and involves a first reversible apoptotic step where the luminal epithelium begins to detach from the alveolar structures and is shed into the lumen. The second step consists of an irreversible phase where the alveoli completely collapse and adipocytes begin to grow into the remaining space (253). Stat3, a key regulator of mammary gland involution, has been shown to induce the expression of negative regulatory subunits of PI3K, resulting in diminished signaling through AKT (254). SLK has previously been shown to be activated downstream of PI3K in mammary epithelial cells and has been implicated in apoptotic signaling (14,16,17,114). Therefore, it is possible that SLK is required for efficient mammary gland involution and remodelling following pregnancy and lactation. Together, we have shown that SLK does not affect normal luminal epithelial development in the mammary gland of virgin mice up to 12 weeks of age, however a role for SLK in regulating epithelial cell proliferation and apoptosis during pregnancy, lactation and involution cannot be excluded.

7.1.4. Somatic *SLK* mutations in human patients are lethal.

Here, we have shown that an *Slk* gene trap is embryonic lethal in mice. Recently, a two-month-old patient bearing *SLK* mutations was identified with pontine cerebellar hypoplasia, congenital heart disease, heterotaxy, ambiguous genitalia and intestinal

malrotation (personal communication, Dr. Jennifer Wambach, Washington University School of Medicine). Whole exome sequencing of this patient revealed the child to be a compound heterozygote for two predicted deleterious mutations in *SLK*, a premature stop codon following glutamine 876 (Q876stop) and a frameshift mutation at threonine 367 (T367fs) which results in a cryptic stop codon downstream. Interestingly, both parents are phenotypically normal and a sibling harbors only a single mutation. The rarity of observing *SLK* mutations in humans supports a major role for this kinase in regulating normal embryonic development. Patients with compound mutations in *SLK* are likely to die *in utero* or shortly following birth and therefore, these mutations would never be identified in predominantly juvenile or adulthood diseases, such as cancer. These observations coupled with the findings that $SLK^{+/fs}$ animals are viable and phenotypically normal suggests that one copy of wildtype *SLK* is sufficient for normal embryonic development in both humans and mice.

We have since cloned these human mutations and surprisingly found the Q876stop mutant to be a functional hypermorph while the T367fs is catalytically dead (data not shown). Therefore, patients who are compound heterozygotes for both mutations would express two copies of *SLK* which lack the C-terminal ATH domain. This is similar to the *Slk*-targeted gene trap where the β-Geo cassette is inserted downstream of exon 10, resulting in an in-frame splicing event and the expression of an SLK-LacZ fusion protein which lacks the C-terminal ATH domain. This raises the possibility that the observed phenotype may be due in part to the ATH domain regulating scaffolding rather than catalytic activity. In fact, the integrin linked kinase, ILK, has been shown to be required for normal embryonic development in a kinase-independent manner (255). Mice carrying point mutations at putative autophosphorylation sites in ILK are phenotypically normal, whereas mutations that reduce binding to structural actin binding proteins such as alpha-parvin, are lethal (255). To decipher whether the

embryonic lethality that we have observed is due to a catalytic or the kinase-independent scaffolding role for SLK, our lab has generated a kinase-dead SLK^{K63R} knock-in mouse line. We would predict that heterozygous $SLK^{+/K63R}$ mice would be viable like both $SLK^{+/fs}$ mice and patients with a single mutant *SLK* allele. Should the role of SLK in embryonic development be mostly dependent on its catalytic activity, we would expect homozygous $SLK^{K63R/K63R}$ mice to die *in utero* or shortly after birth. However, if SLK kinase activity is dispensable for embryonic development, we would expect $SLK^{K63R/K63R}$ mice to be phenotypically normal and completely viable. Therefore, using murine models and clinical evidence, we have shown that SLK plays an important role in embryonic development, however, the exact mechanisms by which it does so are under ongoing investigation (Figure 7.1.).

7.2. Loss of SLK in HER2/Neu-induced tumors drives a Sox10-positive phenotype.

7.2.1. SLK-deletion accelerates Neu-induced tumor onset.

The characterization of SLK has largely taken place in non-transformed cell lines, including fibroblasts, myoblasts and normal mammary epithelial cells (16,40,41,52,196,198,208,209). In these cells, SLK has been shown to be required for haptotactic cell migration and to regulate cell cycle progression (20,35,41,49,208,209). Here, for the first time, we have generated SLK knockout cells from a primary NeuNDL expressing tumor. In contrast to these previous reports, deletion of SLK in transformed NeuNDL cell lines did not have a dramatic effect on cellular migration or proliferation in a subconfluent monolayer. In non-transformed, normal cell lines, many pro-proliferative and pro-migratory pathways are kept in check and their signaling is maintained at basal levels (256). In these normal cells, SLK signaling may be dominant to those proto-oncogenic pathways which are maintained at low levels. As such, loss of SLK results in a reduced migratory and proliferative

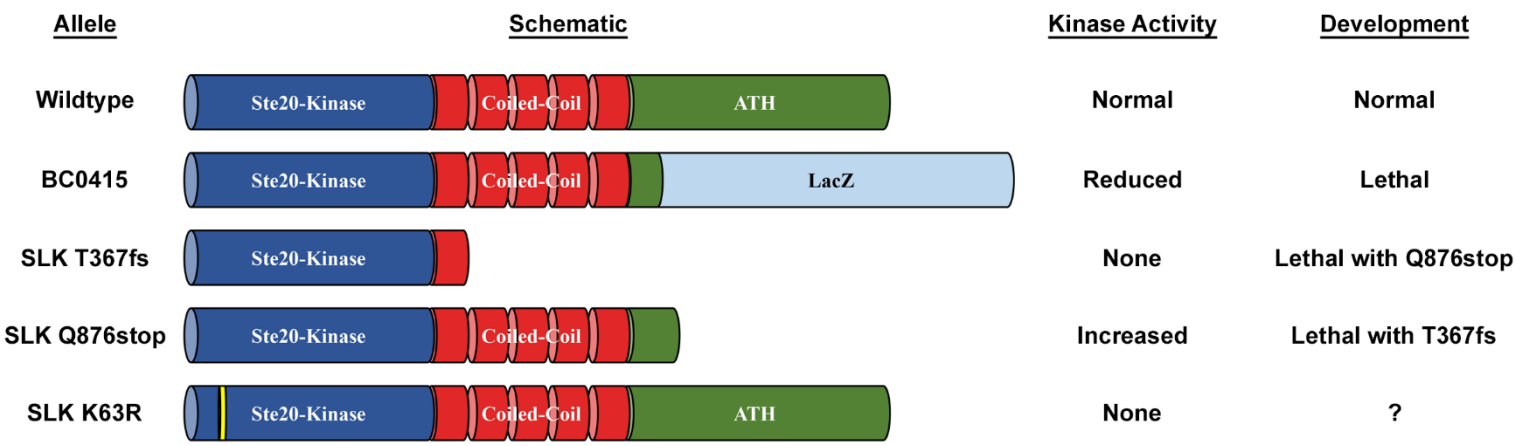

Figure 7.1. A summary of mouse and human SLK alleles and their role in embryonic development. SLK contains a C-terminal kinase domain, central coiled-coil region and an N-terminal ATH domain. Expression of the *Slk-LacZ* fusion allele (BCO415) results in reduced catalytic activity and an early embryonic lethality. A human patient who expressed one *SLK T367fs* (kinase-dead) and one *SLK Q876stop (*hyperactive) allele died at two months of age suggesting that compound heterozygosity of both alleles significantly impairs normal embryonic development. Expression of only one copy of each of these alleles does not result in any significant phenotype. We have generated an SLK^{K63R} knock-in mouse line which is catalytically inactive (mutation represented by a yellow line in the schematic). Interestingly, the lack of an ATH domain in each of these mutations correlates better with the observed severe developmental defects than changes in catalytic activity.

capacity. It is possible that following transformation, oncogenic signals can overcome and bypass SLK-dependent signaling. The constitutive activation of SLK-independent pathways downstream of Neu may provide a possible explanation as to why no differences were observed in haptotactic cell migration and proliferation in the context of our transformed cell line.

7.2.2 SLK is a negative regulator of PDK1 signaling.

Sox10 has previously been shown to modulate mammary stem/progenitor activity, regulate mammary tumor growth and to be highly expressed in basal/triple-negative breast cancers (166,167,184,187). We have demonstrated that deletion of SLK in a Neu-induced mammary tumor model significantly accelerates tumor onset, increases stem/progenitor cell activity and induces *Sox10* expression (Figure 4.3., 9., 10.). We have also shown that Sox10 is able to augment the oncogenic potential of Neu and is sufficient to enhance tumor growth in Neu-positive mammary tumor cells (Figure 4.13., 14.). Despite the obvious importance for Sox10 in breast cancer biology, very little is known regarding the signaling that modulates its expression.

As SLK-deletion results in the induction of *Sox10* in Neu-positive mammary tumor cells, we reasoned that *Sox10* expression may be responsive to Neu/SLK-dependent signaling. Our lab has previously shown that maximal SLK activation downstream of Neu requires active PI3K and PLCγ (114). Here, we have shown that inhibition of the PI3K-signaling module downstream of Neu in SLK knockout tumor cells is sufficient to reduce *Sox10* levels (Figure 6.2.). The role for PI3K-dependent signaling in the regulation of *Sox10* expression is further supported by the elevated levels of PDK1 and AKT activity in SLK knockout tumors and cell lines (Figure 6.3. C, D). Interestingly, inhibition of PI3K or PDK1 resulted in only a partial reduction in *Sox10* mRNA expression whereas inhibition of AKT had a significantly greater

effect. One possibility is that this is due to differential potency of these inhibitors in blocking their targets and downstream signaling.

SLK has been shown to be activated downstream of PI3K following heregulin-stimulation (114). Counterintuitively, the downstream components of the PI3K signaling cascade, PDK1 and AKT, were found to be constitutively activated in SLK knockout mammary tumors and cells (Figure 6.3. C, D). One interpretation is that SLK is activated downstream of Neu and PI3K and acts in a feedback loop to inhibit and dampen this system. Feedback inhibition of the PI3K/AKT signaling cascade is common. For example, AKT activates mTORC1 which phosphorylates and degrades the insulin receptor substrates, preventing membrane scaffolding of PI3K and AKT and reducing their signaling potential (137-139).

We reasoned that SLK does not act at the level of PI3K or PTEN themselves as no differences in intracellular PIP_3 were detected in the $SLK^{fl/fl}$ or $SLK^{-/-}$ NDL cell lines (Figure 6.3. B). Therefore, we tested whether SLK plays a role in inhibiting PDK1 to prevent its constitutive activation. In this model, PDK1 would be localized to the membrane in the presence of a constitutively active Neu and recruit SLK. SLK would in turn become activated and feedback on PDK1 to dampen PI3K-dependent signaling. Supporting this model, we observed that membrane recruitment and maximal activation of SLK required PDK1 activity and that in the absence of SLK, PDK1 could not be dephosphorylated following heregulin-stimulation (Figure 6.4.). Therefore, these data suggest that PDK1 is required to activate SLK which in turn is required to dephosphorylate PDK1 (Figure 7.2.).

Loss of the negative feedback regulation of PDK1 in SLK-deficient mammary tumor cells results in the constitutive activation of AKT. We have shown that SLK deletion in these tumors results in an AKT-dependent induction of *Sox10* (Figure 6.10.) and increase in

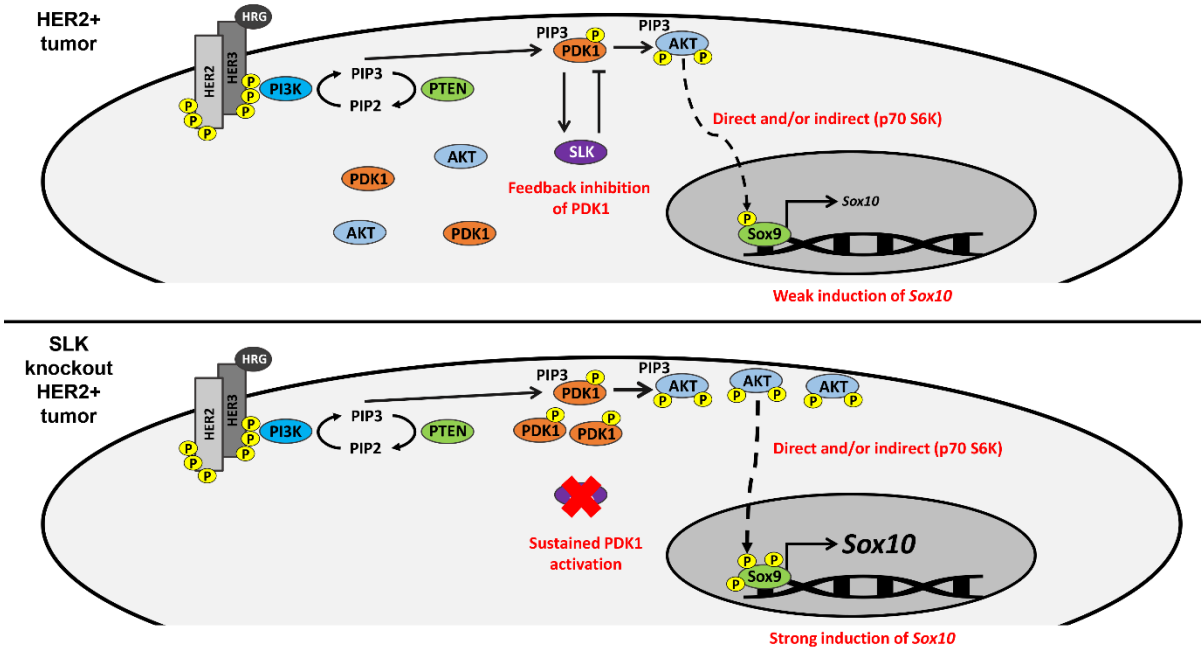

Figure 7.2. Summary model of the role of SLK in Neu-induced mammary tumorigenesis. In HER2/Neu-induced mammary tumors, HER2/Neu becomes activated at the cell membrane and recruits PI3K. In turn, PI3K phosphorylates inositol lipid substrates which bind to the plasma membrane and subsequently recruits PDK1 and AKT. At the membrane, PDK1 becomes phosphorylated and activates both AKT and SLK. SLK negatively inhibits PDK1 to prevent hyperactivation of this signaling axis. AKT can directly phosphorylate Sox9 which is sufficient to induce the transcription of *Sox10*. SLK deletion in this model removes the feedback inhibition on PDK1, resulting in constitutive activation of PDK1 and AKT. Ultimately, the increase in AKT activity results in a strong induction of *Sox10* by modulating Sox9 activity.

mammary stem/progenitor activity (Figure 6.5). Recently, overexpression of a splice variant of the HER2 gene which lacks exon 16 (d16HER2) was also shown to induce *SOX10* expression and drive an increase in self-renewal capabilities (257). The deletion of exon 16 results in the expression of stable and constitutively active HER2 homodimers which ultimately results in a significant hyperactivation of AKT compared to overexpression of wildtype HER2 (257). Interestingly, both SLK deletion in Neu-induced mammary tumors and overexpression of a constitutively active d16HER2 splice variant both hyperactivate AKT and result in increased expression of *Sox10*. These data support the notion that *Sox10* is an AKT-responsive gene at least in the context of HER2-positive luminal-cell derived breast cancers.

7.2.3. SLK-deletion drives a more basal/stem-like breast cancer.

One characteristic of mammary stem cells is the ability for these cells to form mammospheres in anchorage independent conditions and in the absence of any serum components (258). The mammosphere assay directly measures stem/progenitor activity and stem cell self-renewal in mammary cell lines (259,260). Using this assay, we have observed that the $SLK^{fl/fl}$ NDL cell line has a basal mammosphere forming efficiency of approximately 1% in both primary and secondary passages (Figure 4.10. B). Conditional deletion of SLK in these cells results in a significant increase in the mammosphere forming potential, suggesting that SLK may maintain the cells in a differentiated state or repress stem/progenitor activity. Additionally, SLK may be responsible for keeping PDK1/AKT signaling in check, which has been shown to be essential in maintaining embryonic stem cell stemness and pluripotency (261,262). We have identified that Sox10, a regulator of mammary stem/progenitor activity, is upregulated in $SLK^{-/-}$ NDL cells (184). Stable overexpression of Sox10 in the SLK wildtype NDL line was sufficient to significantly increase primary and secondary mammosphere forming efficiency by two-fold compared to vector alone (Figure 4.12. F). Despite this increase

in mammosphere forming efficiency, Sox10 was not sufficient to induce foci formation in Rat-1 fibroblasts above control levels (Figure 4.13. A, B). It did however cooperate with Neu to increase its transforming activity (Figure 4.13 C, D). This suggests that although Sox10 can increase mammary stem/progenitor activity, it is not sufficient to transform normal cells and is therefore unlikely to be an oncogene. Furthermore, this would support the hypothesis that SLK-deficient tumors have an accelerated tumor onset due to the upregulation of Sox10 enhancing Neu-mediated mammary epithelial cell transformation. Whether Sox10 can cooperate with other known oncogenes or enhance transformation in the absence of tumor suppressors remains to be tested.

Stem/progenitor activity of HER2-positive, trastuzumab sensitive breast carcinoma cell lines has been shown to be dependent on signaling through both PI3K and AKT (263). Treatment of these cells with the PI3K inhibitor, LY-294002, significantly reduced the proportion of aldehyde dehydrogenase-positive mammary stem cells (263). As SLK plays a role in regulating PDK1 and AKT, we hypothesized that the increase in stem/progenitor cell activity induced by the loss of SLK was dependent on PI3K signaling. Consistent with these observations, treatment of SLK knockout mammary tumor cells with PI3K, PDK1 or AKT inhibitors significantly reduced their mammosphere forming potential (Figure 6.5. A, B). These data validate the importance for PI3K signaling in regulating the function of mammary stem/progenitor cells and further support the notion that SLK is required to dampen PI3K-dependent signaling. Additionally, we have shown that Sox10 plays a major role in regulating mammary stem/progenitor activity downstream of PI3K-pathway inhibition, with forced expression of Sox10 rescuing mammosphere forming efficiency in the presence of LY-294002, PDK1 inhibitor II or MK-2206 (Figure 6.5. C, D). Together, these data strongly support the hypothesis that Sox10 is a master regulator of mammary stem/progenitor cell

activity and highlights the importance of the PI3K/AKT signaling cascade in regulating this process.

7.2.4. Sox10 is a marker of triple-negative breast cancers.

The TNBC subtype accounts for approximately 10% of all breast cancer cases and has the poorest clinical outcome of all breast cancer subtypes (57,64-66). Diagnosis of TNBC tumors often relies on identifying an absence of HER2-, ESR1- or PGR-positivity in tumor biopsies and the largest barrier to effective treatment is that no known oncogenic drivers have been identified for this subtype (57,58). To identify potential biomarkers within each of these subtypes, we analyzed expression data from 1246 invasive breast cancer samples from the TCGA database.

To identify potential biomarkers within each molecular subtype we chose to perform our analysis using a log2 fold change of 4 (16-fold) cut-off. This was chosen as any biomarker defining these subtypes should have a robust difference in expression. This cut-off resulted in 112 significantly changed genes between each subtype, with no more than 25 genes comprising any one cluster. We believe that these clusters form a manageable list of genes that can be considered as potential biomarkers for each group. Although arbitrarily defined, the identification of HER2 and ESR1/PGR as markers of their corresponding subtype validates our approach. More stringent cut-offs, such as a log2 fold change of 5 (32-fold) or greater may be applied to this data set to identify more rigorous biomarkers of each subtype.

Interestingly, our analysis identified distinct gene signatures for both the HER2-positive and Luminal A/B subtypes. A number of these genes play important roles in tumor progression or as biomarkers of these subtypes (220-222,224,225). One caveat to our approach is that we cannot distinguish whether the expression of any given gene is downregulated (e.g. promoter hypermethylation) in two of the three breast cancer subtypes, or conversely, whether

that gene is induced (e.g. chromosome duplication) in one subtype. One possible method to address this caveat would be to include gene expression data from matched normal tissue as a baseline measure to elucidate whether expression is induced or repressed in the tumor. Fully elucidating these gene signatures may be very important in deriving more thorough subtype classifications beyond the hormone receptors and to identify novel therapeutic strategies in the treatment of these breast cancer subtypes.

One of the most induced genes within the TNBC subtype was *SOX10*, validating that it is a potential biomarker of the TNBC subtype. This also raises the possibility that Sox10-targeted therapies may be beneficial in treating TNBC patients. Although interfering with transcription factor activity can be challenging therapeutically, it has proven to be successful in several clinical trials (264). Furthermore, identifying specific target genes, pathways and processes regulated by Sox10 in the context of breast cancer may provide a novel therapeutic approach in the treatment of the TNBC subtype.

Although Sox10 is highly expressed in the TNBC cluster, we have also observed that a subset of Luminal A/B tumors also express *SOX10* (Figure 5.3., 5.4.). Initially this observation would argue against Sox10 being an independent marker of the TNBC subtype, however, Luminal A/B tumors which have high levels of *SOX10* also express high levels of *AR* (223). Recently, it has been reported that this high expression of *SOX10* is specific to Luminal A-like breast cancers and Sox10 might therefore be another marker to distinguish the Luminal A and B subtypes (187). Assessing tumors for both *AR* and *SOX10* expression may provide a novel method for distinguishing TNBC tumors from the small proportion of Luminal A tumors which express *SOX10*. Of note, the Luminal A/B patients fall within three major subgroups which can be defined by high *ESR1*-expression with low *PGR*-expression, low *ESR1*-expression with high *PGR*-expression or a median level of expression of both receptors

(Figure 5.1., 5.3.). Interestingly, high Sox10-expression within the Luminal A/B subtype falls within this last subgroup with an average expression of both *ESR1* and *PGR*.

7.2.5. Luminal acquisition of Sox10 may be distinct from basal acquisition.

Here, we have reported that *Sox10* expression can be acquired in Neu-induced mammary tumors and cell lines. Although we have not determined whether the acquisition of *Sox10* expression *in vivo* is restricted to a luminal or basal epithelial cell type. A recent report has estimated that Sox10 is expressed in 100% of basal-like and only 70% of luminal-like tumor cells (187). Therefore, one possible explanation for the induction of *Sox10* following SLK deletion in the Neu-induced mammary tumor cells is that these cells have acquired a basal-like signature. However, we have observed that $SLK^{-/-}$ NDL cells retain high levels cytokeratin 8, a luminal epithelial marker, which argues against this possibility (Figure 4.7. D). Additionally, both $SLK^{fl/fl}$ and $SLK^{-/-}$ NDL cells do not express the basal epithelial marker, cytokeratin 5, further supporting the claim that they have maintained their luminal lineage (data not shown). Alone, these data do not support a mechanism whereby the loss of SLK induces a switch from a luminal to a basal epithelial subtype and a more in-depth characterization of these markers would be required to test this. Interestingly, we and others have observed that *Sox10* is not highly expressed in mammary epithelial tumor cell lines grown in 2-D culture, including basal epithelial and TNBC tumor lines (187). This further supports our observations that the induction of *Sox10* in our luminal epithelial Neu-positive mammary tumor cells is dependent on specific signaling that is perturbed following SLK deletion and not due to a switch from a luminal to a basal cell type.

Sorting of luminal epithelial tumor cells into $Sox10^{High}$ and $Sox10^{Low}$ populations has shown that Sox10-positive cells exhibit increased mammary stem/progenitor, neural crest-like and mesenchymal features and gene signatures (184,187). Following SLK knockout we have

only observed an increase in mammary stem/progenitor activity (Figure 4.10. A, B) coupled with the differential expression of 26 genes (Figure 4.9. A). As Sox10 is a transcription factor that is significantly induced following SLK deletion, we were initially concerned at the small number of genes that were differentially regulated. Although several genes including *Pdgfrb* and *Lgr6* appeared in both our dataset and in $Sox10^{High}$ luminal tumor cells derived from an MMTV-PyMT tumor, most genes were not differentially regulated in our dataset (187). One possibility for the lack of mesenchymal target genes within our dataset is the conflicting roles of Sox10 and SLK in regulating EMT. High levels of Sox10 have been linked to dedifferentiation and the acquisition of a mesenchymal gene signature (184,187). However, SLK knockdown has been shown to delay EMT and maintain an epithelial cell state (52). Despite these differences, the most likely explanation for the limited number of differentially regulated genes is that our microarray analysis was performed on total RNA from a mixed population of cells. Given that Sox10 correlates with intratumoral heterogeneity (187), it is unlikely that 100% of cultured cells have acquired *Sox10* expression following SLK deletion. This is further confounded by the high number of cell lines that have been shown to have downregulated *Sox10* with a closed chromatin structure at its promoter (187). Using a Sox10-reporter construct would allow for the dissection of Sox10-expressing SLK knockout cells on which RNA-seq, ChIP-seq and ATAC-seq could be performed. Ultimately, these experiments would allow us to fully identify the epigenetic landscape of $Sox10^{High}/SLK^{Low}$ Neu-positive mammary tumor cells.

7.4. Targeting AKT as a Promising Therapeutic for Herceptin-Resistant and Triple-negative Breast Cancer.

7.4.1. Sox9 is activated downstream of AKT and is required for *Sox10* induction.

Here, we have identified that Sox9 activity is modulated in an AKT-dependent manner (Figure 6.10. A), which has been shown to contribute to maximal transcriptional activity (265). We have also shown that Sox9 is sufficient for the induction of *Sox10* in luminal Neu-positive mammary tumor cells (Figure 6.12.). Lastly, Sox9 is highly phosphorylated in human triple-negative breast cancers and this correlates with the high levels of Sox10 in these samples (Figure 6.9. B, E). We have determined that an AKT-dependent pathway regulates *Sox10* transcription through the -6904/-5995 fragment of the Sox10 promoter (Figure 6.10. B). Therefore, we reasoned that Sox9 phosphorylation may play a role in regulating *Sox10* induction. Interestingly, Sox9 is bound equally to this promoter element in both $SLK^{fl/fl}$ and $SLK^{-/-}$ NDL cells (Figure 6.11.). These data suggest that Sox9 phosphorylation does not affect its DNA binding activity. However, phosphorylation of Sox9 may still affect its transcriptional output without altering its ability to bind DNA. One possibility is that phosphorylation at this site is required to recruit transcriptional cofactors which may be required for maximal activity.

We have shown that AKT can directly phosphorylate Sox9 *in vitro* (Figure 6.10. D) and that Sox9 activity is impaired downstream of AKT inhibition (Figure 6.10. A). Although we predict that AKT directly phosphorylates Sox9 at serine 181, this remains to be tested. Our lab is currently generating a Sox9 S181A mutant which will be used to assess whether AKT phosphorylates this site. There is also the possibility that the phosphorylation that we have observed is an *in vitro* artifact, however, our data still suggests that Sox9 activity is modulated in an AKT-dependent manner (Figure 7.2.). One alternate possibility is that AKT directly phosphorylates and inhibits the activity of a phosphatase which targets Sox9. However, only several protein phosphatases have been identified as direct AKT substrates, with most being involved in regulating cell cycle (266,267). It is also likely that this phosphorylation may be mediated by a kinase that is downstream of AKT. In fact, S6K is activated by mTOR

downstream of AKT and has a consensus phosphorylation recognition motif which matches that of Sox9 S181 (268). To test these predictions, *in vitro* kinase assays would have to be performed with recombinant S6K. Additionally, we would predict that treatment with rapamycin to inhibit mTOR would inactivate S6K and in turn would supress Sox9 activation and subsequently decrease *Sox10* expression.

To validate the role of Sox9 in regulating the transcription of *Sox10*, we performed luciferase assays using the AKT-responsive element from the Sox10 promoter. Surprisingly, myc-Sox9 or the myc-Sox9 S181A mutant are both capable of activating luciferase expression from the -6904/-5995 fragment of the Sox10 promoter under basal conditions (Figure 6.12. lanes 6 and 10). This was also observed for the collagen II promoter, where the induction by both Sox9 constructs is relatively high above background (237). In the context of the collagen II promoter, wildtype Sox9 was sufficient to boost luciferase activity following co-transfection with the catalytic subunit of PKA, whereas the Sox9 S181A mutant failed to do so (237). Similarly, treatment of the myc-Sox9 transfected cells with heregulin increased luciferase activity two-fold above the untreated sample (Figure 6.12. lanes 6 and 7). However, expression of the phosphodeficient mutant abrogated this effect (Figure 6.12. lanes 10 and 11). This suggests that Sox9 transcriptional activity can regulate the Sox10 promoter independent of its DNA binding capacity. Another possible interpretation may be that Sox9 phosphorylation at S181 and/or S211 responds to inductive signals but basally can still dimerize with endogenous Sox9 and activate transcription.

7.4.2. Sox10-positive breast cancers may benefit from AKT inhibition.

We and others have reported that triple-negative and basal/stem-like breast cancers can be defined by a high level of *SOX10* expression (166,167,187). Here, we have uncovered a novel link between constitutive activation of AKT, Sox9 phosphorylation and the induction of

Sox10 expression. Although our findings were observed in Neu-induced luminal mammary tumors and cells, it is possible that a similar mechanism exists in all breast cancers with a high level of PI3K/AKT pathway activation. In fact, oncogenic activation of the PI3K/AKT signaling pathway is frequent in TNBC and most commonly occurs following *PIK3CA* gain-of-function mutations or *P53* inactivation (269,270). Treatment of triple-negative breast cancer cell lines with the allosteric AKT inhibitor, MK-2206, inhibits tumor growth and increases sensitivity to other chemotherapeutic agents (271). Several clinical trials for TNBC have shown that AKT inhibitors, including MK-2206, have a synergistic effect with paclitaxel and significantly improve progression-free and overall survival (150,272,273). In addition to regulating cell survival and promoting tumor growth (131), we have shown that AKT controls the expression of *Sox10*. Therefore, we propose that therapeutic targeting of AKT would be sufficient to decrease mammary tumor stem/progenitor activity by downregulating *SOX10* expression in TNBC.

We have shown that Sox9 activation downstream of AKT is sufficient to induce *Sox10* expression. Consistent with the elevated levels of *SOX10* in human TNBC, these tumors often present with activating mutations in the catalytic subunit of PI3K and therefore increased AKT activity (269). We have corroborated these results and observed a significant increase in Sox9 activity in TNBC patient samples by immunohistochemistry (Figure 6.9. E). Therefore, we predict that mutational activation of PI3K in triple-negative breast cancers activates an AKT/Sox9 signaling axis which induces *SOX10* expression. Additionally, a recent murine model for TNBC has identified a high frequency of both *Egfr* and *Fgfr2* amplifications (270). FGF-signaling has previously been shown to induce the expression of both *Sox9* and *Sox10* (184,191). Given these data, we propose that *Fgfr2* amplifications in TNBC are sufficient to upregulate *Sox9* expression and gain-of-function mutations in *PIK3CA* would be sufficient to

increase Sox9 activity in an AKT-dependent manner. Therefore, TNBC cancers may possess two distinct mechanisms to maximally activate Sox9. Therefore, the combinatorial treatment of triple-negative breast cancers with FGFR and AKT inhibitors may target two distinct signaling pathways that drive *SOX10* expression by blocking both the induction and activation of Sox9.

One of the largest barriers to the effective treatment of HER2-positive breast cancers is the rapid acquisition of Herceptin-resistance (63,102). Four major mechanisms that modulate Herceptin resistance have been identified and include: obstacles preventing Herceptin binding to HER2, failure to trigger and immune response, signaling through alternate pathways and the upregulation of HER2 downstream pathways (274). Relevant to this work, Herceptin-resistant breast cancer cell lines have significantly elevated levels of phosphorylated active AKT compared to parental cell lines (275). As both chronic Herceptin treatment and SLK deletion result in the hyperactivation of AKT, we speculate that these Herceptin-resistant tumors may have also acquired *SOX10* expression. Therefore, it is possible that Herceptin-resistant tumors with high levels of AKT activity, may be dependent on the oncogenic and stem/progenitor activities of Sox10.

7.5. Significance, Conclusions and Future Directions.

Here, we have provided the first evidence that SLK is required for normal embryonic development. Interestingly, these findings directly translate to the clinic where a patient who is compound heterozygote for two deleterious mutations in *SLK* presented with numerous development abnormalities and died perinatally. This suggests that SLK plays a critical role in embryonic development and deciphering its exact role in regulating this process is a subject of ongoing research within our lab.

Contrary to our initial hypothesis, we have observed that SLK-deletion accelerated HER2/Neu-induced mammary tumorigenesis. We have uncovered a novel role for SLK in negative regulating the PI3K/PDK1 signaling axis downstream of HER2/Neu. For the first time, SLK has been shown to be required for the downregulation of PDK1 activity following heregulin-stimulation. Consequently, SLK-deletion in these Neu-induced mammary tumors results in the hyperactivation of PDK1 and its downstream effector AKT. These data build on our previous findings showing that SLK is activated downstream of Neu in a PI3K-dependent manner. Here we have begun to expand on this novel role for SLK in mammary tumorigenesis.

Lastly, we have linked SLK-deletion in HER2/Neu-positive mammary tumors to the induction of *Sox10* and an increase in mammary stem/progenitor activity. To date, Sox10 has been validated as a marker of triple-negative and basal-like tumors. Interestingly, we have shown that *Sox10* expression can also be acquired in a subset of Neu-positive, luminal tumors that have lost SLK to regulate a similar stem/progenitor program. We believe that the loss of negative feedback on the PDK1/AKT signaling axis caused by SLK-deletion, is sufficient to upregulate Sox9 activity. Additionally, Sox9 expression is sufficient to activate the Sox10 promoter in an AKT-dependent manner and its activity is correlated with Sox10 expression in human breast cancer samples. Therefore, we have uncovered a novel signaling axis through AKT/Sox9 which is sufficient to induce *Sox10* expression in SLK-deficient Neu-positive breast cancers.

Currently, our lab is investigating the possibility that Sox10 may drive stem cell activity and tumorigenesis in HER2-positive tumors that lose a dependence on HER2-signaling. This is of interest in the case of Herceptin-resistant breast cancers, where hyperactivation of the PI3K signaling cascade may induce AKT/Sox9-dependent *SOX10* expression. Acquired expression of *SOX10* within these cancers may drive chemotherapeutic

resistance and increased tumor growth. Therefore, we predict that pharmacological inhibition of AKT in Herceptin-resistant or triple-negative breast cancers would decrease Sox9 activity and downregulate *SOX10* expression, ultimately reducing stem/progenitor activity and tumor growth. Additionally, combination therapy of HER2-positive tumors with both Herceptin and MK-2206 may result in increased clinical efficacy by simultaneously repressing both SLK- and Sox10-dependent signaling pathways.

References

1. Hunter T. A thousand and one protein kinases. Cell **1987**;50:823-9
2. Hunter T. Protein kinases and phosphatases: the yin and yang of protein phosphorylation and signaling. Cell **1995**;80:225-36
3. Hanks SK, Quinn AM, Hunter T. The protein kinase family: conserved features and deduced phylogeny of the catalytic domains. Science **1988**;241:42-52
4. Kingsley DM. The TGF-beta superfamily: new members, new receptors, and new genetic tests of function in different organisms. Genes Dev **1994**;8:133-46
5. Clutterbuck E, Shields JG, Gordon J, Smith SH, Boyd A, Callard RE*, et al.* Recombinant human interleukin 5 is an eosinophil differentiation factor but has no activity in standard human B cell growth factor assays. Eur J Immunol **1987**;17:1743-50
6. Manning G, Whyte DB, Martinez R, Hunter T, Sudarsanam S. The protein kinase complement of the human genome. Science **2002**;298:1912-34
7. Hanks SK, Hunter T. Protein kinases 6. The eukaryotic protein kinase superfamily: kinase (catalytic) domain structure and classification. FASEB J **1995**;9:576-96
8. Hanks SK, Quinn AM. Protein kinase catalytic domain sequence database: identification of conserved features of primary structure and classification of family members. Methods Enzymol **1991**;200:38-62
9. Davis RJ. The mitogen-activated protein kinase signal transduction pathway. J Biol Chem **1993**;268:14553-6
10. Fanger GR, Gerwins P, Widmann C, Jarpe MB, Johnson GL. MEKKs, GCKs, MLKs, PAKs, TAKs, and tpls: upstream regulators of the c-Jun amino-terminal kinases? Curr Opin Genet Dev **1997**;7:67-74
11. Zhao ZS, Leung T, Manser E, Lim L. Pheromone signalling in Saccharomyces cerevisiae requires the small GTP-binding protein Cdc42p and its activator CDC24. Mol Cell Biol **1995**;15:5246-57
12. Sells MA, Chernoff J. Emerging from the Pak: the p21-activated protein kinase family. Trends Cell Biol **1997**;7:162-7
13. Itoh S, Kameda Y, Yamada E, Tsujikawa K, Mimura T, Kohama Y. Molecular cloning and characterization of a novel putative STE20-like kinase in guinea pigs. Arch Biochem Biophys **1997**;340:201-7
14. Sabourin LA, Rudnicki MA. Induction of apoptosis by SLK, a Ste20-related kinase. Oncogene **1999**;18:7566-75
15. Yamada E, Tsujikawa K, Itoh S, Kameda Y, Kohama Y, Yamamoto H. Molecular cloning and characterization of a novel human STE20-like kinase, hSLK. Biochim Biophys Acta **2000**;1495:250-62
16. Sabourin LA, Tamai K, Seale P, Wagner J, Rudnicki MA. Caspase 3 cleavage of the Ste20-related kinase SLK releases and activates an apoptosis-inducing kinase domain and an actin-disassembling region. Mol Cell Biol **2000**;20:684-96
17. Hao W, Takano T, Guillemette J, Papillon J, Ren G, Cybulsky AV. Induction of apoptosis by the Ste20-like kinase SLK, a germinal center kinase that activates apoptosis signal-regulating kinase and p38. J Biol Chem **2006**;281:3075-84
18. Cybulsky AV, Takano T, Guillemette J, Papillon J, Volpini RA, Di Battista JA. The Ste20-like kinase SLK promotes p53 transactivation and apoptosis. Am J Physiol Renal Physiol **2009**;297:F971-80
19. Zhang YH, Hume K, Cadonic R, Thompson C, Hakim A, Staines W*, et al.* Expression of the Ste20-like kinase SLK during embryonic development and in the murine adult central nervous system. Brain Res Dev Brain Res **2002**;139:205-15

20. Burakov AV, Zhapparova ON, Kovalenko OV, Zinovkina LA, Potekhina ES, Shanina NA*, et al.* Ste20-related protein kinase LOSK (SLK) controls microtubule radial array in interphase. Mol Biol Cell **2008**;19:1952-61
21. Delarosa S, Guillemette J, Papillon J, Han YS, Kristof AS, Cybulsky AV. Activity of the Ste20-like kinase, SLK, is enhanced by homodimerization. Am J Physiol Renal Physiol **2011**;301:F554-64
22. Schaar DG, Varia MR, Elkabes S, Ramakrishnan L, Dreyfus CF, Black IB. The identification of a novel cDNA preferentially expressed in the olfactory-limbic system of the adult rat. Brain Res **1996**;721:217-28
23. Pike AC, Rellos P, Niesen FH, Turnbull A, Oliver AW, Parker SA*, et al.* Activation segment dimerization: a mechanism for kinase autophosphorylation of non-consensus sites. EMBO J **2008**;27:704-14
24. Luhovy AY, Jaberi A, Papillon J, Guillemette J, Cybulsky AV. Regulation of the Ste20-like kinase, SLK: involvement of activation segment phosphorylation. J Biol Chem **2012**;287:5446-58
25. Pawson T, Scott JD. Signaling through scaffold, anchoring, and adaptor proteins. Science **1997**;278:2075-80
26. Nolen B, Taylor S, Ghosh G. Regulation of protein kinases; controlling activity through activation segment conformation. Mol Cell **2004**;15:661-75
27. Al-Zahrani KN, Baron KD, Sabourin LA. Ste20-like kinase SLK, at the crossroads: a matter of life and death. Cell Adh Migr **2013**;7:1-10
28. Sicheri F, Moarefi I, Kuriyan J. Crystal structure of the Src family tyrosine kinase Hck. Nature **1997**;385:602-9
29. Meng W, Swenson LL, Fitzgibbon MJ, Hayakawa K, Ter Haar E, Behrens AE*, et al.* Structure of mitogen-activated protein kinase-activated protein (MAPKAP) kinase 2 suggests a bifunctional switch that couples kinase activation with nuclear export. J Biol Chem **2002**;277:37401-5
30. Hu J, Liu J, Ghirlando R, Saltiel AR, Hubbard SR. Structural basis for recruitment of the adaptor protein APS to the activated insulin receptor. Mol Cell **2003**;12:1379-89
31. Pombo CM, Bonventre JV, Molnar A, Kyriakis J, Force T. Activation of a human Ste20-like kinase by oxidant stress defines a novel stress response pathway. EMBO J **1996**;15:4537-46
32. Graves JD, Gotoh Y, Draves KE, Ambrose D, Han DK, Wright M*, et al.* Caspase-mediated activation and induction of apoptosis by the mammalian Ste20-like kinase Mst1. EMBO J **1998**;17:2224-34
33. Yan Y, Tulasne D, Browaeys E, Cailliau K, Khayath N, Pierce RJ*, et al.* Molecular cloning and characterisation of SmSLK, a novel Ste20-like kinase in Schistosoma mansoni. Int J Parasitol **2007**;37:1539-50
34. Cybulsky AV, Takano T, Papillon J, Guillemette J, Herzenberg AM, Kennedy CR. Podocyte injury and albuminuria in mice with podocyte-specific overexpression of the Ste20-like kinase, SLK. Am J Pathol **2010**;177:2290-9
35. Ellinger-Ziegelbauer H, Karasuyama H, Yamada E, Tsujikawa K, Todokoro K, Nishida E. Ste20-like kinase (SLK), a regulatory kinase for polo-like kinase (Plk) during the G2/M transition in somatic cells. Genes Cells **2000**;5:491-8
36. O'Reilly PG, Wagner S, Franks DJ, Cailliau K, Browaeys E, Dissous C*, et al.* The Ste20-like kinase SLK is required for cell cycle progression through G2. J Biol Chem **2005**;280:42383-90
37. Craig SW, Johnson RP. Assembly of focal adhesions: progress, paradigms, and portents. Curr Opin Cell Biol **1996**;8:74-85
38. Mitra SK, Schlaepfer DD. Integrin-regulated FAK-Src signaling in normal and cancer cells. Curr Opin Cell Biol **2006**;18:516-23
39. Brown MC, Turner CE. Paxillin: adapting to change. Physiol Rev **2004**;84:1315-39

40. Wagner S, Flood TA, O'Reilly P, Hume K, Sabourin LA. Association of the Ste20-like kinase (SLK) with the microtubule. Role in Rac1-mediated regulation of actin dynamics during cell adhesion and spreading. J Biol Chem **2002**;277:37685-92
41. Wagner S, Storbeck CJ, Roovers K, Chaar ZY, Kolodziej P, McKay M*, et al.* FAK/src-family dependent activation of the Ste20-like kinase SLK is required for microtubule-dependent focal adhesion turnover and cell migration. PLoS One **2008**;3:e1868
42. Etienne-Manneville S, Hall A. Integrin-mediated activation of Cdc42 controls cell polarity in migrating astrocytes through PKCzeta. Cell **2001**;106:489-98
43. Van Aelst L, D'Souza-Schorey C. Rho GTPases and signaling networks. Genes Dev **1997**;11:2295-322
44. Nobes CD, Hall A. Rho, rac, and cdc42 GTPases regulate the assembly of multimolecular focal complexes associated with actin stress fibers, lamellipodia, and filopodia. Cell **1995**;81:53-62
45. Guilluy C, Rolli-Derkinderen M, Loufrani L, Bourge A, Henrion D, Sabourin L*, et al.* Ste20-related kinase SLK phosphorylates Ser188 of RhoA to induce vasodilation in response to angiotensin II Type 2 receptor activation. Circ Res **2008**;102:1265-74
46. Chaar Z, O'Reilly P, Gelman I, Sabourin LA. v-Src-dependent down-regulation of the Ste20-like kinase SLK by casein kinase II. J Biol Chem **2006**;281:28193-9
47. Gates RE, King LE, Jr., Hanks SK, Nanney LB. Potential role for focal adhesion kinase in migrating and proliferating keratinocytes near epidermal wounds and in culture. Cell Growth Differ **1994**;5:891-9
48. Bershadsky A, Chausovsky A, Becker E, Lyubimova A, Geiger B. Involvement of microtubules in the control of adhesion-dependent signal transduction. Curr Biol **1996**;6:1279-89
49. Quizi JL, Baron K, Al-Zahrani KN, O'Reilly P, Sriram RK, Conway J*, et al.* SLK-mediated phosphorylation of paxillin is required for focal adhesion turnover and cell migration. Oncogene **2013**;32:4656-63
50. Palazzo AF, Gundersen GG. Microtubule-actin cross-talk at focal adhesions. Sci STKE **2002**;2002:pe31
51. Kaverina I, Krylyshkina O, Small JV. Regulation of substrate adhesion dynamics during cell motility. Int J Biochem Cell Biol **2002**;34:746-61
52. Conway J, Al-Zahrani KN, Pryce BR, Abou-Hamad J, Sabourin LA. Transforming growth factor beta-induced epithelial to mesenchymal transition requires the Ste20-like kinase SLK independently of its catalytic activity. Oncotarget **2017**;8:98745-56
53. Wang K, Hong RL, Lu JB, Wang DL. Ste20-like kinase is upregulated in glioma and induces glioma invasion. Neoplasma **2018**;65:185-91
54. Ghoncheh M, Pournamdar Z, Salehiniya H. Incidence and Mortality and Epidemiology of Breast Cancer in the World. Asian Pac J Cancer Prev **2016**;17:43-6
55. Perou CM, Sorlie T, Eisen MB, van de Rijn M, Jeffrey SS, Rees CA*, et al.* Molecular portraits of human breast tumours. Nature **2000**;406:747-52
56. Sorlie T, Perou CM, Tibshirani R, Aas T, Geisler S, Johnsen H*, et al.* Gene expression patterns of breast carcinomas distinguish tumor subclasses with clinical implications. Proc Natl Acad Sci U S A **2001**;98:10869-74
57. Cheang MC, Chia SK, Voduc D, Gao D, Leung S, Snider J*, et al.* Ki67 index, HER2 status, and prognosis of patients with luminal B breast cancer. J Natl Cancer Inst **2009**;101:736-50
58. Goldhirsch A, Wood WC, Coates AS, Gelber RD, Thurlimann B, Senn HJ*, et al.* Strategies for subtypes--dealing with the diversity of breast cancer: highlights of the St. Gallen International Expert Consensus on the Primary Therapy of Early Breast Cancer 2011. Ann Oncol **2011**;22:1736-47

59. Brenton JD, Carey LA, Ahmed AA, Caldas C. Molecular classification and molecular forecasting of breast cancer: ready for clinical application? J Clin Oncol **2005**;23:7350-60
60. Guy CT, Webster MA, Schaller M, Parsons TJ, Cardiff RD, Muller WJ. Expression of the neu protooncogene in the mammary epithelium of transgenic mice induces metastatic disease. Proc Natl Acad Sci U S A **1992**;89:10578-82
61. Mansour EG, Ravdin PM, Dressler L. Prognostic factors in early breast carcinoma. Cancer **1994**;74:381-400
62. Dankort DL, Muller WJ. Signal transduction in mammary tumorigenesis: a transgenic perspective. Oncogene **2000**;19:1038-44
63. Wolff AC, Hammond ME, Schwartz JN, Hagerty KL, Allred DC, Cote RJ*, et al.* American Society of Clinical Oncology/College of American Pathologists guideline recommendations for human epidermal growth factor receptor 2 testing in breast cancer. Arch Pathol Lab Med **2007**;131:18-43
64. Carey LA, Dees EC, Sawyer L, Gatti L, Moore DT, Collichio F*, et al.* The triple negative paradox: primary tumor chemosensitivity of breast cancer subtypes. Clin Cancer Res **2007**;13:2329-34
65. Kennecke H, Yerushalmi R, Woods R, Cheang MC, Voduc D, Speers CH*, et al.* Metastatic behavior of breast cancer subtypes. J Clin Oncol **2010**;28:3271-7
66. Brouckaert O, Wildiers H, Floris G, Neven P. Update on triple-negative breast cancer: prognosis and management strategies. Int J Womens Health **2012**;4:511-20
67. Schechter AL, Stern DF, Vaidyanathan L, Decker SJ, Drebin JA, Greene MI*, et al.* The neu oncogene: an erb-B-related gene encoding a 185,000-Mr tumour antigen. Nature **1984**;312:513-6
68. Moasser MM. The oncogene HER2: its signaling and transforming functions and its role in human cancer pathogenesis. Oncogene **2007**;26:6469-87
69. Gullick WJ, Srinivasan R. The type 1 growth factor receptor family: new ligands and receptors and their role in breast cancer. Breast Cancer Res Treat **1998**;52:43-53
70. Fuller SJ, Sivarajah K, Sugden PH. ErbB receptors, their ligands, and the consequences of their activation and inhibition in the myocardium. J Mol Cell Cardiol **2008**;44:831-54
71. Dankort DL, Wang Z, Blackmore V, Moran MF, Muller WJ. Distinct tyrosine autophosphorylation sites negatively and positively modulate neu-mediated transformation. Mol Cell Biol **1997**;17:5410-25
72. Harari D, Yarden Y. Molecular mechanisms underlying ErbB2/HER2 action in breast cancer. Oncogene **2000**;19:6102-14
73. Menard S, Tagliabue E, Campiglio M, Pupa SM. Role of HER2 gene overexpression in breast carcinoma. J Cell Physiol **2000**;182:150-62
74. Venter DJ, Tuzi NL, Kumar S, Gullick WJ. Overexpression of the c-erbB-2 oncoprotein in human breast carcinomas: immunohistological assessment correlates with gene amplification. Lancet **1987**;2:69-72
75. Graus-Porta D, Beerli RR, Daly JM, Hynes NE. ErbB-2, the preferred heterodimerization partner of all ErbB receptors, is a mediator of lateral signaling. EMBO J **1997**;16:1647-55
76. Baulida J, Kraus MH, Alimandi M, Di Fiore PP, Carpenter G. All ErbB receptors other than the epidermal growth factor receptor are endocytosis impaired. J Biol Chem **1996**;271:5251-7
77. Lenferink AE, Kramer RH, van Vugt MJ, Konigswieser M, Di Fiore PP, van Zoelen EJ*, et al.* Superagonistic behaviour of epidermal growth factor/transforming growth factor-alpha chimaeras: correlation with receptor routing after ligand-induced internalization. Biochem J **1997**;327 (Pt 3):859-65
78. Waterman H, Sabanai I, Geiger B, Yarden Y. Alternative intracellular routing of ErbB receptors may determine signaling potency. J Biol Chem **1998**;273:13819-27

79. Lee JW, Soung YH, Seo SH, Kim SY, Park CH, Wang YP*, et al.* Somatic mutations of ERBB2 kinase domain in gastric, colorectal, and breast carcinomas. Clin Cancer Res **2006**;12:57-61
80. Fleishman SJ, Schlessinger J, Ben-Tal N. A putative molecular-activation switch in the transmembrane domain of erbB2. Proc Natl Acad Sci U S A **2002**;99:15937-40
81. Xie D, Shu XO, Deng Z, Wen WQ, Creek KE, Dai Q*, et al.* Population-based, case-control study of HER2 genetic polymorphism and breast cancer risk. J Natl Cancer Inst **2000**;92:412-7
82. Montgomery KG, Gertig DM, Baxter SW, Milne RL, Dite GS, McCredie MR*, et al.* The HER2 I655V polymorphism and risk of breast cancer in women < age 40 years. Cancer Epidemiol Biomarkers Prev **2003**;12:1109-11
83. Benusiglio PR, Lesueur F, Luccarini C, Conroy DM, Shah M, Easton DF*, et al.* Common ERBB2 polymorphisms and risk of breast cancer in a white British population: a case-control study. Breast Cancer Res **2005**;7:R204-9
84. Hudziak RM, Schlessinger J, Ullrich A. Increased expression of the putative growth factor receptor p185HER2 causes transformation and tumorigenesis of NIH 3T3 cells. Proc Natl Acad Sci U S A **1987**;84:7159-63
85. Di Fiore PP, Pierce JH, Kraus MH, Segatto O, King CR, Aaronson SA. erbB-2 is a potent oncogene when overexpressed in NIH/3T3 cells. Science **1987**;237:178-82
86. Benz CC, Scott GK, Sarup JC, Johnson RM, Tripathy D, Coronado E*, et al.* Estrogen-dependent, tamoxifen-resistant tumorigenic growth of MCF-7 cells transfected with HER2/neu. Breast Cancer Res Treat **1992**;24:85-95
87. Muthuswamy SK, Li D, Lelievre S, Bissell MJ, Brugge JS. ErbB2, but not ErbB1, reinitiates proliferation and induces luminal repopulation in epithelial acini. Nat Cell Biol **2001**;3:785-92
88. Bargmann CI, Hung MC, Weinberg RA. Multiple independent activations of the neu oncogene by a point mutation altering the transmembrane domain of p185. Cell **1986**;45:649-57
89. Weiner DB, Liu J, Cohen JA, Williams WV, Greene MI. A point mutation in the neu oncogene mimics ligand induction of receptor aggregation. Nature **1989**;339:230-1
90. Muller WJ, Sinn E, Pattengale PK, Wallace R, Leder P. Single-step induction of mammary adenocarcinoma in transgenic mice bearing the activated c-neu oncogene. Cell **1988**;54:105-15
91. Bouchard L, Lamarre L, Tremblay PJ, Jolicoeur P. Stochastic appearance of mammary tumors in transgenic mice carrying the MMTV/c-neu oncogene. Cell **1989**;57:931-6
92. Cardiff RD, Muller WJ. Transgenic mouse models of mammary tumorigenesis. Cancer Surv **1993**;16:97-113
93. Siegel PM, Dankort DL, Hardy WR, Muller WJ. Novel activating mutations in the neu proto-oncogene involved in induction of mammary tumors. Mol Cell Biol **1994**;14:7068-77
94. Siegel PM, Ryan ED, Cardiff RD, Muller WJ. Elevated expression of activated forms of Neu/ErbB-2 and ErbB-3 are involved in the induction of mammary tumors in transgenic mice: implications for human breast cancer. EMBO J **1999**;18:2149-64
95. Ursini-Siegel J, Hardy WR, Zuo D, Lam SH, Sanguin-Gendreau V, Cardiff RD*, et al.* ShcA signalling is essential for tumour progression in mouse models of human breast cancer. EMBO J **2008**;27:910-20
96. Drebin JA, Link VC, Weinberg RA, Greene MI. Inhibition of tumor growth by a monoclonal antibody reactive with an oncogene-encoded tumor antigen. Proc Natl Acad Sci U S A **1986**;83:9129-33
97. Baselga J, Norton L, Albanell J, Kim YM, Mendelsohn J. Recombinant humanized anti-HER2 antibody (Herceptin) enhances the antitumor activity of paclitaxel and doxorubicin against HER2/neu overexpressing human breast cancer xenografts. Cancer Res **1998**;58:2825-31

98. Saez R, Molina MA, Ramsey EE, Rojo F, Keenan EJ, Albanell J*, et al.* p95HER-2 predicts worse outcome in patients with HER-2-positive breast cancer. Clin Cancer Res **2006**;12:424-31
99. Guarneri V, Frassoldati A, Bottini A, Cagossi K, Bisagni G, Sarti S*, et al.* Preoperative chemotherapy plus trastuzumab, lapatinib, or both in human epidermal growth factor receptor 2-positive operable breast cancer: results of the randomized phase II CHER-LOB study. J Clin Oncol **2012**;30:1989-95
100. Gayle SS, Arnold SL, O'Regan RM, Nahta R. Pharmacologic inhibition of mTOR improves lapatinib sensitivity in HER2-overexpressing breast cancer cells with primary trastuzumab resistance. Anticancer Agents Med Chem **2012**;12:151-62
101. Stemke-Hale K, Gonzalez-Angulo AM, Lluch A, Neve RM, Kuo WL, Davies M*, et al.* An integrative genomic and proteomic analysis of PIK3CA, PTEN, and AKT mutations in breast cancer. Cancer Res **2008**;68:6084-91
102. Gajria D, Chandarlapaty S. HER2-amplified breast cancer: mechanisms of trastuzumab resistance and novel targeted therapies. Expert Rev Anticancer Ther **2011**;11:263-75
103. Gril B, Palmieri D, Bronder JL, Herring JM, Vega-Valle E, Feigenbaum L*, et al.* Effect of lapatinib on the outgrowth of metastatic breast cancer cells to the brain. J Natl Cancer Inst **2008**;100:1092-103
104. Harbeck N, Beckmann MW, Rody A, Schneeweiss A, Muller V, Fehm T*, et al.* HER2 Dimerization Inhibitor Pertuzumab - Mode of Action and Clinical Data in Breast Cancer. Breast Care (Basel) **2013**;8:49-55
105. Badache A, Hynes NE. A new therapeutic antibody masks ErbB2 to its partners. Cancer Cell **2004**;5:299-301
106. Agus DB, Akita RW, Fox WD, Lewis GD, Higgins B, Pisacane PI*, et al.* Targeting ligand-activated ErbB2 signaling inhibits breast and prostate tumor growth. Cancer Cell **2002**;2:127-37
107. Lee-Hoeflich ST, Crocker L, Yao E, Pham T, Munroe X, Hoeflich KP*, et al.* A central role for HER3 in HER2-amplified breast cancer: implications for targeted therapy. Cancer Res **2008**;68:5878-87
108. Dang C, Iyengar N, Datko F, D'Andrea G, Theodoulou M, Dickler M*, et al.* Phase II study of paclitaxel given once per week along with trastuzumab and pertuzumab in patients with human epidermal growth factor receptor 2-positive metastatic breast cancer. J Clin Oncol **2015**;33:442-7
109. Adjuvant Pertuzumab and Trastuzumab in Early HER2-Positive Breast Cancer. N Engl J Med **2017**;377:702
110. Arnould L, Gelly M, Penault-Llorca F, Benoit L, Bonnetain F, Migeon C*, et al.* Trastuzumab-based treatment of HER2-positive breast cancer: an antibody-dependent cellular cytotoxicity mechanism? Br J Cancer **2006**;94:259-67
111. Shi Y, Fan X, Deng H, Brezski RJ, Rycyzyn M, Jordan RE*, et al.* Trastuzumab triggers phagocytic killing of high HER2 cancer cells in vitro and in vivo by interaction with Fcgamma receptors on macrophages. J Immunol **2015**;194:4379-86
112. Bang YJ, Giaccone G, Im SA, Oh DY, Bauer TM, Nordstrom JL*, et al.* First-in-human phase 1 study of margetuximab (MGAH22), an Fc-modified chimeric monoclonal antibody, in patients with HER2-positive advanced solid tumors. Ann Oncol **2017**;28:855-61
113. Benlimame N, He Q, Jie S, Xiao D, Xu YJ, Loignon M*, et al.* FAK signaling is critical for ErbB-2/ErbB-3 receptor cooperation for oncogenic transformation and invasion. J Cell Biol **2005**;171:505-16
114. Roovers K, Wagner S, Storbeck CJ, O'Reilly P, Lo V, Northey JJ*, et al.* The Ste20-like kinase SLK is required for ErbB2-driven breast cancer cell motility. Oncogene **2009**;28:2839-48

115. Marone R, Hess D, Dankort D, Muller WJ, Hynes NE, Badache A. Memo mediates ErbB2-driven cell motility. Nat Cell Biol **2004**;6:515-22
116. Yuan TL, Cantley LC. PI3K pathway alterations in cancer: variations on a theme. Oncogene **2008**;27:5497-510
117. Alimandi M, Romano A, Curia MC, Muraro R, Fedi P, Aaronson SA*, et al.* Cooperative signaling of ErbB3 and ErbB2 in neoplastic transformation and human mammary carcinomas. Oncogene **1995**;10:1813-21
118. Holbro T, Beerli RR, Maurer F, Koziczak M, Barbas CF, 3rd, Hynes NE. The ErbB2/ErbB3 heterodimer functions as an oncogenic unit: ErbB2 requires ErbB3 to drive breast tumor cell proliferation. Proc Natl Acad Sci U S A **2003**;100:8933-8
119. Prigent SA, Gullick WJ. Identification of c-erbB-3 binding sites for phosphatidylinositol 3'-kinase and SHC using an EGF receptor/c-erbB-3 chimera. EMBO J **1994**;13:2831-41
120. Schulze WX, Deng L, Mann M. Phosphotyrosine interactome of the ErbB-receptor kinase family. Mol Syst Biol **2005**;1:2005 0008
121. Cantley LC. The phosphoinositide 3-kinase pathway. Science **2002**;296:1655-7
122. Vanhaesebroeck B, Guillermet-Guibert J, Graupera M, Bilanges B. The emerging mechanisms of isoform-specific PI3K signalling. Nat Rev Mol Cell Biol **2010**;11:329-41
123. Lemmon MA. Membrane recognition by phospholipid-binding domains. Nat Rev Mol Cell Biol **2008**;9:99-111
124. Auger KR, Serunian LA, Soltoff SP, Libby P, Cantley LC. PDGF-dependent tyrosine phosphorylation stimulates production of novel polyphosphoinositides in intact cells. Cell **1989**;57:167-75
125. Shaw RJ, Cantley LC. Ras, PI(3)K and mTOR signalling controls tumour cell growth. Nature **2006**;441:424-30
126. Nagata Y, Lan KH, Zhou X, Tan M, Esteva FJ, Sahin AA*, et al.* PTEN activation contributes to tumor inhibition by trastuzumab, and loss of PTEN predicts trastuzumab resistance in patients. Cancer Cell **2004**;6:117-27
127. Manning BD, Toker A. AKT/PKB Signaling: Navigating the Network. Cell **2017**;169:381-405
128. Alessi DR, Andjelkovic M, Caudwell B, Cron P, Morrice N, Cohen P*, et al.* Mechanism of activation of protein kinase B by insulin and IGF-1. EMBO J **1996**;15:6541-51
129. Kunkel MT, Ni Q, Tsien RY, Zhang J, Newton AC. Spatio-temporal dynamics of protein kinase B/Akt signaling revealed by a genetically encoded fluorescent reporter. J Biol Chem **2005**;280:5581-7
130. Calleja V, Alcor D, Laguerre M, Park J, Vojnovic B, Hemmings BA*, et al.* Intramolecular and intermolecular interactions of protein kinase B define its activation in vivo. PLoS Biol **2007**;5:e95
131. Manning BD, Cantley LC. AKT/PKB signaling: navigating downstream. Cell **2007**;129:1261-74
132. Alessi DR, James SR, Downes CP, Holmes AB, Gaffney PR, Reese CB*, et al.* Characterization of a 3-phosphoinositide-dependent protein kinase which phosphorylates and activates protein kinase Balpha. Curr Biol **1997**;7:261-9
133. Sarbassov DD, Guertin DA, Ali SM, Sabatini DM. Phosphorylation and regulation of Akt/PKB by the rictor-mTOR complex. Science **2005**;307:1098-101
134. Liu P, Gan W, Chin YR, Ogura K, Guo J, Zhang J*, et al.* PtdIns(3,4,5)P3-Dependent Activation of the mTORC2 Kinase Complex. Cancer Discov **2015**;5:1194-209
135. Andjelkovic M, Jakubowicz T, Cron P, Ming XF, Han JW, Hemmings BA. Activation and phosphorylation of a pleckstrin homology domain containing protein kinase (RAC-PK/PKB) promoted by serum and protein phosphatase inhibitors. Proc Natl Acad Sci U S A **1996**;93:5699-704

136. Gao T, Furnari F, Newton AC. PHLPP: a phosphatase that directly dephosphorylates Akt, promotes apoptosis, and suppresses tumor growth. Mol Cell **2005**;18:13-24
137. Manning BD. Balancing Akt with S6K: implications for both metabolic diseases and tumorigenesis. J Cell Biol **2004**;167:399-403
138. Shah OJ, Hunter T. Turnover of the active fraction of IRS1 involves raptor-mTOR- and S6K1-dependent serine phosphorylation in cell culture models of tuberous sclerosis. Mol Cell Biol **2006**;26:6425-34
139. Rodrik-Outmezguine VS, Chandarlapaty S, Pagano NC, Poulikakos PI, Scaltriti M, Moskatel E*, et al.* mTOR kinase inhibition causes feedback-dependent biphasic regulation of AKT signaling. Cancer Discov **2011**;1:248-59
140. Cross DA, Alessi DR, Cohen P, Andjelkovich M, Hemmings BA. Inhibition of glycogen synthase kinase-3 by insulin mediated by protein kinase B. Nature **1995**;378:785-9
141. Inoki K, Li Y, Zhu T, Wu J, Guan KL. TSC2 is phosphorylated and inhibited by Akt and suppresses mTOR signalling. Nat Cell Biol **2002**;4:648-57
142. Kops GJ, de Ruiter ND, De Vries-Smits AM, Powell DR, Bos JL, Burgering BM. Direct control of the Forkhead transcription factor AFX by protein kinase B. Nature **1999**;398:630-4
143. Du K, Montminy M. CREB is a regulatory target for the protein kinase Akt/PKB. J Biol Chem **1998**;273:32377-9
144. Nielsen MD, Luo X, Biteau B, Syverson K, Jasper H. 14-3-3 Epsilon antagonizes FoxO to control growth, apoptosis and longevity in Drosophila. Aging Cell **2008**;7:688-99
145. van der Vos KE, Coffer PJ. The extending network of FOXO transcriptional target genes. Antioxid Redox Signal **2011**;14:579-92
146. Nantel F, Monaco L, Foulkes NS, Masquilier D, LeMeur M, Henriksen K*, et al.* Spermiogenesis deficiency and germ-cell apoptosis in CREM-mutant mice. Nature **1996**;380:159-62
147. Barton K, Muthusamy N, Chanyangam M, Fischer C, Clendenin C, Leiden JM. Defective thymocyte proliferation and IL-2 production in transgenic mice expressing a dominant-negative form of CREB. Nature **1996**;379:81-5
148. Mayer IA, Arteaga CL. The PI3K/AKT Pathway as a Target for Cancer Treatment. Annu Rev Med **2016**;67:11-28
149. Carpten JD, Faber AL, Horn C, Donoho GP, Briggs SL, Robbins CM*, et al.* A transforming mutation in the pleckstrin homology domain of AKT1 in cancer. Nature **2007**;448:439-44
150. Wisinski KB, Tevaarwerk AJ, Burkard ME, Rampurwala M, Eickhoff J, Bell MC*, et al.* Phase I Study of an AKT Inhibitor (MK-2206) Combined with Lapatinib in Adult Solid Tumors Followed by Dose Expansion in Advanced HER2+ Breast Cancer. Clin Cancer Res **2016**;22:2659-67
151. Ma CX, Sanchez C, Gao F, Crowder R, Naughton M, Pluard T*, et al.* A Phase I Study of the AKT Inhibitor MK-2206 in Combination with Hormonal Therapy in Postmenopausal Women with Estrogen Receptor-Positive Metastatic Breast Cancer. Clin Cancer Res **2016**;22:2650-8
152. Hirai H, Sootome H, Nakatsuru Y, Miyama K, Taguchi S, Tsujioka K*, et al.* MK-2206, an allosteric Akt inhibitor, enhances antitumor efficacy by standard chemotherapeutic agents or molecular targeted drugs in vitro and in vivo. Mol Cancer Ther **2010**;9:1956-67
153. Berta P, Hawkins JR, Sinclair AH, Taylor A, Griffiths BL, Goodfellow PN*, et al.* Genetic evidence equating SRY and the testis-determining factor. Nature **1990**;348:448-50
154. Schepers GE, Teasdale RD, Koopman P. Twenty pairs of sox: extent, homology, and nomenclature of the mouse and human sox transcription factor gene families. Dev Cell **2002**;3:167-70
155. Rehberg S, Lischka P, Glaser G, Stamminger T, Wegner M, Rosorius O. Sox10 is an active nucleocytoplasmic shuttle protein, and shuttling is crucial for Sox10-mediated transactivation. Mol Cell Biol **2002**;22:5826-34

156. Harley VR, Lovell-Badge R, Goodfellow PN. Definition of a consensus DNA binding site for SRY. Nucleic Acids Res **1994**;22:1500-1
157. Mertin S, McDowall SG, Harley VR. The DNA-binding specificity of SOX9 and other SOX proteins. Nucleic Acids Res **1999**;27:1359-64
158. van Beest M, Dooijes D, van De Wetering M, Kjaerulff S, Bonvin A, Nielsen O*, et al.* Sequence-specific high mobility group box factors recognize 10-12-base pair minor groove motifs. J Biol Chem **2000**;275:27266-73
159. Wegner M. All purpose Sox: The many roles of Sox proteins in gene expression. Int J Biochem Cell Biol **2010**;42:381-90
160. Werner MH, Huth JR, Gronenborn AM, Clore GM. Molecular basis of human 46X,Y sex reversal revealed from the three-dimensional solution structure of the human SRY-DNA complex. Cell **1995**;81:705-14
161. Bowles J, Schepers G, Koopman P. Phylogeny of the SOX family of developmental transcription factors based on sequence and structural indicators. Dev Biol **2000**;227:239-55
162. Guth SI, Wegner M. Having it both ways: Sox protein function between conservation and innovation. Cell Mol Life Sci **2008**;65:3000-18
163. Weider M, Wegner M. SoxE factors: Transcriptional regulators of neural differentiation and nervous system development. Semin Cell Dev Biol **2017**;63:35-42
164. Harris ML, Buac K, Shakhova O, Hakami RM, Wegner M, Sommer L*, et al.* A dual role for SOX10 in the maintenance of the postnatal melanocyte lineage and the differentiation of melanocyte stem cell progenitors. PLoS Genet **2013**;9:e1003644
165. Shakhova O, Cheng P, Mishra PJ, Zingg D, Schaefer SM, Debbache J*, et al.* Antagonistic cross-regulation between Sox9 and Sox10 controls an anti-tumorigenic program in melanoma. PLoS Genet **2015**;11:e1004877
166. Cimino-Mathews A, Subhawong AP, Elwood H, Warzecha HN, Sharma R, Park BH*, et al.* Neural crest transcription factor Sox10 is preferentially expressed in triple-negative and metaplastic breast carcinomas. Hum Pathol **2013**;44:959-65
167. Ivanov SV, Panaccione A, Nonaka D, Prasad ML, Boyd KL, Brown B*, et al.* Diagnostic SOX10 gene signatures in salivary adenoid cystic and breast basal-like carcinomas. Br J Cancer **2013**;109:444-51
168. Tong X, Li L, Li X, Heng L, Zhong L, Su X*, et al.* SOX10, a novel HMG-box-containing tumor suppressor, inhibits growth and metastasis of digestive cancers by suppressing the Wnt/beta-catenin pathway. Oncotarget **2014**;5:10571-83
169. Zhang S, Zhu C, Zhu L, Liu H, Liu S, Zhao N*, et al.* Oncogenicity of the transcription factor SOX8 in hepatocellular carcinoma. Med Oncol **2014**;31:918
170. Barrionuevo F, Georg I, Scherthan H, Lecureuil C, Guillou F, Wegner M*, et al.* Testis cord differentiation after the sex determination stage is independent of Sox9 but fails in the combined absence of Sox9 and Sox8. Dev Biol **2009**;327:301-12
171. Barrionuevo F, Scherer G. SOX E genes: SOX9 and SOX8 in mammalian testis development. Int J Biochem Cell Biol **2010**;42:433-6
172. O'Bryan MK, Takada S, Kennedy CL, Scott G, Harada S, Ray MK*, et al.* Sox8 is a critical regulator of adult Sertoli cell function and male fertility. Dev Biol **2008**;316:359-70
173. Portnoi MF, Dumargne MC, Rojo S, Witchel SF, Duncan AJ, Eozenou C*, et al.* Mutations involving the SRY-related gene SOX8 are associated with a spectrum of human reproductive anomalies. Hum Mol Genet **2018**;27:1228-40
174. De Santa Barbara P, Bonneaud N, Boizet B, Desclozeaux M, Moniot B, Sudbeck P*, et al.* Direct interaction of SRY-related protein SOX9 and steroidogenic factor 1 regulates transcription of the human anti-Mullerian hormone gene. Mol Cell Biol **1998**;18:6653-65

175. Vidal VP, Chaboissier MC, de Rooij DG, Schedl A. Sox9 induces testis development in XX transgenic mice. Nat Genet **2001**;28:216-7
176. Jakob S, Lovell-Badge R. Sex determination and the control of Sox9 expression in mammals. FEBS J **2011**;278:1002-9
177. Gonen N, Futtner CR, Wood S, Garcia-Moreno SA, Salamone IM, Samson SC*, et al.* Sex reversal following deletion of a single distal enhancer of Sox9. Science **2018**;360:1469-73
178. Guo X, Xiong L, Sun T, Peng R, Zou L, Zhu H*, et al.* Expression features of SOX9 associate with tumor progression and poor prognosis of hepatocellular carcinoma. Diagn Pathol **2012**;7:44
179. Prevostel C, Blache P. The dose-dependent effect of SOX9 and its incidence in colorectal cancer. Eur J Cancer **2017**;86:150-7
180. Lin SC, Chou YT, Jiang SS, Chang JL, Chung CH, Kao YR*, et al.* Epigenetic Switch between SOX2 and SOX9 Regulates Cancer Cell Plasticity. Cancer Res **2016**;76:7036-48
181. Jeselsohn R, Cornwell M, Pun M, Buchwalter G, Nguyen M, Bango C*, et al.* Embryonic transcription factor SOX9 drives breast cancer endocrine resistance. Proc Natl Acad Sci U S A **2017**;114:E4482-E91
182. Herbarth B, Pingault V, Bondurand N, Kuhlbrodt K, Hermans-Borgmeyer I, Puliti A*, et al.* Mutation of the Sry-related Sox10 gene in Dominant megacolon, a mouse model for human Hirschsprung disease. Proc Natl Acad Sci U S A **1998**;95:5161-5
183. Southard-Smith EM, Kos L, Pavan WJ. Sox10 mutation disrupts neural crest development in Dom Hirschsprung mouse model. Nat Genet **1998**;18:60-4
184. Dravis C, Spike BT, Harrell JC, Johns C, Trejo CL, Southard-Smith EM*, et al.* Sox10 Regulates Stem/Progenitor and Mesenchymal Cell States in Mammary Epithelial Cells. Cell Rep **2015**;12:2035-48
185. Kim J, Lo L, Dormand E, Anderson DJ. SOX10 maintains multipotency and inhibits neuronal differentiation of neural crest stem cells. Neuron **2003**;38:17-31
186. Pozniak CD, Langseth AJ, Dijkgraaf GJ, Choe Y, Werb Z, Pleasure SJ. Sox10 directs neural stem cells toward the oligodendrocyte lineage by decreasing Suppressor of Fused expression. Proc Natl Acad Sci U S A **2010**;107:21795-800
187. Dravis C, Chung CY, Lytle NK, Herrera-Valdez J, Luna G, Trejo CL*, et al.* Epigenetic and Transcriptomic Profiling of Mammary Gland Development and Tumor Models Disclose Regulators of Cell State Plasticity. Cancer Cell **2018**
188. Harris ML, Baxter LL, Loftus SK, Pavan WJ. Sox proteins in melanocyte development and melanoma. Pigment Cell Melanoma Res **2010**;23:496-513
189. Antonellis A, Huynh JL, Lee-Lin SQ, Vinton RM, Renaud G, Loftus SK*, et al.* Identification of neural crest and glial enhancers at the mouse Sox10 locus through transgenesis in zebrafish. PLoS Genet **2008**;4:e1000174
190. Cheung M, Briscoe J. Neural crest development is regulated by the transcription factor Sox9. Development **2003**;130:5681-93
191. Chen Z, Huang J, Liu Y, Dattilo LK, Huh SH, Ornitz D*, et al.* FGF signaling activates a Sox9-Sox10 pathway for the formation and branching morphogenesis of mouse ocular glands. Development **2014**;141:2691-701
192. Zhu YT, Jia Y, Hu L, Qi C, Prasad MK, McCallion AS*, et al.* Peroxisome-proliferator-activated receptor-binding protein (PBP) is essential for the growth of active Notch4-immortalized mammary epithelial cells by activating SOX10 expression. Biochem J **2009**;425:435-44
193. Kelleher RJ, 3rd, Flanagan PM, Kornberg RD. A novel mediator between activator proteins and the RNA polymerase II transcription apparatus. Cell **1990**;61:1209-15

194. Dutton JR, Antonellis A, Carney TJ, Rodrigues FS, Pavan WJ, Ward A*, et al.* An evolutionarily conserved intronic region controls the spatiotemporal expression of the transcription factor Sox10. BMC Dev Biol **2008**;8:105
195. Storbeck CJ, Daniel K, Zhang YH, Lunde J, Scime A, Asakura A*, et al.* Ste20-like kinase SLK displays myofiber type specificity and is involved in C2C12 myoblast differentiation. Muscle Nerve **2004**;29:553-64
196. Storbeck CJ, Al-Zahrani KN, Sriram R, Kawesa S, O'Reilly P, Daniel K*, et al.* Distinct roles for Ste20-like kinase SLK in muscle function and regeneration. Skelet Muscle **2013**;3:16
197. Min L, Zhang C, Qu L, Huang J, Jiang L, Liu J*, et al.* Gene regulatory pattern analysis reveals essential role of core transcriptional factors' activation in triple-negative breast cancer. Oncotarget **2017**;8:21938-53
198. Pryce BR, Al-Zahrani KN, Dufresne S, Belkina N, Labreche C, Patino-Lopez G*, et al.* Deletion of the Ste20-like kinase SLK in skeletal muscle results in a progressive myopathy and muscle weakness. Skelet Muscle **2017**;7:3
199. Howe GA, Addison CL. RhoB controls endothelial cell morphogenesis in part via negative regulation of RhoA. Vasc Cell **2012**;4:1
200. Cancer Genome Atlas N. Comprehensive molecular portraits of human breast tumours. Nature **2012**;490:61-70
201. Collado-Torres L, Nellore A, Kammers K, Ellis SE, Taub MA, Hansen KD*, et al.* Reproducible RNA-seq analysis using recount2. Nat Biotechnol **2017**;35:319-21
202. Rossant J, Cross JC. Placental development: lessons from mouse mutants. Nat Rev Genet **2001**;2:538-48
203. Kurosaka S, Kashina A. Cell biology of embryonic migration. Birth Defects Res C Embryo Today **2008**;84:102-22
204. Bedzhov I, Graham SJ, Leung CY, Zernicka-Goetz M. Developmental plasticity, cell fate specification and morphogenesis in the early mouse embryo. Philos Trans R Soc Lond B Biol Sci **2014**;369
205. Machicoane M, de Frutos CA, Fink J, Rocancourt M, Lombardi Y, Garel S*, et al.* SLK-dependent activation of ERMs controls LGN-NuMA localization and spindle orientation. J Cell Biol **2014**;205:791-9
206. Fokin AI, Klementeva TS, Nadezhdina ES, Burakov AV. SLK/LOSK kinase regulates cell motility independently of microtubule organization and Golgi polarization. Cytoskeleton (Hoboken) **2016**;73:83-92
207. Al-Zahrani KN, Sekhon P, Tessier DR, Yockell-Lelievre J, Pryce BR, Baron KD*, et al.* Essential role for the SLK protein kinase in embryogenesis and placental tissue development. Dev Dyn **2014**;243:640-51
208. Storbeck CJ, Wagner S, O'Reilly P, McKay M, Parks RJ, Westphal H*, et al.* The Ldb1 and Ldb2 transcriptional cofactors interact with the Ste20-like kinase SLK and regulate cell migration. Mol Biol Cell **2009**;20:4174-82
209. Baron KD, Al-Zahrani K, Conway J, Labreche C, Storbeck CJ, Visvader JE*, et al.* Recruitment and activation of SLK at the leading edge of migrating cells requires Src family kinase activity and the LIM-only protein 4. Biochim Biophys Acta **2015**;1853:1683-92
210. Cui Y, Wang W, Dong N, Lou J, Srinivasan DK, Cheng W*, et al.* Role of corin in trophoblast invasion and uterine spiral artery remodelling in pregnancy. Nature **2012**;484:246-50
211. Lumbers ER, Yu ZY, Gibson KJ. The selfish brain and the barker hypothesis. Clin Exp Pharmacol Physiol **2001**;28:942-7

212. Pringle KG, Kind KL, Sferruzzi-Perri AN, Thompson JG, Roberts CT. Beyond oxygen: complex regulation and activity of hypoxia inducible factors in pregnancy. Hum Reprod Update **2010**;16:415-31
213. Juers DH, Matthews BW, Huber RE. LacZ beta-galactosidase: structure and function of an enzyme of historical and molecular biological importance. Protein Sci **2012**;21:1792-807
214. Cybulsky AV, Guillemette J, Papillon J, Abouelazm NT. Regulation of Ste20-like kinase, SLK, activity: Dimerization and activation segment phosphorylation. PLoS One **2017**;12:e0177226
215. Huang PY, Kandyba E, Jabouille A, Sjolund J, Kumar A, Halliwill K*, et al.* Lgr6 is a stem cell marker in mouse skin squamous cell carcinoma. Nat Genet **2017**;49:1624-32
216. Bertucci F, Finetti P, Cervera N, Esterni B, Hermitte F, Viens P*, et al.* How basal are triple-negative breast cancers? Int J Cancer **2008**;123:236-40
217. Safarpour D, Pakneshan S, Tavassoli FA. Androgen receptor (AR) expression in 400 breast carcinomas: is routine AR assessment justified? Am J Cancer Res **2014**;4:353-68
218. Christenson JL, Trepel JB, Ali HY, Lee S, Eisner JR, Baskin-Bey ES*, et al.* Harnessing a Different Dependency: How to Identify and Target Androgen Receptor-Positive Versus Quadruple-Negative Breast Cancer. Horm Cancer **2018**
219. Park S, Koo J, Park HS, Kim JH, Choi SY, Lee JH*, et al.* Expression of androgen receptors in primary breast cancer. Ann Oncol **2010**;21:488-92
220. Veeraraghavan J, Tan Y, Cao XX, Kim JA, Wang X, Chamness GC*, et al.* Recurrent ESR1-CCDC170 rearrangements in an aggressive subset of oestrogen receptor-positive breast cancers. Nat Commun **2014**;5:4577
221. Cornen S, Guille A, Adelaide J, Addou-Klouche L, Finetti P, Saade MR*, et al.* Candidate luminal B breast cancer genes identified by genome, gene expression and DNA methylation profiling. PLoS One **2014**;9:e81843
222. Garczyk S, von Stillfried S, Antonopoulos W, Hartmann A, Schrauder MG, Fasching PA*, et al.* AGR3 in breast cancer: prognostic impact and suitable serum-based biomarker for early cancer detection. PLoS One **2015**;10:e0122106
223. Al-Zahrani KN, Cook DP, Vanderhyden BC, Sabourin LA. Assessing the efficacy of androgen receptor and Sox10 as independent markers of the triple-negative breast cancer subtype by transcriptome profiling. Oncotarget **2018**;9:33348-59
224. Bivin WW, Yergiyev O, Bunker ML, Silverman JF, Krishnamurti U. GRB7 Expression and Correlation With HER2 Amplification in Invasive Breast Carcinoma. Appl Immunohistochem Mol Morphol **2017**;25:553-8
225. Tsang JY, Kwok YK, Chan KW, Ni YB, Chow WN, Lau KF*, et al.* Expression and clinical significance of carcinoembryonic antigen-related cell adhesion molecule 6 in breast cancers. Breast Cancer Res Treat **2013**;142:311-22
226. Baniwal SK, Little GH, Chimge NO, Frenkel B. Runx2 controls a feed-forward loop between androgen and prolactin-induced protein (PIP) in stimulating T47D cell proliferation. J Cell Physiol **2012**;227:2276-82
227. Kim YJ, Lim H, Li Z, Oh Y, Kovlyagina I, Choi IY*, et al.* Generation of multipotent induced neural crest by direct reprogramming of human postnatal fibroblasts with a single transcription factor. Cell Stem Cell **2014**;15:497-506
228. Malta TM, Sokolov A, Gentles AJ, Burzykowski T, Poisson L, Weinstein JN*, et al.* Machine Learning Identifies Stemness Features Associated with Oncogenic Dedifferentiation. Cell **2018**;173:338-54 e15
229. Wahlbuhl M, Reiprich S, Vogl MR, Bosl MR, Wegner M. Transcription factor Sox10 orchestrates activity of a neural crest-specific enhancer in the vicinity of its gene. Nucleic Acids Res **2012**;40:88-101

230. Gray A, Olsson H, Batty IH, Priganica L, Peter Downes C. Nonradioactive methods for the assay of phosphoinositide 3-kinases and phosphoinositide phosphatases and selective detection of signaling lipids in cell and tissue extracts. Anal Biochem **2003**;313:234-45
231. Jin SG, Xiong W, Wu X, Yang L, Pfeifer GP. The DNA methylation landscape of human melanoma. Genomics **2015**;106:322-30
232. Li LC, Dahiya R. MethPrimer: designing primers for methylation PCRs. Bioinformatics **2002**;18:1427-31
233. Salas TR, Reddy SA, Clifford JL, Davis RJ, Kikuchi A, Lippman SM*, et al.* Alleviating the suppression of glycogen synthase kinase-3beta by Akt leads to the phosphorylation of cAMP-response element-binding protein and its transactivation in intact cell nuclei. J Biol Chem **2003**;278:41338-46
234. Zheng WH, Kar S, Quirion R. Insulin-like growth factor-1-induced phosphorylation of the forkhead family transcription factor FKHRL1 is mediated by Akt kinase in PC12 cells. J Biol Chem **2000**;275:39152-8
235. Wang Q, Liu L, Pei L, Ju W, Ahmadian G, Lu J*, et al.* Control of synaptic strength, a novel function of Akt. Neuron **2003**;38:915-28
236. Jeong CH, Cho YY, Kim MO, Kim SH, Cho EJ, Lee SY*, et al.* Phosphorylation of Sox2 cooperates in reprogramming to pluripotent stem cells. Stem Cells **2010**;28:2141-50
237. Huang W, Zhou X, Lefebvre V, de Crombrugghe B. Phosphorylation of SOX9 by cyclic AMP-dependent protein kinase A enhances SOX9's ability to transactivate a Col2a1 chondrocyte-specific enhancer. Mol Cell Biol **2000**;20:4149-58
238. Baker RE, Schnell S, Maini PK. A clock and wavefront mechanism for somite formation. Dev Biol **2006**;293:116-26
239. Goldbeter A, Pourquie O. Modeling the segmentation clock as a network of coupled oscillations in the Notch, Wnt and FGF signaling pathways. J Theor Biol **2008**;252:574-85
240. Adams RH, Porras A, Alonso G, Jones M, Vintersten K, Panelli S*, et al.* Essential role of p38alpha MAP kinase in placental but not embryonic cardiovascular development. Mol Cell **2000**;6:109-16
241. Giroux S, Tremblay M, Bernard D, Cardin-Girard JF, Aubry S, Larouche L*, et al.* Embryonic death of Mek1-deficient mice reveals a role for this kinase in angiogenesis in the labyrinthine region of the placenta. Curr Biol **1999**;9:369-72
242. Wojnowski L, Zimmer AM, Beck TW, Hahn H, Bernal R, Rapp UR*, et al.* Endothelial apoptosis in Braf-deficient mice. Nat Genet **1997**;16:293-7
243. Hatano N, Mori Y, Oh-hora M, Kosugi A, Fujikawa T, Nakai N*, et al.* Essential role for ERK2 mitogen-activated protein kinase in placental development. Genes Cells **2003**;8:847-56
244. Qu J, Li X, Novitch BG, Zheng Y, Kohn M, Xie JM*, et al.* PAK4 kinase is essential for embryonic viability and for proper neuronal development. Mol Cell Biol **2003**;23:7122-33
245. Tian Y, Lei L, Cammarano M, Nekrasova T, Minden A. Essential role for the Pak4 protein kinase in extraembryonic tissue development and vessel formation. Mech Dev **2009**;126:710-20
246. Ott MO, Bober E, Lyons G, Arnold H, Buckingham M. Early expression of the myogenic regulatory gene, myf-5, in precursor cells of skeletal muscle in the mouse embryo. Development **1991**;111:1097-107
247. Oakes SR, Hilton HN, Ormandy CJ. The alveolar switch: coordinating the proliferative cues and cell fate decisions that drive the formation of lobuloalveoli from ductal epithelium. Breast Cancer Res **2006**;8:207
248. Anderson SM, Rudolph MC, McManaman JL, Neville MC. Key stages in mammary gland development. Secretory activation in the mammary gland: it's not just about milk protein synthesis! Breast Cancer Res **2007**;9:204

249. Watson CJ. Involution: apoptosis and tissue remodelling that convert the mammary gland from milk factory to a quiescent organ. Breast Cancer Res **2006**;8:203
250. Li N, Zhang Y, Naylor MJ, Schatzmann F, Maurer F, Wintermantel T*, et al.* Beta1 integrins regulate mammary gland proliferation and maintain the integrity of mammary alveoli. EMBO J **2005**;24:1942-53
251. Naylor MJ, Li N, Cheung J, Lowe ET, Lambert E, Marlow R*, et al.* Ablation of beta1 integrin in mammary epithelium reveals a key role for integrin in glandular morphogenesis and differentiation. J Cell Biol **2005**;171:717-28
252. Johnson TM, Antrobus R, Johnson LN. Plk1 activation by Ste20-like kinase (Slk) phosphorylation and polo-box phosphopeptide binding assayed with the substrate translationally controlled tumor protein (TCTP). Biochemistry **2008**;47:3688-96
253. Lund LR, Romer J, Thomasset N, Solberg H, Pyke C, Bissell MJ*, et al.* Two distinct phases of apoptosis in mammary gland involution: proteinase-independent and -dependent pathways. Development **1996**;122:181-93
254. Abell K, Bilancio A, Clarkson RW, Tiffen PG, Altaparmakov AI, Burdon TG*, et al.* Stat3-induced apoptosis requires a molecular switch in PI(3)K subunit composition. Nat Cell Biol **2005**;7:392-8
255. Lange A, Wickstrom SA, Jakobson M, Zent R, Sainio K, Fassler R. Integrin-linked kinase is an adaptor with essential functions during mouse development. Nature **2009**;461:1002-6
256. Hanahan D, Weinberg RA. The hallmarks of cancer. Cell **2000**;100:57-70
257. Castagnoli L, Ghedini GC, Koschorke A, Triulzi T, Dugo M, Gasparini P*, et al.* Pathobiological implications of the d16HER2 splice variant for stemness and aggressiveness of HER2-positive breast cancer. Oncogene **2017**;36:1721-32
258. Shaw FL, Harrison H, Spence K, Ablett MP, Simoes BM, Farnie G*, et al.* A detailed mammosphere assay protocol for the quantification of breast stem cell activity. J Mammary Gland Biol Neoplasia **2012**;17:111-7
259. Ponti D, Costa A, Zaffaroni N, Pratesi G, Petrangolini G, Coradini D*, et al.* Isolation and in vitro propagation of tumorigenic breast cancer cells with stem/progenitor cell properties. Cancer Res **2005**;65:5506-11
260. Harrison H, Farnie G, Howell SJ, Rock RE, Stylianou S, Brennan KR*, et al.* Regulation of breast cancer stem cell activity by signaling through the Notch4 receptor. Cancer Res **2010**;70:709-18
261. Ling LS, Voskas D, Woodgett JR. Activation of PDK-1 maintains mouse embryonic stem cell self-renewal in a PKB-dependent manner. Oncogene **2013**;32:5397-408
262. Romorini L, Garate X, Neiman G, Luzzani C, Furmento VA, Guberman AS*, et al.* AKT/GSK3beta signaling pathway is critically involved in human pluripotent stem cell survival. Sci Rep **2016**;6:35660
263. Korkaya H, Paulson A, Iovino F, Wicha MS. HER2 regulates the mammary stem/progenitor cell population driving tumorigenesis and invasion. Oncogene **2008**;27:6120-30
264. Bhagwat AS, Vakoc CR. Targeting Transcription Factors in Cancer. Trends Cancer **2015**;1:53-65
265. Kumar D, Lassar AB. The transcriptional activity of Sox9 in chondrocytes is regulated by RhoA signaling and actin polymerization. Mol Cell Biol **2009**;29:4262-73
266. Feng C, Yu A, Liu Y, Zhang J, Zong Z, Su W*, et al.* Involvement of protein kinase B/AKT in early development of mouse fertilized eggs. Biol Reprod **2007**;77:560-8
267. Xu W, Yuan X, Jung YJ, Yang Y, Basso A, Rosen N*, et al.* The heat shock protein 90 inhibitor geldanamycin and the ErbB inhibitor ZD1839 promote rapid PP1 phosphatase-dependent inactivation of AKT in ErbB2 overexpressing breast cancer cells. Cancer Res **2003**;63:7777-84

268. Pei JJ, An WL, Zhou XW, Nishimura T, Norberg J, Benedikz E*, et al.* P70 S6 kinase mediates tau phosphorylation and synthesis. FEBS Lett **2006**;580:107-14
269. Cossu-Rocca P, Orru S, Muroni MR, Sanges F, Sotgiu G, Ena S*, et al.* Analysis of PIK3CA Mutations and Activation Pathways in Triple Negative Breast Cancer. PLoS One **2015**;10:e0141763
270. Liu H, Murphy CJ, Karreth FA, Emdal KB, White FM, Elemento O*, et al.* Identifying and Targeting Sporadic Oncogenic Genetic Aberrations in Mouse Models of Triple-Negative Breast Cancer. Cancer Discov **2018**;8:354-69
271. Sangai T, Akcakanat A, Chen H, Tarco E, Wu Y, Do KA*, et al.* Biomarkers of response to Akt inhibitor MK-2206 in breast cancer. Clin Cancer Res **2012**;18:5816-28
272. Kim SB, Dent R, Im SA, Espie M, Blau S, Tan AR*, et al.* Ipatasertib plus paclitaxel versus placebo plus paclitaxel as first-line therapy for metastatic triple-negative breast cancer (LOTUS): a multicentre, randomised, double-blind, placebo-controlled, phase 2 trial. Lancet Oncol **2017**;18:1360-72
273. Costa RLB, Han HS, Gradishar WJ. Targeting the PI3K/AKT/mTOR pathway in triple-negative breast cancer: a review. Breast Cancer Res Treat **2018**;169:397-406
274. Pohlmann PR, Mayer IA, Mernaugh R. Resistance to Trastuzumab in Breast Cancer. Clin Cancer Res **2009**;15:7479-91
275. Chan CT, Metz MZ, Kane SE. Differential sensitivities of trastuzumab (Herceptin)-resistant human breast cancer cells to phosphoinositide-3 kinase (PI-3K) and epidermal growth factor receptor (EGFR) kinase inhibitors. Breast Cancer Res Treat **2005**;91:187-201